SAPIENZA
UNIVERSITÀ DI ROMA

PhD School of Pharmaceutical Sciences XXXI cycle
"Sapienza" University of Rome

DESIGN OF HISTONE METHYLTRANSFERASE AND DEACETYLASE MODULATORS: APPLICATIONS IN CANCER AND NON-CANCER DISEASES

Doctoral Dissertation
Submitted by

Roberta Mazzone

Department of Chemistry and Technologies of Drug
Faculty of Pharmacy and Medicine
"Sapienza" University of Rome

Supervisor

Professor **Antonello Mai** Ph.D. (tutor and main supervisor)

Department of Chemistry and Technologies of Drug, "Sapienza" University of Rome, P.le Aldo Moro, 5 - 00185 – Rome, Italy.

Adjunct Professor **Paul Brennan** Ph.D. (foreign supervisor)

Principal investigator (PI) in Medicinal Chemistry at the Target Discovery Institute and Structural Genomics Consortium (SGC) in NDM Research Building, Old Road Campus, Roosevelt Dr, Oxford OX3 7FZ, UK.

LIST OF PUBLICATIONS:

1: The Emerging Role of Epigenetics in Human Autoimmune Disorders. **Mazzone R.**, Artico M., Taurone S., Ralli M., Mai A., and Greco A. submitted to Clin Epigenetics, **2018**.

2: Development of Alkyl Glycerone Phosphate Synthase Inhibitors: Structure-Activity Relationship and Effects on Ether Lipids and Epithelial-Mesenchymal Transition in Cancer Cells. Stazi G., Battistelli C., Piano V., **Mazzone R.**, Marrocco B., Louie SM., Zwergel C., Antonini L., Patsilinakos A., Ragno R., Viviano M., Sbardella G., Ciogli A., Fabrizi G., Cirilli R., Strippoli R., Marchetti A., Tripodi M., Nomura D. K., Mattevi A., Mai A., and Valente S. Eur J Med Chem. **2018:** 163: 722-735.

3: Identification of novel quinazoline derivatives as potent antiplasmodial agents. Bouchut A., Rotili D., Pierrot C., Valente S., Lafitte S., Schultz J., Hoglund U., **Mazzone R.**, Lucidi A., Fabrizi G., Pechalrieu D., Arimondo PB., Skinner-Adams TS., Chua MJ., Andrews KT., Mai A., Khalife J., Eur J Med Chem. **2018**: 277-291. doi: 10.1016/j.ejmech.2018.10.041.

4: A Quinoline-Based DNA Methyltransferase Inhibitor as a Possible Adjuvant in Osteosarcoma Therapy. Manara MR., Valente S., Cristalli C., Nicoletti G., Landuzzi L., Zwergel C., **Mazzone R**., Stazi G., Arimondo P., Pasello M., Guerzoni C., Picci P., Nanni P., Lollini PL., Mai A., Scotlandi K., Mol Cancer Ther. **2018**: 1881-1892. doi:10.1158/1535-7163.MCT-17-0818.

5: Novel polyamine-based Histone deacetylases-Lysine demethylase 1 dual binding inhibitors. Milelli A, Marchetti C., Turrini E., Catanzaro E., **Mazzone R.**, Tomaselli D., Fimognari C., Tumiatti V., Minarini A., Bioorg Med Chem Lett. **2018**: 1001-1004. doi: 10.1016/j.bmcl.2018.02.034.

6: Epi-drugs in combination with immunotherapy: a new avenue to improve anticancer efficacy. **Mazzone R.**, Zwergel C., Mai A., and Valente S., Clin Epigenetics. **2017**: 9:59. doi.org/10.1186/s13148-017-0358-y.

Abbreviations

AceCSA: acetyl-CoA synthetase

AEBP2: adipocyte enhancer-binding protein 2

agRNAs: antigene RNAs

AMC: aminomethylcoumarin

ANTE2/3: adenine nucleotide transporters 2/3

BAT: brown adipose tissue

BCA: bicinchoninic acid

BDNF: brain-derived neurotrophic factor

BITIC: brain tumor initiating cells

bp: base pairs

cccDNA: closed circular DNA

CML: chronic myeloid leukemia

CREB: cyclic adenosine monophosphate response element-binding protein

CSP1: carbamoyl phosphate synthetase 1

CTCF: CCCTC-binding factor

CTCL: cutaneous T-cell lymphoma

*Ct*PRC2: *Chaetomium thermophilum* PRC2

CypD: cyclophilin D

DHP: 1,4-dihydropyridine

DLBCL: diffuse large B cell lymphoma

DNA-PK: DNA-dependent protein kinase

DNMT: DNA methyltransferase

DNMTi: DNMT inhibitors

Dot1: disruptor of telomeric silencing

DSBs: DNA double-strand breaks

EED: embryonic ectoderm development

EGFR: epidermal growth factor receptor

ELP3: elongation protein 3

EM: electronic microscopy

EMT: epithelial mesenchymal transition

EZH2: enhancer of Zeste homolog 2

FAST1: frataxin antisense transcript 1

FDA: food and drug administration

FRDA: Friedreich's ataxia

FXN: frataxin

GDH: glutamate dehydrogenase

GNAT: Gcn5-related N-acetyltransferases

GRag: glucocorticoid receptor agonist

HBV: hepatitis B virus

HDAC: histone deacetylase

HDACi: HDAC inhibitors

HDR: homologous recombination directed repair

HEK: human embryonic cells

HER2: human epidermal receptor 2

HLM: human liver microsomes

HMGCS2: hydroxymethylglutaryl-CoA-synthase 2

HMT: histone methyltransferase

HSC: hematopoietic stem cells

HsPRC2: human PRC2 complex

Hsts: *S. cerevisiae* homologs of Sir2

IDH2: isocitrate dehydrogenase 2

iNOS: inducible nitric oxide synthase

JARID2: jumonji and AT-rich interaction domain 2

JmjC: jumonji C

KDM: lysine demethylase

KIX: kinase inducible binding domain

KMT: lysine methyltransferase

L3MBTL1: Lethal 3 malignant brain tumor 1

LSD1: lysine demethylase

LXR: nuclear liver X receptor

MYB: myeloblastosis

MM: multiple myeloma

MnSOD: manganese superoxide dismutase

MORF: monocytic leukemia zinc-finger protein related factor

MOZ: monocytic leukemia zinc-finger protein

mPTP: mitochondrial permeability transition pore

NAD: nicotinamide adenine dinucleotide

NAM: nicotinamide

NATs: natural antisense transcripts

N-CoR: nuclear receptor co-repressor

NDA: nicotinamidase

NDCLC: non-small cell lung carcinoma

NES: nuclear export signal

ncRNAs: non-coding RNAs

NTCP: cotransporting polypeptide

NuRD: nucleosome remodeling and deacetylating

ORIs: origins of replication

PARP1: (ADPR) polymerase 1

PCAF: p300/CBP-associated factor

PRC1: polycomb repressive complex 1

PRC2: polycomb repressive complex 2

PR-DUB: polycomb repressive deubiquitinase

PTCL: peripheral T cell lymphoma

RbAp48: Rb-associated protein 48

RBBP4/7: retinoblastoma-binding protein 4 or 7

RF: reactivation fold

ROS: reactive oxygen species

SAHA: suberoyl hydroxamic acid

SAL: SET activation loop

SAM: S-adenosylmethionine

SAR: structure-activity relationship

SPA: scintillation proximity assay

Sir2: silent information regulator 2

SMRT thyroid hormone receptors

SUZ12: suppressor of Zeste 12

PEPCK1: phosphoenolpyruvate carboxykinase 1

PhoRC: pho-repressive complex

PRMT: arginine methyltransferase

PTMs: post-translational modifications

TAMRA: carboxytetramethylrhodamine

TCA: tricarboxylic acid

TTC: trinucleotide

Tip60: TAT interacting proteins 60

TKi: tyrosine kinase inhibitors

TSA: Trichostatin A

TSS: transcription start site

UOX: urate oxidase

VEGF: vascular endothelial growth factor

VLCAD: acyl-CoA dehydrogenase

WT: wild-type

ZBG: zing binding group

ZF: zinc finger

XIAP: X-linked inhibitor of apoptosis protein

Table of contents

“I can't explain chemistry. I really can't. I haven't got a clue what it's all about. It just happens. It's like falling in love. You can't explain why you fall in love or explain why it's this particular person.”

Elaine Stritch

1 INTRODUCTION

Chapter 1: Epigenetics

1. Epigenetics

The term “epigenetics” was originally described by the Britain Conrad Waddington (1905-1975) in 1940 as “the branch of biology which studies the casual interactions between genes and their products, which bring the phenotype into being”. [1] Over the time, the word epigenetics has changed into the definition of “*the study of heritable changes in gene expression that occur independently of changes in the primary DNA sequence*”. Thus, epigenetics can be considered as a link between genotype and phenotype: even though the majority of cells share an identical genotype in a multicellular organism, individual development produces a wide variety of cell types with different profiles of gene expression and distinct cellular functions. Epigenetics modulates the accessibility to the DNA by affecting the local regulation of the chromatin state, through several biochemical mechanisms that include histone post-translational modifications (PTMs), [2, 3] DNA methylation and hydroxymethylation, [4] replacement of canonical histones with histone variants, [5] ATP-dependent nucleosome remodeling, [6] and non-coding RNAs (ncRNAs). [7] A growing body of evidence has drawn the attention of the scientific community by indicating the potential vulnerability to environmental changes of epigenetic mechanisms that control gene expression. The correlation between cigarette smoking, alcohol consumption and dietary intake and genome-wide or loci-specific epigenetic changes have been intensely investigated over the past years. [8] However, the list of environmental factors capable of inducing epigenetic errors seems to be underestimated entirely and exposure to apparently inoffensive products such as hair dye should also be taken into consideration. [9] The association between environmental factors and disease risk has been investigated for a wide variety of disorders such as cancer, diabetes, obesity, heart disease, and a host of psychiatric disorders like mania, depression, and schizophrenia. [2, 10] Cancer was the first human disease linked to epigenetic alterations, and when in 1983 widespread loss of DNA methylation was observed for the first time in colorectal cancer, this was followed by an extraordinary increase in the number of studies investigating this association. [11] The epigenetic aberrations, unlike genetic mutations, are potentially reversible and can be restored to their normal state through the epigenetic therapy. Epigenetic mechanisms have emerged with increasing prominence as disease-related factors in the medical literature over the past decades.

1.1 The human genome

Chromatin is the state in which DNA is condensed within the cell. The nucleosome is the basic unit of chromatin, and it is composed of two copies each of the four core histones (H3, H4, H2A, H2B) with 147 base pairs (bp) of DNA wound around it. Positively charged residues in the histones contact the

phosphate backbone of the DNA every ~10.4 bp, providing 14 relatively weak histone DNA contacts. However, when added together, these contacts provide positional stability. The conserved domain of histone proteins, of about 70 amino acids, consists of three α-helix regions, named histone-fold, and is implicated in the formation of the two H3-H4 and H2A-H2B heterodimers through a head to tail interaction. The DNA between each nucleosome, termed DNA linker, is connected with the histone H1, which is bound to the outside of the nucleosome core particle, forming a full chromatosome, and stabilizing higher-order chromatin structures. Nucleosomes are found every 200 bp, and they form a characteristic 'beads on a string' structure with their coating DNA. Histones are predominantly globular proteins, except for their variable and unstructured N-terminal "tails". The tails are particularly rich in lysine and arginine residues making them extremely basic. This region is the site of numerous post-translational modifications that are proposed to modify its charge and thereby alter DNA accessibility and protein/protein interactions with the nucleosome. In general, nucleosomes impede transcription of the DNA by physical obstruction, as well as by bending the DNA, thus reducing its availability to transcription factors. However, an astonishing number of PTMs that occur on histones, including acetylation, methylation, phosphorylation, ubiquitinylation, sumoylation, ADP ribosylation, deamination and, more recently, propionylation and butyrylation, have been widely described (Fig. 1.1). [2, 12]

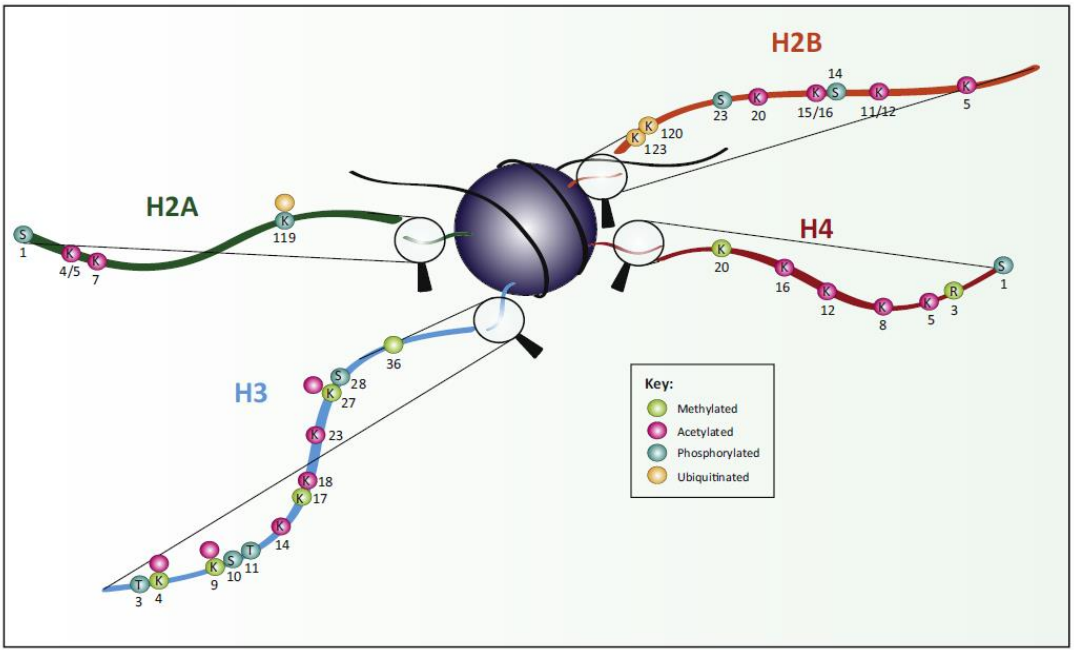

Figure 1.1: Post-translational modifications of the histone tails. [13]

Additionally, histone modifications usually recruit effector proteins to activate downstream signaling, block the access of remodeling complexes, or influence the recruitment of chromatin modifiers and transcription factors.

1.1.1 Epigenome: writing, reading and erasing

As aforementioned, the histone N-terminal portion is the target of several epigenetic modifications that lead to the alteration of the chromatin structure. In a cell, the histone modification patterns are regulated by different epigenetic players classified in writers, readers, and erasers according to their specific role in adding, recognizing and removing these chemical marks, respectively. Therefore, this "protein machinery" have a direct physical impact on the structure of chromatin (e.g., loss or gain of charges, resulting in a modified chromatin packaging and structure). The result is a broad array of epigenetic proteins considered as potential targets for drug discovery. In details, the erasers, such as histone deacetylases (HDACs) and histone demethylases, remove the PTMs and prepare the histones for other modifications. The writers include enzymes such as histone acetylases, kinases, DNA and histone methyltransferases (HMTs) and ubiquitin ligases. The writers catalyze the PMTs on the DNA or the proteins and may impose epigenetic heritability such as DNA methylation through copying and maintaining the modification. Other modifications, such as histone acetylation, react rapidly to environmental stimuli and are therefore more dynamic. Readers of PTMs include proteins with specific domains, such as bromo-, chromo-, tudor-, MBT-, PWWP-, WD40- and PHD-domains, which bind to the specific modification. Therefore, the readers, which are often found in large protein complexes, interpret the modification and place changes in chromatin structure. (Fig. 1.2)

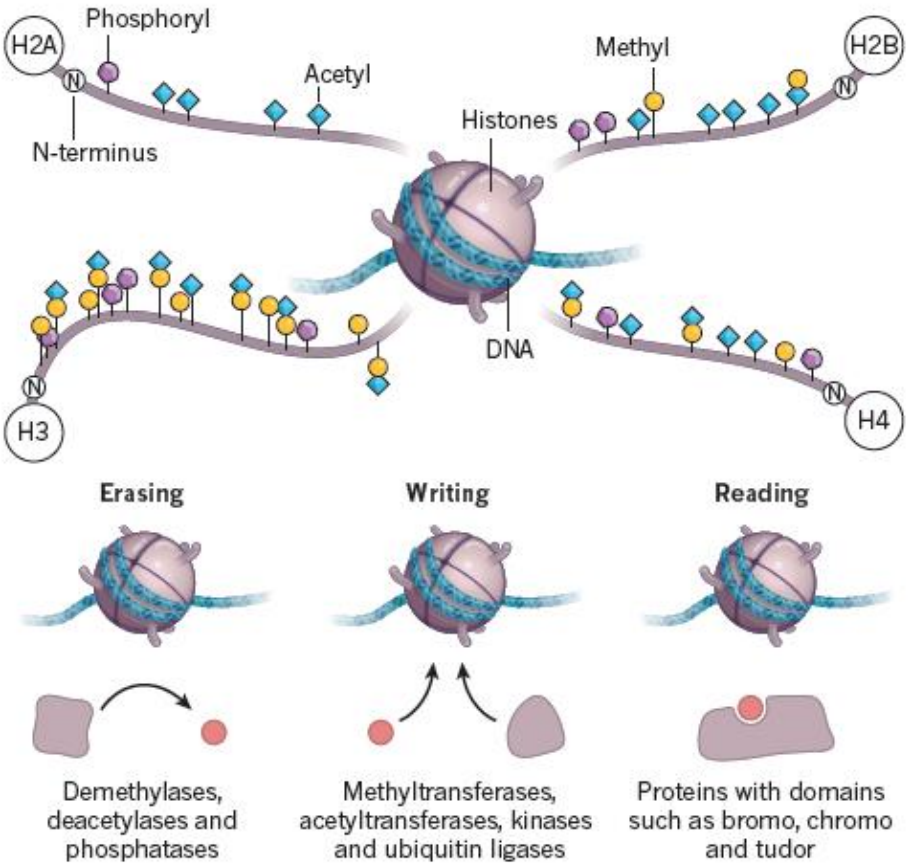

Figure 1.2: Writers, erasers and readers. [14]

Even though much has been explored so far, there is still a lot to disclose in order to give an exhaustive explanation of the epigenetic landscape.

1.1.2 Chromatin remodeling and histone posttranslational modifications

Chromatin remodeling refers to the dynamic and reversible modifications that occur on chromatin structure, allowing the access of compacted genomic DNA to the regulatory transcription machinery proteins, and thereby control gene expression. Such remodeling is mainly determined by:

1) Covalent histone modifications by specific enzymes (e.g., HATs, deacetylases, methyltransferases)
2) ATP-dependent chromatin remodeling complexes which either move, reject or restructure nucleosomes.

Therefore, histone-modifying enzymes that catalyze addition or removal of various chemical elements on histones are responsible to affect the binding affinity between histones and DNA, and thus loosening or tightening the condensed DNA wrapped around histones. For example, methylation of specific lysine residues in H3 and H4 causes further condensation of DNA around histones, thus leading to gene repression. On the contrary, histone acetylation induces the relaxing of chromatin increasing gene expression. As a result, chromatin exists in two different conformations: euchromatin and heterochromatin. The term euchromatin refers to its highly condensed state and transcriptional inactivation, while heterochromatin refers to relaxed and transcriptionally active chromatin (Fig. 1.3). [11]

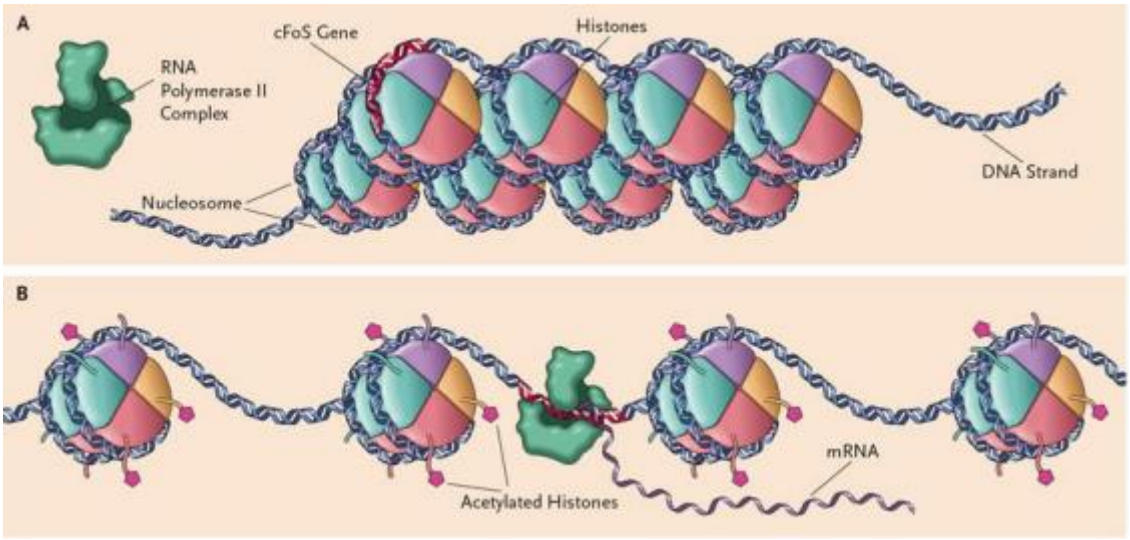

Figure 1.3: a) Heterochromatin (condensed chromatin) **b**) Euchromatin (relaxed chromatin).

By contrast, chromatin remodelers use ATP hydrolysis energy to change the packaging state of chromatin, working with other DNA elements to control chromosomal processes (enhancer, promoter, replication origins) (Fig. 1.4). [15] There are currently four different families of chromatin remodeling complexes: SWI/SNF, ISWI, CHD, and INO80. [16-18] All four use ATP hydrolysis to alter histone-DNA contacts and share a similar ATPase domain. However, all four are also specialized for specific purposes and biological contexts, imparted by unique domains living in their catalytic ATPases and also by their unique related subunits.

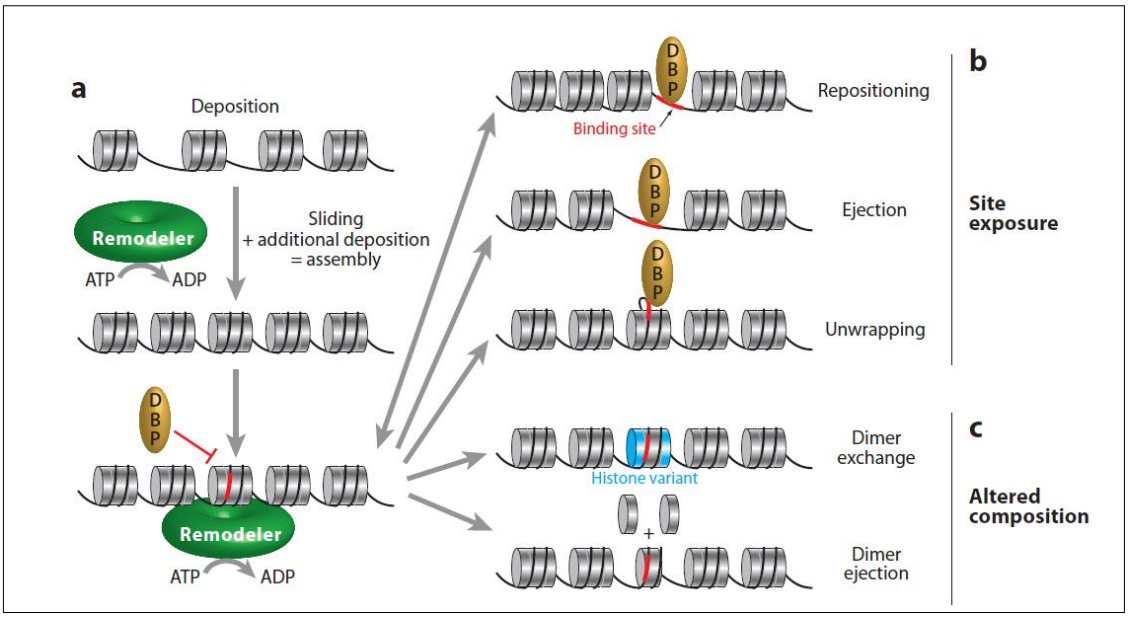

Figure 1.4: The different outcomes of chromatin remodeling. Remodelers (green) can assist in chromatin assembly by moving already deposited histone octamers, generating room for additional deposition (a). Remodeler action on a nucleosome array results in various products that can be classified in two categories: (b) site exposure, in which a site (red) for a DNA-binding protein (DBP), initially occluded by the histone octamer, becomes accessible by nucleosomal sliding (repositioning), or nucleosomal eviction (ejection), or localized unwrapping, and (c) altered composition, in which the nucleosome content is modified by dimer replacement [exchange of H2A-H2B dimer with an alternative dimer containing a histone variant (blue)] or through dimer ejection. [19]

1.2 Histone modifications

PTMs on histone proteins play crucial roles in the establishment of transcriptional states and consequently control cellular states. Since Vincent Allfrey's pioneering studies in the early 1960s, a large number of PTMs have been identified on histone proteins. [20] A great effort in understanding how these modifications may affect the chromatin structure come out with the discovery of the high-resolution X-ray crystal structure of nucleosome in 1997. [21] Since chromatin is ubiquitous, PTMs could influence many other DNA processes that include repair, replication, and recombination. Actually, the field of PTMs is growing with many new sites of modifications and their modifiers being identified. All these efforts are put together to gain a better understanding of how histone PTMs modulate chromatin function.

Histone tails constitute the 25-30% of the mass of each histone and are sensible to proteases, thus having a large surface to establish potential interactions with other proteins. H3 and H4 histone tails represent the ideal target for the previously mentioned PTMs and contribute to regulating the highly-ordered structure of chromatin. Indeed, H4 is able to interact with the next nucleosome's dimer H2A-H2B. [22, 23] It is commonly accepted that the multi-protein complexes of transcription factors can read and decipher the "histone code" thus activating or repressing gene transcription. Several enzymes have been reported in literature able to modify and determine changings in chromatin structure, allowing to better understand the epigenome, as a whole. Among them, the enzymes responsible for acetylation, as well as for methylation, phosphorylation, ubiquitination, sumoylation, ADP-ribosylation and proline isomerization have been described. [24, 25] Furthermore, since these modifications are reversible, enzymes capable of removing these modifications have been identified too. Additionally, the abundance of PTMs on histone tails, sometimes direct to the same/close sites or target different histone tails, can set a cross-talk between them. [26] However, their interplay is quite sophisticated to explain considering that an epigenetic mark can thus inhibit or induce the imposition of a second mark, or it can be read and activate secondary processes. In this regard, while acetylation, methylation, phosphorylation, and ubiquitination are generally involved in gene activation, methylation, ubiquitination, sumoylation and proline isomerization are also involved in gene silencing.

1.2.1 Histone methylation and demethylation

Histone methylation mainly occurs on the side chain of lysine (K) and arginine (R). Among them, lysine methylation is considered one of the most versatile chemical modifications. Indeed, lysine residues can be mono-methylated, di-methylated, or tri-methylated and second, methylation of different histone residues can be associated with either gene activation or silencing. On the other hand, arginine can be just (symmetrically or asymmetrically) mono- or di-methylated at its guanidine moiety by arginine methyltransferases (PRMTs), and its methylation levels are often associated with gene activation.

Lysine methylation is tightly regulated by histone lysine methyltransferases (KMT) and demethylases (KDMs). For many years, protein methylation was believed to be irreversible, stable and static. However, in 2004 after the discovery of the first demethylase (LSD1), [27] this process was considered as reversible and dynamic, involved in the regulation of a variety of processes. [28] Since methylation does not change the lysine charge or arginine residue, its effect on chromatin structure seems to be indirect. Remarkably, both classes of enzymes are often regulated by one or more chromatin binding domains that recognize distinct histone methylation marks. SUV39H1 targeting H3K9 was the first KMT identified. [29] Strikingly, all of HKMTs contain a so-called SET domain that accommodates the enzymatic activity, except Dot1 that does not possess a SET domain. In fact, Dot1 consists of only an evolutionarily conserved protein named Dot1 (disruptor of telomeric silencing; also called Kmt4) that methylates H3K79 within the histone globular core. In any case, all the KMTs catalyze the transfer of a methyl group

from S-adenosylmethionine (SAM) to a lysine ε-amino group. Extensive studies have been carried out to identify the histone methylation sites that include H3 lysine 9 (H3K9), H3K4, H3K27, H3K36, H3K79, and H4K20. Among them, common sites of methylation associated with gene activation are H3K4, H3K36, and H3K79. On the contrary, gene inactivation sites include H3K9 and H3K27. The most widely studied KMTs and KDMs are listed in table 1.1.

Histone lysine locus	Methyltransferase	Demethylase
H3K4	hMLL1 (KMT2A) hMLL2 (KMT2B) hMLL3 (KMT2C) hMLL4 (KMT2D) hMLL5 (KMT2E) hET1A (KMT2F) hSET1B (KMT2G) ASH1 (KMT2H) SMYD1 (KMT3D) SMYD2 (KMT3C) SMYD3 (KMT3E) Sc/Sp SET1 SET7/9 (KMT7)	LSD1(KDM1A) LSD2 (KDM1B) JHDM1A (KDM2A) JHDM1B (KDM2B) JARID1A (KDM5A) JARID1B (KDM5B) JARID1C (KDM5C) JARID1D (KDM5D) NO66
H3K9	SUV39H1 (KMT1A) SUV39H2 (KMT1B) G9a (KMT1C) GLP (KMT1D) SETDB1 (KMT1E) SETDB2 (KMT1F) RIZ1 (KMT8) CLL8 SpClr4	LSD1 (KDM1A) JHDM2A (KDM3A) JHDM2B (KDM3B) JHDM3A (KDM4A) JMJD2B (KDM4B) JMJD2C (KDM4C) JMJD2D (KDM4D) JHDM1D (KDM7) PHF8
H3K27	EZH2 (KMT6)	UTX (KDM6A) JMJD3 (KDM6B)
H3K36	Sc/Sp SET2 (KMT3A) SET3 NSD1 (KMT3B) NSD2	JHDM1A (KDM2A) JHDM1B (KDM2B) FBXL10 JMJD2A (KDM4A)

	NSD3 SMYD2 (KMT3C) METNASE(SETMAR)	JMJD2B (KDM4B) JMJD2C (KDM4C) JMJD5(KDM8)
H3K79	Sc/Sp DOT1 h DOT1L (KMT4)	Not described
H4K20	h MMSET Pr-SET7/8 (KMT5A) SpSet 9 SUV420H1(KMT5B) SUV420H2 (KMT5C) NSD1(KMT3B)	PHF8(KDM7B)

Table 1.1: The methyltransferases and demethylase for histone H3 and H4.

Histone lysine methylation is known to be implicated in several fundamental cellular processes including transcription, cell identity and genome stability. Aberration in histone lysine methylation-controlled regulatory cues is generally observed in cancer. [30] Two families of lysine demethylases have been identified so far: the amine oxidases and jumonji C (JmjC)-domain-containing, iron-dependent dioxygenases. These enzymes are highly conserved from yeast to humans and demethylate histone and non-histone substrates. Instead, arginine demethylases still remain more elusive.

1.2.1.1 Insights into the role of H4K20 methylation status

As previously mentioned, HMTs can act as either repressive or active marks. For histone lysine methylation, modification of H3K4, H3K36, and of H3K79 have been associated with transcriptional activation, whereas methylation of H3K9, H3K27, and H4K20 are marks of repressive chromatin states. [31, 32] However, different methylation states obtained by a combination of various methylation marks could help the recognition of distinct chromatin regions or the total chromosomes. [33] In this regard, a controlled interplay between different histone lysine methylation systems is required by the combinatorial nature of HMTs. [34] Therefore, loss of a given HMTase may also influence the methylation on lysine residues for which the enzyme has no intrinsic activity. [35]

H4K20 is an essential repressive chromatin domain conserved among eukaryotes, such as *Schizosaccharomyces pombe*, *Caenorhabditis elegans*, *Drosophila*, and mammals, but is not present in *Saccharomyces cerevisiae.* It was one of the first PTMs to be discovered even if only recently the catalyzing enzymes have been identified. (5-7) In mammalian cells, most of histone H4 methylation is present in the N terminal tail of Lys20. In 2004, Schotta and co-workers studied all three H4K20 methylation states in mammalian chromatin using high selective antibodies by UBI for discriminating

each H4K20 methylation level. In details, they demonstrated for the first time that H4K20me3 is a novel and evolutionarily conserved domain of pericentric heterochromatin. [36] Due to the strikingly similar enrichment of H4K20 and H3K9 trimethylation at pericentric heterochromatin, they analysed H4K20me3 accumulation both in wild-type and *Suv39h dn MEFs* mitotic spreads. They showed a loss of pericentric H4K20 trimethylation only in mitotic spreads from suv39h, whereas the chromosomal arms display enriched signals. These data confirm the crucial role of Suv39h enzymes in directing H4K20 trimethylation.

Furthermore, each methylation state results in distinct biology: mono- (H4K20me1) and dimethylated H4K20 (H4K20me2) are involved in DNA replication and DNA damage repair, whereas trimethylated H4K20 (H4K20me3) is a hallmark of silenced heterochromatic regions. [14, 37] In mammals, the different H4K20 methylation states are established through specific enzymes. There is only one well-known mono-methylating enzyme, SETD8/PR-SET7 [38, 39], whereas the majority of di- and tri-methylation is catalyzed by Suv420h1 and Suv420h2, two highly homologous methyltransferases with a unique N-terminal domain and Zn-binding post-SET domain. [36] In proliferating cells, the most abundant methylation state was H4K20me2, which was found on ~80% all histone H4 molecules (10,9). In mouse embryonic fibroblast cells, Suv420h1 induces preferentially H4K20me2, whereas Suv420h2 is mainly implicated in H4K20me3. In *in vitro* HMT assays, both enzymes require the mono-methylated state as substrate, and also Suv420h enzymes can convert SET8-mediated H4K20me1 to H4K20me2 and me3 in vivo. [40] Although the establishment of different methylation states is not fully clear to date, Jorgensen *et al.* tried to propose a model, shown in fig. 1.5. [41]

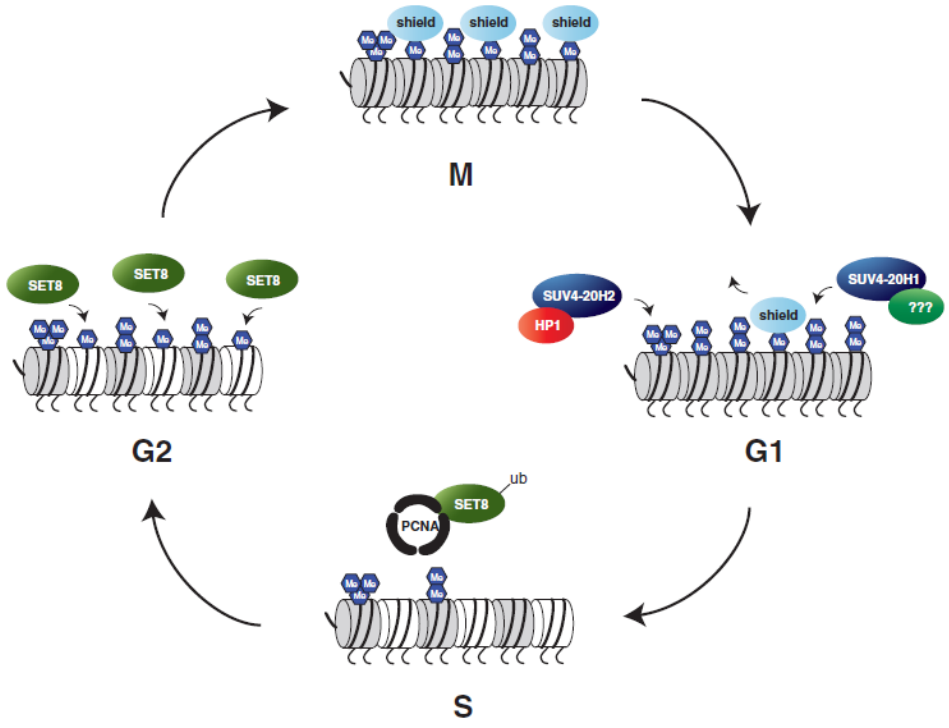

Figure 1.5: Cell cycle regulates the establishment of the different H4K20 methylation states. [41]

In more detail, they found that resting cells in G1 or G0 phase exhibit high levels of H4K20me3 at heterochromatic regions and carry H4K20me2 throughout the genome. In the S phase, very little H4K20me1 is added and towards the end of G1, and in G2, SETD8 establishes H4K20me1. During mitosis, the high level of H4K20me1 is stable and protected from conversion into H4K20me2 or me3. Directly after mitosis, in early G1, mostly H4k20me1 is then converted to H4K20me2 and me3 by Suv420h enzymes.

1.2.1.2 Novel heterochromatic SET domains: Suv420h1 and Suv420h2

As aforementioned, in 2004, Schotta *et al.* identified two novel SET domain proteins able to catalyze the trimethylation of H4K20. [36] The reason to investigate whether Suv39h might possess an intrinsic activity raised from the observation that Suv39h is required for pericentric H4K20 trimethylation. In previous reports, Suv39h enzymes were shown to target only H3K9 position, with a weak activity toward histone H1. [35] By comparing all SET domains that are shared among mouse, *Drosophila* and *S. Pombe*, 12 candidate proteins cDNAs tested were selected. Among them, Cgi-85 (Suv420h1) and Mgc2705 (Suv420h2) were identified as H4K20-specific HMTases. Cgi-85 (876 amino acids) and Mgc2705 (468 amino acids) are two closely related proteins present in mammals. Therefore, they classified these two homologs proteins as novel Su(var) genes, renaming it Suv420h1 and Suv420h2, respectively. Additionally, a small region in the C termini that is shared between the various Suv420h proteins has been detected, as well (Fig. 1.6).

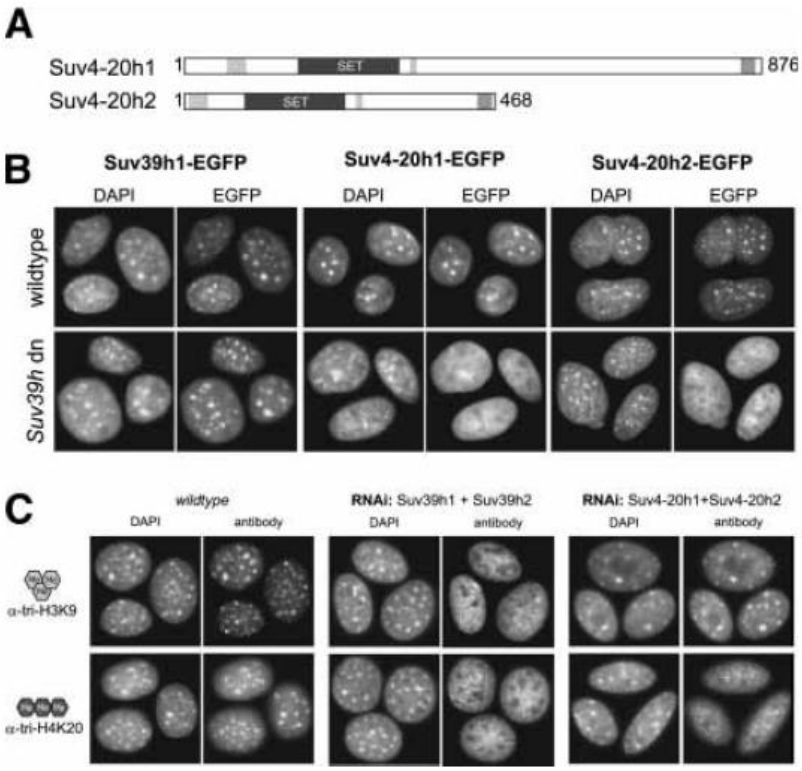

Figure 1.6: Identification of Suv4-20h1 and Suv4-20h2 as heterochromatic H4-K20 trimethylating HMTases. (*A*) Protein structure of Suv4-20h proteins. The SET domain is located in the N terminus and flanked by N- as well as C-terminal extensions of high sequence homology within Suv4-20h orthologous proteins. In addition, there is a conserved region in the C terminus of these proteins. (*B*) EGFP-tagged Suv39h1, Suv4-20h1, and Suv4- 20h2 were expressed in wild-type and *Suv39h* double-null (dn) female MEFs. After fixation, distribution of EGFP-tagged proteins was analyzed by fluorescence microscopy. DAPI dense foci represent pericentric heterochromatin. (*C*) RNAi mediated knock-down of Suv39h and Suv4-20h proteins. Female wildtype MEFs were cotransfected with pEGFP-N1 as transfection marker and pSUPER vector expressing hairpin oligos directed against Suv39h1/Suv39h2 or Suv4-20h1/Suv4-20h2. After 5 d in selection medium, cells were stained with α-trimethyl H3-K9 and α-trimethyl H4-K20 antibodies. Immunostaining was examined in EGFP-positive cells. [36]

Next, the same authors, investigated the activity and substrate specificity of Suv420h, suggesting that both enzymes are nucleosomal HMTases with a preferential activity toward H4K20 trimethylation. [39, 42] This is in contrast with Suv39h function, which prefers an H3K9 mono-methylated position. [35] Additionally, even though H3K9 trimethylation is not necessary for Suv420h activity *in vitro*, cross-talk interactions between nucleosomal H3K9 and H4K20 may exist *in vivo*, thus affecting the enzymatic activity of Suv420h. Finally, an evolutionary conservation of the evident silencing pathway between H3K9 and H4K20 methylation is confirmed by the presence of H4K20 trimethylation from *S. pombe* to mammals.

1.2.1.3 Suv420h1 and Suv420h2 crystal structures

After the isolation and characterization of the two Suv420 family members (also known as Set9/KMT5) of histone H4K20 methyltransferases by Jenuwein's lab in 2004, [36] Tsang *et al.* revealed differences and cellular localization of Suv420h1 (KMT5b)and Suv420h2 (KMT5c) by comparative analysis of their isoforms. [43] Interestingly, Suv420h1 presents two alternatively spliced isoforms that share N-terminal SET-domain including catalytic domain which function substantially depends from the chromatin localization. Suv420h1 and Suv420h2 preferentially dimethylated H4K20 and are responsible for about 80 and 90% of total histone H4 methylation in HeLa and S2 cells, respectively. However, both proteins can trimethylate specific sites in chromatin, and also in mammalian tissues, H4K20me3 has been linked with aging. [43-45] With the aim to assess the enzymatic activity of these two H4K20 methyltransferases quantitatively, Wu and co-workers proposed the first crystal structures, cloning and purifying the catalytic domain of both Suv420h1 (residues 63-335) and Suv420h2 (residues 2-248). Through high-resolution crystallography and radioactivity-based assay, they determined the human Suv420h1 and Suv20h2 structures in complex with the cofactor SAM and their substrate specificity, respectively [46] Considering that the catalytic domains of Suv420h1 Suv420h2 share 65% sequence identity, it is not surprising that their structures are also highly conserved.

In details, the overall structures of the catalytic domain of Suv420h1 and Suv420h2 proteins comprise three subdomains: an N terminal helical domain, a SET domain, and a Zn-binding post-SET domain. It has been observed that Suv420h1 has a bigger N-terminal helical domain than its homologous Suv420h2 as

shown by a 22-residue insertion between the first and second helices. Unfortunately, due to crystallographic disorder, these differences were not highlighted. Additionally, despite their similarity in the N-terminal domain, the SET domains of Suv420h1 and Suv420h2 share low sequence identity but highly conserved structure. The SET domain hosts the active site, and both the SET and post-SET domains are involved in substrate and cofactor binding. [47] The effort to realize the crystals of Suv420h1 and Suv420h2 in complex with a substrate was unsuccessful, so they tried to superimpose such crystal structures with the complex structure of the GLP-H3K9me2 peptide. They showed that likewise GLP, both Suv420h enzymes harbor an aromatic pocket which probably accommodate the target Lys20 of histone H4. In fig. 1.7, the main active sites residues have been shown.

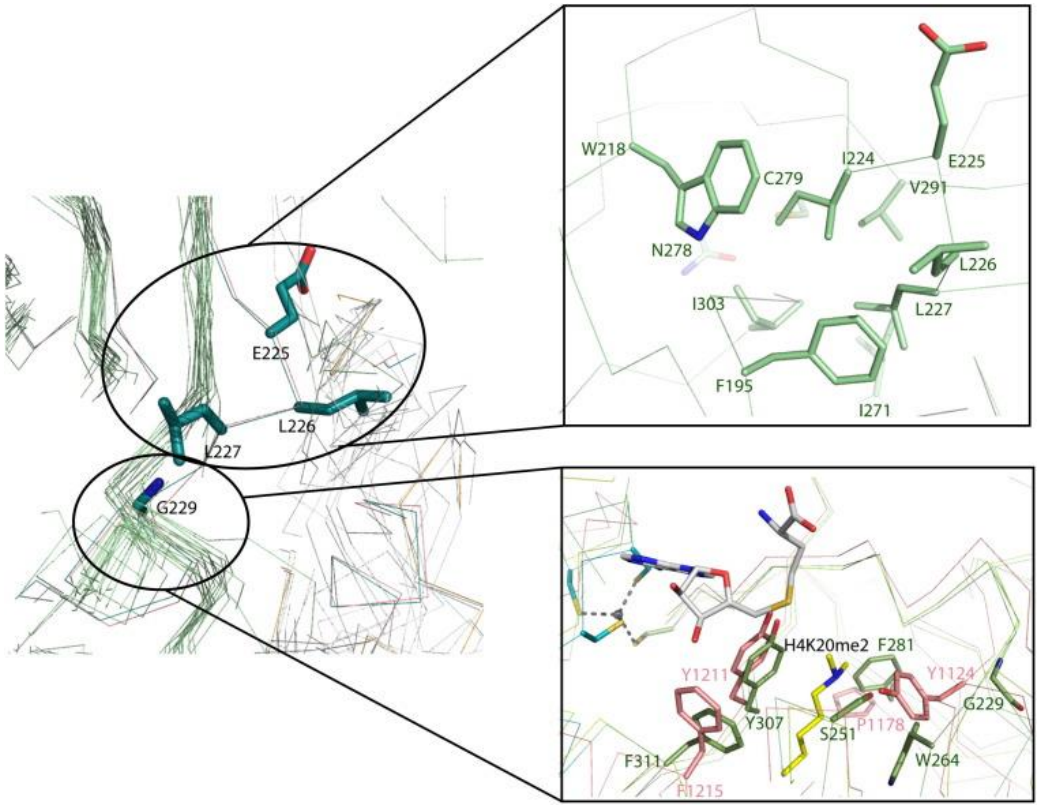

Figure 1.7: Active site of SUV420H1. SUV420H1 and SUV420H2 have a unique structural bulge near the active site. A close-up view of the bulge is shown in the top right panel. Like other SET domain proteins, SUV420H1 and SUV420H2 also have an aromatic pocket, which presumably would accommodate the target lysine K20 of H4. Comparison of the active site of SUV420H1 (green) and GLP (pink, PDB 2RFI) is shown in the bottom right panel. The di-methyl lysine from mouse SUV420H2 structure (PDB 4AU7) is colored in yellow. [46]

Lastly, no histone H4K20 activity was detected, presumably due to a conserved serine residue that attenuates the methylation level forming a hydrogen bond with the target lysine side-chain.

1.3 The potential role of histone H4 in the maintenance of genomic integrity

The first evidence between H4 HMTs and genomic maintenance derived from a study where these enzymes were removed by siRNA in both human cell lines and animal models. [48, 49] RNA interference of SET8 determines severe consequences for the cells, showing a DNA double-strand breaks (DSBs), defective cell cycle progression, reduced cell proliferation and activation of DNA damage checkpoint. [50-52]. Therefore, SET8 plays a pivotal role in cellular homeostasis due to massive DSBs and checkpoint activation after depletion of SET8. [53] Two important studies, supporting the importance of H4 HMTs in genomic stability, have been carried out. In the first one, double knock out of Suv420h show lethality in mice, even though the exact cause of death is unclear. Some hypothesis suggests that the underdevelopment of the lung might be a contributing factor. [54] The other study shows that MEFs lacking Suv420h enzymes displayed low growth rates and early onset of senescence. [54] However, the genomic maintenance by H4 HMTs appears to be multifaceted. In fact, animals genetically modified show different phenotypic outcomes. One important key process in genomic maintenance is the modulation of chromatin both in mitosis and during interphase. Cellular studies suggest that increased of H4K20me3 on specific histone gene promoters is correlated with decreased chromatin compaction in interphase cells on ectopic expression of SET8. [55] By contrast, other authors demonstrated that ectopic expression of SET8 induces a more compact chromatin in interphase cells. [56, 57]. Nevertheless, these differences are currently unexplained, the duration of experiments as well as the degree of SET8 overexpression might be a reasonable justification. Taken together, these very controversial results indicated, however, a pivotal role of SET8 in the regulation of chromatin structure. [48, 50] Indeed, Jørgensen *et al.* supposed that such a role most likely involved H4K20me1, as the compaction is SET8 activity-dependent. [41] Various chromatin compaction factors have been identified, such as Lethal 3 malignant brain tumor 1 (L3MBTL1) in interphase [58], as well as CAP-D3 and CAP-G2, two members of the mitotically operating condensin II complex. [56, 59] Similar to SET8 depletion, phenotypic alterations of L3MBTL1, a candidate tumor suppressor, affected replication and genomic instability. [60] In *in vitro* nucleosomal array studies, Lu *et al.* showed that H4K20me2 and me3 improved chromatin folding. [61] Many other findings support the crucial role of histone H4 in chromatin modulation and its importance in tight regulation. [55-57, 62]

Recently, H4K20 methylating enzymes are also emerging as important regulators of DNA replication. Indeed, seems that H4K20me2 and me3 play central roles in recruitment of Orc complex to the replication origins, thus implicating both SET8 and Suv420h enzymes. [55, 63, 64] Depletion of SET8 methyltransferase activity impairs DNA replication, leading to massive DNA damage and genomic instability. [53] While SET8 is implicated in a more general regulation of chromatin structure around the origins of replication (ORIs), the di- and tri- methylation of H4K20, catalyzed by Suv420h, is directly involved in Orc recruitment. [41] However, it is not fully understood why depletion of SET8 or Suv420h

enzymes causes impairment in DNA replication. Thereby, more coherent studies are needed to resolve this, especially investigating the three methylation states of H4K20.

1.3.1 Suv420h1 and Suv420h2 control DNA repair pathway choice

The main pathways for the repair of DSBs include non-homologous end-joining (NHEJ) and homologous recombination directed repair (HDR). [65, 66] These act mutually exclusive and are activated by 53BPI and BRCA1, respectively. It has become evident that the DNA pathway choice depends on inhibition of DNA end-resection by 53BPI, including its downstream factors RIF1 and MAD2L2. To date, it is not clear how MAD2L2 accumulates at DSBs to take part in DNA repair process regulation and how the NHEJ and HDR repair pathways are properly activated at DSBs with regard to the replication status of DNA. Indeed, NHEJ and HDR operate on DSBs in pre-replicative and post-replicative DNA, respectively. Very recently, Simonetta and co-workers showed that MAD2L2 is recruited to DSBs in H4K20 dimethylated chromatin by forming a protein complex with 53BP1 and RIF1. [67] Likewise to these factors, MAD2L2 was found to arrest DSB accumulation of BRCA1 and, in non-replicated DNA, H4K20me2 led to robust 53BP1-RIF1-MAD2L2 recruitment at DSBs, with the concomitant exclusion of BRCA1. By contrast, in replicated DNA, H4K20me2 promotes the release of such complex, thus allowing the access of BRCA1. Therefore, the differential H4K20 methylation status can be considered an intrinsic mechanism that locally favors the correct recruitment of the 53BP1-RIF1-MAD2L2 complex at DNA DSBs, to engage the right DNA repair pathway.

Specifically, after DNA damage, H4K20me2 recruits 53BPI and other DNA damage proteins, such as gH2A.X, MDC1, and BRCA1, at DSBs sites. [68-70] 53BP1 has a lower affinity for H4K20me1 and, therefore, in Suv420h DKO cells, which have a largely mono-methylated genome, 53BP1 binding to damage sites is less stable, which might explain the delayed repair foci formation. 53BP1 can therefore not efficiently prevent end resection or inhibit HR repair, leading to elevated HR in Suv420h mutant cells. [71]

Recent reports have also identified an important role for H4K20 methylation as an epigenetic mark allowing the recognition of the DNA replication state to recruit the correct DNA repair pathway. [72] First of all, Pellegrino *et al.* reported that replication-associated dilution of H4K20me2 directs the 53BP1-driven repair pathway to pre-replicative chromatin, according to the data presented by Simonetta *et al.* [73] In addition, other recent work showed that direct binding of the TONSL ankyrin repeat domain (ARD) to newly synthesized H4K20me0 histones allowed the recruitment of the TONSL-MMS22L homologous recombination complex to replicated DNA. [74] Despite that BRCA1-dependent ubiquitination is necessary for the removal of 53BP1, even though the exact mechanism of 53BP1 release is unclear. [75]

H4K20me2, together with H3K79me2, is correlated with proper replication licensing. [63, 76] Both H4K20me2 and H3K79me2 are strongly linked to chromatin compaction and are re-established in late G2 instead of in G1. [41, 77] The reason why this happens is maybe due to the fact that both histone

modifications prepare the ground for chromatin condensation in the next phase of the cell cycle, i.e., prophase of mitosis. HDR steps are not feasible on compacted chromatin, so the reactivation of NHEJ at the end of G2 might be a necessity, which improves with the re-establishment of H4K20me2. In addition to H4K20 methylation, H3K9 and H3K27 methylation have also recently been shown to play key roles in the DNA damage response. An in-depth investigation on how the combinatorial modification of these marks and others coordinately contribute to DNA repair will be a tremendous molecular challenge.

1.4 Polycomb repressive complex 2 (PRC2)

Polycomb group (PcG) proteins are transcriptional repressors and the genes encoding many of these proteins were initially characterized in *Drosophila* as key regulators of epigenetic silencing of homeotic genes. [78, 79] Subsequent studies showed that PcG proteins function in the context of large heterochromatic repressive complexes that include Polycomb repressive complex 1 and 2 (PRC1 and PRC2) as well as the more recently discovered Pho-Repressive Complex (PhoRC) and Polycomb Repressive Deubiquitinase (PR-DUB). [80, 81] PRC1 monoubiquitinates Lys119 in histone H2A (H2AK119ub1) and compacts chromatin by binding to nucleosomes, whereas PRC2 methylates lysine 27 in histone H3 (H3K27me3) and regulates cellular differentiation and development. [82, 83] PRC2-mediated histone methylation plays an important role in aberrant gene silencing, and its overexpression and mutations have been found in many types of cancers. Although inhibition of PRC2 has been reported as a promising strategy to fight cancer, significant changes in PRC2 activity by its inhibitors and their mode of interaction has to be carefully considered.

1.4.1 Components of PRC2

The human PRC2 complex is conserved across all multicellular organisms and comprises four core components: enhancer of Zeste homolog 2 (EZH2), embryonic ectoderm development (EED), suppressor of Zeste 12 (SUZ12) and RbAp48. [84-86] To all these subunits that contribute to its biological function and constitute the minimal core complex, additional subunits, including Retinoblastoma-Binding Protein 4 or 7 (RBBP4/7, also known as RBAP48/46), Adipocyte Enhancer-Binding Protein 2 (AEBP2), Jumonji and AT-Rich Interaction Domain 2 (JARID2), and Polycomb-like proteins to form holo-PRC2 complexes, have been identified (Fig. 1.8). [87, 88] The majority of these non-core subunits display intrinsic or DNA binding activity recruiting PRC2 to chromatin and promoting H3K27 methylation. [89]

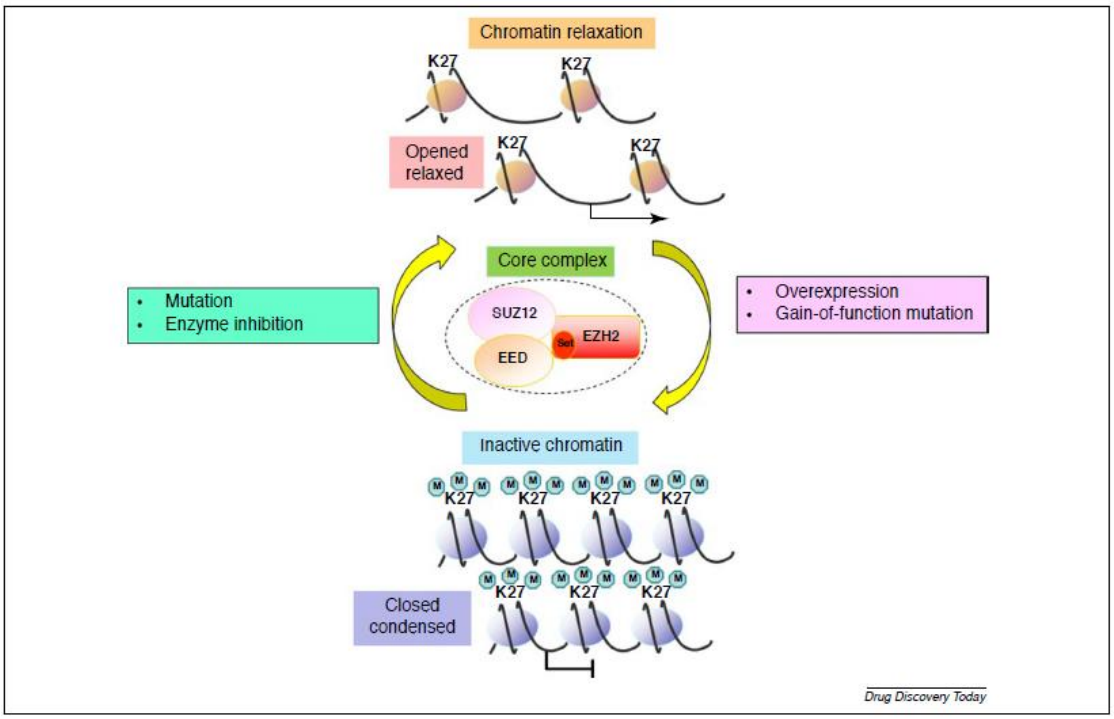

Figure 1.8: PRC2 complex and its function. [90]

Since its discovery, there has been a growing interest in understanding the PRC2 complex architecture in order to better elucidate its function. In 2012, Ciferri *et al.* reported the first crystal structure of the PRC2 complex determined by low-resolution electron microscopy (EM) and subsequent biochemical studies have provided a wealth of information regarding PRC2 subunits assembly, catalysis and allosteric regulation. [91-93]

1.4.1.1 EZH2

As aforementioned, the lysine methyltransferases EZH1 or EZH2 represent the catalytic subunit of the PRC2 complex. They conserve the catalytic SET domain found in many other KMTs using SAM as a co-substrate. EZH1 and EZH2 display a high sequence similarity, with 76 % overall identity and 96 % sequence identity in their catalytic SET domains but they possess different catalytic efficiencies, distinct chromatin binding properties, and expression patterns. EZH1 is expressed both in dividing and non-proliferative differentiated/adult cells, while EZH2 is only active in dividing cells. [78] Besides that, EZH1 typically have lower enzymatic activity than those containing EZH2 and the activity of EZH1/2 depends on interaction with both Suz12 and the WD40 domain in EED-binding domain (EED). Several pieces of evidence suggest that PRC2-EZH2 should establish cellular mono- di- and tri- H3K27me levels, while PRC2-EZH1 is involved in restoring H3K27me1/2/3, probably lost it upon histone exchange or through demethylase activity. [94]

Overexpression of EZH2 has been found mostly in metastatic prostate and breast cancer and has been associated with breast malignancy aggressiveness. [95] The ~750 amino acid EZH2 is characterized by various N terminus region domains such as EED, SANT1 and SET activation loop (SAL) that contains an

extended structural scaffold that allows the interaction with EED and SUZ12, thus maintaining certain conformation changes in the SET domain. [95] However, the catalytic activity of PRC2 depends by the C terminus SET domain of EZH2, which did not exhibit any interaction with EED. [96, 97] Furthermore, structural studies suggest that amino acids 39-68 are involved in the interaction with EED, and this region was the EBD. It has been reported that conformational changes in pre-SET and post-SET domains are important for the binding and the catalysis activity of EED and SUZ12. [98] Among SET domains of KMTs, amino acids G643 and G681 behave as "swing" to improve the flexibility of I-SET domain, leading it to shift between its different conformational states, which distance were found to be 1.6 A. Another interesting domain involved in the interaction with EED is AA40-60, an α-helical domain that could be a potential target for the development of hydrocarbostapled derivatives to disrupt the specific protein interactions. [99]

1.4.1.2 EED

EED is formed by seven WD-40 repeats at its C terminus domain followed by an N-terminal domain. WD-40 is a structural motif of ~40 residues able to recognize various group of ligands such as proteins. [100] Margueron *et al.* have demonstrated that EED interacting with trimethyl-lysine residues on histone tails connected with repressive chromatin marks leads to allosteric activation of PRC2 activity. [101] Thus, mutations of EED prevents the activation of PRC2. Moreover, binding analysis showed that EED binds to H1K26me3, H3K27me3, H3K9me3 and H4K20me3 peptides with dissociation constant Kd of 10–45 mM. [101] Numerous other studies have been carried out to identify which are the main interactions involved in stabilizing the EED-H3K27me peptide complex. [102-104] Additionally, it has been reported by Xu *et al.* that WD-40 domains of EED created a histone methyl-lysine binding motifs that preferentially recognizes the ARKS-motif-containing trimethylated H3K27, H3K9, and H1K26 peptides. [105]

1.4.1.3 SUZ12

As EED, SUZ12 was also described to play an essential part in the PRC2 complex due to its HMTase enzymatic activity. Indeed, this protein is characterized by two conserved evolutionary domains: C terminal VEFS and a zinc finger domain. [106] In PRC2 complex from the yeast *Chaetomium thermophilum* and human, VESF domain in SUZ12 was found to interact with EED and SET regions in EZH2. [107] The importance of the VESF domain lies on its function to preserve the PRC2 assembly formation and to order the activation loop of EZH2, confirmed by mutation studies. [93, 108, 109] For example, mutation of Y231 and Y232 of EED reduces the hydrophobic interaction with amino acid W584 of VESF domain, leading a decrease of *Drosophila* PRC2 activity. [107] Currently, no inhibitors for SUV12 have yet been identified even if this protein may be a crucial target for the development of novel PRC2-based inhibitors.

1.5 PRC2 crystal structure

In 2015, Jiao and Liu determined the first crystal structure of an active PRC2 complex (170 kDa) from the yeast *Chaetomium thermophilum* (*Ct*PRC2), thus offering new insights into its atomic level structure, catalytic mechanism, and allosteric regulation. [92] In this study, they compared two structures of *Ct*PRC2, in both basal and stimulated state, observing the presence of a flexible EZH2 motif being allosterically modulated and regulating the access to the active site. [92] Very recently, Justin *et al.* showed the crystal structure of the human PRC2 complex (HsPRC2) in its stimulated state, composed by EZH2 and EED polypeptides, the VEFS domain with a SAH cofactor, and the two peptides JARID2-K116me3 peptide, and H3K27M peptide (Fig. 1.9**A**). [95, 110] Such complex is organized to form a trilobated tri-dimensional structure, in which two lobes are involved in regulation, whereas the third in catalysis. EED and the N-terminal region of EZH2 are members of the so-called N-lobe. The middle lobe comprises SUZ12 VEFS and the EZH2 domains MCSS and SANT2. Lastly, the pre-SET and SET domains of EZH2, and the N-terminus of the VEFS domain form the catalytic lobe. Nevertheless, the two crystal structures have evident differences, a superimposition of the CtPRC2 and HsPRC2 revealed an interesting evolutionary conservation of the core complex (Fig. 1.9**B**). In addition, the comparison of the structures of the isolated SET domain and the HsPRC2 (Fig. 1.9**C**) reveals key interactions for the allosteric activation of the SET domain. Most importantly, in the isolated SET domain, difference lies in the cSET motif organization where this motif has been found mostly disordered. In fact, partially occupying the substrate binding pocket, it contributes to the auto-inhibited state. By contrast, in HsPRC2 the cSET motif flipped out of the substrate cleft, is available for catalysis. Further information about the HsPRC2 crystal structure, as well as a proper explanation of the oncogenic inhibition of H3K27M, and of the improvement of the catalytic efficiency derived by binding of repressive marks, such as H3K27me3, to the EED subunit are also reported in these papers. [95, 110]

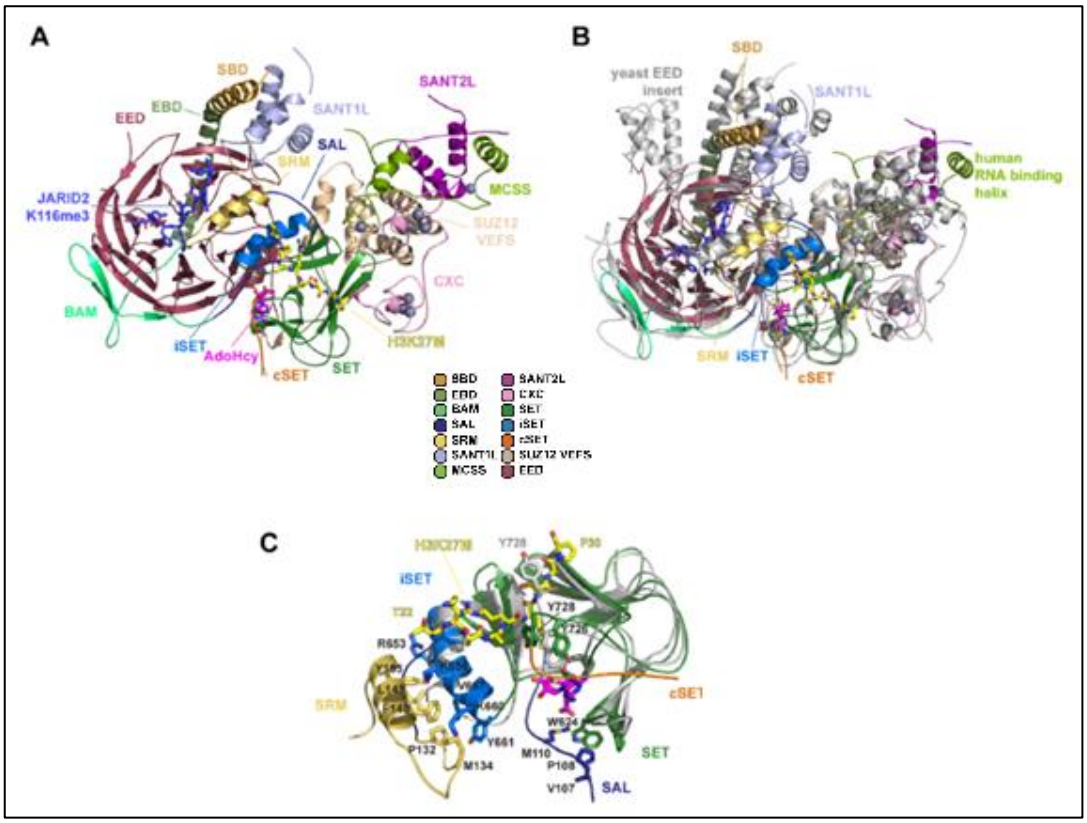

Figure 1.9: Structure and regulation of the HsPRC2 core complex. **A.** HsPRC2 in complex with JARID2K116me3 and H3K27M peptides and SAH (PDB: 5HYN). Proteins, domains, and motifs colour code are included. Peptides and SAH are rendered as sticks, and Zn ions are depicted as spheres. **B.** Superimposition of the stimulated CtPRC2 complex (grey) and the stimulated human PRC2 complex (PDB codes 5KJH and 5HYN). **C.** Structural alignment of the isolated SET domain of EZH2 (grey) and the SAL, SRM, iSET, cSET, and SET domains of EZH2 in the HsPRC2 stimulated complex (PDB codes 4MI0 and 5HYN). [97]

1.6 EZH2 function in cancer

The importance and druggability of EZH2 in cancer biology have been widespread documented. [99, 111, 112] Many studies suggest that EZH2 is required for cancer cell proliferation, migration, invasion, and epithelial-mesenchymal transition (EMT), all of which are linked with cancer initiation, progression, and metastasis. Interestingly, EZH2 is strongly associated with stem cell properties and tumor-initiating cell function. [113-115] Additionally, cancer-related oncogenic signaling pathways are strictly associated with EZH2 transcription, thus EZH2 expression is certainly a clinical biomarker for disease progression and cancer development. [99]

Somatic mutations in the *EZH2* gene have been identified in diffuse large B-cell lymphoma and follicular lymphoma. Indeed, changes of the amino acid tyrosine 641 (Y641) in EZH2 affect its enzyme activity. [116] These mutations were originally associated with a loss-of-function mutation because it reduces the enzymatic activity of EZH2 toward an unmodified substrate. However, Y641 mutant *EZH2* actually has higher activity of mono- to di- and di- to tri-methylation than wild type *EZH2.* [117] Moreover, in diffuse large B-cell lymphoma and follicular lymphoma with *EZH2* mutation, both wild-type and Y641 mutant *EZH2* showed an increase of H3K27me3 in mutant cancer cells than wild-type cells. [117] Thus, the *EZH2* Y641 mutation results as unique gain-of-function mutation. Further validation of the oncogenic

role of the Y641 mutation arises from an engineered mouse model study in which conditional expression of mutant *EZH2* in germinal center B-cells produced germinal center hyperplasia and enhanced lymphoma formation in the presence of Bcl-2 overexpression. [118] Additionally, A687V and A677G mutations have been awarded as activating mutations of *EZH2* in B-cell lymphoma. [119, 120]

Recently, a K27M mutation, H3.3, was found in most of the pediatric high-grade glioma. [121, 122] H3.3 K27M binds to and inhibits EZH2, thus the cells with H3.3 K27M exhibit global reduction of H3K27me3. More relevant, H3K27me3 and EZH2 were also found increased in hundreds of local genes in cells with the H3.3K27M mutation. [123] Consequently, H3K27me3 alterations are closely associated with glioma.

Many findings indicate that EZH2 is mostly overexpressed in multiple cancer types, including prostate, breast, bladder, ovarian, lung, liver, brain, kidney, gastric, oesophagal, and pancreatic cancer and melanoma. [124-132] Unfortunately, EZH2 expression is also correlated with increased proliferation, aggressive behaviour of cancer cells and poor prognosis. Indeed, extensive studies have reported that EZH2, when it is overexpressed, induces cell proliferation, migration, and/or invasion *in vivo*. [133-135] In addition to that, wild-type EZH2 overexpression in mammary epithelial cells *in vivo* enhances mammary tumour initiation induced by human epidermal growth factor receptor 2 (EGFR)/neu expression. [136, 137]

However, in some types of cancer EZH2 behaves like a tumour suppressor. Inactivating mutations of EZH2 are found in patients with myeloid malignancies, inactivating *EZH2* mutations are associated with poor patient survival. [138, 139] Furthermore, 25% of T-cell leukaemia cases possess loss-of-function mutations and ablations of the *EZH2* and *SUZ12* genes. [140] Further evidence of the role of EZH2 as tumour suppressor are described in a study in which conditional deletion of EZH2 in bone marrow cells causes T-cell leukaemia. [141] Once again, mice with conditional deletion of EZH2 in the pancreatic epithelium also exhibit low pancreatic regeneration and acceleration of K-Ras-induced neoplasia. [142] Taken together, these results show that EZH2 function is cell context-dependent, although EZH2 demonstrated to be an oncogenic factor in most solid tumours.

1.7 EZH2 as a therapeutic target

Given the evidence that EZH2 is an important component of PRC2 and a cancer driver, various pharmaceutical companies and scientific organisations have engaged in developing potential and specific inhibitors against it. All inhibitors, reported in the next chapter, target EZH2 and, some of them, have already obtained promising preclinical results. However, most of the human preclinical trials are still underway.

1.7.1 EZH2 inhibitors

An intense investigation has been pursued for the discovery of specific inhibitors of PRC2 mainly due to its well-documented implication in cancer. To date, some EZH2 inhibitors have been obtained, and

human clinical trials are now undergoing, with already great preliminary results. All inhibitors target EZH2 with a SAM competitive binding mechanism to the SET domain. An overview of the most widely reported EZH2 inhibitors is given in figure 1.10.

Tan and co-workers identified a SAM-dependent methyltransferase inhibitor (SAH-hydrolase) by library-based drug screening: the carbocyclic adenosine analogue 3-deazaneplanocin (DZNep, **1**, Fig. 1.10), a derivative of the natural antibiotic neplanocin-A. [143, 144] This compound blocks the methionine cycle and SAM regeneration, thus is an indirect and unselective inhibitor. Preferentially, DZNep induces apoptosis in various haematological malignancies targeting the degradation of EZH2. [145, 146] Indeed, it was reported that DZNep decreases the expression levels of the PRC2 components EZH2, SUZ12 and EED with concomitant loss of H3K27me3 but it is not efficient to inhibit H3K9 methylation. Even though this compound promotes apoptosis in different types of cancer cells, the poor PK and toxicological profile of DZNep prompted the development of novel, potent and selective inhibitors of EZH2.

In 2012 Epizyme, Inc., USA reported EPZ005687 (**2**, Fig. 1.10) as a potent, selective and SAM-competitive small-molecule inhibitor of EZH2 with a Ki of 24 nM. **2** has the potency to inhibit wild-type and EZH2 mutants (Y641 and A677) with a dose-dependent loss of H3K27 methylation and showed great selectivity (>500-fold) over human protein methyltransferases. [147]

Concurrently, Glaxo Smith Kline (GSK), USA disclosed GSK126 via a high-throughput biochemical screening, followed by an extensive medicinal chemistry optimisation (**3**, Fig. 1.10). GSK126 inhibits EZH2 with high potency (IC_{50} = 9.9 nM) compared with EZH1 (IC_{50} = 680 nM) and it was highly selective (>1000-fold) over other methyltransferases. [148] This compound decreases total H3K27me3 levels and reactivates silenced PRC2 target genes. Currently, GSK126 is under evaluation in phase I clinical trials for the treatment of non-Hodgkin's lymphoma (NHL) and other solid tumours. [149] In two cell lines, MGC803 and A549, GSK126 was able to inhibit cell migration and angiogenesis through downregulation of vascular endothelial growth factor (VEGF)-1 expression. [150]

GSK343 (**4**, Fig. 1.10), another potent EZH2 inhibitor, differs from GSK126 because it contains an indazole nucleus instead of an indole. GSK343 is a potent and selective EZH2 inhibitor with IC_{50} of 4 nM in a cell-free assay, showing 60 fold selectivity against EZH1, and >1000 fold selectivity against other histone methyltransferases. Recently, it was found to suppress cancer stem-like phenotypes and reverse mesenchymal transition in glioma cells, thereby regulating the levels of markers involved in epithelial-mesenchymal transition and stemness. [151]

EI1 (**5**, Fig. 1.7), a potent and selective small-molecule inhibitor, inhibits the enzymatic activity of the wild-type (IC_{50} = 15 nM) and Y641N mutant (IC_{50} = 13 nM) of EZH2. EI1 directly binds to the enzyme and competes with the methyl group donor SAM. [152] It is highly selective and displays > 10,000-fold

selectivity for EZH2 over other methyltransferases, and 90-fold selectivity over EZH1. EI1 was found to be effective in the treatment of NHL and other solid tumours. Cells treated with EI1 exhibited a genome-wide reduction of H3K27 methylation and activation of PRC2 target genes. Molecular modelling revealed that I626 and C663 residues near the EI1-binding pocket might contribute to the selectivity. Moreover, EI1 was able to decrease proliferation and to induce cell cycle arrest and apoptosis in Y641 mutant large B-cell lymphoma.

UNC1999 (**6**, Fig. 1.10) is the first orally bioavailable highly potent and selective inhibitor of EZH1 and EZH2. [153] **6** is a SAM-competitive inhibitor and has potency for the wild-type (IC_{50} < 10 nM) and Y641N mutant (EC_{50} of 633 nM) EZH2. [153] Binding mode analysis of UNC1999 within the active site of EZH2 revealed that the secondary amide and pyridone form H-bonds with N688 and H689 residues, whereas indazole is hidden in a hydrophobic pocket. Xu *et al.* showed that UNC1999 and its inactive analogue UNC2400 among MLL-rearranged leukaemia was able to suppress the H3K27me3/2 activity. [154]

Tazemetostat (EPZ-6438, **7**, Fig. 1.10) was developed using a follow-up optimisation of the Epyzime scaffold (EPZ005687, **2**, Fig. 1.10). [155] This compound inhibits EZH2 in a manner competitive with the substrate SAM and displays a 35-fold selectivity versus EZH1 and >4500-fold selectivity relative to 14 other HMTs tested. In addition, **7** showed similar potency for wild-type and the EZH2 mutants (Y646F, A682G, etc.) (Ki = 2.5 nM). In EZH2 mutant NHL, **7** exhibited a potent and selective antitumor activity. Currently, EPZ-6438 is used for the treatment of lymphoma and is in Phase I clinical trials. [156] Very recently, compound **7** entered the clinical arena to study also its effects on B-cell lymphoma, relapsed or refractory non-Hodgkin lymphoma, advanced solid tumours (Phase I), diffuse large B-cell lymphoma (Phase II), and follicular lymphoma (Phase II).

Constellation Pharmaceuticals developed a 2,2,6,6-tetramethylpiperidine-containing compound (**8**, Fig. 1.10) as an EZH2 inhibitor effective in KARPAS-422 lymphoma cells. [157] Unfortunately, due to its poor PK properties, **8** was not suitable for further *in vivo* investigation. In biochemical assays, the indole-based compound CPI-360, reported for the first time in 2015, exhibited a good activity profile as well as in a KARPAS-422 mouse xenograft model.

More recently, using a chemical optimisation study on 8 has been identified compound **9** (CPI-1205, Fig. 1.10) as a highly potent (biochemical IC_{50} = 0.002 μM, cellular EC_{50} = 0.032 μM) and selective EZH2 inhibitor. Vaswani *et al.* have also reported the co-crystal structure of **9** in complex with the human PRC2. [158] This compound showed once again a potent antitumor activity in a KARPAS-422 mouse xenograft model. Compound **9** is currently in Phase I clinical trials for B-cell lymphoma treatment.

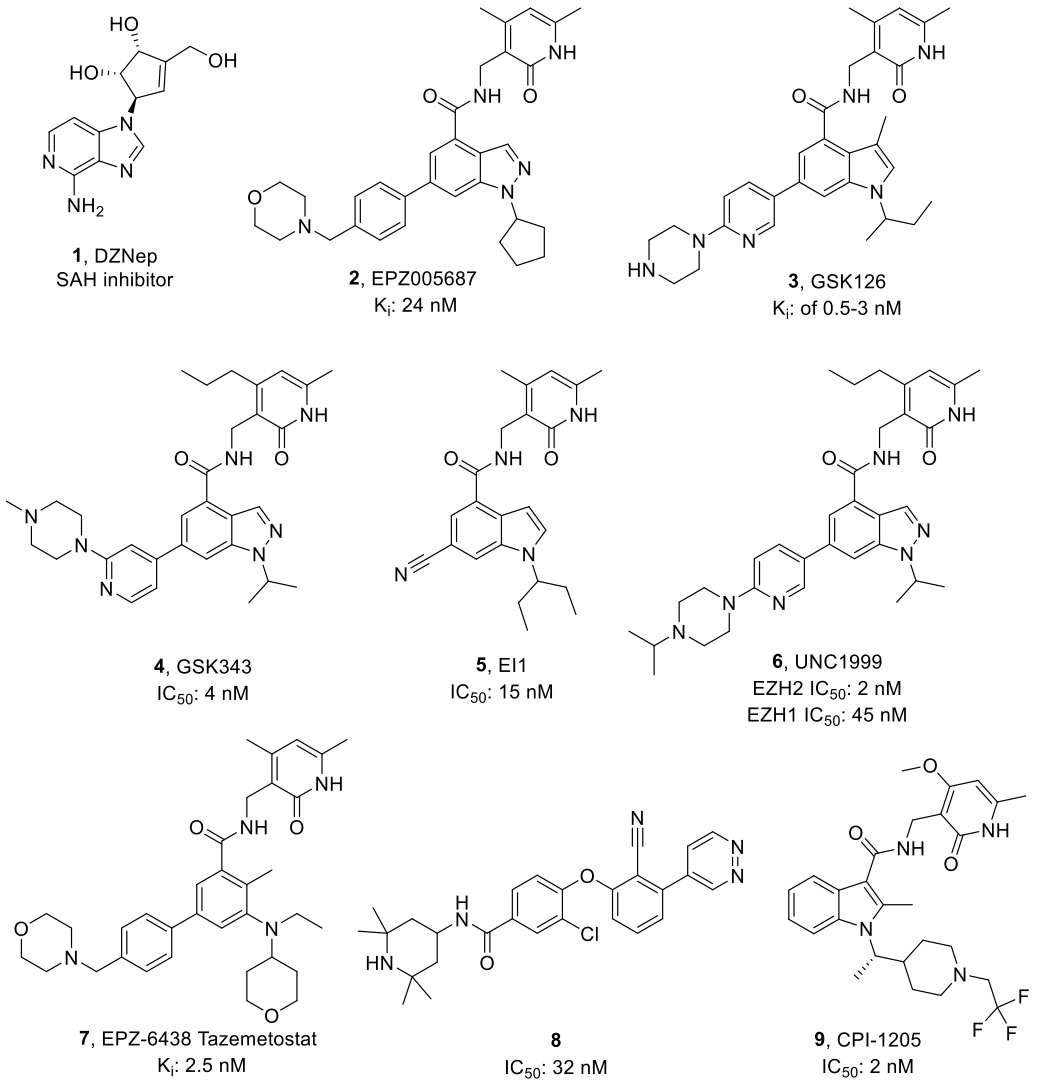

Figure 1.10: chemical structures of the selected EZH2 inhibitors.

1.7.2 EED inhibitors

There is continuing interest in developing novel inhibitors against PRC2 complex, with more acceptable pharmacological properties. Over the last years, many efforts have been provided to discover some inhibitors of EED for the treatment cancers that are dependent on PRC2 activity (Fig. 1.11)

The first PRC2 disruptors astemizole (**10**, Fig. 1.11), an old anti-histamine drug, and the natural product wedelolactone (**11**, Fig. 1.11) have been identified through high-throughput screenings. [159, 160]

In 2016, Novartis discovered five structurally distinct EED binders (**12**-**16**, Fig. 1.11), by using the PRC2 enzymatic assay as the primary screening assay. [161] Compounds **12**-**16** showed low μM activities against PRC2, with a similar inhibition potency against EZH1 and EZH2 and a selectivity over other HMTs (IC_{50} > 100 μM). The co-crystal structure of compounds **12**-**16** in complex with EED have been solved, showing a similar “induced fit” in the H3K27me3 pocket of EED.

Through an optimisation study of compound **15** applying X-ray crystallography guided fragmentation and regrowth, compound **17** (EED226, Fig. 1.11) was discovered as a potent and selective PRC2-EZH2/PRC2-EZH1 inhibitor. This compound showed to reduce globally H3K27 methylation and displays optimal PK properties, encouraging extensive preclinical studies. [162] Binding mode analysis of **17** revealed an allosteric mechanism of action by binding to the H3K27me3 pocket of EED. In addition, **17** modulates gene transcription similar to the SAM-competitive EZH2 inhibitor. Notably, when combined with EZH2 inhibitors, this compound shows a synergistic effect in inhibiting cancer cell growth. [163]

Novartis scientists also developed compound **18** from the HTS hit **12** (Fig. 1.11). Its activity was validated in cell-based assays, showing similar results than what observed after the treatment with EZH2 inhibitor. [164]

Concomitantly, AbbVie Inc. identified a novel potent and selective EED binder, compound **19** (A-395, Fig. 1.11). It binds EED in the H3K27me3 binding pocket and reduces H3K27 methylation *in vitro* by inhibiting PRC2 activation. Also, **19** was found to be selective against several PMTs as well as a panel of other methyl-lysine binding proteins. Compound **19** was also efficacious in cell lines with acquired resistance to SAM-competitive EZH2 inhibitors. Lastly, **19** proved to be effective in a diffuse large B-cell lymphoma (DLBCL) xenografted mouse model. [165]

Characterisation of the binding of trimethylated Jarid2 (116Kme3) to EED at low micromolar potency (Kd = 3 μM) provided a rational starting point for peptide optimisation to target the reader interface of EED. Recently, through a coupled combinatorial and structure-based design approach, Barnash *et al*. discovered the first peptidomimetic EED ligands (**20** and **21**, UNC5114 and UNC5115, Fig. 1.11). Unfortunately, both the binding mode and the exact mechanism on how they inhibit PRC2 are not yet fully elucidated. Evidently, the novel peptidomimetic binders are allosteric inhibitors, targeting the methyl-lysine reader function. [166]

Surprisingly, Novartis discovered MAK683 (**22**, Fig. 1.11) as an allosteric inhibitor of PRC2, with potential antineoplastic activity. It selectively binds to the domain of EED interacting with trimethylated H3K27me3, which leads to a conformational change in the EED-H3K27me3-binding pocket thus preventing the interaction of EED with EZH2. This binding disrupted the EED–EZH2 interaction and reduced the PRC2 activity. Currently, this compound is in phase I/II clinical trials for the treatment of adult patients with advanced malignancies (NCT02900651). MAK683 was also tested in patients with DLBCL, nasopharyngeal carcinoma and potentially other solid tumours.

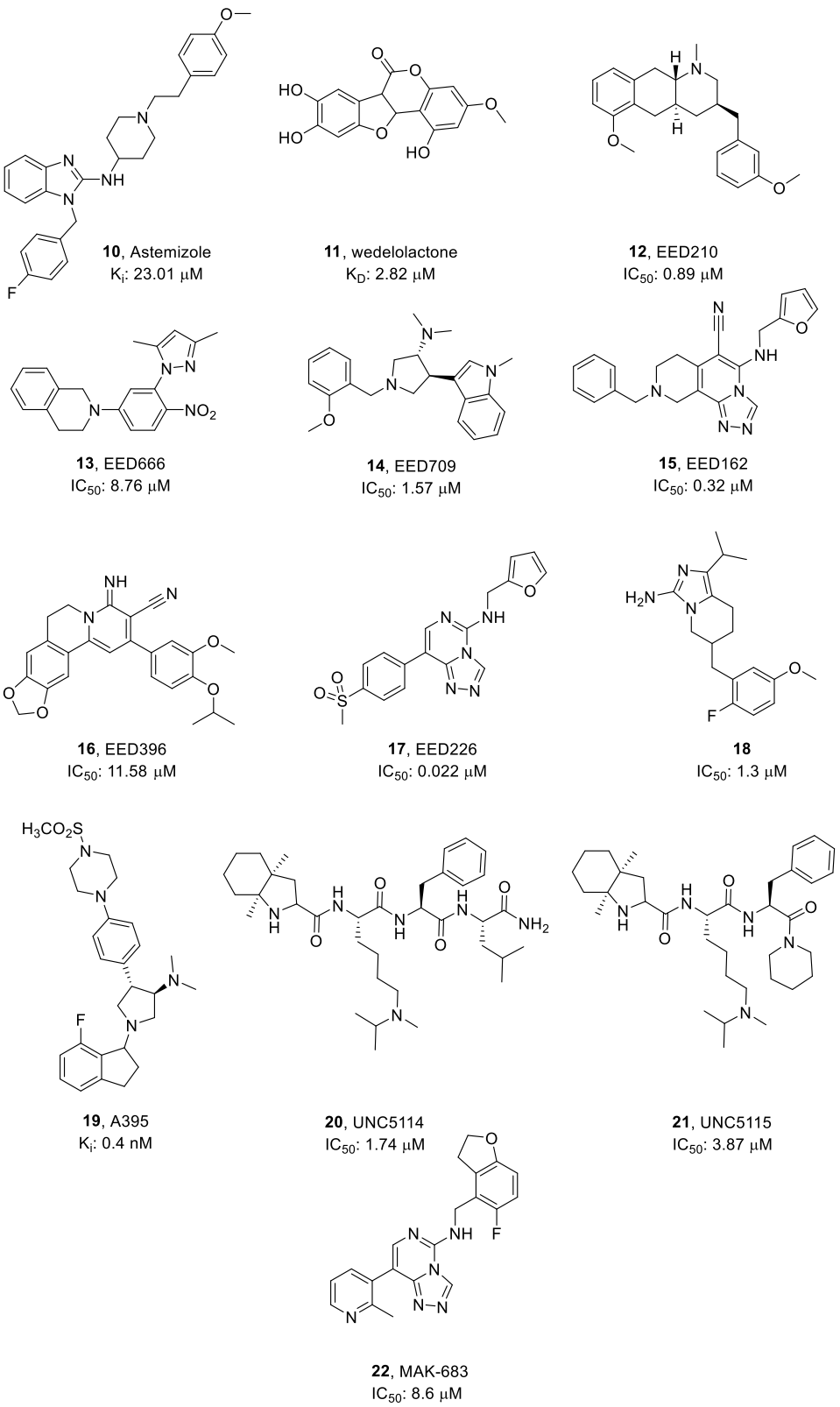

Figure 1.11: Chemical structures of selected EED inhibitors.

1.8 Histone acetylation

Chromatin structure and function can be affected by various HMTs of the amino-terminal tails of nucleosomal histones, of which lysine acetylation is the best characterised. Acetylation is thought to

increase DNA accessibility through the neutralisation of the positive charge of lysine residues. This modification correlates mostly with transcriptional activation, but it is also implicated in DNA replication, histone deposition, and DNA repair. Histone acetylation also regulates protein-protein interactions, as some acetylated lysines are recognised by bromodomains, which are found in many proteins that regulate chromatin function. [167] Histone acetylation and deacetylation are usually catalysed by HAT and HDAC activities (Fig. 1.12). [168-170]

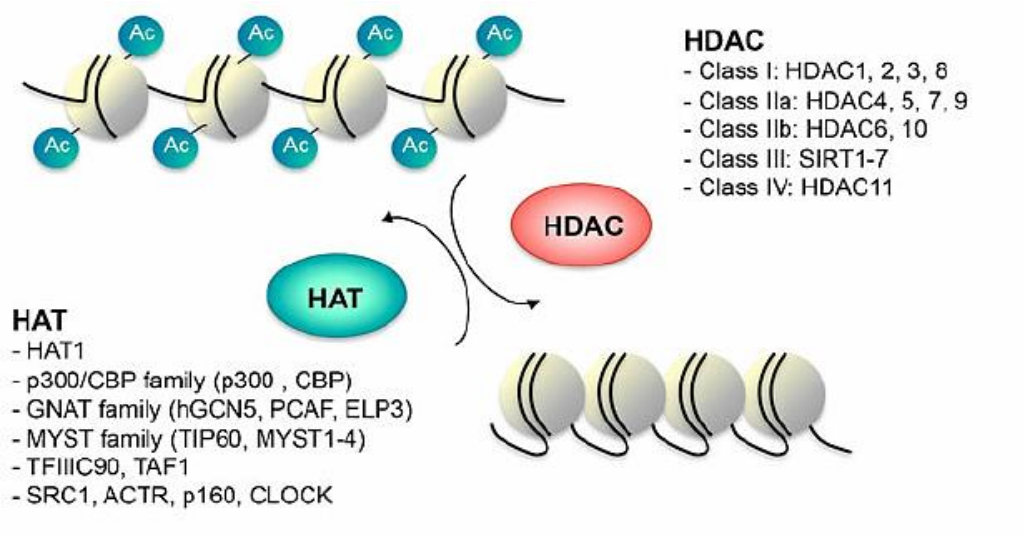

Figure 1.12: Histone acetyltransferase (HAT) and histone deacetylase (HDAC) families. Illustration of chromatin conformation according to the HAT/HDAC balance. The acetylation levels of nucleosome histone tails, at lysine residues, are determined through the interplay between acetylation and deacetylation mechanisms engaged respectively through HATs and HDACs enzymes. [168]

HATs induce chromatin relaxation through acetylation of the lysine residues on N- terminal tails of histones by transferring an acetyl group donor from acetyl-coenzyme-A. This event allows more access to transcriptional factors, transcriptional regulatory complexes and RNA polymerases to promoter regions of DNA. Conversely, HDACs remove the acetyl group from lysine in the histone tail, thus restoring the positive charge and leading chromatin condensation. Thus, the function of this class of enzymes is that of "turn off" the gene transcription. [171, 172] HATs and HDACs control the dynamic acetylation equilibrium not only of histones but also non-histone proteins and play a crucial role in apoptosis, proliferation, differentiation, angiogenesis, cancer treatment, neuroprotection, and anti-inflammatory effects. HATs and HDACs are classified into many families that are often conserved from yeast to humans. [173]

1.8.1 Histone acetyltransferases (HATs)

After several decades of research on histone acetylation, the majority of the functional properties of acetylation have been documented, with recent findings of non-histone protein acetylation. As

previously mentioned, histones undergo acetylation in order to yield a more relaxed chromatin structure resulting in reduced electrostatic interactions between the lysine in the histone tail and the negatively charged phosphate group on DNA. Then, acetylated histones recruit bromodomain-containing proteins, thereby enhancing gene expression. [173]

Since the isolation of the Gcn5 HAT from *Tetrahymena* by Allis and coworkers [174], and the identification of HAT1 by Sternglanz and coworkers [175] and Gottschling and coworkers [176], many other HATs have been identified from yeast to man.

Nowadays, HATs are broadly classified into cytoplasmic type A and nuclear type B HATs. Further, nuclear HATs are sub-classified into 5 major families: 1) Gcn5-related N-acetyltransferases (GNAT), 2) p300/cyclic adenosine monophosphate response element-binding protein (CREB) binding protein (CBP), 3) MOZ, yeast YBF2, SAS2, and TIP60 (MYST), 4) transcription factor-related HATs, and 5) nuclear receptor-associated HATs.

GCN5, a member of GNAT family, was the first acetyltransferase identified. Most of GNAT members are involved in amino acids synthesis 5 (Gcn5), elongation protein 3 (ELP3), p300/CBP-associated factor (PCAF), chromodomain on chromosome Y protein, and others. [177, 178]

GNATs are characterised by a conserved acetyltransferase domain as bromodomain, whose function is to recognize acetylated lysine residues and the transcriptional coactivator ADA2-binding domain.

The two paralogs of the p300/CBP family are transcriptional co-activators of p300 and CBP. The most relevant protein interaction domains of p300 and CBP are: the nuclear receptor interaction domain; the CREB and myeloblastosis (MYB)-interaction domain; the kinase-inducible binding domain (KIX), which binds to the Ser-133- phosphorylated kinase-inducible domain region of CREB; the cysteine/histidine regions (CH1 and CH3); and the interferon response-binding domain, which is also the steroid receptor coactivator 1 interacting domain of CBP. [179] Furthermore, other two domains have been identified in p300/CPB: a plant homedomain-type zinc finger motif and a bromodomain with an acetyltransferase activity.

The members of MYST family comprise TAT interacting proteins 60 (Tip60), monocytic leukemia zinc-finger protein (MOZ), males absent on the first (MOF), monocytic leukemia zinc-finger protein-related factor (MORF) and human acetylase binding to ORC1 (HBO1), have a 240 amino acid-long MYST region with a canonical acetyl-CoA-binding site and a C2HC-type zinc finger motif.

The majority of the MYST family acetyltransferases possess a chromodomain implicated in protein-protein interactions. [180]

Several proteins related to HAT activities have been identified with transcriptional activation through hormonal signals. This family has been classified as nuclear receptor coactivators. [24]

Since HATs are involved in many different biological processes including cell cycle progression, DNA damage and hormone signalling, dysregulation of its function are correlated with several human diseases, such as solid tumours, leukaemias, viral infections, diabetes, and inflammatory disorders. [181,

182] However, the development of potent HATs inhibitors has not progressed as the development of HDAC inhibitors.

1.8.2 Histone deacetylases (HDACs)

Until now, 18 HDACs have been found in humans. The huge deacetylase family can be classified into four classes by the structure, function, sub-cellular localisation and pattern of expression as well as homology to yeast HDACs. [183]

Class I, II and IV HDACs, numbered according to their chronological order of discovery, comprise classical HDACs, which are zinc-dependent amidohydrolases, sensitive to Zn^{2+} chelating compounds such as hydroxamic acids. By contrast, Class III HDACs belong to the recently discovered sirtuin family and are homologous to the yeast Silent information regulator 2 (Sir2) family of proteins. Being NAD+-dependent enzymes, sirtuins are not sensitive to hydroxamic acid-derived HDAC inhibitors. Proposed catalytic mechanism of class I, II and IV HDACs is illustrated in figure 1.13, whereas that of class III HDACs is depicted in figure 1.14. [184]

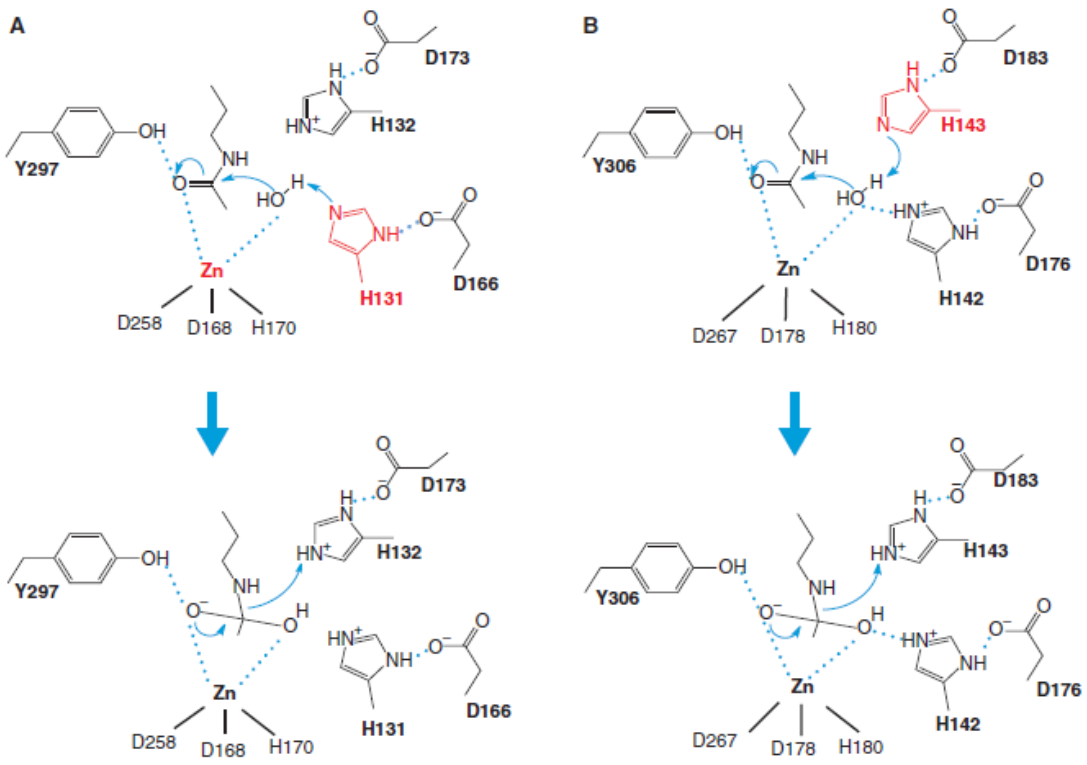

Figure 1.13: Catalytic mechanism of HDACs. Two models for the catalytic mechanism of the Zn-dependent HDAC reaction have been proposed. (**A**) A model proposed from the HDLPstructure. The HDLP catalytic core consists of a tubular pocket, a zinc-binding site, and active-site residues (in bold) of a tyrosine (Y297) and two histidines (H131 and H132) that make hydrogen bonds to two aspartic acids (D166 and D173). One of these catalytic histidines (red) facilitates the nucleophilic attack at the

substrate carbonyl by activating a water molecule coordinated with the zinc ion. Initially, two tandem histidine residues (H131 and H132) were proposed to function as Asp-His charge relay systems, typical of serine proteases such as chymotrypsin and chymotrypsinogen in the enzyme reaction. The active site zinc ion is coordinated by three residues (two aspartic acids and one histidine). (**B**) A model proposed from the HDAC8 structure, in which the other histidine residue (red) plays an essential role in the electron transfer. Hydrogen bond interactions are drawn in dotted lines. [185]

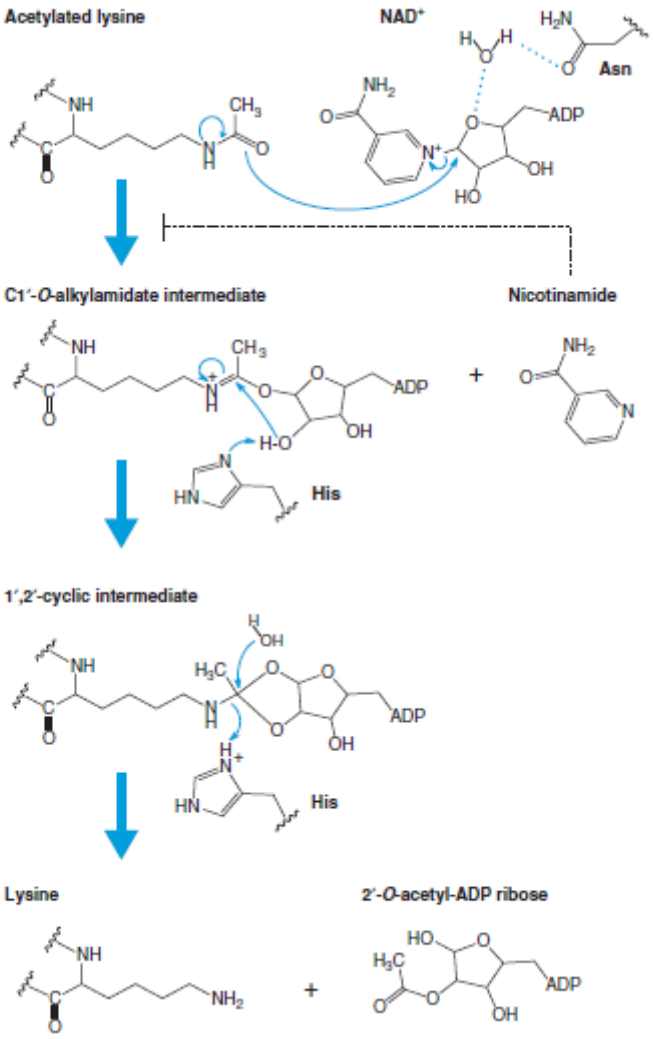

Figure 1.14: Catalytic mechanism of sirtuins (Class III). Proposed mechanism of the NAD^+-dependent deacetylase reaction. The first step of the reaction involves the nucleophilic addition of the acetamide oxygen to the C1 position of the nicotinamide ribose to form a C1 -O-alkylamidate intermediate and free nicotinamide. Next, the 2-hydroxy group of the NAD^+ ribose is activated by an active site histidine residue that, in turn, attacks the C1′-O-alkylamidate to form the 1′,2′-cyclic intermediate. The 1, 2-cyclic intermediate is then attacked by an activated water molecule resulting in the formation of deacetylated lysine and 2-O-acetyl-ADP ribose. 2-O-acetyl-ADP ribose can be readily converted to 3-O-acetyl-ADP ribose in aqueous solution by nonenzymatic intramolecular transesterification. Thus, nicotinamide, the deacetylated peptide, and a mixture of 2′- and 3′-O-acetyl-ADP ribose are the final reaction products. [185]

Class I HDACs (HDAC1, 2, 3, and 8) are closely related to the yeast (*Saccharomyces cerevisiae*) transcriptional regulator RPD3. Class II HDACs (HDAC4, 5, 6, 7, 9 and 10), further divided into class IIa (HDAC4,5,7 and 9) and IIb (HDAC6 and 10), share similar domains to the deacetylase HDA1. [186] Class III HDACs, also known as sirtuins, include SIRT1, SIRT2, SIRT3, SIRT4, SIRT5, SIRT6, and SIRT7. The sole member of class IV HDACs is HDAC11. In fact, although HDAC11 shares certain features belonging to both class I and II HDACs, it cannot be classified into these classes due to its overall low sequence similarity. [187] Currently, since class I HDACs are expressed in several cell types, whereas class II HDACs

are more restricted, it is thought that they might be involved in cellular differentiation and developmental processes. [188, 189]

1.8.2.1 Class I HDACs

HDAC1 and HDAC2 share approximatively 82% of sequence identity and are inactive when reproduced by recombinant techniques, demonstrating that other cofactors occur for their activity. In fact, *in vivo* both HDAC1 and HDAC2 display activity within a complex of proteins able to either modulate their deacetylase activity or to recruit HDACs to the promoters of genes. [190] Three protein complexes have been discovered that contain both HDAC1 and HDAC2: Sin3, nucleosome remodeling and deacetylating (NuRD) and Co-REST. Both Sin3 (also known as mSin3A) and NuRD complexes have a core that holds HDAC1 and HDAC2, Rb-associated protein 48 (RbAp48) and RbAp46. [190, 191] Additionally, HDAC1 and HDAC2 can directly bind to DNA binding proteins including the cellular nuclear matrix regulatory protein Yin and Yang 1 (YY1), Rb binding protein-1 and Sp1. [192-195] Besides the regulation of HDAC1 and HDAC2 by the availability of co-repressors, a second means of regulating activity is via PTMs. Indeed, both HDAC1 and HDAC2 undergo to phosphorylation. Hyperphosphorylated HDAC1 and HDAC2 show an increase in their deacetylase activity and, at the same time, the disruption of complex-formation between HDAC1 and HDAC2 and, between HDAC1 and mSin3A/YY1. On the contrary, when hypophosphorylated, HDAC1 and HDAC2 exhibit decreased activity with concomitant increase of complex formation.

HDAC3 was discovered by searching the GenBank database for DNA and protein sequences with homology to HDAC1 and HDAC2. [196] Likewise HDAC1 and HDAC2, HDAC3 suppresses transcription, binds to and is recruited by transcription factors. HDAC3 is evolutionarily most closely to HDAC8, with 34% overall sequence identity. [197] Several studies indicate that HDAC3 expression is restrictive to certain tissues, and HDAC1, HDAC2, HDAC3, and HDAC8 can be localised to the cytoplasm or specialised cellular organelles. Silencing mediator for retinoic acid and thyroid hormone receptors (SMRT) and nuclear receptor co-repressor (N-CoR) are fundamental for HDAC3 deacetylase activity. Both SMRT and N-CoR, two distinct but highly related proteins, have a conserved deacetylase-activating domain for HDAC3 activation. [198]

1.8.2.2 Class II HDACs

HDAC4, HDAC5, and HDAC6 were discovered together with sequence similarity to yeast HDA1. [199] Interestingly, HDAC6 contains an internal duplication of two deacetylase catalytic domains arranged in tandem which function is independent of each other. [199] HDAC6 is evolutionarily most closed related to HDAC10 and possess a HUB domain (HDAC6-, USP3-, and Brap2-related zinc finger motif) on the C-terminus. This domain is a signal for ubiquitination, suggesting that HDAC6 is subjected to degradation.

Thus, HDAC6 acts as a tubulin deacetylase and controls microtubule-dependent cell motility. [200] HDAC6 is present both in the cytoplasm and in the nucleus in a complex together with HDAC11. However, the HDAC11 function has been less investigated compared to the other HDACs but seems to have many interesting and valuable features. [192, 201, 202]

HDAC7 was first isolated as a protein that interacts with SMRT and has three repression domains where the third deacetylase activity is independent of the other two. [193]

The HDAC9 catalytic domain is located on the N-terminus, as for class I HDACs. Three known splice variants of HDAC9 have been detected: HDAC9a, HDAC9b, and HDAC9c/HDRP. The latter lacks the catalytic domain and shares 50% homology to the N-terminus of HDAC4 and HDAC5. [203] Since HDAC9 was found to interact with MEF2 (CaMK/14-3-3), a likely function in muscle differentiation has been assumed. [204]

HDAC10 is mostly related to HDAC6 (37% overall similarity). [205] HDAC10 has a catalytic domain on its N-terminus, a nuclear export signal (NES) and a second putative catalytic domain on the C-terminus. Both HDAC6 and HDAC10 are subclassified as Class IIb. Moreover, due to the presence of two putative Rb binding proteins, a potential role in the regulation of the cell cycle by HDAC10 has been hypothesized. Most importantly, HDAC10 can interact with other HDACs, except for HDAC6, suggesting that it functions as a recruiter rather than as a deacetylase. However, several reports confirm that HDAC10 displays a deacetylating activity. [205-207]

1.8.2.3 Class IV HDACs

HDAC11 is the unique member of the Class IV HDACs and was first discovered by Basic Local Alignment Search Tool searches of GenBank database. [187] It has similar sequence identity to the catalytic domains of both Class I and II HDACs. HDAC11 regulates the protein stability of DNA replication factor CDT1. [208] However, both HDAC10 and HDAC11 are the less studied and poorly understood HDACs in the classical HDAC family.

1.8.2.4 Class III HDACs

S. cerevisiae homologs of Sir2 (Hsts) was first described by Lorraine Pillus and Jef Boeke that also observed how this protein is conserved from bacteria to humans. [209] Subsequent studies identified five human sirtuins (SIRT1, SIRT2, SIRT3, SIRT4, and SIRT5) by using *S. cerevisiae* Sir2 amino acid sequence as a probe. [210] Later, two additional human sirtuins (SIRT6 and SIRT7) were discovered using human SIRT4 as a probe. Overall, the seven sirtuins share 22%-50% amino acid sequence identity and, 27%-88% identity in the conserved catalytic domains.

Among them, SIRT1 is the most similar to Sir2 protein and has a robust deacetylase activity that's why has been extensively studied. Surprisingly, sirtuins possess two enzymatic activities: mono-ADP-ribosyltransferase and histone deacetylase. *In vitro*, additional protein lysine desuccinylase and

demalonylase activity have been found in SIRT5. [211] Another interesting feature of sirtuins is their localisation: SIRT1 and SIRT2 are in the nucleus and cytoplasm, SIRT3 in the nucleus and mitochondria, SIRT4 and SIRT5 only in the mitochondria, SIRT6 exclusively in the nucleus, and SIRT7 in the nucleolus. As Class I, II, and IV, sirtuins also have non-histone substrates, at least in eukaryotes. The most essential characteristics of sirtuins including their specific enzymatic activity, localisation, histone, and non-histone deacetylation target as well as their effects on pathologies have been reported in table 1.2.

Sirtuin	**Localisation**	**Enzymatic Activity**	**Histone deacetylation target**	**Non-histone deacetylation target**	**Pathology**
SIRT1	Nuclear/ cytoplasmatic	Deacetylase	H3K9ac H1K26ac H4K16ac	Hif-1α, Hif-2α MYC	Neurodegenerative diseases. Cancer: acute myeloid leukaemia, colon, prostate, ovarian, glioma, breast, melanoma, lung adenocarcinoma.
SIRT2	Nuclear/ cytoplasmatic	Deacetylase	H3K56ac H4K16ac	Tubulin Foxo3a EIF5A P53, G6PD, MYC	Neurodegenerative diseases. Cancer: brain tissue, glioma.
SIRT3	Mitochondrial	Deacetylase	H3K56ac H4K14ac	SOD2, PDMC1a, IDH2, GOT2, FoxO3a	Neurodegenerative diseases. Cancer: B cell chronic lymphocytic leukaemia, mantle cell lymphoma, chronic lymphocytic leukaemia, breast, gastric.
SIRT4	Mitochondrial	ADP-ribosyltransferase	Unknown	GDH, PDH	Cancer: breast, colorectal.
SIRT5	Mitochondrial	Malonyl, succinyl, glutaryl	Unknown	CPS1	Cancer: pancreatic, breast, non-small cell

		deacetylase			lung carcinoma.
SIRT6	Nuclear	Deacetylase, ADP-ribosyltransferase, long-chain fatty acyl deacetylase	H3K9ac H3K56ac	Unknown	Cancer: breast, colon.
SIRT7	Nuclear	Deacetylase	H3K18ac	Hif-1α, Hif-2α	Cancer: liver, testis, spleen, thyroid, breast.

Table 1.2: Sirtuin location, activity, and effects on pathologies. [212]

1.8.2.4.1 Sirt1

The nuclear and cytoplasmic Sirt1 is the most extensively studied mammalian sirtuin isotype. Thus far, more than 50 cellular substrates have been identified. Sirt1 showed to regulate transcription directly via deacetylation of histones H1, H3 and H4 [212-214] and indirectly by deacetylation of transcription factors such as FOXO1, FOXO4, NF-*k*b, HIF1α, and HIF2α. [215-217] PCAF and p300 and KDAC1 deacetylating activities depending on Sirt1 deacetylation, represent further ways of an indirect transcriptional regulation. Therefore, Sirt1 is implicated in modulating diverse cellular processes. [218] In particular, Sirt1 has been found to regulate apoptosis by deacetylating the tumour suppressor proteins p53, p73 and Ku70. [219] Thus, deacetylated tumour suppressor proteins result inactive with a consequent antiapoptotic effect mediated by Sirt1. The anticancer activity display by some Sirt1 inhibitors is mainly related to p53 hyperacetylation. [220, 221] Additionally, Sirt1 can decrease the tumour suppressor effects of p53 by deacetylation of the proto-oncogene BLC6. [222] By pharmacological inhibition of BLC6, a hallmark of B-cell lymphoma, the increase of BLC6 acetylation determines the promising effect in cell culture and mouse models for this disorder. [220] Furthermore, deacetylation and activation of KAP1 by Sirt1, another transcriptional corepressor involved in the NHEJ pathway, represents a further antiapoptotic effect of Sirt1. [223] However, Yeung *et al.* reported that Sirt1 can mediate both pro- and antiapoptotic effects dependent on the cellular context, thus Sirt1 can act either as tumour promotor or tumour suppressor. [224] These evidences elucidated the opposite behaviour of Sirt1 in tumorigenesis. Various metabolic processes are also regulated by Sirt1 because, as for all sirtuin isotypes, the catalytical activity of Sirt1 is strictly related to the availability of the cofactor NAD^+. That phenomena directly links the sirtuin activity to the energetic state of the cells. Overexpression of Sirt1 in mice induces a caloric restriction state such as improvement of insulin sensitivity, enhancement of mitochondrial biogenesis and a lower incident of age-related diseases. [225] Recently, it has been reported that Sirt1 plays a crucial role in age-related arterial dysfunction. [226-228] Sirt1-dependent deacetylation and activation of the acetyl-CoA synthetase (AceCSI) determine an increase in endogenous fatty acid synthesis. [229] In addition, the nuclear liver X receptor (LXR) that

regulates cholesterol biosynthesis and other factors implicated in lipid metabolism are positively regulated and activated by Sirt1 via deacetylation. [230] The Sirt1-mediated deacetylation of FOXO1 leads to an increase in adiponectin transcription. [231] Besides the role of Sirt1 in enhancing insulin effects, additional studies demonstrated that Sirt1 is also involved in the stimulation of the insulin secretion of pancreatic β cells by transcriptional repression of UCP2. [232]

Moreover, Sirt1 can maintain glucose homeostasis under calorie restriction. During fasting, the intracellular levels of pyruvate are elevated. So, overexpression of Sirt1 in liver cells induces the activation of the coactivator PGC-1α by deacetylation, leading to transcriptional activation of genes involved in gluconeogenesis and glycogenolysis with an increase of glucose levels in the blood. [233, 234]

Sirt1 is also implicated in protein metabolism by deacetylation of the autophagy proteins Atg5, Atg7, and Atg8. [235, 236] Its activity can be differently modulated either by physiological inhibitors such as nicotinamide or by endogenous regulator proteins like the active regulator of Sirt1 (AROS) and deleted in breast cancer DBC1 or by PMTs (e.g., phosphorylation and sumoylation). [237, 238]

In recent years, encouraged by the beneficial effects of Sirt1 overexpression and calorie restriction, respectively, extensive studies have been started with the aim to identify small-molecules activators of Sirt1. Actually, several clinical studies are underway to investigate Sirt1 activators as a novel therapeutic approach to treat several diseases including diabetes, cancer, sepsis, psoriasis and so on. Surprisingly, Sirt1 expression has also been linked to several neuronal processes, such as Huntington's disease, Alzheimer's disease, and Parkinson's disease. Indeed, Sirt1 has been found to mediate neuroprotective effects, however it is also involved in neuropathology. In a mouse model of Huntington's disease, Sirt1 overexpression improved survival and the expression of brain-derived neurotrophic factor (BDNF). [239] Conversely, pharmacological inhibition of Sirt1 in multiple animal and cell-based models of Huntington's disease leads to alleviate the pathology. Despite these contradictory evidences, Selisistat, a potent and selective Sirt1 inhibitor, has already completed both phase I and phase II clinical trials for the treatment of Huntington's disease. [240, 241]

1.8.2.4.2 Sirt2

The mammalian ortholog of Hst2 from yeast is the primary cytosolic protein Sirt2. It is mainly bounds to the microtubule network and deacetylases the α-subunit at K40Ac. [242] Deacetylation of α-tubulin, also catalyzed by KDAC6, is considered important for cell cycle regulation and cell motor functions. [243] Sirt2, by regulating anaphase-promoting complex/cyclosome (APC/C) activity through deacetylation of its cofactors, is able to maintain genome integrity and to suppress tumorigenesis. [244] An important role of Sirt2 is the global deacetylation of H4K16Ac during mitosis influencing directly cell progression and genome stability. [245, 246] Although Sirt2 is considered a tumour suppressor, some reports showed an opposite role in tumorigenesis, at least in some types of cancer. Both KDAC6 and Sirt2 were

found to deacetylate and activate the oncoprotein K-RAS, thus inhibiting either of them, Sirt2 has a devastating effect on the growth properties and leads the expression of K-RAS mutants. [247] Indeed, targeting Sirt2 or KDAC6 might be a novel strategy to fight cancer expressing mutant forms of K-RAS. Furthermore, p53 was identified as a substrate of Sirt2, and its deacetylation induces the downregulation of p53-mediated tumour suppression. [248] However, in C6 glioma cells, Sirts was shown to act as tumour promotor. [249] Furthermore, deacetylation of NF*k*B leads the regulation of immune and inflammatory response by Sirt2. [250] In addition, Sirt2 reduces the cellular reactive oxygen species (ROS) levels by the deacetylation of the transcription factor FOXO3a, resulting in an increased transcription of the mitochondrial antioxidant manganese superoxide dismutase (MnSOD). [251] During oxidative stress, Sirt2, deacetylating the glucose-6-phosphate dehydrogenase (G6PD), maintains NADPH homeostasis and promotes cell survival. [252] However, in macrophages Sirt2 exhibits proinflammatory effects by the transcriptional activation of the inducible nitric oxide synthase (iNOS). [253]

Moreover, Sirt2 has an essential role in carbohydrate metabolism due to the degradation inhibition of phosphoenolpyruvate carboxykinase 1 (PEPCK1) proteasomal. Indeed, an elevated level of PEPCK1 has been linked with the pathogenesis of diabetes mellitus type 2, thus targeting Sirt2 could be an interesting choice to treat such disease. [254]

Other observations show that Sirt2 is preferentially involved in the pathogenesis of some neurodegenerative diseases. [255] For example, by pharmacological inhibition of Sirt2 in a cellular model of Parkinson's disease, lower level of the α-synuclein-mediated neurotoxicity has been detected. [256] Finally, Sirt2 has been reported to deacetylate H3K18A in bacteria-infected cell lines, opening new options for potential therapeutics in bacterial infections. [257]

1.8.2.4.3 Sirt3

Sirt3 shows the most robust deacetylase activity among the mitochondrial sirtuins and can undergo proteolytic cleavage upon translocation to the mitochondrion. Full-length (FL) SIRT3 is proposed to be inactive until it is translocated and proteolytically processed within the mitochondrion to an active 28 kDa protein. It has been reported to deacetylate a range of metabolic enzymes such as glutamate dehydrogenase (GDH), acetyl-CoA-synthase 2 (AceCS2), ATP-synthase,271 hydroxymethylglutaryl-CoA-synthase 2 (HMGCS2), and isocitrate dehydrogenase 2 (IDH2). [258-260] Other physiological Sirt3 substrates are complex I, FOXO3a, heat shock protein 10 (HSP10), and Ku70. [261-263] Although Sirt3 has the highest sequential overlap with Sirt2, the effect of its substrate conversion is much more similar to Sirt1.

In mice, overexpression of Sirt3 causes increased protection against ROS and removes the onset of age-related diseases such as cardiac hypertrophy or tissue fibrosis. [264] Recent findings outline the emerging role and therapeutic use of Sirt3 in cardiovascular diseases. [265, 266] In humans, the improved Sirt3 expression has been correlated with survival at oldest ages. [267] Likewise Sirt1, Sirt3

acts either as a tumor suppressor or tumour promotor dependent on cell context or tumour type. [268, 269] An overview of the main function of Sirt3 is illustrated in table 1.30.

Function	Gene symbol	Gene name	References
Energy metabolism			
Glycolysis	PPID	Peptidylprolyl isomerase D (cyclophilin D)	[270]
Fatty acid oxidation	ACADL	ACADL Long-chain Acyl-CoA dehydrogenase (LCAD)	[271]
Ketone body synthesis	HMGCS2	3-Hydroxy-3-methylglutaryl-CoA synthase 2, mitochondrial	[272]
Acetate metabolism	ACSS2	Acyl-CoA synthetase short-chain family member 2	[229, 258]
Urea cycle	OTC	Ornithine transcarbamylase	[273]
Amino acid catabolism	GLUD1	Glutamate dehydrogenase 1 (GDH)	[259]
Mitochondrial protein synthesis	MRPL10	Mitochondrial ribosomal protein L10	[274]
	NDUFA9	NADH dehydrogenase (ubiquinone) 1 α subcomplex 9	[275]
Oxidative phosphorylation	SDHA	Succinate dehydrogenase complex, subunit A, flavoprotein	[276, 277]
	ATP5a	F_1F_0-ATPase subunit α	[278]
TCA cycle	IDH2	Isocitrate dehydrogenase 2, mitochondrial	[279]
Oxidative stress			
Transcriptional activation	FOXO3a	Forkhead box O3a	[261, 280]
ROS	SOD2	Superoxide dismutase 2, mitochondrial (MnSOD)	[281, 282]
	OPA1	Optic atrophy 1	[283, 284]
Apoptosis	XRCC6	X-ray repair cross-complementing 6 (Ku70)	[261]

Table 1.3: Known targets of Sirt3 and function. [285]

In details, SIRT3 can control a wide range of important biological processes including regulation of nuclear gene expression, metabolic control, neuroprotection, cardiovascular disease, cancer, and

ageing. SIRT3 can regulate characteristic mitochondrial processes like protein deacetylation. Some other organs and active metabolic tissues, including brown adipose tissue (BAT), heart, and kidney also accommodate significant concentrations of SIRT3. SIRT3 impacts energy metabolism processes (e.g., tricarboxylic acid cycle, respiratory chain, fatty acid b-oxidation, and ketogenesis) by targeting the specific enzymes. Other functions of Sirt3 are the control of the flow of mitochondrial oxidative pathways as well as the rate of ROS production. SIRT3 also plays a role in multiple additional metabolic processes from acetate metabolism to BAT thermogenesis, often by controlling mitochondrial pathways through the deacetylation of target enzymes. The role of SIRT3 in physiology is crucial and an interesting subject for research. Protein acetylation regulates global mitochondrial function. Moreover, SIRT3-knockout mice revealed many relevant aspects of SIRT3 in physiology. As previously said, SIRT3 can interact with FOXO3a to activate antioxidant genes like MnSOD and catalase, whose gene products reduce ROS, thus positively affecting disorders such as cardiac hypertrophy and interstitial fibrosis. [280]. SIRT3-knockout mice are prone to age-related disorders like cancer, cardiac hypertrophy, and metabolic syndrome. [286]. Frequency in the opening of mitochondrial permeability transition pore (mPTP) can lead to mitochondrial dysfunction. mPTP is regulated by cyclophilin D (CypD) which is a substrate of SIRT3. The deletion of SIRT3 in cardiac muscle provides a stimulus to increase the opening of mPTP, leading SIRT3 KO mice to hamper the mitochondrial function in the heart. SIRT3-knockout rodents also develop pulmonary arterial hypertension. [287] SIRT3 controls stress response in hematopoietic stem cells (HSC) and improves regenerative capability in aged HSCs, monitoring tissue homeostasis, as well. [288] SIRT3 can also manage NAD^+ levels to regulate mitochondrial function, offering protection against liver injury associated with fatty liver and/or acute kidney injury. [289] SIRT3 KO mice are not able to preserve SOD2 homeostasis and ROS level, thus they suffer from mild endothelial dysfunction when fed with high cholesterol diet. [290] Overall, the most relevant biological and pathophysiological functions of SIRT3 are cancer control, neuroprotection, enhanced longevity, energy homeostasis and oxidative stress tolerance.

1.8.2.4.3.1 Sirt3 structures

In the last few years, 25 crystal structures of human Sirt3 have been solved including *apo* and peptide-bound form as well as in complex with the cofactor NAD^+. Sirt3 was co-crystallized with inhibitor/activator of other sirtuin isotypes, such as the indole derivative EX-527 and resveratrol and its derivatives. The binding mode for these compounds was found similar to the other sirtuins. Disch *et al.* reported a series of thieno[3,2-d]pyrimidine-6-carboxamide derivatives as potent nanomolar sirtuin inhibitors. [291] The resolved crystal structures showed that such compounds bind to the catalytic pocket in a similar way, occupying both the acetyl-lysine substrate channel as well as the nicotinamide C-pocket. In details, the carboxamide group of the thieno[3,2-d]pyrimidine-6-carboxamide core mimics

the corresponding group of nicotinamide or the sirtuin inhibitor EX-527. Very recently, Sirt1 has been co-crystallized with an ELT inhibitor, showing the same binding mode of Sirt3 (Fig. 1.15). [292]

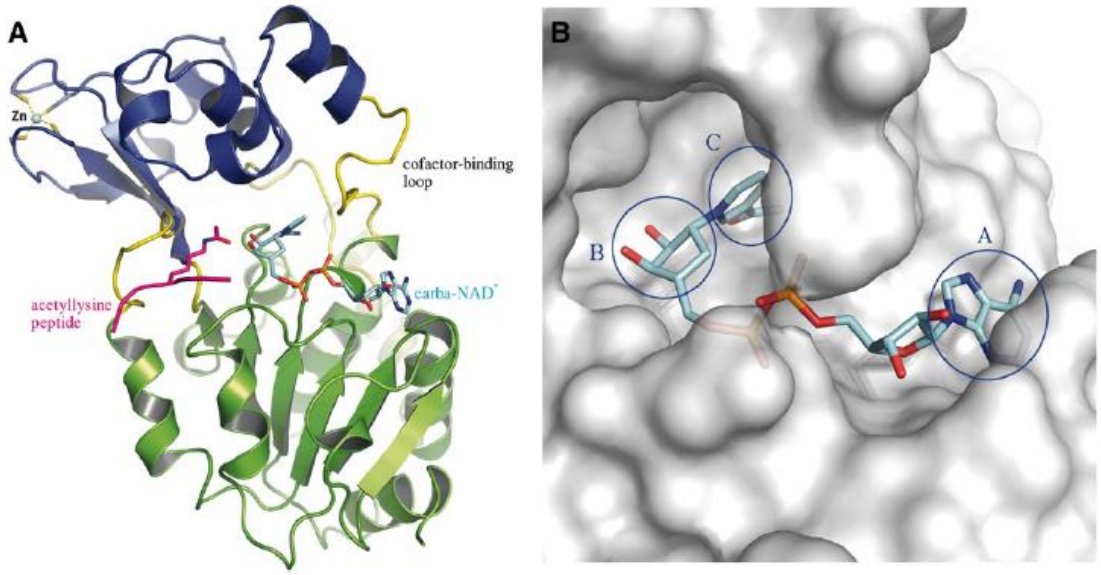

Figure 1.15: (**A**) Overall structure of sirtuins, Sirt3 (PDB ID 4FVT) as example. The structure of Sirt3 is shown as a cartoon model. The zinc-binding domain and Rossmann fold domain are coloured in blue and green, respectively. The four loops (including the cofactor-binding loop) that connect the subdomains are coloured in yellow. Substrate peptide is coloured in pink and the cofactor analogue carba-NAD^+ is shown as cyan sticks. The zinc ion is shown as cyan sphere. (**B**) NAD^+-binding pocket; carba-NAD^+ is shown as cyan sticks.

Notably, Sirt3 crystal structure in complex with the known Sirt1 activator SRT1720, also found to inhibit Sirt3, revealed that SRT1720 binds at the acetyl-lysine binding pocket of Sirt3. [293] The compound makes a tight sandwich-like interaction with the bound NAD^+ cofactor. However, when ADPR was used for crystallisation instead of NAD^+ , no inhibitor molecule was observed in the binding pocket, thus suggesting the importance of SRT1720-nicotinamide interaction. [293]

1.8.2.4.4 Sirt4

Initially, Sirt4 was described as an ADP-ribosyltransferase enzyme involved in the regulation of insulin secretion by ADP-ribosylating the adenine nucleotide transporters (ANT2/3) and the GDH. [294] The ADP-ribosylation of GDH, both substrate of Sirt4 and Sirt3, induces a reduced enzymatic activity. Oxidative deamination from glutamate into α-ketoglutarate, a substrate of tricarboxylic acid (TCA) cycle, is catalysed by GDH. Since elevated cellular ATP levels are determined by improving substrate conversion in the TCA, inhibition of GDH by Sirt4 reduces ATP levels and, thereby decreasing insulin secretion from pancreatic β cells. Recently, Sirt4 has shown to act as a lysine deacetylase, as well. [295] Moreover, its deacetylating activity has been associated with several cellular functions such as cell ageing and proliferation, regulation of lipid metabolism and ATP homeostasis. [296] As the other sirtuins, Sirt4 acts as a tumour suppressor in many types of tumours. [297, 298] To date, Sirt4 has been

reported to also regulate the activity of pyruvate dehydrogenase complex (PDH), a protein complex responsible for the production of Acetyl-CoA, thus acting as a lipoamidase. [299]

1.8.2.4.5 Sirt5

Sirt5 represents the main mitochondrial demalonylase, desuccinylase, and deglutarylase. [211, 300] However it also has a deacetylase activity. Sirt5 exhibits a crucial role in ammonia detoxification through the deacetylation of the carbamoyl phosphate synthetase 1 (CSP1), the rate-limiting enzyme of the urea cycle. [301] CSP1 has been found to be desuccinylated and deglutarylated by Sirt5, too. [211] By desuccinylation of SOD1, Sirt5 reduces cellular ROS levels. [302] Other important targets of Sirt5 are the urate oxidase (UOX) and the HMGCS2, which is involved in the synthesis of ketone in humans. [303, 304] Recently, acyl-CoA dehydrogenase (VLCAD) and cytochrome c, a major regulator of apoptosis and the mitochondrial respiratory chain, have been found desuccinylated and deacetylated by Sirt5, respectively. [260, 305] Moreover, Sirt5 showed to be essential for the metabolic homeostasis under basal conditions. [306] In cardiac phenotype of Sirt5-deficient mice, an enhanced incidence of hypertrophic cardiomyopathy was observed, identifying Sirt5 as a regulator of cardiac function. [307]

1.8.2.4.5.1 Sirt5 crystal structures

Up to date, seventeen crystal structures of Sirt5 from human and zebra fish have been solved (Fig. 1.16).

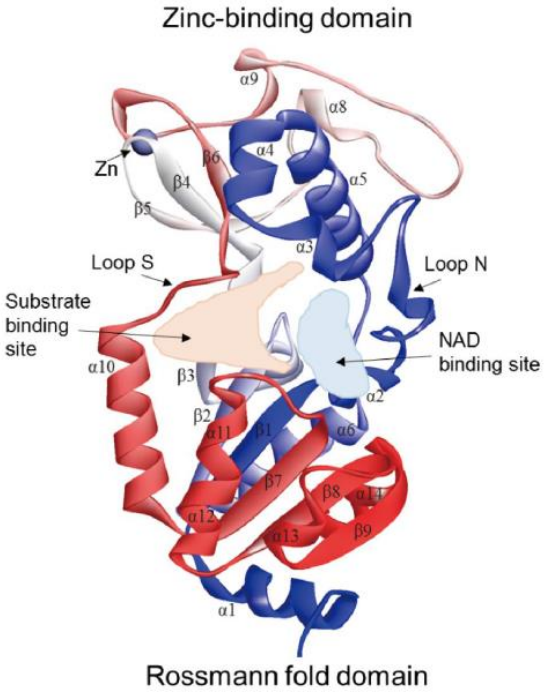

Figure 1.16: The overall structure of Sirt5.

In 2006, the first crystal structures of Sirt5 in complex with ADPR as well as with the drug suramin was discovered. Interestingly, suramin binds to the active cleft located between the substrate and the cofactor-binding pockets of two sirtuin monomers. [308] Since Sirt5 showed to be an effective demalonylase/desuccinylase both *in vitro* and in vivo [309, 310], the analysis of the crystal structure of Sirt5-substrate highlighted the importance of the interaction between succinylated lysine and the side chain of Arg105 and Tyr102 as a mechanism for substrate acyl discrimination. [211] Notably, these amino acid residues produce isotypes and substrate acyl specific inhibitor effects. [311, 312] Furthermore, peptide-based Sirt5 inhibitors developed by acyl-group modifications, were utilised to investigate the effects of substrate lysine modifications in a more systematic fashion. [313] Due to the larger acyl residues, in the Sirt5 crystal structures, Arg105 displays different conformations, allowing its interaction with Tyr102. Thus, analogues of the substrate CSP1 were designed and synthesised by introducing the acyl group at the lysine chain, such as oxalyl, malonyl and succinyl. Crystal structures of zebra fish Sirt5 with the analogues CPS1 peptides exhibit H-bond to Tyr98 as well as a salt bridge between the carboxyl group of the acyl moiety and Arg101, corresponding to Arg105 in human.

1.8.2.4.6 Sirt6

Sirt6 is localised only in the nucleus and has a histone deacetylase, ADP-ribosyltransferase, and lysine deacetylase activity. [314, 315] However, initially Sirt6 was described as ADP-ribosyltransferase due to its low deacetylase activity that is upregulated by long-chain fatty acids. [316]

Importantly, Sirt6 promotes DNA repair through ADP-ribosylation of poly (ADPR) polymerase 1 (PARP1) and the nucleus protein KAP1. [317] Therefore, Sirt6 acts as a regulator of genome stability. [314, 318] Histone substrates of Sirt6 include H3K9Ac and H3K56Ac, and their conversion has been associated with immune modulation, longevity, and DNA repair. [319] By hydrolysing long-chain fatty acyl lysines, Sirt6 controls the secretion of TNFα. [315] Additionally, anti-inflammatory properties have been awarded to Sirt6, due to its implication in rheumatoid arthritis. [320]

1.8.2.4.7 Sirt7

Sirt7 is the least understood sirtuin isotype. Sirt7 is located in the nucleoli where, by deacetylation of a subunit of RNA polymerase I (Pol I) PAF53, activates the rRNA transcription. [321, 322]

Notably, Sirt7 stabilises the transformed state of cancer cells via deacetylation of H3K18Ac. [323] In HCC and colorectal cancer, Sirt7 was found upregulated, and also its depletion markedly suppresses the tumorigenicity. [324, 325] Another vital function of Sirt7 is that to transcriptional regulate the mitochondrial genes by deacetylation and activation of the transcription factor GABPβ1. [326] Further known targets of Sirt7 are the DNA-dependent protein kinase (DNA-PK), p53 and MEF-2C. [327] However, the highly controversial deacetylase activity of Sirt2 is probably due to the very low and

undetectable enzymatic conversion. Tang et al. suggested that Sirt7 deacetylase activity is, however, activate by DNA. [328]

1.9 HDAC inhibitors as anticancer drugs

HDAC inhibition was found to have a substantial effect on their fate. [329] HDAC inhibitors (HDACi) may act specifically against the only several types of HDACs (HDAC isoform-selective inhibitors), but also against all types of HDACs (pan-inhibitors). HDACi can be divided at least into five classes: (I) hydroxamic acids (hydroxamates); (II) short chain fatty (aliphatic) acids; (III) benzamides; (IV) cyclic tetrapeptides; and (V) sirtuin inhibitors including the pan-inhibitor nicotinamide and the specific SIRT1 and SIRT2 inhibitors sirtinol and cambinol, respectively (table 1.4).

Class	HDAC Inhibitor	Target HDAC Class	Clinical Status
hydroxamic acids	Trichostatin A	Pan	Preclinical
	SAHA	Pan	approved for cutaneous T-cell lymphoma
	Panobinostat	Pan	approved for multiple myeloma
	Givinostat	Pan	phase II clinical trials—relapsed leukaemia and multiple myeloma
	Resminostat	Pan	phase I and II clinical trials—hepatocellular carcinoma
	Abexinostat	Pan	phase II clinical trial—B-cell lymphoma
	Quisinostat	Pan	phase I clinical trial—multiple myeloma
	Rocilinostat	II	phase I clinical trial—multiple myeloma
	Practinostat	I, II and IV	phase II clinical trial—prostate cancer
	CHR-3996	I	phase I clinical trial—advanced/metastatic solid tumours refractory to standard therapy
short-chain fatty acids	Valproic acid	I and IIa	approved for epilepsia, bipolar disorders and migraine, phase II clinical trials—several studies
	Phenylbutyric acid	I, II	phase I clinical trials—several studies
benzamides	Entinostat	I	phase II clinical trials—breast cancer, Hodgkin´s lymphoma, non-small cell lung cancer, phase III clinical trial—hormone receptor-positive breast cancer
	Tacedinaline	I	phase III clinical trial—non-small cell lung cancer and pancreatic cancer
	4SC202	I	phase I clinical trial—advanced hematological malignancies
	Mocetinostat	I, IV	phase II clinical trials—Hodgkin´s lymphoma cyclic

tetrapeptides	Romidepsin	I	approved for cutaneous T-cell lymphoma
sirtuins inhibitors	Nicotinamide	all class III	phase III clinical trial—laryngeal cancer
	Sirtinol	SIRT 1 and 2	Preclinical
	Cambinol	SIRT 1 and 2	Preclinical
	EX-527	SIRT 1 and 2	cancer preclinical, phase I and II clinical trials—Huntington disease, glaucoma

Table 1.4: Overview of selected HDAC inhibitors.

(I) Trichostatin A (TSA) was the first natural hydroxamate identified as HDACi but due to its toxicity is used exclusively in laboratory experiments. Vorinostat (suberoyl hydroxamic acid, SAHA) is structurally similar to TSA and was the first Food and Drug Administration (FDA)-approved HDACi for the treatment of relapsed and refractory cutaneous T-cell lymphoma in 2006. (CTCL). Belinostat (PXD-101), and Panobinostat (LBH589) have been approved by FDA for therapy of peripheral T cell lymphoma (PTCL) and multiple myeloma (MM) in 2014 and 2015, respectively. Currently, the pan-HDAC inhibitors givinostat (ITF2357), resminostat (4SC201), abexinostat (PCI24781) and quisinostat (JNJ-26481585) are under clinical investigation. Moreover, selective HDACi such as rocilinostat (CY1215, a selective class II inhibitor) that belongs to the group of hydroxamic acids and CHR-3996, a selective inhibitor of class I, undergo clinical trials, too.

(II) The aliphatic acids, such as valproic acid (VPA), butyric acid and phenyl butyric acid are relatively weak HDACi. VPA is registered for the therapy of epilepsy, bipolar disorders, and migraines and is now tested in clinical studies as an anticancer drug.

(III) Entinostat (MS-275-SNDX-275), tacedinaline (CI994) and 4SC202 are benzamide derivatives that inhibit class I HDACs. Mocetinostat (MGD0103) is a selective inhibitor of classes I and IV HDACs.

(IV) The cyclic tetrapeptides include the bicyclic depsipeptide romidepsin (FK228, FR901228), approved by FDA and EMA for the treatment of CTCL in 2009. Depsipeptide is a unique HDAC pro-drug, which is converted and reduced intracellularly into a form containing a functional sulphydryl group that binds to the zinc in the active site pocket of class I HDACs. [330]

(V) Among sirtuin inhibitors, nicotinamide (pan-inhibitor) and the specific SIRT1 and SIRT2 inhibitors sirtinol, cambinol and EX-527 are now under evaluation in different types of neurodegenerative disorders and cancers. [331]

Therefore, various compounds with HDAC inhibiting activity are now preclinically investigated. The typical side effects of those HDACi, which are not the class-specific and have been observed in all their types, are thrombocytopenia, neutropenia, diarrhoea, nausea, vomiting, and fatigue. [332]

HDACi induce cancer cell cycle arrest, differentiation and cell death. Moreover, they reduce angiogenesis and modulate immune response. [333] The hypothesis of "epigenetic vulnerability of

cancer cells", proposed by Dawson and Kouzarides, [334] is a cause of relative specificity of HDACi. In fact, this hypothesis supposed that normal and cancer cells have differing multiplied epigenetic regulatory mechanisms. Thus, HDACs may be vital for the maintenance of a set of key genes needed for survival and growth of cancer cells but not of normal ones. [334]

Mechanisms of anticancer effects of HDACi are not uniform; they may be different and depend on a type of cancer, on the individual HDACi and its dose. [335] However, it is thought that normal cells are relatively resistant to HDACi treatment, whereas cancer cells are more sensitive and undergo growth arrest, inhibited differentiation and cell death (Fig. 1.17). [336, 337]

In many tumour cell lines, HDACi cause upregulation of the cell cycle gene p21 by blocking the cyclin/CDK complexes, thus leading to cell cycle arrest and inhibiting differentiation. [338, 339]

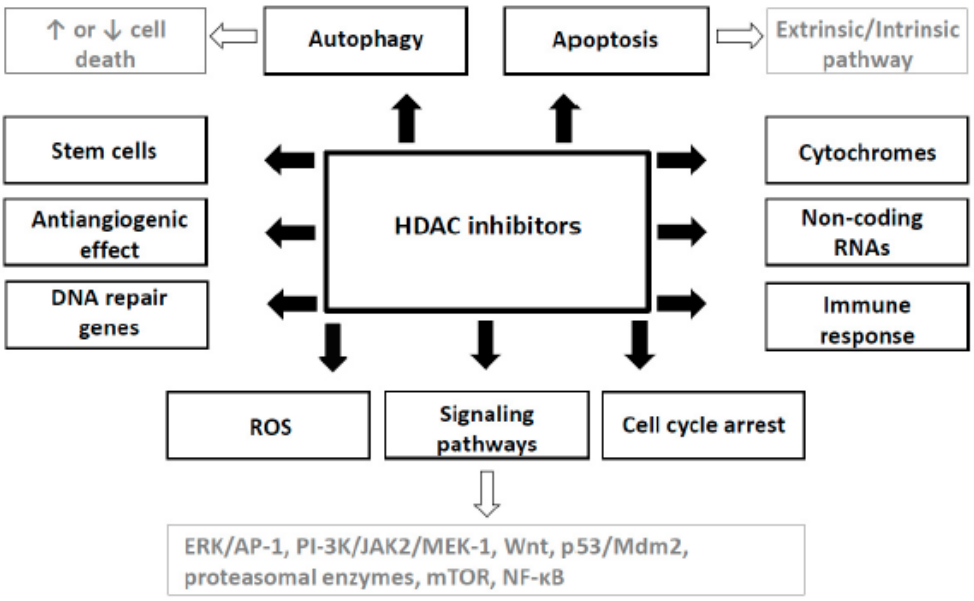

Figure 1.17: Mechanism of anticancer effects of HDAC inhibitors. [340]

Moreover, by modulating the balance between pro- and anti-apoptotic proteins, HDACi cause tumour cell death. [341] Pro-apoptotic genes Bmf and Bim, and TRAIL and DR5 induced by HDAC inhibition that upregulates the intrinsic and extrinsic apoptosis pathways. [342, 343] Overall, in tumor cells exposed to HDACi pro-apoptotic genes involved in the extrinsic (TRAIL, DR5, FAS, FAS-L, and TNF-α) and/or intrinsic apoptotic pathways (BAX, BAK and APAF1) are up-regulated, while anti-apoptotic genes (Bcl-2 and XIAP (X-linked inhibitor of apoptosis protein)) are downregulated. [344]

Hyperacetylation of p53 promotes both cell cycle blockage and the expression of pro-apoptotic genes. [345] HDAC inhibition also increases the stability and transcriptional activity of RUNX3, which in turn induces p21 and Bim, leading apoptosis and cell cycle arrest of tumour cells. [346, 347] By blocking tumour angiogenesis and inhibiting intracellular stress response pathway, HDACi may also compromise

tumour cell survival. [348] Additionally, HDACi can affect cancer angiogenesis and inhibit cellular stress response pathways, thereby interfering with the metastatic process.

Indeed, HDAC inhibition influences stress responses by decreasing the expression of VEGFR, increasing the formation of intracellular ROS, and affecting the handling of misfolded proteins. [349, 350] Hyperacetylation of the chaperone protein HSP90 by HDACi results in the degradation of cancer-related client proteins, thus leading the dysregulation of chaperone activity which is to protect client proteins from their degradation. [351]

However, the role of HDACi induced autophagy in the death of cancer cells is still controversial. [352, 353]

The effect of HDAC inhibition has also been investigated in cancer stem cells. Indeed, epigenetic changes are crucial for reprogramming of somatic cells into pluripotent stem cells. [354] It was described as HDACi can maintain normal human hematopoietic stem cells by modifying chromatin structure and make it more accessible to transcription factors. [355] A recent study showed that HDACi such as VPA, SAHA, and MS-275, increase the expression of CD133, a marker of cancer stem cells, in neuroblastoma cancer cells. [356]

Further understanding of the mechanisms of action of HDACi are certainly needed to overcome their major limitations, such as toxicity.

Chapter 2: Polypharmacology in epigenetics

2. Polypharmacology

For many years, many efforts have been provided to overcome the major limitations of current therapies that mostly rely on the development of target-specific inhibitors. More than 150 years ago, Paul Ehrlich coined the term “magic bullet” that means the pharmacological therapy can provide an effective remedy for a disease or condition without deleterious side effects. This concept has long been debated by many health professionals and researchers because of the off-target responses which may involve toxicity. Importantly, even selective drugs are not free by drug-drug interactions, which also represent a challenge, especially for chronic diseases. [357] Based on these evidences, pharmaceutical companies, as well as scientific organizations, wondered whether target-based drug discovery approach was a better choice than multi-target modulation for successful therapies. [358] The right answer may be searched in the etymology of the term “polypharmacology”.

Polypharmacology means the capability of one drug to simultaneously and specifically interact with multiple targets. This potential and innovative therapeutic approach relies on the search of “master key compounds” to fight several multifactorial pathologies, such as central nervous system (CNS) disorders that required the use of different medicines due to the complexity instead of single-target inhibition. [359]

A “master key compound” is essentially a molecule that binds to a given number of targets, thus producing beneficial effects without affecting undesirable off-targets. [360]

The interest in the polypharmacology field has been increased significantly, with almost 200 articles published in the past three years. [361] However, the road ahead in polypharmacology drug discovery might be hard to achieve, the development of poly-drugs is currently possible. Computational methods, as well as tools for in silico drug discovery, represent certainly a starting point for the development of multi-target compounds. Indeed, more effective drugs could be obtained through a multi-target approach, even though is more complicated than the one drug- one target strategy. [362] Generally, the combination of two or more drugs with diverse target properties may lead to unexpected side effects due to their interaction in human bodies. [363] Such interactions can depend on several factors including the nature of the drug structures, the target as well as drug concentrations. Therefore, poly-drugs may have a “dual-face”.

2.1 Polypharmacology in drug discovery

Currently, most concepts in drug discovery refer to the interaction of one drug with multiple targets. In this regard, drug “repurposing” or “repositioning” takes place as an innovative view for the identification of a novel clinical use for compounds already approved for a particular disorder. [360] The

most relevant features of drug repurposing involve that drugs may have activity against more than one target, thus being poly-drugs. For many years, more than one definition of repurposing concept has been proposed. However, recently, Langedijik *et al.* [364] tried to uniform such diverse and sometimes opposite definitions to offer an overview of the main characteristics that include:

a) general concept: strategy, process, approach; b) action performed: identifying, using or developing;

c) innovative use: for a different disease, patient population, dosage or route of administration; d) the product itself: an existing or abandoned pharmaceutical active ingredient, patent, medicinal product, and so on.

To date, several potential activities have been attributed for some compounds, and further investigation is undoubtedly needed to evaluate if alternative activities of these compounds can be validated and, thereby, approved for alternative indication. For example, olsalazine, an anti-inflammatory drug, was identified by chemoinformatic-based virtual screening approaches a novel hypomethylating agent. [365] Thus, olsalazine is currently under investigation as a potential epigenetic drug. Looking into this proof-of-concept, additional computational studies have been carried out aiming to repurpose approved drugs as potential epi-drugs.

2.2 Polypharmacology in epigenetic: from single to multi-target approach

The increasing number of epi-drugs therapies targeting multiple disorders, first of all, cancer, sometimes fail in clinical trials due to the dynamic and reversible nature of epi-modification. However, the multi-target approach might be useful and effective to overcome potential mechanism(s) of resistance caused by redundancy and robustness of biological pathways. Various signal pathways, as well as cross-talk among genetic, epigenetic and biological processes, require, therefore, a more complex therapeutic approach. Indeed, it becomes increasingly evident that aiming at a single pharmacological target would not be an accurate strategy. Epigenetics play a key role in the establishment and maintenance of several diseases including diabetes, cancer, autoimmune and neurodegenerative disorders. Since the complexity of epigenetic mechanism is not yet fully elucidated, it appears very difficult to design therapies targeting them. In fact, only a few epi-drugs have been approved for the treatment of malignancies with positive outcomes. [366, 367] Currently, the trend to shift towards epi-polypharmacology drugs has been taken into account in order to acquire a superior therapeutic effect and eventually reduce drug-related doses and toxicity, as well. [358] However, predicting the efficacy of multi-target drugs in complex systems is more difficult than in a single-target based approach. Notably, many different epigenetic biological targets share cofactors, such as NAD^+ and Zn^{2+}, thus is possible to drive the design and synthesis of cofactor inhibitors with polypharmacological properties. [368] Another relevant approach is the design of hybrid compounds that share structural elements containing in different epi-drugs that bind to their specific epigenetic target. So, the use of hybrid molecules or drug combinations seems to be a promising strategy for personalised medicine. This approach has led the

development of pan-demethylase inhibitors by combining the pharmacophore of both histone demethylases LSD1 and JmjC inhibitors, thus producing molecules with an increased methyltransferase activity towards H3K4 and H3K9. Moreover, the new hybrid molecule shows selective apoptosis for cancer cells, without affecting normal cells. In other cases, compounds though to selectively inhibit specific epigenetic targets revealed polypharmacology against other epi-targets. [369] That phenomena happened when our research group developed analogues of AMI-5, a small molecule inhibitor of protein arginine and histone lysine methyltransferases. In fact, some of the AMI-5 derivatives display activity towards multiple epigenetic targets, including protein and histone methyl and acetyltransferases. [370]

2.2.1 Single epi-target approach

Drug discovery process can be described at least by three fundamental steps: the identification of the target, the discovery of molecules modulating its function and the evaluation of the drug efficacy in *in vivo* models (Fig. 2.1).

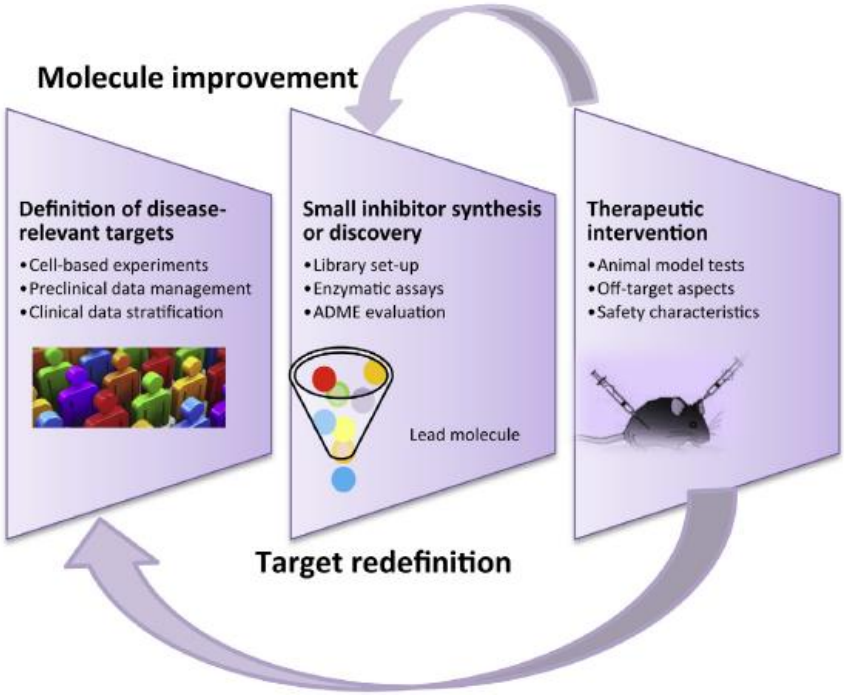

Figure 2.1: Drug discovery process.[371]

The "ideal" molecule must be highly selective, specific and potent against a specific target. The first step in drug discovery process is the analysis of chemical libraries of small synthetic molecules or natural products to identify substances that have a desirable therapeutic effect. It has become common practice to use high throughput screening of large compounds libraries to identify hits that are then tested in cells, and then in animals for efficacy.

Overall, modern drug discovery involves the identification of screening hits, medicinal chemistry and optimisation of those hits to improve the affinity, selectivity, efficacy/potency, metabolic stability, and oral bioavailability. Once a compound that fulfils all of these requirements has been identified, it will begin the process of drug development before clinical trials.

However, it is very difficult to find hit compounds that comply with all of the previously mentioned characteristics, probably due to intrinsic cell biology. For example, TSA is a very potent but toxic HDACi, thus there are no possible clinical applications. [372] It is known that the network system involves resistance mechanisms to bypass the drug-induced inhibition/activation effect, thus reducing drug efficacy as well as potency in vivo. Moreover, many epi-enzymes exist as large families so that cross-talk interactions can be observed and, in addition, their inhibition can affect both cancer and normal cells. [373, 374] Although targeting redundant enzymatic classes, HDACi and DNMTi represent the first epigenetic-based mono-therapies approved by FDA, while several histone demethylases and methyltransferase inhibitors are currently in clinical trials. In Table 2.1 epi-drugs approved by FDA or in current clinical trials are reported.

	Compound	Target specificity	Indication	Status
1	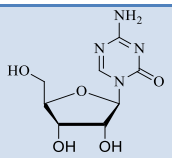 Azacitidine	DNMT	Myelodysplastic syndrome	Approved FDA, 2004
2	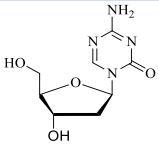 Decitabine	DNMT	Myelodysplastic syndrome	Approved FDA, 2006
3	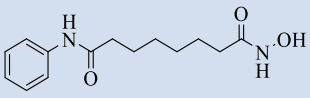 Vorinostat	HDAC	Cutaneous T-cell lymphoma	Approved FDA, 2006
4	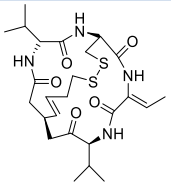 Romidepsin	HDAC	Cutaneous T-cell lymphoma	Approved FDA, 2009

5	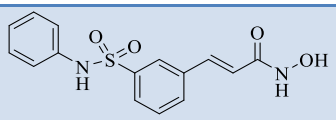 Belinostat	HDAC	Peripheral T-cell lymphoma	Approved FDA, 2014
6	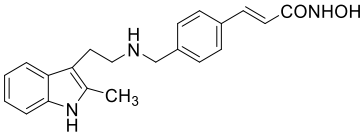 Panobinostat	HDAC	Multiple mieloma	Approved FDA, 2015
7	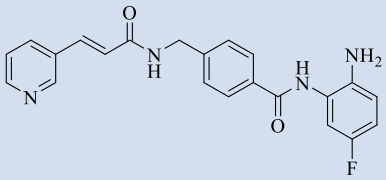 Chidamide	HDAC	Peripheral T-cell lymphoma	Approved CFDA, 2006
8	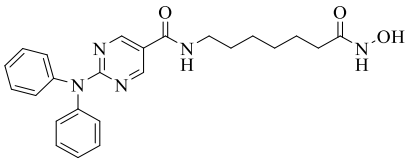 Rocilinostat	HDAC6	Multiple myeloma	Phase II
9	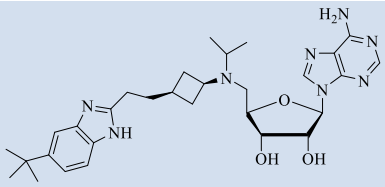 EPZ-5676	DOT1L	Mixed-lineage Leukaemia (MLL)	Phase I
10	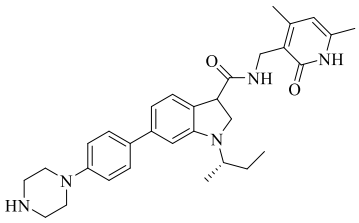 GSK2816126	EZH2	Acute myeloid leukaemia, Non-Hodgkin lymphoma and Multiple myeloma	Phase I/II
11	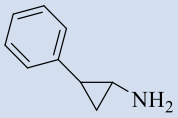 Tranylcypromine	LSD1	Acute Myelogenous Leukaemia	Phase I

12	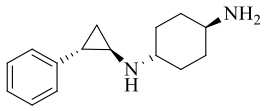 ORY-1001	LSD1	Leukaemia	Phase I/II
13	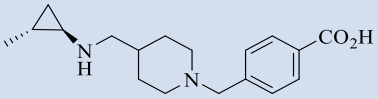 GSK2879552	LSD1	Leukaemia	Phase I
14	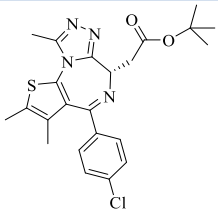 JQ1	BET family bromodomain	A variety of cancers including Nut midline carcinoma	Phase I

Table 2.1: Approved epigenetic modulators and potential clinical candidates.

Certainly, in some cases single-target display high selectivity, thus providing maximal efficacy and minimal side effects. One example of effective single-target drugs is the class of EZH2 inhibitors, such as GSK126, one of the most selective small molecule inhibitors of EZH2. [375] Other known single-target agents, belonging to the same class of GSK126, are EPZ-6438, EPZ005678 and EI1, found to be powerful and selective mutated EZH2 inhibitors. EPZ-6438 is more effective in EZH2-mutant NHL, inhibiting selectively H3K27 methylation in lymphoma and other cancer cells. [147, 155, 376] In 2013, a phase I/II clinical trial of EPZ-6438 for the treatment of relapsed or refractory B-cell lymphoma or advanced-state solid tumours was opened (NCT01897571).

2.2.2 Combination epi-therapy

Inhibitors already validated as effective in monotherapy might be combined to increase efficacy. Indeed, the combination of single epi-drugs with known efficacy as monotherapy can offer many advantages. Since all molecules used in combination have *well-known* molecular targets, the major effort is to identify unexpected interactions between molecules in cellular pathways involved in the same pathology, seeking for synergistic or additive effects. However, different PK, as well as PD properties of combined drugs, might prevent any synergistic/additive effect. For example, in early phase, clinical trials HDACi, used as single agents, have shown limited benefit for the treatment of myeloproliferative disorders. However, in various cancer cell lines, by inhibiting DNA methyltransferase (DNMT) activity, co-administration of HDACi synergistically improve the expression of silenced tumour suppressors and

promote cell death and differentiation. [377, 378] Currently several clinical trials are evaluating the effect of decitabine in combination with SAHA [379] (NCT00275080, NCT01130506, NCT00882206, NCT00357708, NCT01483690, NCT00479232, NCT01593670, NCT02412475), mainly for the treatment of MDS. Moreover, many other trials combining HDACi and DNMTi are ongoing [373, 380]. In phase II (NCT00477386) and phase I/II (NCT01498445) clinical trials, decitabine was combined with carboplatin [381] or decitabine (Dacogen) [382] for the treatment of ovarian cancer and chronic myeloid leukaemia (CML), respectively.

Preclinical and clinical studies have been carried out to demonstrate that the inhibition of HDAC activity enhances the antitumor effect of tamoxifen in several ER-positive breast cancer cell lines and tamoxifen resistant-breast tumours. (NCT00365599, NCT01194427, NCT02395627).

2.2.3 Multi epi-target approach

As aforementioned, the principle of multi-target chromatin-modifying drugs is the design and synthesis of small molecules capable of interacting simultaneously with different epigenetic marks, such as histone acetylation/methylation and DNA methylation. Ideally, a multi-target epi-drug redresses the action or expression of several proteins contributing to disease status, rather than completely deleting the function of a single target which affects dramatically cellular pathways and network (Fig. 2.2).

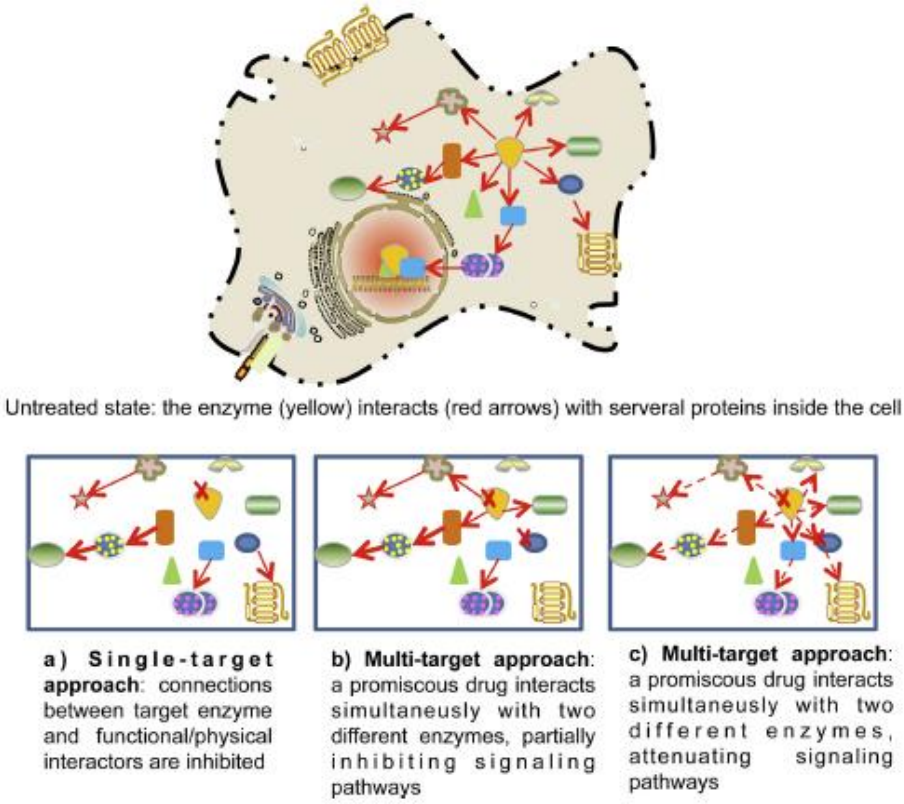

Figure 2.2: Single-target versus multi-target approach. The cellular network, composed of several molecular entities (shapes) interacting with each other (arrows) in a physical or functional way, is schematically reported. Shapes and arrows are both

potentially druggable. The node is here reported as a point connected by a large number of arrows. Arrows proceed from one molecule to another and have different prevalence as indicated by thicker lines. [371]

Therefore, the multi-target approach evaluates the effect of drugs within the cellular context composed of several molecular entities that interact with each other in a functional way. While a single-target approach abolishes all possible interactions of the selected target, a multi-target approach involves either the partial inhibition or modulation of selected targets, thus enabling to guide a pathway in the desired direction. [371]

Multi-targets strategies interfering with the natural direction of a signalling pathway may improve the efficacy of inhibitory effects, thus obtaining the desired result.

Multi-target epi-drugs are mostly obtained by fusing two or more molecules targeting different enzymes. Fusion can be achieved by connecting compounds with a linker that is removed under physiological conditions (pro-drugs) or by a stable linker allowing an individual element of a drug to interact with its specific target without interferences by its counterpart.

Finally, a third option is to fuse molecules together by preserving and connecting only reactive and functional groups (usually the pharmacophores). The latter more complicated strategy allows to produce hybrid molecules (Fig. 2.3).

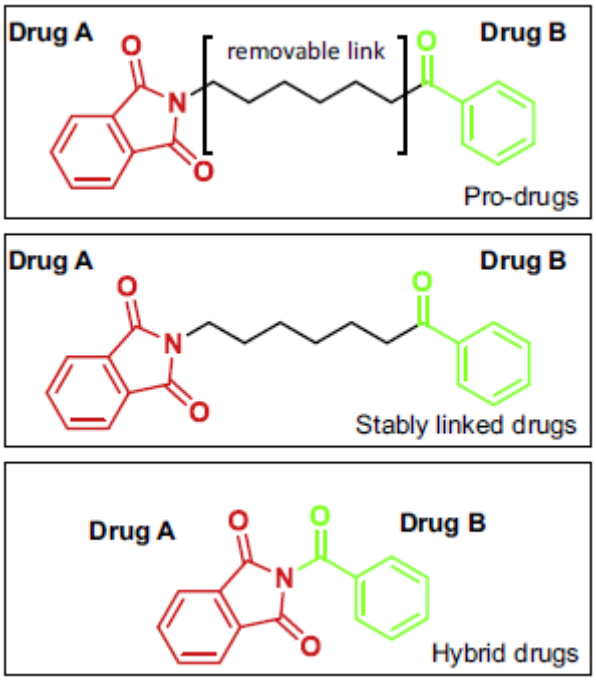

Figure 2.3: Schematic representation of fused molecules (pro-drugs, stably linked drugs, and hybrid drugs). [371]

Multi-target epi-drugs comprise molecules that act individually on one or more epigenetic targets or can regulate different pathways involved in the same pathology, such as cancer. [383] Overall, the pros and cons of epi-drug discovery approaches are depicted in table 2.2.

	PROS	CONS
Single-target epi-drugs	• Highly selective for disease-relevant single targets • In vitro assays • One pharmacokinetic and pharmacodynamic analysis • Conventional clinical trials	• Complex biochemical processes • Resistance mechanisms • Unexpected side effects • High toxicity
Multi-target epi-drugs	• Simultaneous inhibition • Reduced toxicity • Standard development program • Standard clinical trials • Multi-selective action	• Complex chemistry • Costly production • Non-selective action • Low potency • Impossible to obtain "in sequence" activity
Combination of epi-drugs	• Many combinations available • Sequenced action • Flexible formulation • Combination of dosages • Proof-of-concept clinical trials • Drug repositioning	• Different pharmacokinetics and pharmacodynamics to combine • "Combination versus part" clinical trials • Drug-drug interaction • Unexpected side effects

Table 2.2: An overview of the pros and cons of epi-drugs discovery approaches.

2.3 Molecular hybrids in drug discovery

The hybridisation of biologically active compounds is gaining momentum worldwide because it is considered a powerful tool for drug discovery used to target various diseases, such as cancer, tuberculosis, and HIV. Indeed, hybrid molecules can offer a better therapeutic outcome for the treatment of serveral illnesses than conventional classic cure. These superior chemical entities possess druggable properties with potential enzymatic activity against two or more different enzymes.

In the last few years, molecular hybrids investigation is becoming an attractive topic for many researchers, thus is in great expansion. The main goals for designing hybrids are: (a) to achieve improved activity, (b) to gain higher selectivity, (c) to lower toxicity of drugs. [384]

2.3.1 An overview of drugs as multi-target epigenetic modulators

The most exciting strategy in polypharmacology is, therefore, combining pharmacophores for multiple epigenetic targets in a single molecule. In figure 2.4 are reported two molecules (**15**, **16**) obtained by chemical manipulation of the natural products curcumin and psammaplins, respectively. At 1 µM, compound **15** displayed an inhibitory activity against histone methylation, acetylation, and deacetylation, while compound **2** inhibited HDAC1, DNMT and SIRT1. [385] Furthermore, our research group working on analogues of the lysine-specific demethylase inhibitor tranylcypromine (**17**, Fig. 2.4), discovered a dual inhibitor of lysine demethylation (simultaneously targeting LSD1/JmjC lysine

demethylases) by both mechanisms of action, probably due to the introduction of an additional metal binding motif. [369]

GlaxoSmithKline developed dual HDAC inhibitors by modifying a hit series for bromodomain binding. Among the newly derivatives, compound **18** (Fig. 2.4) was found to inhibit both HDAC1 and BRD4, with an IC_{50} value of 250 nM and a K_d of 50 nM, respectively. Additionally, **18** was able to increase H4 acetylation levels and decrease c-myc levels in cells, as well. [386] Unfortunately, a pharmacological combination of single HDAC and BRD inhibitors displayed a superior inhibitory effect than **18**. However, dual targeting agents have also been designed with the aim to get an improvement of the primary epigenetic mechanism of action. In this perspective, the clinical candidate HDACi MS-275 was conjugated to a NO donor to effort compound **19** (Fig. 2.4). The novel hybrid **19** was effective against HDACs and cyclic GMP signalling pathway by enhancing the post-translational S-nitrosylation of HDAC2, probably due to the increased NO levels. [387] Over the last years, great efforts in the development of bromodomain ligands as potential therapeutic targets have been provided. The major limitations, however, arise from their transient effect that can be reversed by increased expression of the target bromodomain. To overcome this issue, very recently the bromodomain JQ-1, which displays a nanomolar activity, has been linked to thalidomide, a drug used for the treatment of MM. Thalidomide's mechanism of action consists of the recruitment of cereblon, a cullin-dependent ubiquitin ligase that marks protein for degradation by the proteasome. Two hybrid compounds (**20**, **21**, Fig. 2.4) have been synthesised showing promising cellular effects by binding their bromodomain targets. Indeed, **20** and **21** hamper the recruitment of cereblon, thus affecting protein degradation. Additionally, when compared to JQ-1, they showed a longer lasting effect. Surprisingly, compound **7** also provided efficacy in a mouse AML xenograft at 50 mg/kg. [388, 389]

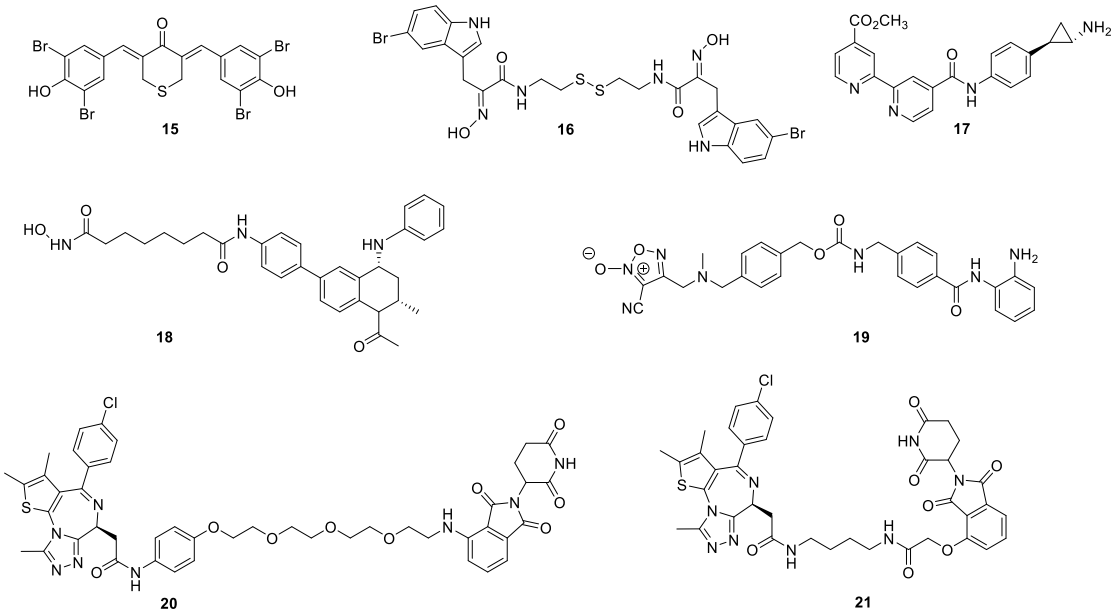

Figure 2.4: Examples of dual epigenetic targeting compounds.

2.3.2 HDAC inhibitors in polypharmacology

HDACi are mainly investigated as dual targeting agents because of their wide structural variety and feasibility to accommodate on the surface binding cap a high degree of different chemical entities. Due to the importance of the zing binding group (ZBG) in HDAC inhibition, different chemical moieties inhibiting the same or another epi-enzyme have been attached to *well-known* HDACi through an appropriate linker. [390] Rationale for the development of multi-targets HDACi arises from several studies wherein synergistic effects by co-administration of HDACi with other epi-drugs have been observed. For example, in *in vivo* and *in vitro* model studies the simultaneous intake of HDACi and tyrosine kinase inhibitors (TKi) enhance the final anti-cancer effect. [391] Some of the approved TKi have been chosen to design novel dual HDAC/TK inhibitor such as lapitinib (**22**, Fig. 2.5) [392], ruxolitinib (**23**, Fig. 2.5) [393], and piclilisib (**24**, Fig. 2.5). [394] As aforementioned, the hybrid compounds are characterised by a hydroxamic acid or benzamide as ZBG connected by different linkers to the kinase inhibitors scaffold.

One of the most interesting hybrids is CUCD-101, got by chemical manipulation of erlotinib with the introduction of the hydroxamic acid group and a spacer linked to the quinazoline moiety. CUCD-101 showed to inhibit HDACs in the nanomolar range, EGFR and the human epidermal receptor 2 (HER2) in carcinogenesis. Moreover, CUCD-101 can regulate both proliferation and migration state of erlotinib-resistant non-small cell lung carcinoma (NDCLC) HCC827 through the downregulation of E-cadherin and MET, AKT and HER3 compensatory pathways. [395, 396] To date, this novel modifier is in phase I/Ib trials to evaluate its safety and oral tolerability in cancer patients. Recently, a phase Ib open-label study is underway to evaluate the effect of CUCD-101 in patients with advanced head and neck, liver, gastric, and breast cancer as well as NSCLC (ClinicalTrials.gov Identifier: NCT01171924). Numerous other inhibitors have been synthesised starting from the quinazoline scaffold. [397, 398] Among them, the hydroxamic acid lapitinib analog (an EGFR/HER2 TKi) showed dual nanomolar inhibition against HDACs and EGFR/HER2 kinases, thus is in advanced clinical trials. In literature were also reported some examples of molecules able to interact with HDACs even with non-kinase targets. [399, 400] Pursuing the idea of “combined therapy” as well as innovative multi-target drugs, a very promising approach is representing by dual HDACs/LSD1 inhibitors. Both epigenetic targets are overexpressed in several types of human cancer cell lines inducing the tumour suppressor genes silencing. Simultaneous inhibition of HDAC and LSD1 results in a synergic activity to fight cellular growth, migration, and invasion.

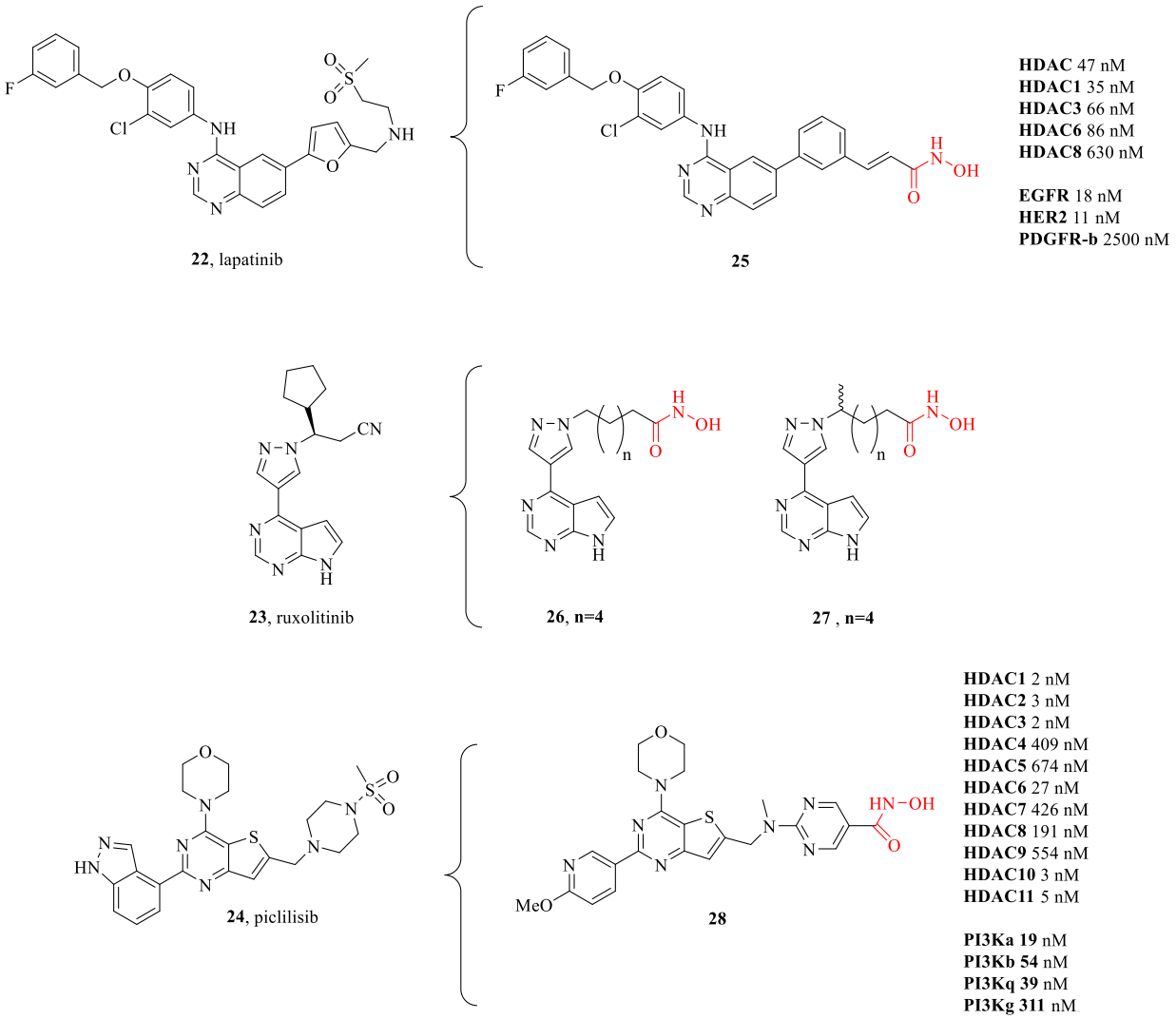

Figure 2.5: Structures and IC_{50} values of selected dual HDAC/TKi inhibitors. (adapted from Epigenetic polypharmacology: a new frontier in epi-drug discovery, Tomaselli *et al.*, not yet submitted).

Noteworthy, in the series of N-substituted tranylcypromine derivatives linked to hydroxamic portion, a novel dual HDAC/LSD1 inhibitor has found to inhibit LSD1 in the micromolar range and HDAC1/2 in a nanomolar range, respectively. However, a weak MAO-A inhibitory effect has been observed, as well. Moreover, it displayed a strong anti-proliferative activity in A-549, MCF-7, MCF-803, SW-620 human cancer cell lines. [394] Furthermore, the goal to target both HDAC and BRD4 arises from the evidence that both enzymes take part in acetylation processes with similar genetic and biological effects. So, many studies have been carried out to design novel HDAC/BRD4 inhibitors. [401-403] Very recently, Kalin *et al.* developed a series of dual HDAC/LSD1 inhibitors targeting the CoREST complex. Among the newly derivatives, a novel dual HDAC/LSD1 inhibitor, obtained by linking the benzamidine as ZBG to an amine oxidase warhead through a propyl-phenyl portion, was found to create a ternary complex 1:1:1 HDAC1:LSD1:CoREST stoichiometry showing almost irreversible HDAC1 inhibitory activity with a quite LDS1 inhibition and an interesting selectivity against MAO A and B, and LSD2. In cell-based assays, it

exhibited a superior anti-proliferative activity against cutaneous squamous carcinoma and various melanoma lines than MS-275. Additionally, it also displays a lower toxicity towards keratinocytes and melanocytes. [404]

2.3.3 EZH2 in polypharmacology

In 2015, Xu *et al.* reported for the first time specific enzymatic dual inhibition of EZH2 and EZH1 as a promising therapeutic strategy for MLL-rearranged leukaemia. [154] They show that the dual inhibitor UNC1999 was able to reduce efficiently cell proliferation both *ex vivo* and *in vivo*, even more efficiently than the selective EZH2 inhibitor GSK126. The importance of this study targeting simultaneously EZH1 and EZH2, rely on the possibility to further investigate the function and role of EZH1 that still remain unclear and poorly understood. The interest in EZH2 in combination therapy has grown considerably over the last few years. For example, in preclinical models of EZH2-mutant NHL, EPZ-6438 was combined with either conventional NHL-directed chemotherapy [405] or with prednisolone, a glucocorticoid receptor agonist (GRag). GSK126 and etoposide association was evaluated in prostate cancer, as well. [406] Recently, an important patented study (WO 2014077784) described how the association between EZH2 inhibitors and IFNγ for cancer treatment led to sensitise MYC-dependent prostate cancer cells (DU145, PC3) to IFNγ treatment by inhibiting EZH2 activity. Currently, combining EZH2 inhibitors with several epigenetic drugs is a valuable strategy, as suggested by several scientific evidence proving epigenetic crosstalk. [407] A recent study on glioblastoma brain tumour-initiating cells (BTIC), reported first that the EZH2 inhibitor UNC1999 showing a cytotoxic activity in the low micromolar range in different BTIC, also had synergistic effects with dexamethasone. In details, UNC1999 in combination with dexamethasone efficiently arrested tumor growth *in vivo*. In addition, in the same cell lines, the combination of EZH2 and HDAC inhibitors displayed synergistic effects *in vitro*, increasing apoptosis and causing DNA damage. [408]

Very recently, the multi-target approach has also been applied to design novel epi-drugs targeting EZH2, with promising results in cancer. Fox example, several studies have been carried out to realise dual G9a/EZH2 inhibitors as potential therapy for triple negative breast cancer. Specifically, using a cell-based assay, based on the substrate competitive EHMT2 inhibitor BIX01294, Curry *et al.* identified proof-of-concept compounds able to induce re-expression of a subset of genes consistent with dual HKMT inhibition in MDA-MB-231 breast cancer cells. [409] In another study, Coward *et al.* discovered a dual inhibitor of G9a/EZH2 that mediates the upregulation of genes typically repressed by EZH2 (JMJD3, KRT17, FBX032) at 10 Um and the downregulation of H3K9Me2/ H3K27Me3 methylation levels. [410]

3 Design, synthesis and biological evaluation of novel SIRT3/5 activators

3.1 Sirtuin modulators

The potential role of sirtuins in the pathogenesis of several disorders has prompted research groups worldwide to develop small-molecule modulators of sirtuin activity. Thus, innovative approaches, such as high-throughput screening, fragment-based or computer-based screening have been applied with the aim to identify novel sirtuin modulators. However, despite very little information about sirtuin modulation, the use of silico methods allowed to discover several promising sirtuin modulators. To date, the clinical potential of sirtuin inhibitors still remains unknown and, only one sirtuin inhibitors, selisistat, has entered clinical trials [241, 411], probably due to the lack of potency, isotype selectivity or suitable physicochemical properties of SIRT inhibitors. Nowadays, most sirtuin inhibitors target Sirt1-3 and, very recently, Sirt4-7 pharmacological inhibition is also under investigation.

3.1.1 Small molecules inhibitors of Sirtuins

Class III HDACs, known as sirtuins, are linked to several age-related diseases, such as cancer, diabetes, cardiovascular diseases, inflammation and neurodegeneration as presented in chapter 1. Most of the research focused on the role of SIRT1 and SIRT2 on the regulation of H4K16 acetylation and the association with gene silencing, as well as on p53 deacetylation and the resulting decreased tumour growth. By phenotypic assay, SIRT inhibitors have revealed beneficial effects against misfolded protein-related diseases and, presumably, these compounds can be used in several neurodegenerative diseases such as Parkinson and Huntington diseases; inhibitors are furthermore designed for the treatment of cancer, muscle disorders, and HIV infections. [286, 412, 413]

Many SIRT modulators, used alone or in combination with other epigenetic modulators or known drugs, have been described so far. [414]

Nicotinamide (NAM) (**1**, Fig. 3.1) is one of the products of the deacetylation catalysed by sirtuins. **1** is the endogenous inhibitor of all sirtuin isotypes and, in particular, inhibits both SIRT1 and SIRT2 with an IC_{50} of 50 µM and 100 µM, respectively. [415]

Identified in 2001 from a yeast-based screening for inhibitors of Sir2, splitomicin (**2**, Fig. 3.1), despite being substantially inactive against hSIRTs, was the starting point for the development of several SIRT1/2 inhibitors. Among them, HR-73 was found to inhibit SIRT1 in a single-digit micromolar and impair HIV transcription through affecting the Tat protein acetylation (**3**, Fig. 3.1). [413]

In 2005, scientists of Elixir Pharmaceuticals discovered the indole EX-527 (Selisistat or SEN0014196) (**4**, Fig. 3.1), the first drug-like and selective Sirt1 inhibitor. With an IC_{50} value of 98 nM, EX-527 belongs to

the most potent Sirt1-selective inhibitors until now. Both EX-527, as well as its analog CHIC35 (**5**, Fig. 3.1) [414], have a carboxamide moiety mimicking the amide group of nicotinamide. Among all reported beneficial effects, the most promising one was the alleviation of pathology in multiple animal and cell models of Huntington's disease after treatment with **4**. [416] Meanwhile, EX-527 has completed Phase I and Phase II clinical trials for the treatment of Huntington's disease and was found to be safe and well tolerated. [240, 241]

In 2001, by a high-throughput phenotypic screen, Grozinger *et al.* identified the hydroxynaphthaldehyde derivative sirtinol (**6**, Fig. 3.1) as a dual Sirt1/2 inhibitor. [417] Although varying IC_{50} values have been published, sirtinol seems to inhibit Sirt2 slightly better than Sirt1. Two further inhibitors with a hydroxynaphthaldehyde scaffold are salermide (**7**, Fig. 3.1) and cambinol (**8**, Fig. 3.1). [220, 418]
Salermide, which is analogue of sirtinol with "reverse amide" structure, is a selectiveSirt2 inhibitor that induces tumour-specific cell-death in a wide range of human cancer cell lines (mainly MOLT4, KG1A, SW480, and Raji). [418, 419] **7** induces cancer-specific pro-apoptotic effect by reactivating pro-apoptotic genes, such as CASP8, TNF, TNFRSF10B, and PUMA and up-regulating DR5. [420]

On the other hand, cambinol was discovered in 2006 as a moderate SIRT1/2i that induces hyperacetylation of p53, α-tubulin, FOXO3a, and Ku70 in NCI-H460 and HeLa cancer cells; promotes apoptosis in BCL-6-expressing Burkitt lymphoma cells, and reduces tumour growth in a xenograft model. It is also endowed with anticancer effects on hepatocellular carcinoma tumour models *in vitro* and in vivo and reduces neuroblastoma formation in n-myc transgenic mice. [421]
Through a focused library screening, AGK2 (**9**, Fig. 3.1) was identified as a single-digit micromolar SIRT2i selective over SIRT1/3 being able to inhibit the deacetylation of α-tubulin in HeLa cells. AGK2 rescues dopaminergic neurons from α-synuclein toxicity, thus protecting against Parkinson. [256] Likely through SIRT2 inhibition, AGK2 also induces caspase-3-dependent death in glioma cells. [249]

Tenovin-1 (**10**, Fig. 3.1) and its water-soluble analogue tenovin-6 (**11**, Fig. 3.1) as SIRTi were discovered through a cell-based screen designed to detect p53 activators. Tenovin-6 is a micromolar SIRT1-3i that increases the level of p53K382ac; shows cytotoxic effects on melanoma cells, delaying the growth of ARN8-derived xenograft tumours (355); and induces apoptosis in gastric cancer cells [422] and in chronic myeloid leukaemia cells, thus decelerating the disease progression in mice models. [423]
Several other classes of inhibitors have been discovered, including polyanionic compounds as suramin (**12**, Fig. 3.1). [424]

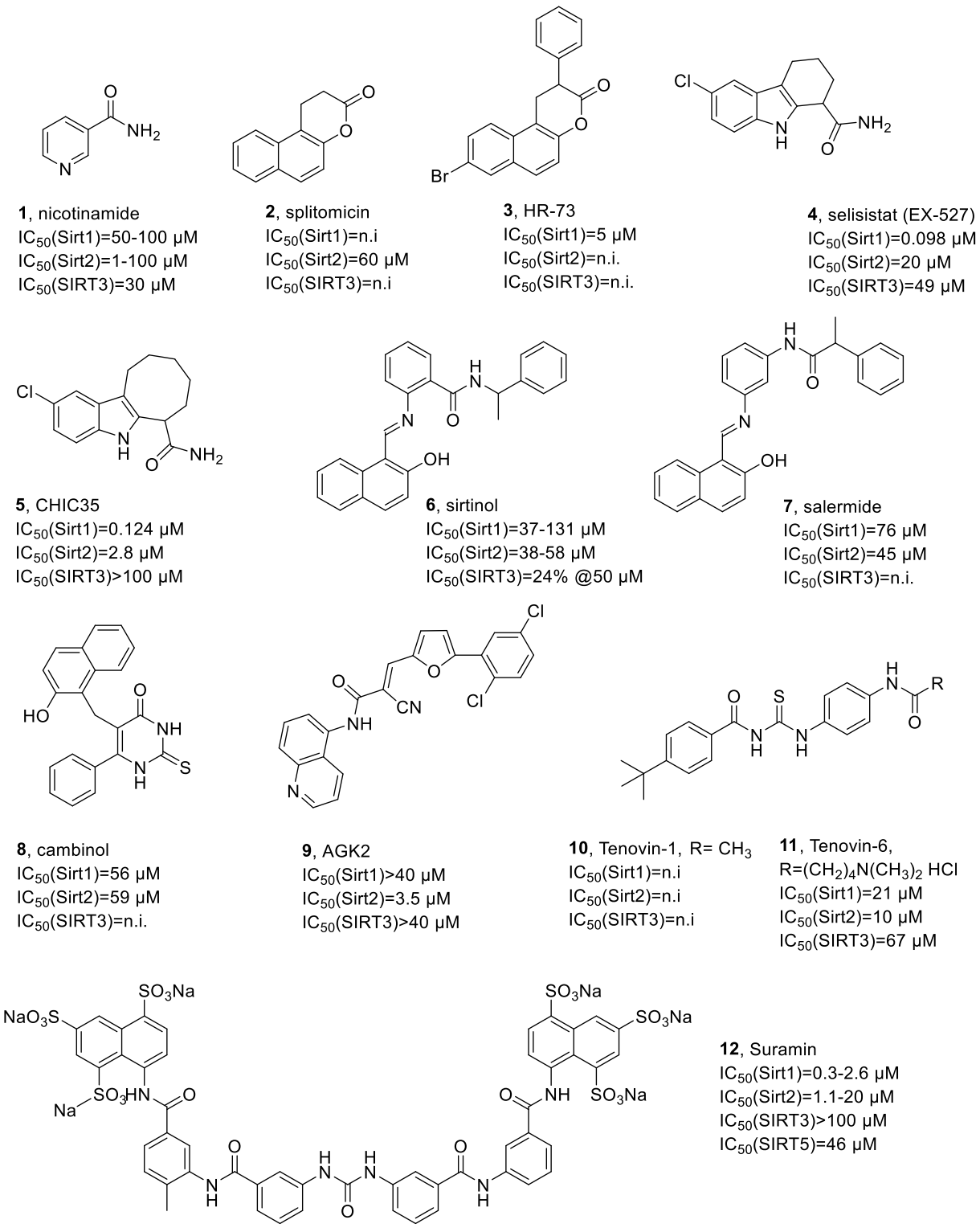

Figure 3.1: Chemical structures and IC_{50} values of Sirt inhibitors.

About 100 years after its initial discovery as an antiprotozoal agent, the polyanionic naphthyl urea **12** was identified as a potent Sirt1 inhibitor by Howitz *et al.* [425, 426]

12 is an antagonist of an adenosine receptor, approved for the treatment of trypanosomiasis and onchocerciasis. Suramin is a symmetric polyanionic naphthylurea that displaying a wide range of

biological properties. **12** has higher activity on SIRT1 (IC_{50} = 297 nM) rather than SIRT2 (IC_{50} = 1150 nM). Biochemical studies showed that suramin is a non-competitive inhibitor against both NAD^+ and the acylated substrate. [427]

3.1.2 Small-molecule Sirtuin activators

For many years, many efforts have been undertaken with the aim to develop small-molecule activators of Sirt1 due to its beneficial effects on calorie restriction or Sirt1 overexpression. [428-430] The first compounds discovered as Sirt1 activators were derivatives of plant polyphenols, including resveratrol, a phytoalexin found in grapes. Resveratrol (**13**, Fig. 3.2) administration was found to extend lifespan in yeast, *Caenorhabditis elegans*, *Drosophila*, fishes, and bees. Mice treated with resveratrol displays improved mitochondrial functions and protection against high-fat diet-induced obesity, while in obese mice, treatment with resveratrol leads to an increased health span and lifespan. [431] Over the past years, the effective SIRT1 activation by resveratrol and other SRT compounds has been highly debated because only the use in the enzyme-based assays with labeled substrates allowed to see activation, whereas in the presence of natural substrates no activation was observed. [432] However, direct SIRT1 activation by resveratrol has been confirmed later, and it has been shown that there are subtle structural and positional requirements to detect SIRT1 activation with some of its natural substrates (e.g., FOXO3a and PGC-1α), and finally the co-crystal structure of a mini-h SIRT1-activator complex was solved. [292, 433] However, attempts to identify novel sirtuin activators had never been stopped. The first Sirt1 activators classes that showed no structural analogies to resveratrol were the 1,4 dihydropyridines developed by our research group [434, 435] and the quinoxalines (**14**, Fig. 3.2). [436] Some 1,4 dihydropyridine analogues, such as MC2563 (**15**, Fig. 3.2) were identified as activators of not only Sirt1 but also of Sirt2 and Sirt3. [434] Indeed, the activating effect of MC2563 was reported to be relevant in cells by the induction of a hypoacetylation of the tubulin network. [434] Several high-throughput screens, as well as wide structure-activity relationship (SAR) investigation, were performed by Sirtris Pharmaceuticals in order to identify novel potential Sirt1 activators (**16**, **17**, Fig. 3.2). These efforts result in the discovery of several highly potent and drug-like Sirt1 activators that showed to activate Sirt3 via a Glu230-dependent mechanism. [437, 438] All sirtuins were reported as isotype-selective for Sirt1, apart from SRT1720, which additionally displays a potent Sirt3 inhibitory activity. [293, 439]

Therefore, identified in 2007 by high-throughput screening as selective SIRT1 activators more potent than resveratrol, SRT compounds (SRT1460 (**18**), SRT1720 (**19**), SRT2183 (**20**); Fig. 3.2) can reproduce most of the beneficial effects of resveratrol *in vivo*. In diet-induced and genetically obese ($Lep^{ob/ob}$) mice, compounds **18**, **19**, and **20** improve insulin sensitivity, lower plasma glucose, and increase mitochondrial capacity. Moreover, in Zucker (*fa/fa*) rats, the same compounds improve whole-body

glucose homeostasis and insulin sensitivity. [440] Due to their very promising activities, some of the most potent SRTs are currently in clinical trials for the treatment of different age-related diseases. [441, 442]

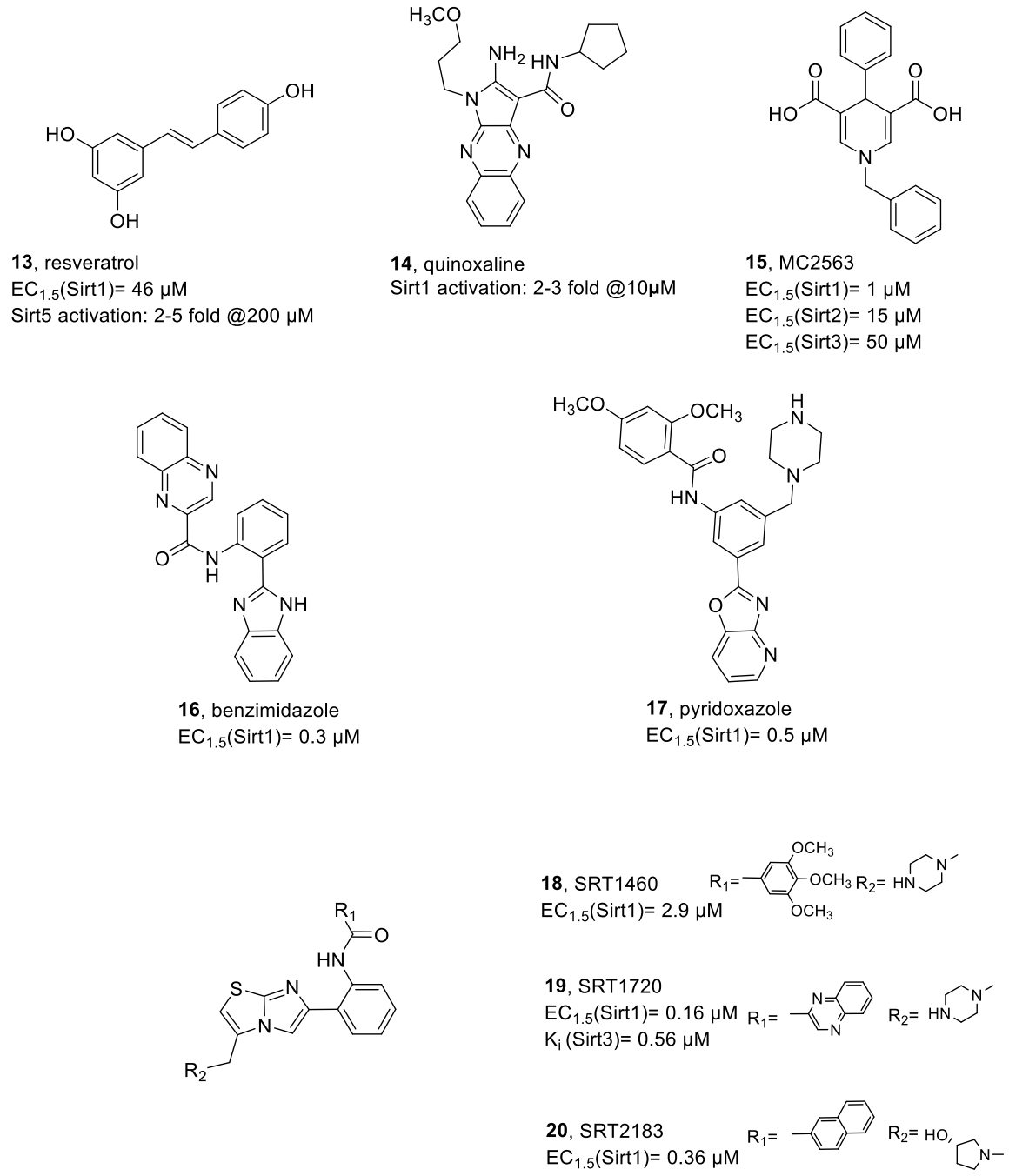

Figure 3.2: Chemical structures and $EC_{1.5}$ values of Sirt activators.

SRT1720 has been intensively studied both in cellular and animal models where was found to stimulate a range of beneficial effects including the activation of fatty acid metabolism and mitochondrial biogenesis, improvement of insulin sensitivity, suppression of inflammation, and extension of lifespan. [441, 443] Conversely, in *in vivo* studies, Pacholec *et al.* reported that SRT1720 neither led to blood

glucose levels reduction nor to improved mitochondrial biogenesis. [444] In breast cancer cells, SRT1720 was able to enhance cell migration and lung metastasis. [445]

Thus far, several sirtuin activators have already entered a series of clinical trials, but very little information about their outcome is available. In these current clinical studies, sirtuin are mainly investigated for the treatment of diabetes type 2, COPD, psoriasis, colitis ulcerosa, and cardiovascular diseases.

3.2 Chemical scaffolds for Sirt1 activation

Currently, the most potent scaffolds required for sirt1 activation in age-related conditions (obesity, metabolic and cardiovascular disorders, inflammatory/autoimmune diseases, neurodegeneration, and cancer) are:

I. Pyrido[3,2-b][1,4]oxazocines (STAC-8, **21**, Fig. 3.3), with an EC1.5 of 1.2 μM for STAC-8, which shows promising activities in different age-related disease models including obesity and metabolic disorders, inflammatory and autoimmune disorders, cardiovascular disease, hepatic steatosis, neurodegeneration, and cancer. [442, 446, 447]
II. azabenzimidazoles (STAC-5, **22**, Fig. 3.3), with and EC1.5 of 0.4 μM for STAC-5, which also shows to be effective in different age-related disease models. [442, 448, 449]

As aforementioned, over the past years, it has been in-depth debated the effective SIRT1 activation by resveratrol and other SRT compounds, because the activation was only observed in enzyme assays using aminomethylcoumarin (AMC)- or carboxytetramethylrhodamine (TAMRA)-labelled substrates, rather than in the presence of natural substrates. [450] Thus, it was questioned if the action of resveratrol and SRT compounds on SIRT1 was the result of a direct activation or rather the indirect modulation of other pathways, such as AMPK activation and/or PDE inhibition. [451] However, recently, direct SIRT1 activation has been confirmed, providing subtle structural and positional requirements to detect SIRT1 activation with some of its natural substrates (e.g., FOXO3a and PGC-1α). [446] Moreover, E230K or E230A SIRT1 mutation abolishes enzyme activation as well as binding of SRT compounds, thus suggesting an assisted allosteric activation mechanism that enables the deacetylation through a stable binding of activators to the enzyme-substrate complex. [451]

Lastly, the crystal structure of a SRT compound bound to an engineered minimally functional hSIRT1 has been reported, unambiguously confirming the direct allosteric activation of SIRT1 by small molecules. [292] The 1,4-dihydropyridine (DHP) scaffold (**23**, Fig. 3.3) has been described by our research group in 2009 as a new chemotype for SIRT activation. Selected DHPs induced hypoacetylation of α-tubulin in U937 cells, high NO release in HaCat cells, and ameliorated skin repair in a mouse model of wound healing. In myoblasts, they improved mitochondrial density and functions through activation of the

SIRT1/AMPK axis. A water-soluble analogue displayed antiproliferative activity and increased H4K16ac deacetylation in a panel of cancer cells at 8– 35 μM. [434]

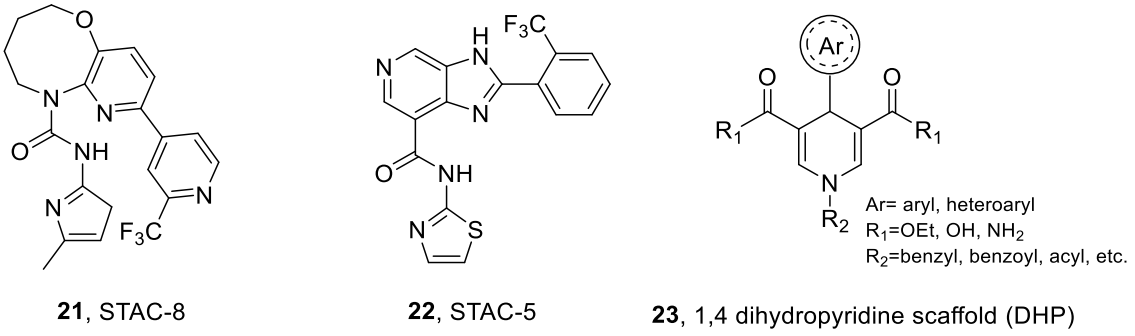

21, STAC-8 **22**, STAC-5 **23**, 1,4 dihydropyridine scaffold (DHP)

Figure 3.3: Chemical scaffolds for Sirt1 activation.

Very recently, the cardiac anti-hypertrophic effects of the natural compound honokiol (**24**, Fig. 3.4) were described. In mice, Honokiol was found to block and reverse cardiac hypertrophy by pharmacological activation (increased expression and activity) of mitochondrial SIRT3. [452]

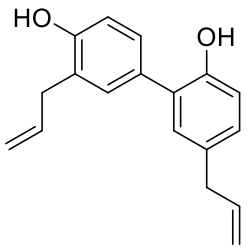

24, Honokiol

Figure 3.4: Honokiol.

3.3 Mechanisms of small-molecule-induced enzyme activation

Most efforts in chemical biology were carried out in order to identify small-molecule tools or drugs that inhibit enzyme function. In literature, small-molecule enzyme inhibitors are widely described rather than activators, even if in recent years is coming out the area of “small-activators in drug discovery”, given their importance in many cellular processes. Importantly, activators provide a means to better understand the enzymatic activation mechanism(s) behind their action. Many enzymes such as proteases, kinases, and phosphatases are stored in dormant forms that await activation by PTMs, including proteolysis and phosphorylation, or by interactions with other proteins or metabolites. Such mechanisms typically stabilise an active enzyme conformation. Synthetic small-molecule activators can often promote similar transitions. Unlike inhibitors, the target for the phenotype is not fundamental for activators. In addition, an inhibitor often requires an IC_{90} or even IC_{95} (inhibitor concentration at 90% to

95% enzyme inhibition) to block such phenotypic effects because, in many cases, small amounts of active enzyme are sufficient to trigger a signalling cascade, thus driving biological responses. By the same token, the concentration of an allosteric activator may only need an AC10 (activator concentration at 10% maximal activation level). Therefore, such small-molecule activators extend the target landscape for drug discovery. There are almost a dozen examples of mechanistically well characterised small-molecule activators for enzymes, such as regulators of proteases, kinases, deacetylases, dehydrogenases, phosphatases, and nucleases. [453] These activators exploit four means of inducing enzyme activity (Fig. 3.5):

- **A1**: small molecules can bind to an allosteric site directly on the catalytic domain of a dormant enzyme to induce a conformational change, which can occur cooperatively with the substrate.
- **A2**: proteases are typically expressed as inactive precursors, or zymogens, that need to be processed by an upstream protease, or auto-processed, to form the active, mature enzyme. Small molecules can interact directly with the catalytic domain of a protease and enhance this activating, irreversible PTM.
- **B1**: small molecules can bind to an allosteric site on regulatory subunits of an enzyme to promote an active conformation.
- **B2**: oligomerisation of some enzymes can promote activation. Thus, small molecules that facilitate oligomerisation, either by binding to an allosteric site on the catalytic domain or by interacting with a regulatory subunit, can enhance activity.

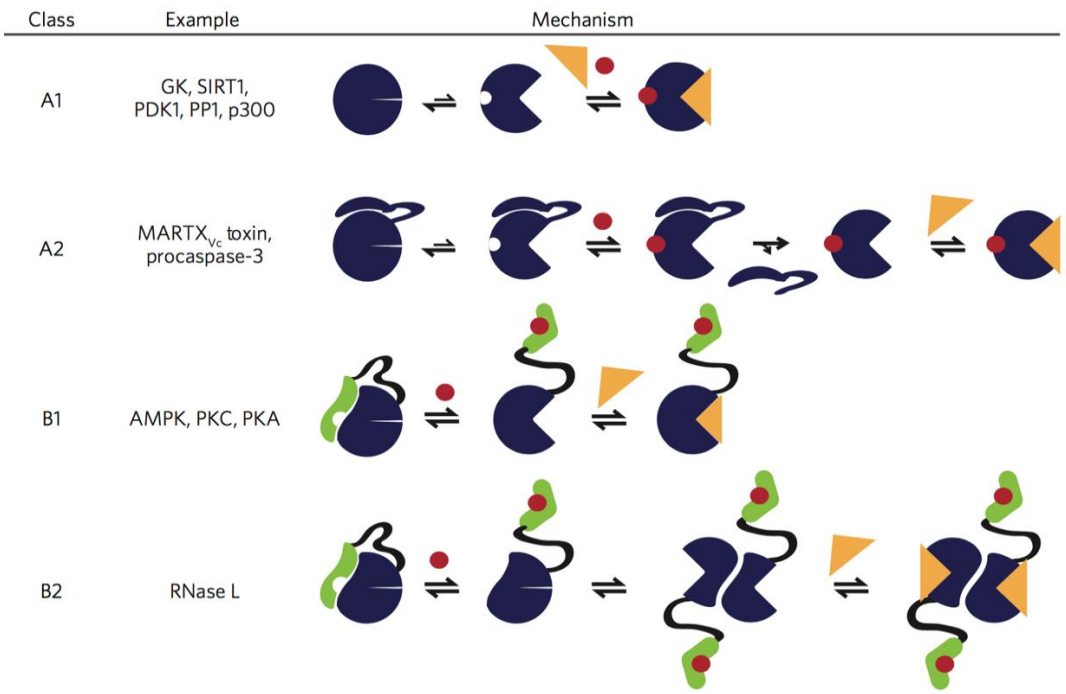

Figure 3.5: Mechanisms of small-molecule-induced enzyme activation. Four general mechanisms have been identified for small-molecule activation of an enzyme (blue circles). A closed enzyme active site indicates an inactive conformation, whereas an open active site, which binds substrate (orange triangle), indicates an active conformation. Type A mechanisms are defined

by a direct binding interaction between the small-molecule activator (red dot) and an allosteric site on the enzyme's catalytic domain. Type A1 involves a direct binding interaction to stabilise an active conformation; this often requires the presence of substrate. Type A2 is a direct binding interaction that results in an irreversible, activating post-translational modification, such as proteolysis. Type B mechanisms are defined by the activator binding to a regulatory subunit (green subunit), which can either be covalently linked to the catalytic domain (as depicted) or an isolated subunit of the complex. Type B1 involves an activating conformational change in the catalytic domain as a result of binding to the regulatory subunit. Type B2 requires additional oligomerisation of the catalytic domain to generate the active enzyme. For simplicity, many potential conformational states of the enzymes are not shown in the figure. [453]

3.4 Rational of the project

Modulation of Sirtuins activity is retained a promising therapeutic strategy for the treatment of cancer, cardiovascular, metabolic, inflammatory, and neurodegenerative diseases. Among the mitochondrial sirtuins (SIRT3, -4 & -5), SIRT3 is the only one exhibiting robust deacetylase activity. [259] The substrates of SIRT3 are very diverse including enzymes, which serve unique and critical functions regulating metabolism, cell survival, and longevity. SIRT3 deficiency manifests in reduced cellular ATP and increased ROS levels. [267, 273] SIRT3-knockout mice have 50% lower ATP levels than their wild-type littermates and are susceptible to develop cardiac hypertrophy at an early age, cancer (mainly hepatocellular carcinoma), and age-related hearing loss. Similarly, SIRT3 levels are reduced in many experimental models of cancer, diabetes mellitus, and heart failure as well as in older patients (over 60s) with sedentary lifestyle. In human studies, an increased SIRT3 level was associated to an extended lifespan of humans, whereas a decreased enzymatic activity of SIRT3 has been associated with metabolic syndrome, indicating a key role of SIRT3 in the regulation of human ageing. These studies suggest that higher SIRT3 intracellular expression would be a strategy to ameliorate/prevent many diseases and health deficiencies related to ageing. Particularly, the discovery of a pharmacological activator of SIRT3 is highly desirable for the treatment of diseases associated with SIRT3 deficiency. [271, 280, 454-456] Furthermore, very recently Ren *et al.* identified SIRT3 as a novel host factor epigenetically restricting Hepatitis B virus (HBV) covalently closed circular DNA (cccDNA) transcription and replication by acting cooperatively with SUV39H1 and SETD1A histone methyltransferases. These data provided a rational for the use of SIRT3 activators in the prevention or treatment of HBV infection. [457]
In a previous study by our group the potential of the 1,4-dihydropyridine scaffold in developing sirtuin ligands was rationalised. [434] A series of 1,4-dihydropyridine-based derivatives was thus prepared, and the assessment of their SIRT1-3 deacetylase activities revealed the importance of the substituent at the N1 position of the dihydropyridine structure on sirtuin activity. In particular, the presence of a benzyl group at N1 conferred potent SIRT1 activation and, to a lesser extent, also SIRT2 and -3 activations.

In a following study, several related compounds were synthesised to investigate SIRT1-activation SAR. [435] Selected compounds were able to accelerate tissue renewal in a mouse model of skin repair, and displayed anticancer effect in different cancer cell lines. From these series of DHPs, one compound bearing an acyl function at the N1-position of the DHP scaffold (MC2791, Fig. 3.6) displayed selective

activation of SIRT3 over SIRT1, -2 and -5. This specific SIRT3 activation was confirmed by mass spectrometry analysis as well as by SIRT3-activators binding affinity experiments. Another compound bearing carbonyl group at N1 was synthesised (MC2789, Fig.3.6), however, it was not reported in the study. [435] The inspiration for its design came from the synthetic SIRT1 activator SRT1460, as shown in figure 3.6.

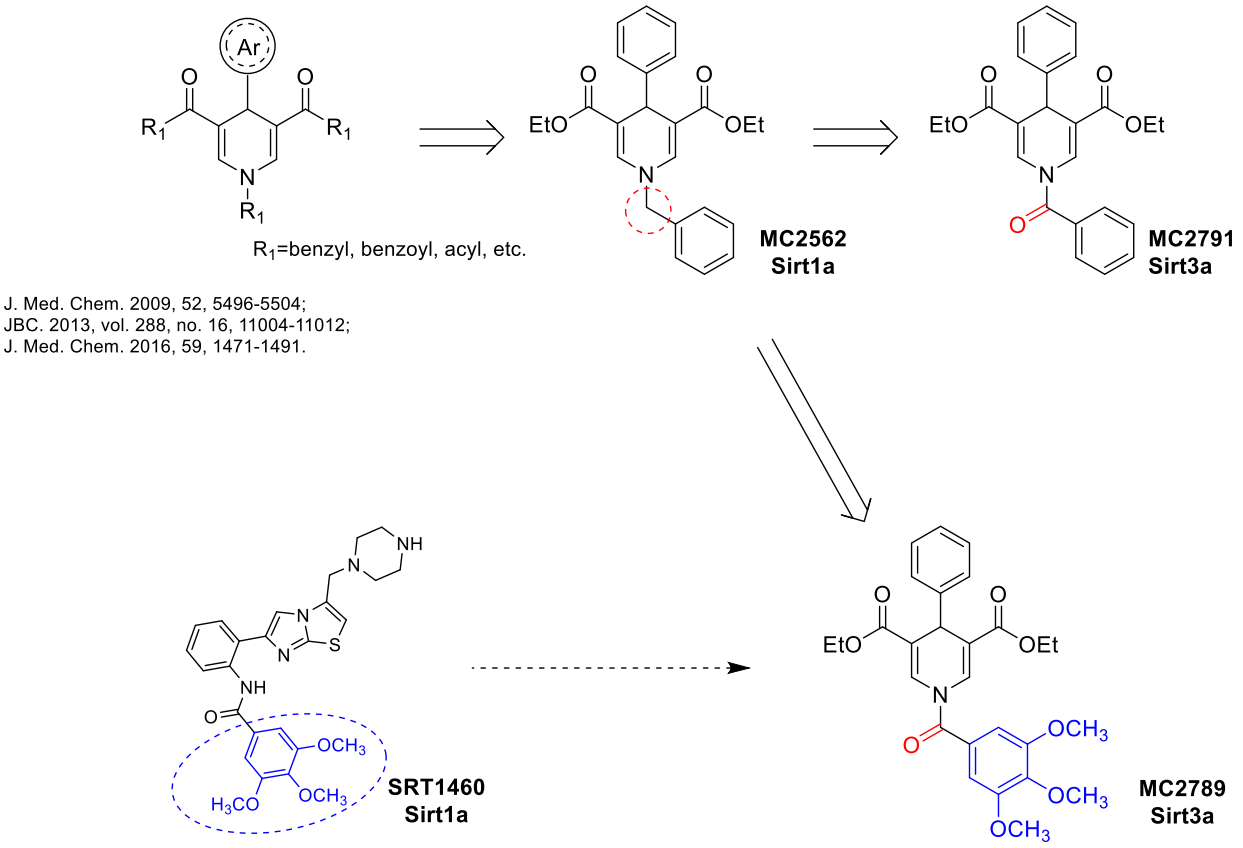

Figure 3.6: Design of MC2791 and MC2789.

Therefore, we planned to resynthesize and rescreen some selected N1 carbonyl DHPs, showing poor Sirt1 activation, against other natural endogenous sirtuin substrates (Sirt1, -2, -3 and -5) to validate their inhibition potency and isoform selectivity, as well. Surprisingly, the carbonyl group at N1 turned out to strongly increase the activity on SIRT3. Strikingly, the two hits MC2791 and MC2789 showed significantly stronger effects, activating Sirt3~3.5 and 5-fold, respectively (Fig. 3.7).

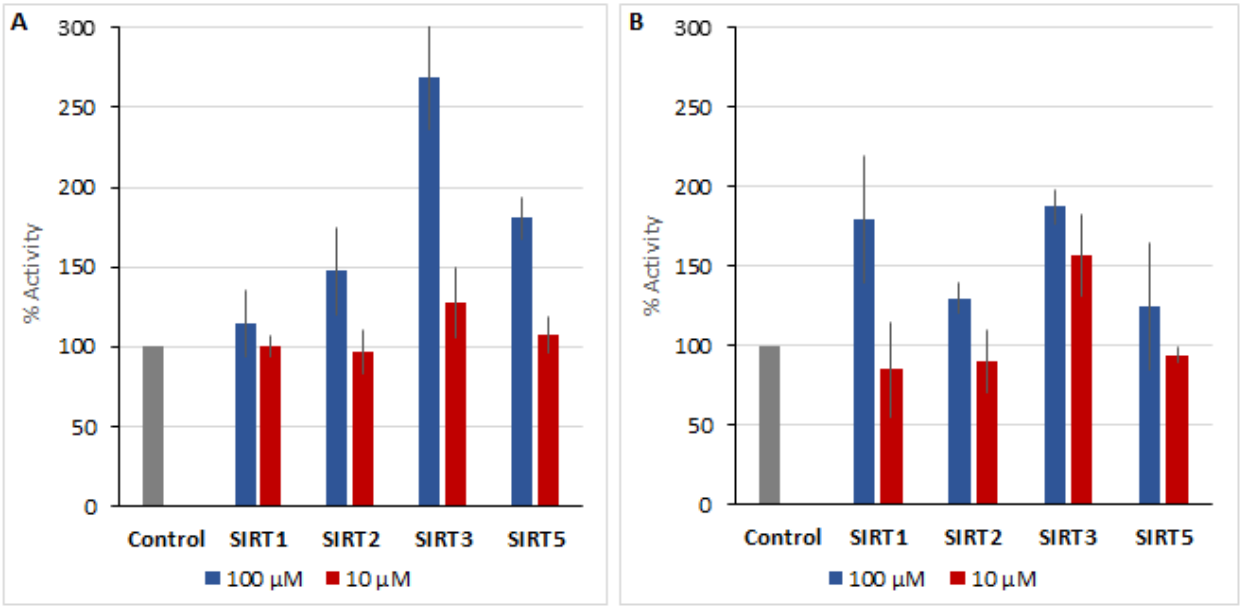

Figure 3.7: Sirt3 activation by MC2789 (**A**) and MC2791 (**B**).

Control reactions for compound effects on the coupled enzymes nicotinamidase and glutamate dehydrogenase (GDH) showed negligible effects, confirming that the activators act directly on Sirt3.

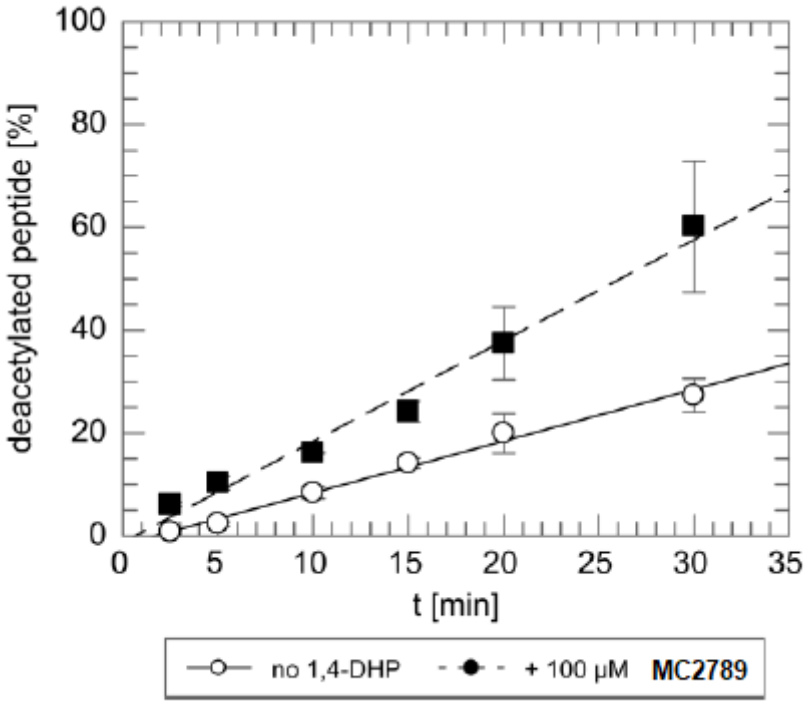

Figure 3.8: Mass spectrometry (MS)-based activity assay.

For additional confirmation of direct Sirt3 activation, we tested compound effects in a mass spectrometry (MS)-based activity assay that directly analyses acetylation levels of non-modified substrate, rendering it insensitive to artefacts. MC2789 activated Sirt3-dependent deacetylation of the

ACS2 peptide also in the MS-based assay (Fig. 3.8), confirming that our 1,4-DHP-based compounds are direct Sirt3 activators.

To characterise the isoform selectivity of our Sirt3 activators, we tested the parent compound MC2562 and the strongest Sirt3 activators, MC2791, and MC2789, against Sirt1, 2, and 5. Using the same coupled assay as for Sirt3 and the same concentrations for the enzyme, NAD^+, and the substrate (peptide for Sirt1: acetylated p53; Sirt2: acetylated tubulin; Sirt5: succinylated CPS1), MC2562 activated Sirt1 slightly better than Sirt3, consistent with the previous "Fluor-de-Lys" FdL results. [434] The compound showed no significant effects against Sirt2 and Sirt5. The novel Sirt3-activating compounds MC2791 and MC2789, in contrast, showed no significant activating effects on Sirt1, 2, and 5, thus MC2791 and MC2789 are Sirt3 selective activators.

The moderate potencies of MC2791 and MC2789 prompted us to screen for more potent derivatives. We generated new series of compounds by varying their "top" or "bottom" with other substituents at C1 or C4 position of the DHP scaffold, respectively (Fig. 3.9).

The chemical manipulations applied to the structure of MC2791 and MC2789 to improve their selectivity towards SIRT3 were the following:

a) on the **MC2791** structure we replaced the C4-phenyl ring with different isosteric rings, such as 2- or 3-furyl or 2- or 3-thienyl rings, keeping fixed the benzoyl group at N1, or we inserted at the ortho, meta or para position of C4-phenyl ring some substituents (chloro, methoxy, methyl). In addition, we prepared some N1-aroyl analogues replacing the N1-benzoyl moiety with various mono- or bicycle aroyl/phenylsulfonyl/cyclohexyl portions or with different isosteric rings. Then, we introduced at *meta* or *para* position of the C1-benzoyl ring, some electron-withdrawing (fluoro, chloro, bromo, nitro, cyano) substituents.

b) on the **MC2789** structure we removed one or two methoxy groups at *meta* and/or *para* position of the N1-benzoyl ring and we replaced the benzoyl moiety with the benzyl one. Moreover, we introduced at the *ortho, meta,* or *para* position of the C4-phenyl, keeping fixed the trimethoxy-benzoyl group at N1, some electron-withdrawing (fluoro, chloro, bromo, nitro, cyano) as well as electron-releasing (methyl, amino) substituents. In attempt to realize a ligand/co-substrate for Sirt3, we replaced the para methoxy group of MC2789 with a crotonyl substituent. Lastly, we also inserted at the para position of the C4 phenyl ring a (4-methylpiperazin-1-yl)methyl group as a salifiable function to improve the water solubility of MC2789.

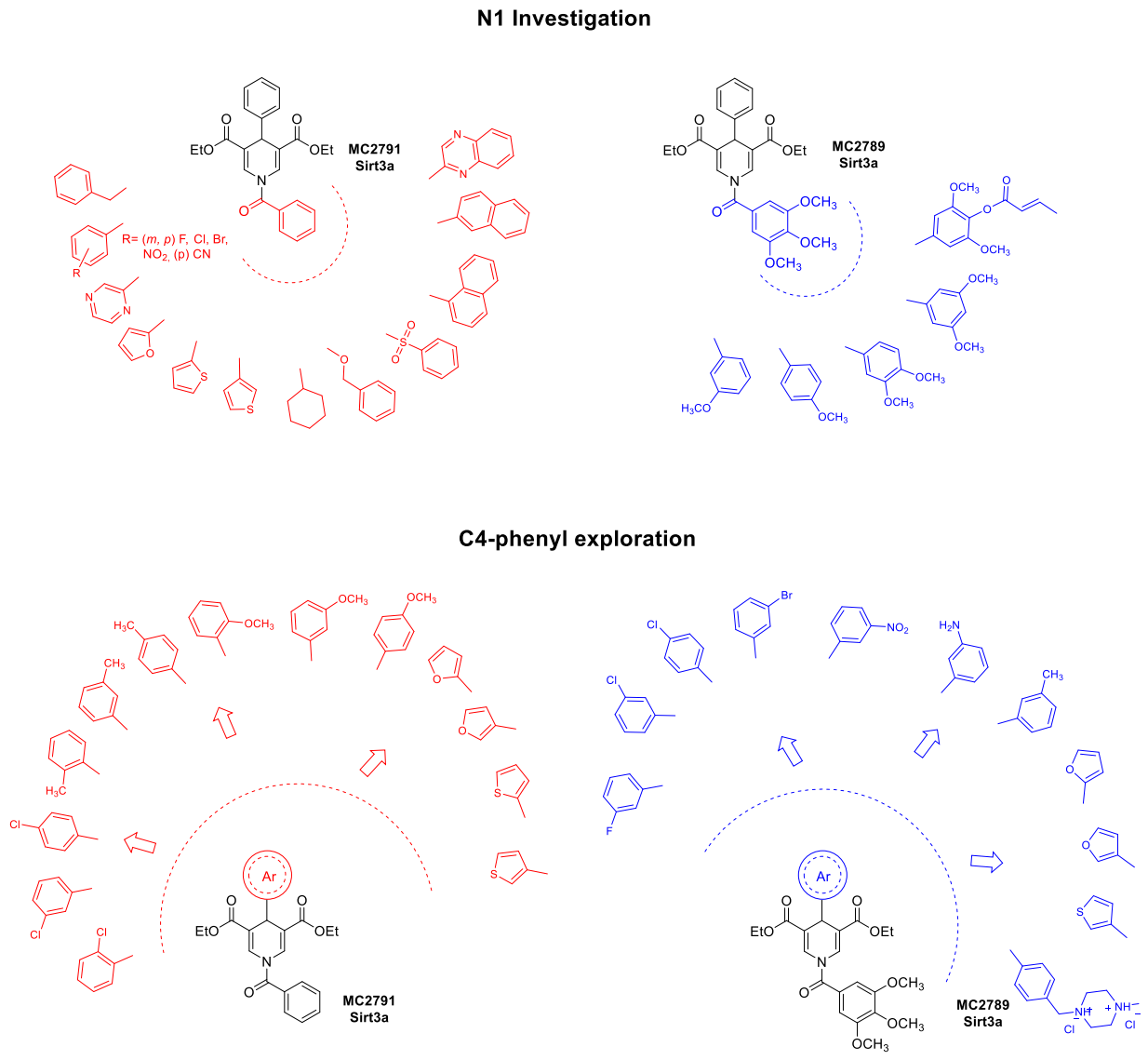

Figure 3.9: New set of dihydropyridines bearing carbonyl group at N1.

At a later stage, our collaborator Prof. Steegborn screened both series of MC2791 and MC2789 derivatives for the activation of Sirt3/Sirt5 against physiological substrates and in cellular settings. Interestingly, we found that some of the newly derivatives displayed increased either SIRT3 or Sirt5 activation, thus resulting in highly selective lead structures towards these two aformentioned isoforms (Fig. 3.10). Additionally, other tested compounds showed to activate both Sirt3 and Sirt5 with a similar potency. Importantly, Sirt5 is a weak deacetylase and acts primarily as a protein lysine desuccinylase and deglutarylase. Sirt5 regulates metabolic enzymes and stress response proteins, has been implicated in metabolic adaptations to protein-rich diet, fasting, and long term CR, and seems to contribute to metabolic dysfunctions and neurodegeneration. [458]

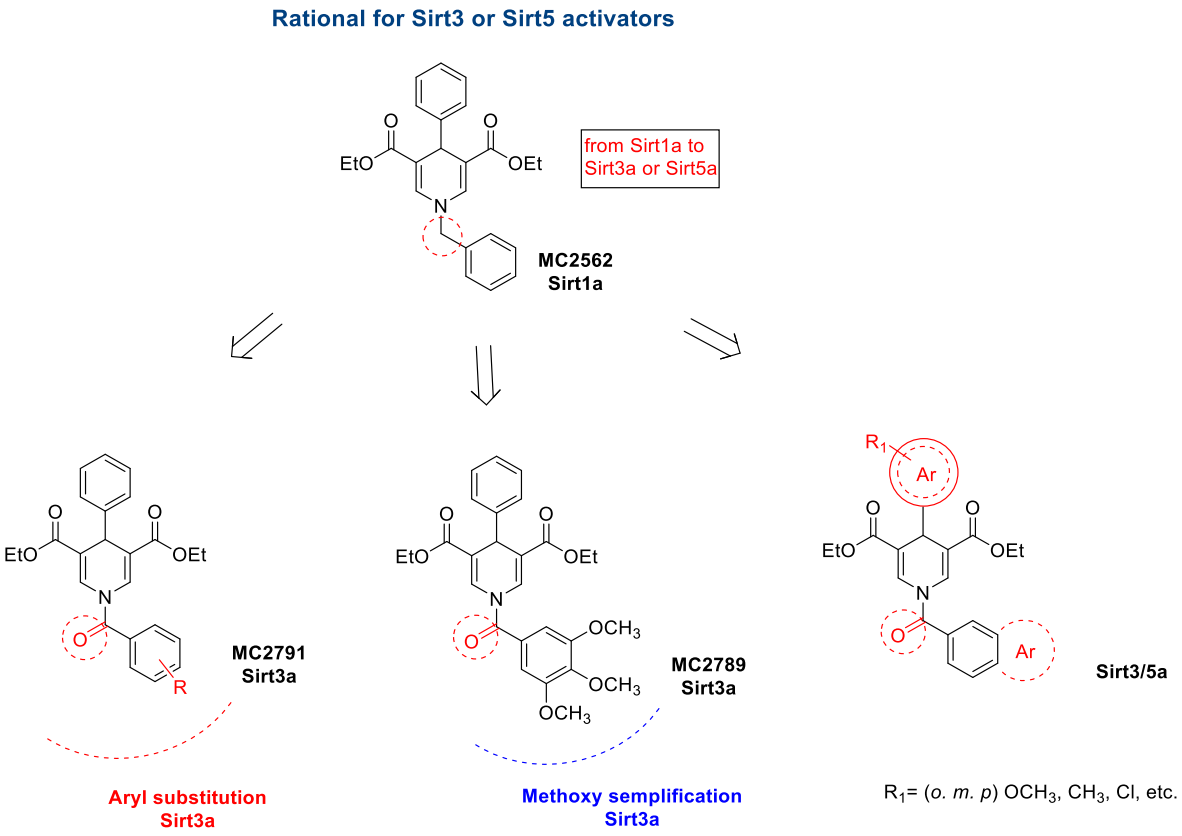

Figure 3.10: Rational for Sirt3 or Sirt5 activators.

3.5 Chemistry

The N1-aroyl-3,5-carbethoxy-4-aryl DHPs **1a-a'**, **2** and the N1-phenylsulfonyl analogue **3** were prepared by using the following procedure: (i) multicomponent cyclocondensation between benzaldehyde or the benzylamine (**2**), ethyl propiolate, and ammonium acetate (except for **1B,** Scheme 3.1); (ii) heating at 80 °C in glacial acetic acid to obtain the intermediate compounds **10**; (iii) N1-acylation with triethylamine and the appropriate acyl chloride (for **10a-a'**) or phenylsulfonyl chloride (for **3**) to afford the desired final compounds **1a-a'** (Scheme 3.1, **1A** and **1C**).

Scheme 3.2 shows the synthesis of the final compounds **4a-m**, **5b-c**, **5e**, **5j-k**, **5m-q** and **6**. Here, multicomponent cyclocondensation between benzaldehyde (properly substituted), ethyl propiolate, and ammonium acetate, gave the intermediates **11a-q** which underwent to acylation with the proper acyl chloride (**4** or **5**) to afford the final compounds **4a-m**, **5b-c**, **5e**, **5j-k**, **5m-q** and **6** (Scheme 2**A**). A multicomponent reaction between ethyl propiolate, the commercially available 4-(4-methylpiperazin-1-yl)- methylbenzaldehyde, and 2,3,4-trimethoxybenzoyl chloride (**9u**), according to what was reported for **11a-q**, followed by treatment with 4 M HCl in 1,4- dioxane, afforded compound **6** as dihydrochloride salt (Scheme 3.2, **2B**).

Scheme 3.1

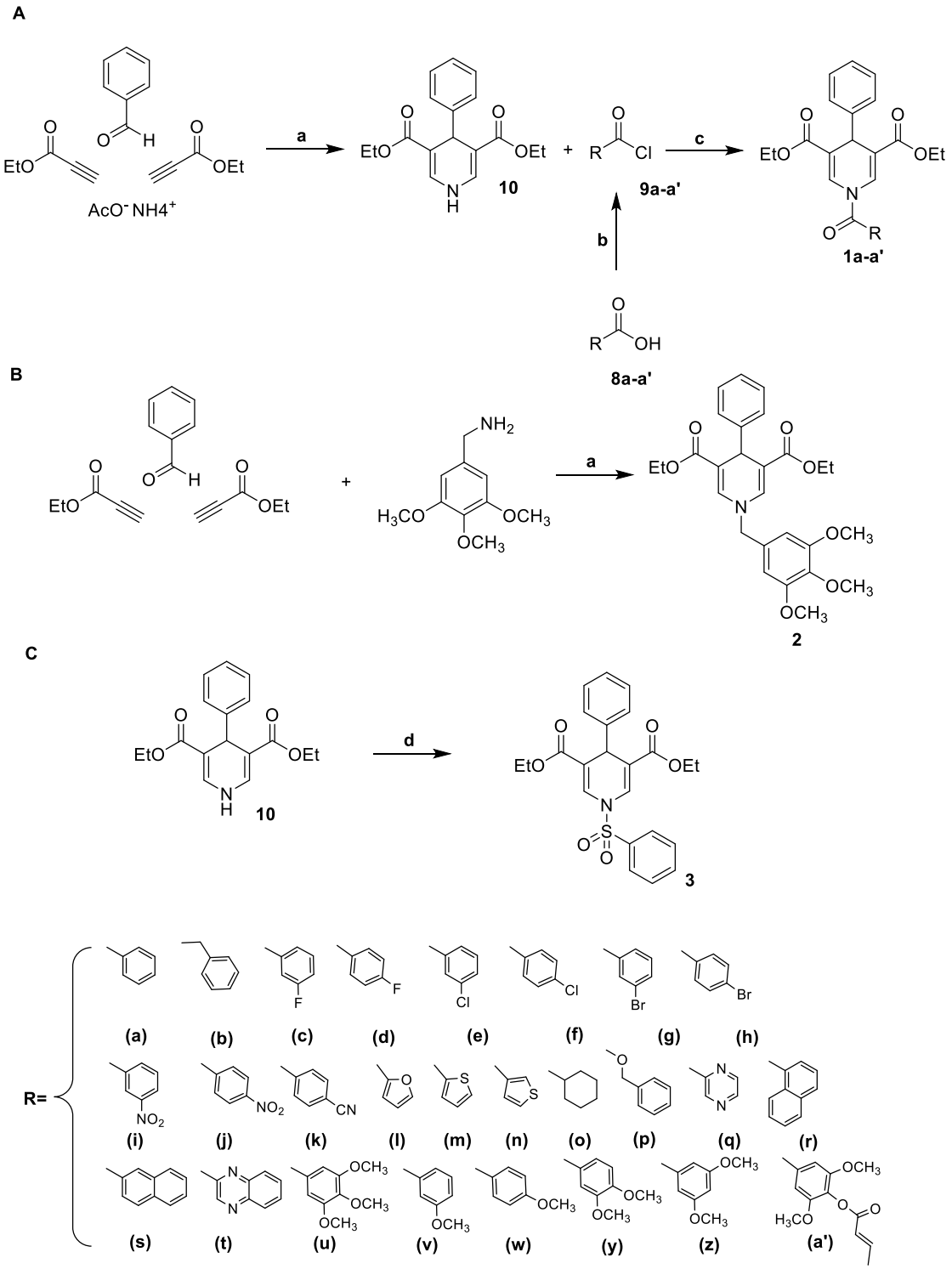

Reagents and conditions: (**a**) CH_3COOH, 80 °C, 8 hrs; (**b**) $SOCl_2$, toluene, 1hr; (**c**) Et_3N, dry DCM, rt, overnight; (**d**) Et_3N, $PhSO_2Cl$, dry DCM, rt, overnight.

Scheme 3.2

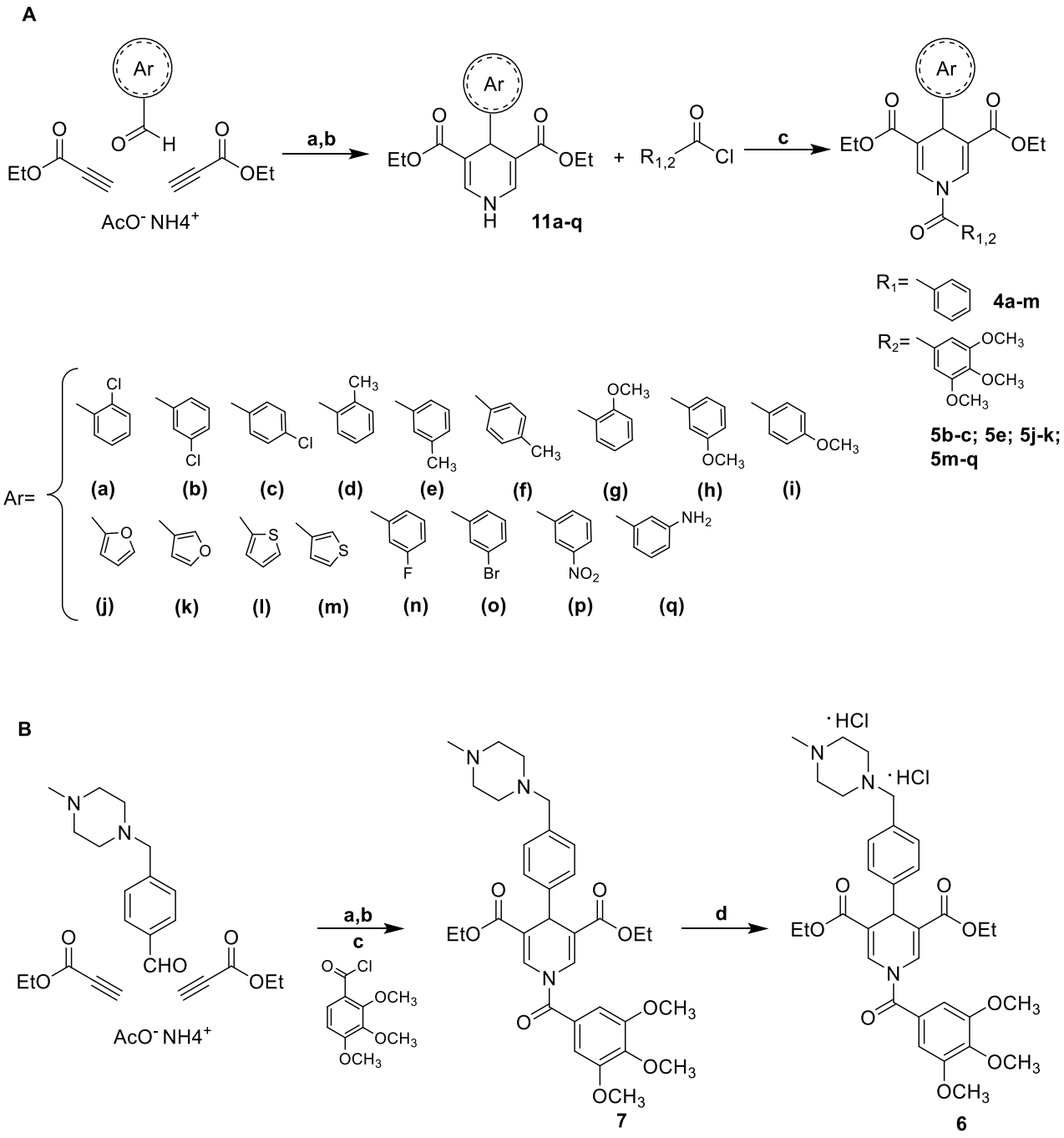

Reagents and conditions: (**a**) CH_3COOH, 80 °C, 8 hrs; (**b**) $SOCl_2$, toluene, 1hr; (**c**) Et_3N, dry DCM, rt, overnight; (**d**) 4 M HCl in 1,4-dioxane, tetrahydrofuran, 0 °C.

Table 3.1: Chemical-Physical Data of Compounds **1a-a'**, **2**, **3**, **4a-m, 5b-c**, **5e**, **5j-k**, **5m-q** and **6**.

LAB CODE	COMPOUND	CHEMICAL STRUCTURE	M.P (°C)	YIELD	RECRYSTALLIZATION SOLVENT

MC2791	**1a**	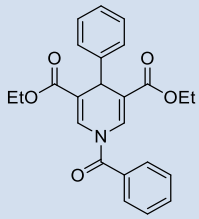	107-109°C	20.3%	Cyclohexane
MC4208	**1b**	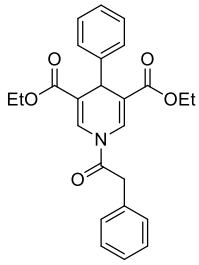	152-154°C	14.1%	Benzene
MC4158	**1c**	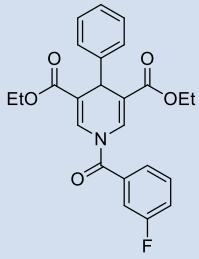	124-126°C	85.2%	Cyclohexane/Benzene
MC4168	**1d**	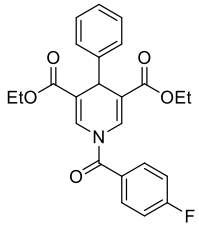	122-124°C	93.6%	Cyclohexane
MC4172	**1e**	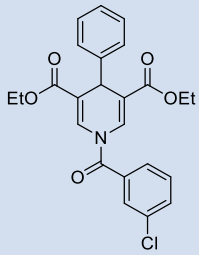	153-155°C	61.8%	Benzene
MC4166	**1f**	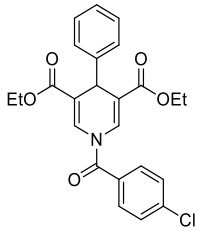	122-124°C	65%	Cyclohexane
MC4181	**1g**	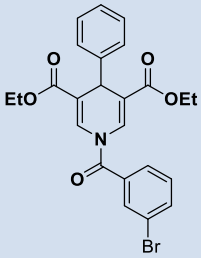	154-156°C	68.7 %	Benzene

MC4185	**1h**	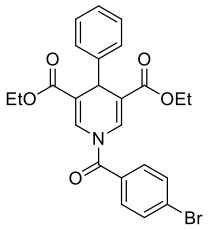	140-142°C	71.6 %	Cyclohexane/Benzene
MC4165	**1i**	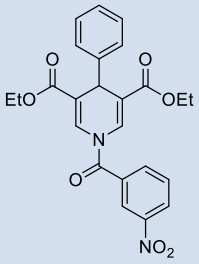	146-148°C	63%	Cyclohexane/Benzene
MC4167	**1j**	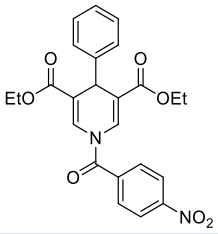	108-110°C	65.6 %	Cyclohexane
MC4177	**1k**	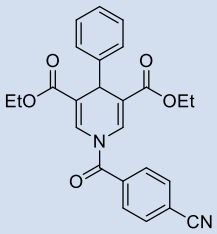	155-157°C	60.4%	Benzene
MC4204	**1l**	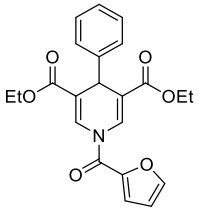	125-127°C	12.2%	Benzene
MC4188	**1m**	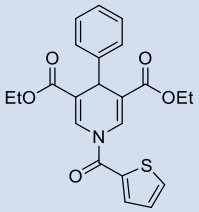	142-144°C	56.4%	Cyclohexane/Benzene
MC4186	**1n**	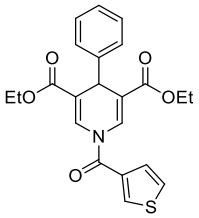	113-115°C	51.2%	Cyclohexane
MC4199	**1o**	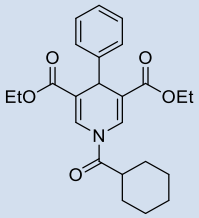	92-94°C	17%	Cyclohexane

MC2792	**1p**	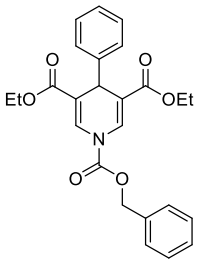	85-87°C	78%	Cyclohexane
MC2870	**1q**	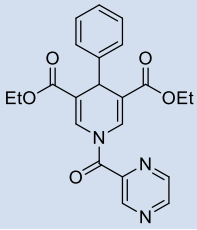	127-129°C	69%	Cyclohexane
MC2861	**1r**	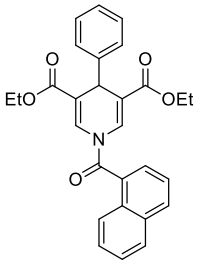	140-142°C	75%	Toluene
MC2790	**1s**	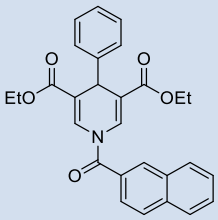	123-125°C	78%	Cyclohexane
MC2788	**1t**	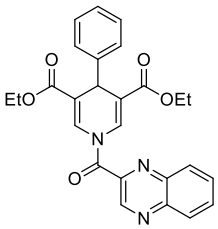	142-144°C	65%	Toluene
MC2789	**1u**	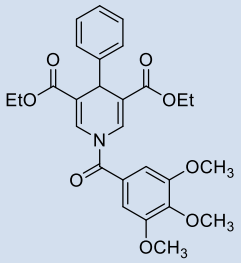	174-176°C	34.8%	Benzene/Acetonitrile
MC4164	**1v**	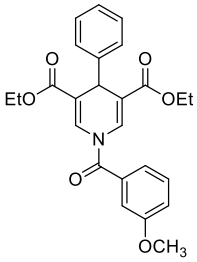	134-136°C	58.2 %	Cyclohexane/Benzene

MC4182	**1w**	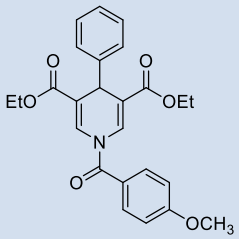	131-133°C	17.9%	Cyclohexane/Benzene
MC4175	**1y**	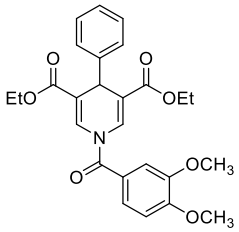	174-176°C	27.6%	Benzene/Acetonitrile
MC4176	**1z**	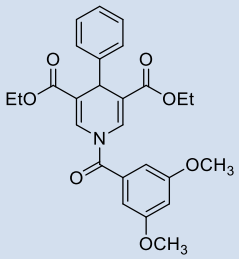	158-160°C	64.3%	Benzene/Acetonitrile
MC4054	**1a'**	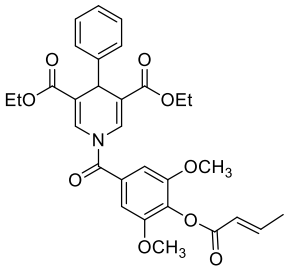	161-163°C	45.6%	Benzene
MC4001	**2**	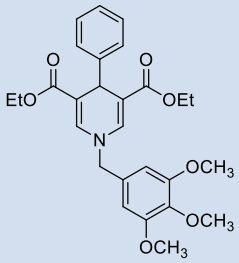	128-130°C	42.3%	Cyclohexane
MC2867	**3**	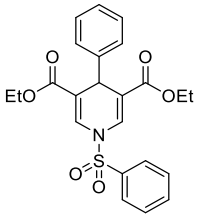	155-157°C	76%	Toluene
MC3139	**4a**	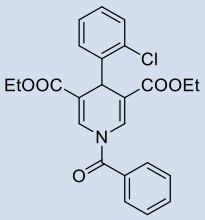	127-129°C	80%	Cyclohexane

MC3140	**4b**	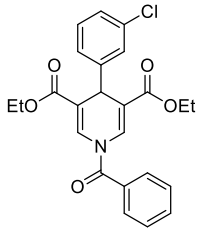	120-122°C	94%	Cyclohexane
MC3156	**4c**	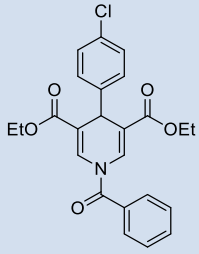	119-121°C	85%	Cyclohexane
MC3169	**4d**	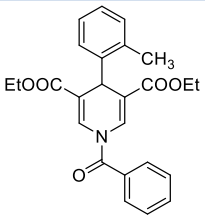	110-112°C	92%	Cyclohexane
MC3170	**4e**	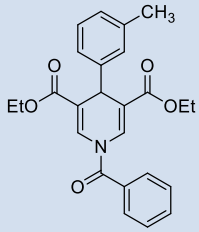	97-99°C	83%	Cyclohexane
MC3171	**4f**	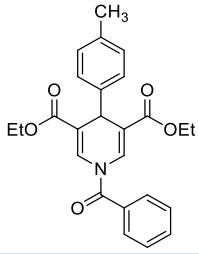	119-121°C	87%	Cyclohexane
MC3131	**4g**	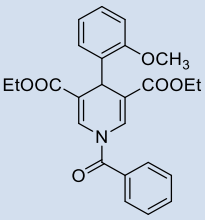	137-140°C	88%	Cyclohexane/Toulene
MC3138	**4h**	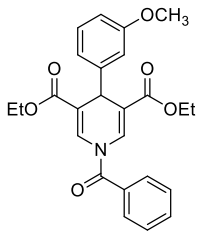	68-71°C	87.5%	Cyclohexane
MC3132	**4i**	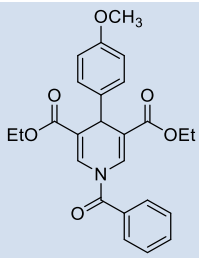	185-187°C	89%	Toluene/Acetonitrile

MC3193	**4j**	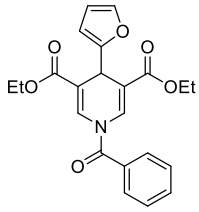	65-67°C	89.7%	Cyclohexane
MC3224	**4k**	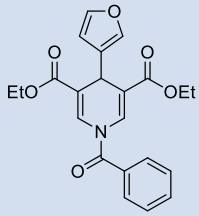	95-97°C	90%	Cyclohexane
MC3191	**4l**	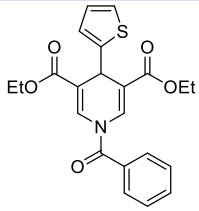	108-110°C	87.7%	Cyclohexane
MC3215	**4m**	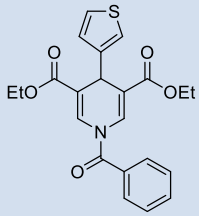	90-92°C	84%	Cyclohexane
MC4070	**5b**	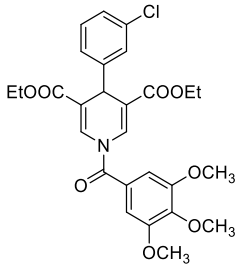	160-162°C	57%	Benzene
MC4069	**5c**	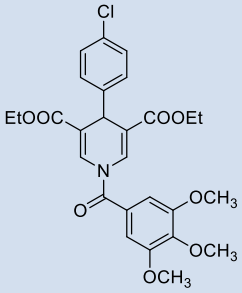	217-219°C	62.4%	Acetonitrile
MC4062	**5e**	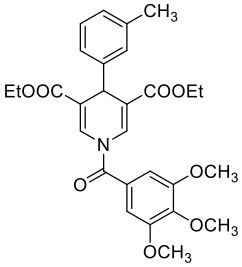	142-144°C	58.9%	Cyclohexane/Benzene

MC4068	**5j**	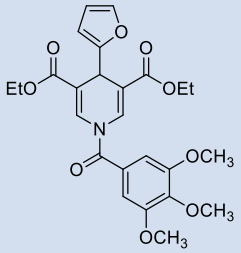	123-125°C	49.2%	Cyclohexane
MC4065	**5k**	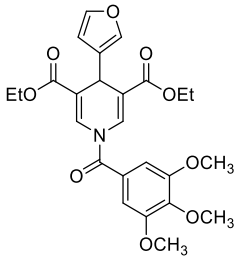	134-136°C	53.2%	Cyclohexane/Benzene
MC4076	**5m**	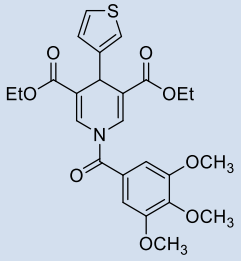	159-161°C	39.2%	Benzene
MC4071	**5n**	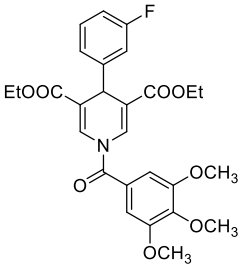	162-164°C	64%	Benzene
MC4077	**5o**	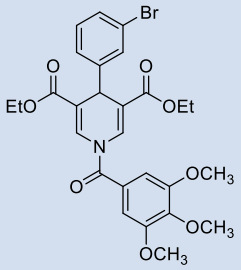	96-98°C	63.4%	Cyclohexane
MC4079	**5p**	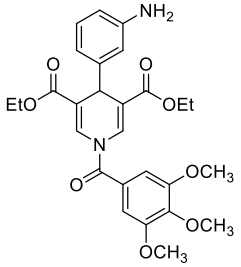	188-190°C	58.9%	Toluene/Benzene
MC4075	**5q**	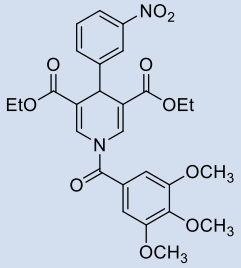	186-188°C	42.2%	Toluene/Benzene

MC4003	**6**	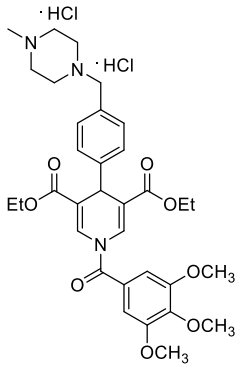	159-161°C	35.6%	Benzene

3.6 Experimental section

Chemistry. Melting points were determined on a Buchi 530 melting point apparatus and are uncorrected. ^{1}H NMR spectra were recorded at 400 MHz on a Bruker AC 400 spectrometer; chemical shifts are reported in δ (ppm) units relative to the internal reference tetramethylsilane (Me_4Si). EIMS spectra of all compounds were recorded with a Fisons Trio 1000 spectrometer; only molecular ions (M+) and base peaks are given.HR-MS spectra of final compounds were recorded with an ESI Orbitrap spectrometer (capillary temperature:275°C, spray voltage 4,0 kV (ESI +) and 3,8 kV (ESI +), sheath gas: 5, tube lens voltage +/- 90 V). The mass spectrometry samples were solubilized in MeOH + 0,01% HCOOH (10^{-5}M). All compounds were routinely checked by TLC and ^{1}H NMR. TLC was performed on aluminum-backed silica gel plates (Merck DC, Alufolien Kieselgel 60 F_{254}) with spots visualised by UV light. All solvents were reagent grade and, when necessary, were purified and dried by standard methods. The concentration of solutions after reactions involved the use of a rotary evaporator operating at a reduced pressure of ca. 20 Torr. Analytical results are within ±0.40% of the theoretical values. All chemicals were purchased from Sigma-Aldrich Chemistry, Milan (Italy), or from Alfa Aesar GmbH, Karlsruhe (Germany), and were of the highest purity.

General procedure for the synthesis of the diethyl 4-aryl-1,4-dihydropyridine-3,5-dicarboxylate intermediates 11a-q and 10: Example diethyl 4-phenyl-1,4-dihydropyridine-3,5-dicarboxylate (10)

To a solution of ethyl propiolate (2 eq, 1.109 g, 11.31 mmol) and NH_4OAc (1 eq, 0.440 g, 5.65 mmol) in glacial acetic acid (5 mL) was added benzaldehyde (1 eq, 0.57 mL, 5.65 mmol). The resulting mixture was heated to 90 °C. After 8 hours the reaction was cooled to room temperature, and the solvent was distilled in the presence of toluene. The remaining residue was purified by column chromatography (silica gel) using EtOAc:Hexane (1:3) as eluent. The product was isolated as a yellow solid (0.24 g, Y=14%).

Mp = 117-118°C.

^{1}H NMR (400MHz, $CDCl_3$) δ: 1.25 (t, 6H, 2x -OCH_2CH_3), 3.88-4.24 (m, 4H, 2x -OCH_2CH_3), 4.92 (s, 1H, ArC*H*-), 6.75 (s, 1H, N*H*), 7.17 (t, 1H, aromatic proton), 7.21-7.52 (m, 6H, aromatic protons and dihydropiridine protons) ppm.

General procedure for the synthesis of the properly substituted acylchlorides intermediates (9a-a')

Example: synthesis of the intermediate 3,4,5-trimethoxybenzoyl chloride (9u)

To a solution of 3,4,5-trimethoxybenzoyc acid (**8u**) (0.188 g, 0.83 mmol, 2.5 eq) in toluene (3 mL) was added $SOCl_2$ (0.3 mL, 4.15 mmol, 12.5 eq). After 1 hour the solvent was distilled and then washed twice with toluene to remove all traces of $SOCl_2$. The product (**9u**) was directly used, without purification, for the following acylation step.

General procedure for the synthesis of the final compounds (1a-a') and (4a-m, 5b-c, 5i-k, 5m, 5n-q** and **6) Example: synthesis of diethyl 4-phenyl-1-(3,4,5-trimethoxybenzoyl)-1,4-dihydropyridine-3,5-dicarboxylate (MC2789, 1u)

To a solution of diethyl 4-phenyl-1,4-dihydropyridine-3,5-dicarboxylate (**10**) (1 eq, 0.100 g, 0.33 mmol) in DCM dry (3 mL) was added TEA (4 eq, 0.185 mL, 1.33 mmol) and then, slowly and on ice bath, the previously synthesized 3,4,5-trimethoxybenzoyl chloride (**9u**) dissolved in DCM dry (3mL) was added too. The reaction was stirred overnight at RT. The solvent was then evaporated, and the remaining residue was purified by column chromatography (silica gel) using EtOAc:Hexane (1:2) as eluent. The product (**1u**) was isolated as a white solid (0.057 g, Y=34,8%).

Mp = 174-176°C

^{1}H NMR (400MHz, $CDCl_3$) δ: 1.11-1.19 (t, 6H, 2x -OCH_2CH_3), 3.82 (s, 6H, -OCH_3), 6.87 (s, 3H, -OCH_3), 3.98-4.12 (m, 4H, 2x -OCH_2CH_3), 4.89 (s, 1H, ArC*H*-), 6.83 (s, 2H, aromatic protons), 7.12-7.15 (m, 1H, aromatic proton), 7.19 (m, 1H, aromatic proton), 7.22-7.24 (d, 2H, aromatic protons), 7.26-7.28 (d, 2H, aromatic protons), 8.06 (s, 1H, dihydropyridine protons) ppm. MS (EI) m/z $[M]^+$: 495.19.

Procedure for the synthesis of the final compound diethyl 4-phenyl-1-(3,4,5-trimethoxybenzyl)-1,4-dihydropyridine-3,5-dicarboxylate (2)

Ethyl propiolate (2 eq, 1.9 mL, 18.84 mmol), benzaldehyde (1eq, 0.82 mL, 9.42 mmol), and (3,4,5-trimethoxyphenyl)methanamine (1 eq, 1.61 mL , 9.42 mmol) in glacial acetic acid (0.5 mL) were heated at 80 °C for 30 min. After cooling, the mixture was poured into water (20 mL) and stirred for 1 h. The solid product was filtered and washed with diethyl ether (3 × 30 mL) to give the pure **2** solid that was recrystallized from cyclohexane.

Mp= 128-130 °C.

^{1}H NMR (400MHz, $CDCl_3$) δ: 1.09-1.12 (t, 6H, 2x -OCH_2CH_3), 3.80 (s, 9H, 3x -OCH_3), 3.95-4.06 (m, 4H, 2x -OCH_2CH_3), 4.45 (s, 2H, -CH_2Ph), 4.85 (s, 1H, ArC*H*-), 6.40 (s, 2H, aromatic protons), 7.07-7.15 (m, 3H, aromatic protons), 7.21-7.25 (m, 4H, aromatic protons), 8.06 (s, 2H, dihydropyridine protons) ppm. MS (EI) m/z $[M]^+$: 481.21.

Procedure for the synthesis of the final compound diethyl 4-(4-((4-methylpiperazin-1-yl)methyl)phenyl)-1-(3,4,5-trimethoxybenzoyl)-1,4-dihydropyridine-3,5-dicarboxylate dihydrochloride (MC4003, 6)

To a solution of diethyl 4-(4-((4-methylpiperazin-1-yl)methyl)phenyl)-1-(3,4,5-trimethoxybenzoyl)-1,4-dihydropyridine-3,5-dicarboxylate **7** (1eq, 0.040g, 0.066 mmol) in dry tetrahydrofuran (2 mL), 4N HCl in 1,4 dioxane (10 eq, 0.2 mL, 0.66 mmol) was added dropwise at 0° C. The resulting solution was left stirring for about 30 min and then allowed to warm at room temperature. After 2 hours the reaction was completed, the solvent was removed by filtration and the solid was washed twice with diethyl ether (2x 5 mL) and dried *in vacuo* to afford the desired product **6** as a white salt. (0.016 g, Y= 35.7 %).

Mp= 159-161 °C.

^{1}H NMR (400MHz, $CDCl_3$) δ: 1.09-1.13 (t, 6H, 2x -OCH_2CH_3), 1.24 (s, 2H, ArCH_2-), 2.05 (s, 3H, -NCH_3), 3.77 (s, 3H, -OCH_3), 3.38-3.52 (m, 8H, piperazine protons), 3.83 (s, 6H, -OCH_3), 4.01-4.07 (m, 4H, 2x -OCH_2CH_3), 4.78 (s, 1H, ArC*H*-), 5.02 (s,2H, NCH_2Ph), 7.06 (s, 2H, aromatic protons), 7.32-7.30 (m, 4H, aromatic protons), 7.94 (s, 2H, dihydropyridine protons), 11.60 (bs, 2H, 2 x NH^+ piperazine) ppm. MS (EI) m/z $[M]^+$: 679.24.

^{1}H-NMR and mass spectra of final compounds:

Diethyl 1-Benzoyl-4-phenyl-1,4-dihydropyridine-3,5-dicarboxylate (MC2791, 1a)

^{1}H NMR (400MHz, $CDCl_3$) δ: 1.08−1.11 (m, *6H*, 2x -OCH_2CH_3), 4.01−4.07 (m, *4H*, 2x -OCH_2CH_3), 4.78 (s, *1H*, ArC*H*-), 7.20−7.21 (m, *1H*, aromatic protons), 7.29−7.35 (m, *4H*, aromatic protons), 7.61−7.64 (m, *2H*, aromatic protons), 7.68−7.73 (m, *4H*, aromatic protons), 7.90 (s, *2H*, dihydropyridine protons) ppm. MS (EI) m/z $[M]^+$: 405.16.

Diethyl 4-phenyl-1-(2-phenylacetyl***)-1,4-dihydropyridine-3,5-dicarboxylate (MC4208, 1b)***

^{1}H NMR (400MHz, $CDCl_3$) δ: 1.20-1.24 (t, 6H, 2x -OCH_2CH_3), 4.05-4.18 (m, 4H, 2x -OCH_2CH_3), 4.85 (s, 1H, ArC*H*-), 7.16-7.26 (m, 5H, aromatic protons), 7.32-7.37 (m, 3H, aromatic protons), 7.40-7.43 (m, 2H, aromatic protons), 8.14-8.18 (s, 2H, dihydropyridine protons) ppm. MS (EI) m/z $[M]^+$: 419.17.

Diethyl 1-(3-fluorobenzoyl)-4-phenyl-1,4-dihydropyridine-3,5-dicarboxylate (MC4158, 1c)

^{1}H NMR (400MHz, $CDCl_3$) δ: 1.19-1.22 (t, 6H, 2x -OCH_2CH_3), 4.06-4.20 (m, 4H, 2x -OCH_2CH_3), 4.96 (s, 1H, ArC*H*-), 7,25-7,21 (m, 1H, aromatic proton), 7.28-7.44 (m, 5H, aromatic protons), 7.40-7.44 (m, 2H, aromatic protons), 7.52-7.57 (m, 1H, aromatic proton), 8.08 (s, 2H, dihydropyridine protons) ppm. MS (EI) m/z $[M]^+$: 439.12.

Diethyl 1-(4-fluorobenzoyl)-4-phenyl-1,4-dihydropyridine-3,5-dicarboxylate (MC4168, 1d)

^{1}H NMR (400MHz, $CDCl_3$) δ: 1.10-1.14 (t, 6H, 2x -OCH_2CH_3), 3.97-4.11 (m, 4H, 2x -OCH_2CH_3), 4.88 (s, 1H, ArC*H*-), 7.14-7.27 (m, 7H, aromatic protons), 7.61-7.65 (m, 2H, aromatic protons), 8.00 (s, 2H, dihydropyridine protons) ppm. MS (EI) m/z $[M]^+$: 423.15.

Diethyl 1-(3-chlorobenzoyl)-4-phenyl-1,4-dihydropyridine-3,5-dicarboxylate (MC4172, 1e)

^{1}H NMR (400MHz, $CDCl_3$) δ: 1.19-1.23 (t, *6H*, 2x -OCH_2CH_3), 4.06-4.20 (m, *4H*, 2x -OCH_2CH_3), 4.96 (s, 1H, ArC*H*-), 7.22-7.25 (m, 1H, aromatic proton), 7.30-7.36 (m, 4H, aromatic protons), 7.47-7.52 (m, 2H, aromatic protons), 7.60-7.63 (m, 1H, aromatic proton), 7.69 (s, 1H, aromatic proton), 8.07 (s, 1H, dihydropyridine proton) ppm. MS (EI) m/z $[M]^+$: 439.12.

Diethyl 1-(4-chlorobenzoyl)-4-phenyl-1,4-dihydropyridine-3,5-dicarboxylate (MC4166, 1f)

^{1}H NMR (400MHz, $CDCl_3$) δ: 1.19-1.23 (t, 6H, 2x -OCH_2CH_3), 4.08-4.19 (m, 4H, 2x -OCH_2CH_3), 4.96 (s, 1H, ArC*H*-), 7.22-7.36 (m, 5H, aromatic protons), 7.53-7.55 (d, 2H, aromatic protons), 7.62-7.64 (d, 2H, aromatic protons), 8.07 (s, 2H, dihydropyridine protons) ppm. MS (EI) m/z $[M]^+$: 439.12.

Diethyl 1-(3-bromobenzoyl)-4-phenyl-1,4-dihydropyridine-3,5-dicarboxylate (MC4181, 1g)

^{1}H NMR (400MHz, $CDCl_3$) δ: 1.19-1.23 (t, 6H, 2x -OCH_2CH_3), 4.06-4.20 (m, 4H, 2x -OCH_2CH_3), 4.96 (s, 1H, ArC*H*-), 7.22-7.25 (m, 1H, aromatic proton), 7.30-7.36 (m, 4H, aromatic protons), 7.41-7.45 (t, 1H, aromatic proton), 7.55-7.57 (d, 1H, aromatic proton), 7.76-7.78 (d, 1H, aromatic proton), 7.85 (s, 1H, aromatic proton), 8.07 (s, 2H, dihydropyridine protons) ppm. MS (EI) m/z $[M]^+$: 483.07.

Diethyl 1-(4-bromobenzoyl)-4-phenyl-1,4-dihydropyridine-3,5-dicarboxylate (MC4185, 1h)

^{1}H NMR (400MHz, $CDCl_3$) δ: 1.19-1.23 (t, 6H, 2x -OHC_2CH_3), 4.06-4.21 (m, 4H, 2x -OCH_2CH_3), 4.96 (s, 1H, ArC*H*-), 7.22-7.25 (m, 1H, aromatic proton), 7.32-7.36 (m, 4H, aromatic protons), 7.54-7.57 (d, 2H, aromatic protons), 7.67-7.72 (d, 2H, aromatic protons), 8.07 (s, 2H, dihydropyridine protons) ppm. MS (EI) m/z $[M]^+$: 483.07.

Diethyl 1-(3-nitrobenzoyl)-4-phenyl-1,4-dihydropyridine-3,5-dicarboxylate (MC4165, 1i)

^{1}H NMR (400MHz, $CDCl_3$) δ: 1.19-1.22 (s*,* 6H, 2x -OCH_2CH_3), 4.08-4.19 (m, 4H, 2x -OCH_2CH_3), 4.98 (s, 1H*,* ArC*H*-), 7.23-7.28 (m, 1H, aromatic proton), 7.31-7.49 (m, 4H, aromatic protons), 7.76-7.80 (t, 1H, aromatic proton), 7.95-7.97 (d, 1H, aromatic proton), 8.04 (s, 2H, dihydropyridine protons), 8.49-8.51 (d, 1H, aromatic proton), 8.58 (s, 1H, aromatic proton) ppm. MS (EI) m/z $[M]^+$: 450.14.

Diethyl 1-(4-nitrobenzoyl)-4-phenyl-1,4-dihydropyridine-3,5-dicarboxylate (MC4167, 1j)

^{1}H NMR (400MHz, $CDCl_3$) δ: 1.19-1.22 (t, 6H, 2x -OCH_2CH_3), 4.08-4.19 (m, 4H, 2x -OCH_2CH_3), 4.97 (s, 1H, ArC*H*-), 7.23-7.28 (m, 1H, aromatic proton), 7.31-7.34 (m, 4H, aromatic protons), 7.84-7.86 (d, 2H, aromatic protons), 8.02 (s, 2H, dihydropyridine protons), 8.41-8.43 (d, 2H, aromatic protons) ppm. MS (EI) m/z $[M]^+$: 450.14.

Diethyl 1-(4-cyanobenzoyl)-4-phenyl-1,4-dihydropyridine-3,5-dicarboxylate (MC4177, 1k)

^{1}H NMR (400MHz, $CDCl_3$) δ: 1.10-1.68 (t, 6H, 2x -OCH_2CH_3), 3.97-4.11 (m, 4H, 2x -OCH_2CH_3), 4.87 (s, 1H, ArC*H*-), 7.17-7.17 (m, 1H, aromatic proton), 7.19-7.21 (m, 2H, aromatic protons), 7.23-7.24 (m, 2H, aromatic protons), 7.68-7.70 (d, 2H, aromatic protons), 7.77-7.79 (d, 2H, aromatic protons), 7.93 (s, 2H, dihydropyridine protons) ppm. MS (EI) m/z $[M]^+$: 430.15.

Diethyl 1-(furan-2-carbonyl)-4-phenyl-1,4-dihydropyridine-3,5-dicarboxylate (MC4204, 1l)

^{1}H NMR (400MHz, $CDCl_3$) δ: 1.13-1.17 (t, 6H, 2x -OCH_2CH_3), 3.99-4.14 (m, 4H, 2x -OCH_2CH_3), 4.88 (s, 1H, ArC*H*-), 6.57-6.59 (m, 1H, aromatic proton), 7.10-7.14 (m, 1H, aromatic proton), 7.18-7.22 (m, 2H, aromatic proton), 7.24-7.26 (m, 2H, aromatic proton), 7.32-7.34 (d, 1H, aromatic proton), 7.65 (m, 1H, aromatic proton), 8.31 (s, 2H, dihydropyridine protons) ppm. MS (EI) m/z $[M]^+$: 495.14.

Diethyl 4-phenyl-1-(thiophene-2-carbonyl)-1,4-dihydropyridine-3,5-dicarboxylate (MC4188, 1m)

^{1}H NMR (400MHz, $CDCl_3$) δ: 1.21-1.25 (t, 6H, 2x -OCH_2CH_3), 4.08-4.23 (m, 4H, 2x -OCH_2CH_3), 4.98 (s, 1H, ArC*H*-), 7.21-7.24 (m, 2H, aromatic protons), 7.28-7.32 (m, 2H, aromatic protons), 7.35-7.37 (m, 2H, aromatic protons), 7.67-7.68 (d, 1H, aromatic proton), 7.76-7.77 (d, 1H, aromatic proton), 8.29 (s, 2H, dihydropyridine protons) ppm. MS (EI) m/z $[M]^+$: 411.11.

Diethyl 4-phenyl-1-(thiophene-3-carbonyl)-1,4-dihydropyridine-3,5-dicarboxylate (MC4186, 1n)

^{1}H NMR (400MHz, $CDCl_3$) δ: 1.20-1.24 (t, 6H, 2x -OCH_2CH_3), 4.07-4.22 (m, 4H, 2x -OCH_2CH_3), 4.97 (s, 1H, ArC*H*-), 7.20-7.36 (m, 5H, aromatic protons), 7.45-7.50 (m, 2H, aromatic protons), 7.97-7.98 (m, 1H, aromatic proton), 8.21 (s, 2H, dihydropyridine protons) ppm. MS (EI) m/z $[M]^+$: 411.11.

Diethyl 1-(cyclohexanecarbonyl)-4-phenyl-1,4-dihydropyridine-3,5-dicarboxylate (MC4199, 1o)

^{1}H NMR (400MHz, $CDCl_3$) δ: 1.12-1.15 (t, 6H, 2x -OCH_2CH_3), 1.18-1.36 (m, 4H, cyclohexane protons), 1.52-1.55 (m, 2H, cyclohexane protons), 1.79-1.86 (m, 2H, cyclohexane protons), 3.98-4.1 (m, 4H, 2x -OCH_2CH_3), 4.80 (s, 1H, ArC*H*-), 7.09-7.19 (m, 5H, aromatic protons), 8.03 (s, 2H, dihydropyridine protons) ppm. MS (EI) m/z $[M]^+$: 411.20.

1-Benzyl-3,5-diethyl-4-phenylpyridine-1,3,5(4H)-tricarboxylate (1p)

^{1}H NMR (400MHz, $CDCl_3$) δ: 1.19−1.26 (m, 6H, 2x -OCH_2CH_3), 4.04−4.23 (m, 4H, 2x -OCH_2CH_3), 4.87 (s, 1H, ArC*H*-), 5.40 (s, 2H, −CH_2Ph), 7.18−7.22 (m, 1H, aromatic proton), 7.24−7.30 (m, 2H, aromatic protons), 7.42−7.48 (m, 5H, aromatic protons), 8.06 (s, 2H, dihydropyridine protons) ppm. MS (EI) m/z $[M]^+$: 421.15.

Diethyl 4-Phenyl-1-(pyrazine-2-carbonyl)-1,4-dihydropyridine-3,5-dicarboxylate (1q)

^{1}H NMR (400MHz, $CDCl_3$) δ: 1.10−1.14 (m, 6H, 2x -OCH_2CH_3), 4.04−4.09 (m, 4H, 2x -OCH_2CH_3), 4.80 (s, 1H, ArC*H*-), 7.18−7.22 (m, 1H, aromatic proton), 7.26−7.30 (m, 4H, aromatic protons), 8.19 (s, 2H,

dihydropyridine protons), 8.85 (s, 1H, pyrazine proton), 8.86 (d, 1H, pyrazine proton) 9.20 (s, 1H, pyrazine proton) ppm. MS (EI) m/z $[M]^+$: 407.15.

Diethyl 1-(2-Naphthoyl)-4-phenyl-1,4-dihydropyridine-3,5-dicarboxylate (MC2861, 1r)

^{1}H NMR (400MHz, $CDCl_3$) δ: 1.17−1.21 (m, 6H, 2x -OCH_2CH_3), 4.05−4.19 (m, 4H, 2x -OCH_2CH_3), 4.99 (s, 1H, ArC*H*-), 7.24−7.25 (m, 1H, aromatic proton), 7.33−7.35 (m, 2H, aromatic protons), 7.40−7.42 (m, 2H, aromatic protons), 7.65−7.72 (m, 3H, aromatic protons), 7.89−7.95 (m, 3H, aromatic protons), 8.23 (s, 1H, aromatic proton), 8.27 (s, 2H, dihydropyridine protons) ppm. MS (EI) m/z $[M]^+$: 455.17.

Diethyl 1-(1-Naphthoyl)-4-phenyl-1,4-dihydropyridine-3,5-dicarboxylate (1s)

^{1}H NMR (400MHz, $CDCl_3$) δ: 1.06−1.16 (m, 6H, 2x -OCH_2CH_3), 4.00−4.19 (m, 4H, 2x -OCH_2CH_3), 4.95 (s, 1H, ArC*H*-), 7.22−7.41 (m, 6H, aromatic protons), 7.59−7.68 (m, 4H, dihydropyridine protons and aromatic protons), 6.28−6.29 (m, 1H, dihydropyridine proton), 7.90−8.10 (m, 4H, aromatic protons) ppm. MS (EI) m/z $[M]^+$: 455.17.

Diethyl 4-Phenyl-1-(quinoxaline-2-carbonyl)-1,4-dihydropyridine-3,5-dicarboxylate (1t)

^{1}H NMR (400MHz, $CDCl_3$) δ: 1.11−1.13 (m, 6H, 2x -OCH_2CH_3), 4.04−4.10 (m, 4H, 2x -OCH_2CH_3), 4.83 (s, 1H, ArC*H*-), 7.21−7.23 (m, 1H, aromatic proton), 7.30−7.34 (m, 4H, aromatic protons), 8.03−8.10 (m, 2H, quinoxaline protons), 8.18 (d, 1H, quinoxaline proton), 8.26 (d, 1H, quinoxaline proton), 8.45 (s, 2H, dihydropyridine protons), 9.41 (s, 1H, quinoxaline proton) ppm. MS (EI) m/z $[M]^+$: 457.16.

Diethyl 4-phenyl-1-(3,4,5-trimethoxybenzoyl)-1,4-dihydropyridine-3,5-dicarboxylate (MC2789, 1u)

^{1}H NMR (400MHz, $CDCl_3$) δ: 1.11-1.19 (t, 6H, 2x -OCH_2CH_3), 3.82 (s, 6H, 2x -OCH_3), 6.87 (s, 3H, -OCH_3), 3.98-4.12 (m, 4H, 2x -OCH_2CH_3), 4.89 (s, 1H, ArC*H*-), 6.83 (s, 2H, aromatic protons), 7.12-7.15 (m, 1H, aromatic proton), 7.19 (m, 1H, aromatic proton), 7.22-7.24 (d, 2H, aromatic protons), 7.26-7.28 (d, 2H, aromatic protons), 8.06 (s, 2H, dihydropyridine protons) ppm. MS (EI) m/z $[M]^+$: 495.19.

Diethyl 1-(3-methoxybenzoyl)-4-phenyl-1,4-dihydropyridine-3,5-dicarboxylate (MC4164, 1v)

^{1}H NMR (400MHz, $CDCl_3$) δ: 1.19-1.28 (t, 6H, 2x -OCH_2CH_3), 3.89 (s, 3H, -OCH_3), 4.07-4.18 (m, 4H, 2x -OCH_2CH_3), 4.96 (s, 1H, ArC*H*-), 7.15-7.24 (m, 4H, aromatic protons), 7.28-7.29 (m, 1H, aromatic proton), 7.31-7.36 (m, 3H, aromatic protons), 7.43-7.47 (t, 1H, aromatic proton), 8.12 (s, 2H, dihydropyridine protons) ppm. MS (EI) m/z $[M]^+$: 435.17.

Diethyl 1-(4-methoxybenzoyl)-4-phenyl-1,4-dihydropyridine-3,5-dicarboxylate (MC4182, 1w)

^{1}H NMR (400MHz, $CDCl_3$) δ: 1.19-1.23 (t, 6H, 2x -OCH_2CH_3), 3.92 (s, 3H, -OCH_3), 4.06-4.19 (m, 4H, 2x -OCH_2CH_3), 4.97 (s, 1H, ArC*H*-), 7.02-7.05 (d, 2H, aromatic protons), 7.21-7.25 (t, 1H, aromatic proton), 7.28-7.38 (m, 4H, aromatic protons), 7.67-7.70 (d, 2H, aromatic protons), 8.12 (s, 2H, dihydropyridine protons) ppm. MS (EI) m/z $[M]^+$: 435.17.

Diethyl 1-(3,4-dimethoxybenzoyl)-4-phenyl-1,4-dihydropyridine-3,5-dicarboxylate (MC4175, 1y)

^{1}H NMR (400MHz, $CDCl_3$) δ: 1.20-1.28 (t, 6H, 2x -OCH_2CH_3), 3.95 (s, 3H, -OCH_3), 3.99 (s, 3H, -OCH_3), 4.06-4.21 (m, 4H, 2x -OCH_2CH_3), 4.97 (s, 1H, ArC*H*-), 6.96-6.99 (d, 1H, aromatic proton), 7.21-7.38 (m, 7H, aromatic protons), 8.15 (s, *2H, dihydropyridine* protons) ppm. MS (EI) m/z $[M]^+$: 465.18.

Diethyl 1-(3,5-dimethoxybenzoyl)-4-phenyl-1,4-dihydropyridine-3,5-dicarboxylate (MC4176, 1z)

^{1}H NMR (400MHz, $CDCl_3$) δ: 1.19-1.23 (t, m, 6H, -OCH_2CH_3), 3.85 (s, 6H, 2x -OCH_3), 4.15 (m, 4H, 2x -OCH_2CH_3), 4.95 (s, 1H, ArC*H*-), 6.67-6.68 (m, 1H, aromatic proton), 6.75-6.76 (d, 2H, aromatic protons), 7.22-7.24 (m, 1H, aromatic proton), 7.28-7.36 (m, 4H, aromatic protons), 8.12 (s, 2H, dihydropyridine protons). MS (EI) m/z $[M]^+$: 465.18.

Diethyl (E)-1-(4-(but-2-enoyloxy)-3,5-dimethoxybenzoyl)-4-phenyl-1,4-dihydropyridine-3,5-dicarboxylate (MC4054, 1a')

^{1}H NMR (400MHz, $CDCl_3$) δ: 1.20-1.24 (t, 6H, 2x -OCH_2CH_3), 2.0-2.02 (d, 3H, -CH_3), 3.87 (s, 6H, 2x –CH_3), 4.09-4.22 (m, 4H, 2x -OCH_2CH_3), 4.98 (s, 1H, ArC*H*-), 6.13-6.17 (d, 1H, -C*H*=CHCO), 6.95 (d, 1H, -CH=C*H*CO), 7.23 (m, 2H, aromatic protons), 7.27-7.38 (m, 5H, aromatic protons), 8.16 (s, 2H, dihydropyridine protons) ppm. MS (EI) m/z $[M]^+$: 549.20.

Diethyl 4-phenyl-1-(3,4,5-trimethoxybenzyl)-1,4-dihydropyridine-3,5-dicarboxylate (MC4001, 2)

^{1}H NMR (400MHz, $CDCl_3$) δ: 1.09-1.12 (t, 6H, 2x -OCH_2CH_3), 3.80 (s, 9H, 3x -OCH_3), 3.95-4.06 (m, 4H, 2x -OCH_2CH_3), 4.45 (s, 2H, -CH_2Ph), 4.85 (s, 1H, ArC*H*-), 6.40 (s, 2H, aromatic protons), 7.07-7.15 (m, 3H, aromatic protons), 7.21-7.25 (m, 4H, aromatic protons), 8.06 (s, 2H, dihydropyridine protons) ppm. MS (EI) m/z $[M]^+$: 481.21.

Diethyl 4-phenyl-1-(phenylsulfonyl)-1,4-dihydropyridine-3,5-dicarboxylate (3)

^{1}H NMR (400MHz, $CDCl_3$) δ: 1.14−1.23 (m, 6H, 2x -OCH_2CH_3), 4.06−4.17 (m, 4H, 2x -OCH_2CH_3), 4.79 (s, 1H, ArC*H*-), 6.84−6.92 (m, 2H, aromatic protons), 7.05−7.15 (m, 3H, aromatic protons), 7.66−7.72 (m, 2H, aromatic protons), 7.76−7.86 (m, 3H, aromatic protons), 7.91−8.00 (m, 2H, dihydropyridine protons) ppm. MS (EI) m/z $[M]^+$: 441.12.

Diethyl 1-benzoyl-4-(2-chlorophenyl)-1,4-dihydropyridine-3,5-dicarboxylate (MC3139, 4a)

^{1}H NMR (400MHz , $CDCl_3$) δ: 1.18−1.21 (m, 6H, 2x -OCH_2CH_3), 4.06−4.19 (m, 4H, 2x -OCH_2CH_3), 5.40 (s, 1H, ArC*H*-), 7.14−7.18 (m, 1H, aromatic proton), 7.23−7.26 (m, 1H, aromatic proton), 7.33−7.36 (m, 2H, aromatic protons), 7.54−7.58 (m, 2H, aromatic protons), 7.62−7.66 (m, 1H, aromatic proton), 7.68−7.71 (m, 2H, aromatic protons), 8.15 (s, 2H, dihydropyridine protons) ppm. MS (EI) m/z $[M]^+$: 439.12.

Diethyl 1-benzoyl-4-(3-chlorophenyl)-1,4-dihydropyridine-3,5-dicarboxylate (MC3140, 4b)

^{1}H NMR (400MHz, $CDCl_3$) δ: 1.21−1.24 (m, 6H,2x -OCH_2CH_3), 4.09−4.20 (m, 4H, -OCH_2CH_3), 4.95 (s, 1H, ArC*H*-), 7.21−7.24 (m, 1H, aromatic proton), 7.25−7.27 (m, 2H, aromatic protons), 7.33 (s, 1H, aromatic

proton), 7.55−7.59 (m, 2H, aromatic protons), 7.65−7.69 (m, 3H, aromatic proton), 8.14 (s, 2H, dihydropyridine protons) ppm. MS (EI) m/z $[M]^+$: 439.12.

Diethyl 1-benzoyl-4-(4-chlorophenyl)-1,4-dihydropyridine-3,5-dicarboxylate (MC3156, 4c)

^{1}H NMR (400MHz, $CDCl_3$) δ: 1.20−1.23 (m, 6H, 2x -OCH_2CH_3), 4.08−4.17 (m, 4H, 2x -OCH_2CH_3), 4.95 (s, 1H, ArC*H*-), 7.30 (s, 4H, aromatic protons), 7.55−7.58 (m, 2H, aromatic protons), 7.63−7.68 (m, 3H, aromatic protons), 8.12 (s, 2H, dihydropyridine protons) ppm. MS (EI) m/z $[M]^+$: 439.12.

Diethyl 1-benzoyl-4-(o-tolyl)-1,4-dihydropyridine-3,5-dicarboxylate (MC3169, 4d)

^{1}H NMR (400MHz, $CDCl_3$) δ: 1.18−1.21 (m, 6H, 2x -OCH_2CH_3), 2.71 (s, 3H, −CH_3), 4.06−4.17 (m, 4H, 2x -OCH_2CH_3), 5.11 (s, 1H, ArC*H*-), 7.10−7.15 (m, 2H, aromatic protons), 7.17−7.18 (m, 2H, aromatic protons), 7.55−7.59 (m, 2H, aromatic protons), 7.63−7.66 (m, 1H, aromatic proton), 7.70−7.71 (m, 2H, aromatic protons), 8.13 (s, 2H, dihydropyridine protons) ppm. MS (EI) m/z $[M]^+$: 419.17.

Diethyl 1-benzoyl-4-(m-tolyl)-1,4-dihydropyridine-3,5-dicarboxylate (MC3170, 4e)

^{1}H NMR (400MHz, $CDCl_3$) δ: 1.20−1.24 (m, 6H, 2x -OCH_2CH_3), 2.36 (s, 3H, −CH_3), 4.08−4.19 (m, 4H, 2x -OCH_2CH_3), 4.93 (s, 1H, ArC*H*-), 7.04 (d, 1H, aromatic proton), 7.14−7.23 (m, 3H, aromatic protons), 7.53−7.58 (m, 2H, aromatic protons), 7.62−7.69 (m, 3H, aromatic protons), 8.12 (s, 2H, dihydropyridine protons) ppm. MS (EI) m/z $[M]^+$: 419.17.

Diethyl 1-benzoyl-4-(p-tolyl)-1,4-dihydropyridine-3,5-dicarboxylate (MC3171, 4f)

^{1}H NMR (400MHz, $CDCl_3$) δ: 1.20−1.25 (m, 6H, 2x -OCH_2CH_3), 2.33 (s, 3H, −CH_3), 4.06−4.18 (m, 4H, 2x -OCH_2CH_3), 4.92 (s, 1H, ArC*H*-), 7.13 (d, 2H, aromatic protons), 7.25 (d, 2H, aromatic protons), 7.53−7.57 (m, 2H, aromatic protons), 7.63 (d, 1H, aromatic proton), 7.68 (d, 2H, aromatic protons), 8.11 (s, 2H, dihydropyridine protons) ppm. MS (EI) m/z $[M]^+$: 419.17.

Diethyl 1-benzoyl-4-(2-methoxyphenyl)-1,4-dihydropyridine-3,5-dicarboxylate (MC3131, 4g)

^{1}H NMR (400MHz, $CDCl_3$) δ: 1.18−1.21 (m, 6H, 2x -OCH_2CH_3), 3.84 (s, 3H, -OCH_3), 4.04−4.16 (m, 4H, 2x -OCH_2CH_3), 5.14 (s, 1H, ArC*H*-), 6.88−6.95 (m, 2H, aromatic protons), 7.20−7.26 (m, 1H, aromatic proton), 7.33−7.36 (m, 1H, aromatic proton), 7.53−7.57 (m, 2H, aromatic protons), 7.61−7.65 (m, 1H, aromatic proton), 7.71−7.73 (m, 2H, aromatic protons), 8.10 (s, 2H, dihydropyridine protons) ppm. MS (EI) m/z $[M]^+$: 435.17.

Diethyl 1-benzoyl-4-(3-methoxyphenyl)-1,4-dihydropyridine-3,5-dicarboxylate (MC3138, 4h)

^{1}H NMR (400MHz, $CDCl_3$) δ: 1.21−1.24 (m, 6H, 2x -OCH_2CH_3), 3.82 (s, 3H, -OCH_3), 4.10−4.17 (m, 4H, 2x -OCH_2CH_3), 4.96 (s, 1H, ArC*H*-), 6.77−6.79 (m, 1H, aromatic proton), 6.93−6.97 (m, 2H, aromatic protons),

7.22−7.26 (m, 1H, aromatic proton), 7.54−7.58 (m, 2H, aromatic protons), 7.62−7.69 (m, 3H, aromatic protons), 8.12 (s, 2H, dihydropyridine protons) ppm. MS (EI) m/z [M]+: 435.17.

Diethyl 1-benzoyl-4-(4-methoxyphenyl)-1,4-dihydropyridine-3,5-dicarboxylate (MC3132, 4i)

^{1}H NMR (400MHz, $CDCl_3$) δ: 1.20−1.24 (m, 6H, 2x -OCH_2CH_3), 3.80 (s, 3H, -OCH_3), 4.10−4.19 (m, 4H, 2x -OCH_2CH_3), 4.91 (s, 1H, ArC*H*-), 6.85 (d, 2H, aromatic protons), 7.26 (s, 2H, aromatic protons), 7.54−7.58 (m, 2H, aromatic proton), 7.63 (d, 1H, aromatic proton), 7.67−7.69 (m, 2H, aromatic protons), 8.10 (s, 2H, dihydropyridine protons) ppm. MS (EI) m/z $[M]^+$: 435.17.

Diethyl 1-benzoyl-4-(furan-2-yl)-1,4-dihydropyridine-3,5-dicarboxylate (MC3193, 4j)

^{1}H NMR (400MHz, $CDCl_3$) δ: 1.25-1.28 (t, 6H, 2x -OCH_2CH_3), 4.15-4.23 (m, 4H, 2x -OCH_2CH_3), 5.15 (s, 1H, ArC*H*-), 6.21 (d, 1H, furan proton), 6.32 (m, 1H, furan proton), 7.32 (d, 1H, furan proton), 7.54-7.57 (t, 2H, aromatic protons), 7.63 (d, 1H, aromatic proton), 7.68-7.70 (d, 2H, aromatic protons), 8.11 (s, 2H, dihydropyridine protons) ppm. MS (EI) m/z [M]+: 395.14.

Diethyl 1-benzoyl-4-(furan-3-yl)-1,4-dihydropyridine-3,5-dicarboxylate (MC3224, 4k)

^{1}H NMR (400MHz, $CDCl_3$) δ: 1.26-1.28 (t, 6H, 2x -OCH_2CH_3), 4.18-4.30 (m, 4H, 2x -OCH_2CH_3), 4.96 (s, 1H, ArC*H*-), 6.36 (s, 1H, furan proton), 7.29 (m, 1H, furan proton), 7.34 (d, 1H, furan proton), 7.53-7.57 (t, 2H, aromatic protons), 7.63-7.68 (m, 3H, aromatic protons), 8.07 (s, 2H, dihydropyridine protons) ppm. MS (EI) m/z [M]+: 395.14.

Diethyl 1-benzoyl-4-(thiophen-2-yl)-1,4-dihydropyridine-3,5-dicarboxylate (MC3191, 4l)

^{1}H NMR (400MHz, $CDCl_3$) δ: 1.25-1.28 (t, 6H, 2x -OCH_2CH_3); 4.15- 4.25 (m, 4H, 2x -OCH_2CH_3); 5.33 (s, 1H, -ArC*H*), 6.93-6.96 (m, 1H, thiophene proton), 6.99-7.00 (m, 1H, thiophene proton); 7.18-7.19 (m, 1H, thiophene proton), 7.53-7.57 (m, 2H, aromatic protons), 7.62-7.64 (d, 1H, aromatic proton), 7.67-7.69 (m, 2H, aromatic protons), 8.09 (m, 2H, dihydropyridine protons) ppm. MS (EI) m/z $[M]^+$: 441.11.

Diethyl 1-benzoyl-4-(thiophen-3-yl)-1,4-dihydropyridine-3,5-dicarboxylate (MC3215, 4m)

^{1}H NMR (400MHz, $CDCl_3$) δ: 1.23-1.26 (t, 6H, 2x -OCH_2CH_3); 4.13- 4.24 (m, 4H, 2x -OCH_2CH_3); 5.13 (s, 1H, -ArC*H*), 7.07-7.09 (d, 1H, thiophene proton), 7.13-7.14 (m, 1H, thiophene proton); 7.23-7.25 (m, 1H, thiophene proton), 7.53-7.57 (m, 2H, aromatic protons), 7.62-7.66 (m, 3H, aromatic protons), 8.09 (m, 2H, dihydropyridine protons) ppm. MS (EI) m/z [M]+: 441.11.

Diethyl 4-(3-chlorophenyl)-1-(3,4,5-trimethoxybenzoyl)-1,4-dihydropyridine-3,5-dicarboxylate (MC4070, 5b)

^{1}H NMR (400MHz, $CDCl_3$) δ: 1.22-1.25 (t, 6H, 2x -OCH_2CH_3), 2.25 (s, 3H, -ArCH_3), 3.87 (s, 3H, -OCH_3), 3.82 (s, 6H, -OCH_3), 4.11-4.21 (m, 4H, 2x -OCH_2CH_3), 4.96 (s, 1H, ArC*H*-), 6.92 (s, 2H, aromatic protons), 6.94-

6.96 (s, 1H, aromatic proton), 7.22-7.23 (m, 2H, aromatic protons), 7.30 (s, 1H, aromatic proton), 8.15 (s, 2H, dihydropyridine protons) ppm. MS (EI) m/z $[M]^+$: 529.15.

Diethyl 4-(4-chlorophenyl)-1-(3,4,5-trimethoxybenzoyl)-1,4-dihydropyridine-3,5-dicarboxylate (MC4069, 5c)

^{1}H NMR (400MHz, $CDCl_3$) δ: 1.21-1.24 (t, 6H, 2x -OCH_2CH_3), 3.91 (s, 6H, -OCH_3), 3.97 (s, 3H, -OCH_3), 4.08-4.21 (m, 4H, 2x -OCH_2CH_3), 4.95 (s, 1H, Ar*CH*-), 6.90 (s, 2H, aromatic protons), 7.27-7.31 (dd, 4H, aromatic protons), 8.15 (s, 2H, dihydropyridine protons) ppm. MS (EI) m/z $[M]^+$: 529.15.

Diethyl 4-(m-tolyl)-1-(3,4,5-trimethoxybenzoyl)-1,4-dihydropyridine-3,5-dicarboxylate (MC4062, 5e)

^{1}H NMR (400MHz, $CDCl_3$) δ: 1.12-1.15 (t, 6H, 2x -OCH_2CH_3), 1.19 (s, 2H, ArCH_2-), 2.25 (s, 3H, -ArCH_3), 3.87 (s, 3H, -OCH_3), 3.82 (s, 6H, -OCH_3), 4.00-4.11 (m, 4H, 2x -OCH_2CH_3), 4.85 (s, 1H, Ar*CH*-), 6.83 (s, 2H, aromatic protons), 6.94-6.96 (s, 1H, aromatic proton), 7.07-7.10 (m, 3H, aromatic protons), 7.19 (m, 4H, aromatic protons), 8.05 (s, 2H, dihydropyridine protons) ppm. MS (EI) m/z $[M]^+$: 509.20.

Diethyl 4-(furan-2-yl)-1-(3,4,5-trimethoxybenzoyl)-1,4-dihydropyridine-3,5-dicarboxylate (MC4068, 5j)

^{1}H NMR (400MHz, $CDCl_3$) δ: 1.17-1.20 (t, 6H, 2x -OCH_2CH_3), 3.82 (s, 6H, 2x -OCH_3), 3.87 (s, 3H, -OCH_3), 4.06-4.20 (m, 4H, 2x -OCH_2CH_3), 5.08 (s, 1H, Ar*CH*-), 6.13-6.14 (d, 1H, furan proton), 6.22-6.24 (m, 1H, furan proton), 6.86 (s, 2H, aromatic protons), 8.04 (s, 2H, dihydropyridine protons) ppm. MS (EI) m/z $[M]^+$: 485.17.

Diethyl 4-(furan-3-yl)-1-(3,4,5-trimethoxybenzoyl)-1,4-dihydropyridine-3,5-dicarboxylate (MC4065, 5k)

^{1}H NMR (400MHz, $CDCl_3$) δ: 1.14-1.21 (t, 6H, 2x -OCH_2CH_3), 3.81 (s, 6H, -OCH_3), 3.87 (s, 3H, -OCH_3), 4.11-4.20 (m, 4H, 2x -OCH_2CH_3), 4.88 (s, 1H, Ar*CH*-), 6.26 (d, 1H, aromatic proton), 6.78 (s, 2H, aromatic protons), 7.19 (s, 1H, furan proton), 8.00 (s, 2H, furan protons) ppm. MS (EI) m/z $[M]^+$: 485.17.

Diethyl 4-(thiophen-3-yl)-1-(3,4,5-trimethoxybenzoyl)-1,4-dihydropyridine-3,5-dicarboxylate (MC4076, 5m)

^{1}H NMR (400MHz, $CDCl_3$) δ: 1.24-1.27 (t, 6H, 2x -OCH_2CH_3), 3.90 (s, 6H, 2x -OCH_3), 3.96 (s, 3H, -OCH_3), 4.15-4.25 (m, 4H, 2x -OCH_2CH_3), 5.14 (s, 1H, Ar*CH*-), 6.88 (s, 2H, aromatic protons), 7.06-7.07 (s, 1H thiophene proton), 7.12 (d, 1H, thiophene proton), 7.23-7.25 (m, 1H, thiophene proton), 7.28 (s. 2H, aromatic protons), 8.11 (s, 2H, dihydropyridine protons) ppm. MS (EI) m/z [M]+: 501.15.

Diethyl 4-(3-fluorophenyl)-1-(3,4,5-trimethoxybenzoyl)-1,4-dihydropyridine-3,5-dicarboxylate (MC4071, 5n)

^{1}H NMR (400MHz, $CDCl_3$) δ: 1.21-1.25 (t, 6H, 2x -OCH_2CH_3), 2.25 (s, 3H, -$ArCH_3$), 3.92 (s, 6H, -OCH_3), 3.97 (s, *3H*, -OCH_3), 4.14-4.23 (m, 4H, 2x -OCH_2CH_3), 4.99 (s, 1H, ArCH-), 6.91-6.95 (m, 3H, aromatic protons), 7.04-7.06 (m, 1H, aromatic proton), 7.16-7.18 (d, 1H, aromatic proton), 7.30 (d, 1H, aromatic proton), 8.15 (s, 2H, dihydropyridine protons) ppm. MS (EI) m/z $[M]^+$: 513.18.

Diethyl 4-(3-bromophenyl)-1-(3,4,5-trimethoxybenzoyl)-1,4-dihydropyridine-3,5-dicarboxylate (MC4077, 5o)

^{1}H NMR (400MHz, $CDCl_3$) δ: 1.22-1.30 (t, 6H, 2x -OCH_2CH_3), 3.93 (s, 6H, 2x -OCH_3), 3.97 (s, 3H, -OCH_3), 3.97 (s, *3H*, -OCH_3), 4.09-4.22 (m, 4H, 2x -OCH_2CH_3), 4.94 (s, 1H, ArCH-), 6.92 (s, 2H, aromatic protons), 7.17-7.21 (t, 1H, aromatic proton), 7.33-7.38 (t, 2H, aromatic protons), 7.45 (m, 1H, aromatic proton), 8.15 (s, 2H, dihydropyridine protons) ppm. MS (EI) m/z $[M]^+$: 573.10.

Diethyl 4-(3-aminophenyl)-1-(3,4,5-trimethoxybenzoyl)-1,4-dihydropyridine-3,5-dicarboxylate (MC4079, 5p)

^{1}H NMR (400MHz, $CDCl_3$) δ: 0.91-0.92 (t, 6H, 2x -OCH_2CH_3), 3.60-3.64 (m, 2H, -$ArNH_2$), 3.91 (s, 6H, -OCH_3), 3.96 (s, 3H, -OCH_3), 4.09-4.23 (m, 4H, 2x -OCH_2CH_3), 4.89 (s, 1H, ArCH-), 6.54-6.55 (d, 1H, aromatic proton), 6.71-6.75 (m, 2H, aromatic protons), 6.91 (m, 2H, aromatic protons), 7.06-7.10 (t, 1H, aromatic proton), 8.13 (s, 2H, dihydropyridine protons) ppm. MS (EI) m/z $[M]^+$: 510.20.

Diethyl 4-(3-nitrophenyl)-1-(3,4,5-trimethoxybenzoyl)-1,4-dihydropyridine-3,5-dicarboxylate (MC4075, 5q)

^{1}H NMR (400MHz, $CDCl_3$) δ: 1.21-1.24 (t, 6H, 2x -OCH_2CH_3), 3.94 (s, 6H, -OCH_3), 3.98 (s, 3H, -OCH_3), 4.08-4.22 (m, 4H, 2x -OCH_2CH_3), 5.10 (s, 1H, ArCH-), 6.95 (s, 2H, aromatic protons), 7.48-7.52 (t, 1H, aromatic proton), 7.81-7.80 (d, 1H, aromatic proton), 8.11-8.13 (d, 1H, aromatic proton), 8.18 (s, 1H, aromatic proton), 8.20 (s, 2H, dihydropyridine protons) ppm. MS (EI) m/z $[M]^+$: 540.17.

Diethyl 4-(4-((4-methylpiperazin-1-yl)methyl)phenyl)-1-(3,4,5-trimethoxybenzoyl)-1,4-dihydropyridine-3,5-dicarboxylate dihydrochloride (MC4003, 6)

^{1}H NMR (400MHz, $CDCl_3$) δ: 1.09-1.13 (t, 6H, 2x -OCH_2CH_3), 1.24 (s, 2H, $ArCH_2$-), 2.05 (s, 3H, -NCH_3), 3.77 (s, 3H, -OCH_3), 3.38-3.52 (m, 8H, piperazine protons), 3.83 (s, 6H, -OCH_3), 4.01-4.07 (m, 4H, 2x -OCH_2CH_3), 4.78 (s, 1H, ArCH-), 5.02 (s,2H, NCH_2Ph), 7.06 (s, 2H, aromatic protons), 7.32-7.30 (m, 4H, aromatic protons), 7.94 (s, 2H, dihydropyridine protons), 11.60 (bs, 2H, 2 x NH^+ piperazine) ppm. MS (EI) m/z $[M]^+$: 679.24.

3.7 Methods

3.7.1 Enzyme-based activation assays

The activity of the final compounds **1a-a', 2, 3, 4a-m, 5b-c**, **5e**, **5j-k**, **5m-q** and **6** against SIRT3 and other isoforms has been evaluated in collaboration with Prof. Steegborn, University of Bayreuth, Germany. In particular, a coupled enzymatic deacetylation assay was used which will be described in detail in the next paragraph.

3.7.1.2 Coupled enzymatic deacetylation assay

This assay links the sirtuin reaction to two additional enzyme activities, thereby enabling a continuous optical read-out. In this continuous activity assay, the sirtuin product NAM is consumed by nicotinamidase (NCA) to form ammonia, which in turn is coupled to α-ketoglutarate by GDH to form glutamate. The latter enzymatic reaction depends on the oxidation of NAD(P)H to $NAD(P)^+$, which can be monitored by an absorption decrease at 340 nm (Fig. 3.9).

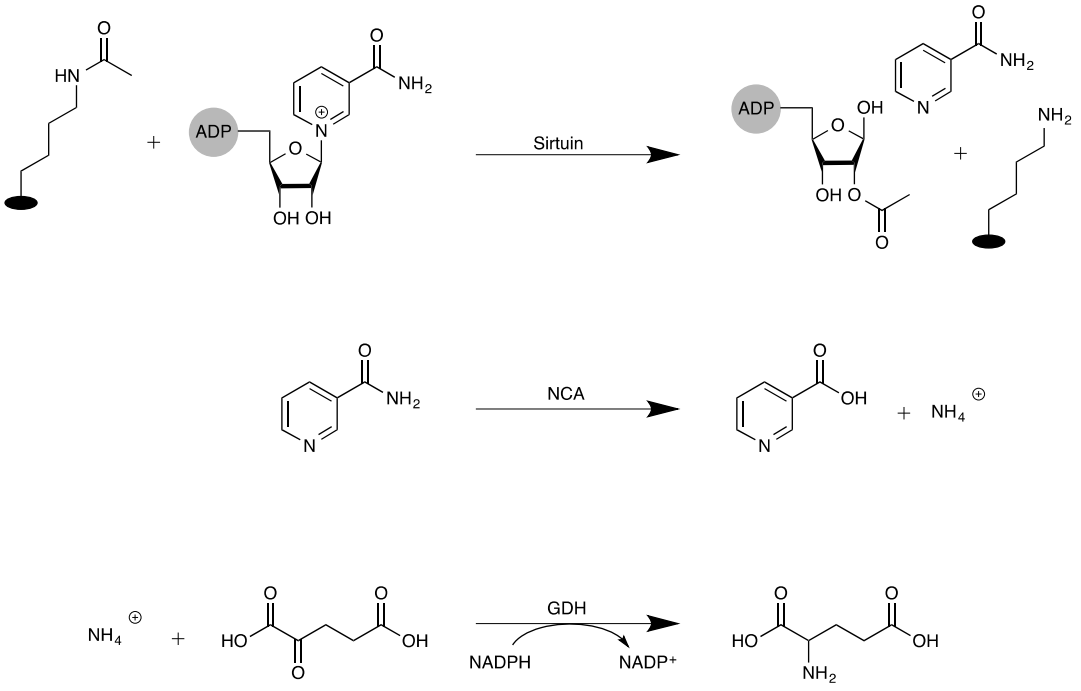

Figure 3.9: Continuous coupled enzymatic sirtuin activity assay. The sirtuin reaction transfers an acyl moiety to ADP-ribose, which is generated by the release of nicotinamide from NAD^+. Subsequently, nicotinamidase (NCA) degrades nicotinamide to nicotinic acid and ammonia, which is then attached to α-ketoglutarate to form glutamate by glutamate dehydrogenase (GDH). This last reaction is driven by NADPH oxidation to $NADP^+$ and can be monitored by a decrease in the absorption at 340 nm.

Although sirtuins differ in their substrate and deacylation specificity, all NAD^+-dependent deacylations catalysed by sirtuins can be monitored by this assay due to the formation of the common coproduct NAM. Given that, to test the activity against the several enzyme isoforms, it must be used the desired

sirtuin isoform and its preferential peptide substrate (Acetylated p53 for SIRT1, α-tubulin for SIRT2, acetylated Acetyl-CoA Synthetase 2 for SIRT3, succinylated Carbamoyl phosphate synthetase 1 for SIRT5).

The coupled continuous assays for different sirtuin isoforms were performed in the following conditions: 1.5 µM sirtuin, 50 µM peptide, 100 µM NAD^+, saturating conditions of GDH (2U), NCA (2 µM), α-ketoglutarate (3.3 mM) and NADPH (500 µM) in 80 µL 50mM phosphate buffer pH 7.8 with 5% final DMSO concentration. In order to ensure stability against oxidation throughout the 60 min reaction, the samples were supplemented with 600 µM DTT. for a better reproducibility, an enzyme master mix and a substrate master mix were prepared, which were used in a ratio of 5:3. The enzyme master mix contained thesirtuin, NAD+, DTT, NCA, GDH, NADPH, and α-ketoglutarate. The substrate master mix contained the sirtuin substrate which is missing in the enzyme master mix. The substrate master mix was dispensed in a 96-well UV plate. The reaction was then started by adding the enzyme master mix, and its progress was monitored by the decreasing absorption at a wavelength of 340 nm at room temperature for 60 min by the microplate-reading spectrophotometer LAMBDA-Scan spectrophotometer (MWG Biotech). Derived raw data were then processed in Microsoft Excel. To perform NAM control for SIRT3, the substrate was replaced by NAM for a final concentration of 100 µM. The following concentrations were instead used to perform compound titrations: 500 µM, 250 µM, 125 µM, 62.5 µM, 31.25 µM, 15.625 µM, 7.3125 µM.

3.7.2 MnSOD assay

We analysed the ability of the activator **1a** (MC2791) to modulate the activation of SOD2 mediated by SIRT3, realising a Western Blot in order to verify if this activator was able to induce the deacetylation of the MnSOD enzyme at the level of acetylated lysine (K68). The 231 WT MDA-MB cells were treated at 8 and 16 hours with the activator **1a** (MC2791) at a concentration of 50 µM. DMSO has been used as a control. After treatment, the pellets were collected from the cells (1 x 106) by centrifugation at 700 xg (5 min at 4 °C) and lysed in 50 µl of lysis buffer (20 mM Tris pH 7.4, 100 mM NaCl, 1 % Triton, 1 mM phenylmethylsulfonylfluoride, 10 µg/ml leupeptin, 10 µg/ml aprotinin). After 30 minutes on ice, the lysates were purified by centrifugation (10 min at 4 °C to 14,000 rpm), and the supernatant was preserved. Protein concentration was determined by Bradford's assay (Bio-Rad Laboratories, Hercules CA). The corresponding equivalent of proteins was run in electrophoresis on a polyacrylamide SDS (PAGE-SDS) gel at 80V for 3 hours, using Kaleidoscope Prestained Standards (Bio-Rad) as molecular weight marker. The proteins were subsequently transferred onto a PVDF membrane for 1.5 hours at 100V. To check the successful transfer and uniformity of the amount of protein loaded in the wells, the filters were coloured with the Ponceau solution.

After a series of washes with TBS-0.1% Tween-20 Buffer (TBS-T), until the red colour disappeared, the phytriums were immersed in a solution of blocking buffer (5% milk in TBS-T) to reduce the non-specific

bonds between the proteins present on the membrane and the antibody to be used in the subsequent detection phase. Subsequently, the membranes were separately incubated with the primary anti-human antibody MnSOD-acetylK68 (AbCam) and with the anti-human anti-MnSOD (AbCam) antibody overnight at 4 °C. At the end of the incubation, the filters were subjected to three TBS-Tween washes of 10 minutes each and incubated for 1 h with the corresponding secondary antibody (diluted in 3% TBS-Tween milk) conjugated with horseradish peroxidase (HRP). At the end of the incubation, the filters were subjected to three washes in PBS-Tween each of 10 minutes. The detection phase of the proteins of interest (MnSOD and MNSODAcK68) was carried out at room temperature using the ECL method (luminol in the presence of peroxidase and H_2O_2 is oxidized with the emission of bluish light that impresses the plate).

3.7.3 HepG2 cell Cultures and Treatments

HepG2 hepatoma cells were maintained in DMEM (GIBCO Life Technologies) supplemented with 10% FBS (Gibco Life Technologies), 1% penicillin/streptomycin (Sigma). HepAD38 cells were maintained in DMEM supplemented with 10% FBS Fetal Clone II Hyclone (Thermoscientific), 1% penicillin/ streptomycin, 200 µg/mL L-Glutamine (Gibco Life Technologies), 50 µg/mL hydrocortisone (Sigma), insulin (Sigma) and 400 mg/mL G418 (GIBCO Life Technologies). HepAD38 cells were grown in the presence of 0.3 µg/mL tetracycline (Sigma). For *TET-off system-stably replicating HepAD38 cells* containing stably integrated the entire genome of Hepatitis B virus (HBV) under Tet control, the initiation of viral replication is strictly regulated by the absence of tetracycline in the growth medium. The previous preparation leads to a high level of HBV DNA production and accumulation of viral intermediates after the cells become confluent. *TET-on system*: after a first 6 day- period in which confluent cells were allowed to replicate HBV from the integrated genome (TET-off) leading to the accumulation of a cccDNA pool into the nucleus, capsids containing pgRNA and mature viral particles into the cytoplasm, 0.3 µg/mL tetracycline was added daily to culture medium for 7 days to inhibit integrated HBV DNA replication and to allow cccDNA transcription. HepG2-NTCP cells were maintained in Dulbecco's Modified Eagle Medium (DMEM) supplemented with heat-inactivated 10% FBS, 1% penicillin/streptomycin. Cells were dosed every 24hrs with small molecules to a final concentration of 25 µM in all experiments. Untreated cells were exposed to the same DMSO (Sigma) final concentration. HepG2 cells were treated 1 h post transfection for 48 h; confluent TET-off system HepAD38 cells were treated for six days; TET-on system HapAD38 cells were treated for six days starting 1 day after the introduction of Tet in the medium; HepG2-NTCP cells were treated one day post infection or 10 days post-infection for 10 days.

3.7.3.1 Gel Electrophoresis and Western Blotting

48 h- and 6 days-treated HepG2 and HepAD38 cells respectively were processed with EpiQuik Total Histone Extraction Kit (Epigentek). Briefly: cells were harvested, pelleted by centrifugation and lysed with the Diluted 1X Pre-Lysis Buffer on ice for 10 min. Cells were centrifuged at 10000 rpm for 1 min at 4 °C, resuspended in Lysis Buffer and incubated on ice for 30 min. Samples were pelleted at 12000 rpm for 5 min at 4 °C and the containing proteins supernatant fraction was added to the Balance-DTT Buffer. Equal amounts of protein were separated by SDS–polyacrylamide gel electrophoresis and transferred on to polyvinylidene fluoride membranes according to standard techniques. Membranes were incubated overnight with an anti-AcH4 antibody (06-866, Millipore), anti-trimethylated H3 Lysine 27 antibody (ab6002, Abcam) and anti-actin antibody (sc-1616 Santa Cruz) and revealed with the 'Western Lightning Chemiluminescent Reagent Plus' (Perkin Elmer, Boston, MA, USA) detection system.

3.7.3.2 MTT assay

The cytotoxicity of epigenetic compound **1a** (MC291) in transfected HepG2 and replicating HepAD38 cells was measured using the 3-(4,5-dimethyl-2-thiazolyl)-2,5-diphenyl-2H-tetrazolium bromide (MTT) assay. The cells were incubated for 48 h with **1a** (MC2791) at a final concentration of 25 µM in duplicate in a 6-well plate together with the respective control treatment (cells incubated with 2 µM doxorubicin (Sigma) as positive control, DMSO only as negative control). The cells were then incubated with the MTT substrate (5 mg/mL in 0.1 M phosphate buffered saline (PBS) (GIBCO Life Technologies) for 4 h. The supernatants were then removed by aspiration, and DMSO (1 mL) was added to the wells. Finally, the optical density was measured at 570 nm with a spectrophotometer (DU 530, Beckmann colter). The data was translated to percentage cell viability relative to the no inhibitor (DMSO) treated control.

3.7.3.3 Flow Cytometric Analysis

Flow cytometric analysis of the cell cycle, FACS analysis, was performed as described below: after 48 h incubation with DMSO (NT cells), 25 µM **1a** (MC2791) treatment and 50 µM cisplatin (Sigma) (positive control) cells were washed with PBS and incubated with 0.25 % trypsin-EDTA (GIBCO Life Technologies) for 10 min at 37 °C. Afterwards, cells were centrifuged and washed twice in PBS, fixed in ice-cold 70% ethanol and incubated 2 h at 4 °C. The cells were centrifuged, washed twice in PBS and stained with a freshly made solution containing 50 µg/mL propidium iodide (PI) (Life technologies), 0.1% Triton x-100 (Sigma) and 40 µg/mL ribonuclease A (Sigma) in PBS. All samples were incubated for 30 min at room temperature in the dark. The percentages of cell cycle distribution were evaluated by PI staining by analytical DNA flow cytometer (Accuri C6, BD Biosciences) and data analysis was performed employing BD Accuri ^{TM} C6 software.

3.7.3.4 ChIP assays

The cccDNA ChIP assays were performed as described here. Cross-linked Chromatin from 48 h transfected HepG2 and 6 days stably replicating HepAD38 cells was subjected to immunoprecipitation for 14–16 hours at 4 °C using antibodies specific to AcH4 (06-866, Millipore; rabbit polyclonal IgG recognizing histone H4, which is tetra-acetylated at lysines 5, 8, 12, and 16). Immunoprecipitations with nonspecific immunoglobulins (ab27478 Abcam) were included in each experiment as negative controls. After the reverse cross-linking, immunoprecipitated chromatin was purified by phenol:chloroform (1:1) extraction and ethanol precipitation and analysed by real-time PCR using selective primers and probes that discriminate between cccDNA and the relaxed circular DNA (OC species) present in the cytoplasmic HBV particles.

3.7.3.5 Transient transfection of full-length HBV DNA genomes

Monomeric linear full-length WT HBV genome was released from the pCR.HBV.A.EcoRI using EcoRI-PvuI (New England Biolabs). Linear HBV monomers were transfected into HepG2 human hepatoma cells using the Mirrus Bio transIT-LT1 (Mir 2300A). Briefly, HepG2 cells were seeded at a density of 2–3 million cells in 100-mm-diameter Petri dishes and transfected 24 hours later with 1 µg of digested HBV DNA. Culture medium was changed one day after transfection and cells were harvested at the indicated times. All transfections included 0.5 µg of a GFP expression vector to assess transfection efficiency (HepG2 cells, range 28%–32%).

3.7.3.6 HepG2-NTCP infection

HepG2-NTCP infections were performed according to Ni Y. *et al.* Briefly, approximately 100-fold concentrated supernatant of 2.2.15 cells were used as HBV inoculum. For infection, cells seeded in 6-well plates were inoculated overnight with a 100 MOI HBV in medium containing 4% polyethylene glycol 8000 (Sigma-Aldrich) and 2.5 % DMSO. After washing with PBS 1X cells were treated or not with epigenetic compounds.

3.7.3.7 Purification and quantification of core particles associated with HBV DNA from HBV-replicating cells

To purify HBV DNA from intracellular core particles, transfected HepG2, infected HepG2-NTCP, and HepAD38 cells were washed once with ice-cold PBS and lysed in 50 mmol Tris-HCl, pH 7.4, 1 mmol EDTA, and 1% NP-40 (lysis buffer A). Nuclei were pelleted by centrifugation (1 minute at 10000 g). The supernatant was adjusted to 100 mmol $MgCl_2$ and treated with 100 mg/mL of DNase I for 60 min at 37 °C. The reaction was stopped by adding EDTA to a final concentration of 25 mmol. Protein was digested with 0.5 mg/mL proteinase K and 1% SDS overnight at 56 °C. Nucleic acids were purified by phenol: chloroform (1:1) extraction and isopropanol precipitation adding 0.1 M NaCl. HBV DNA was quantified

by real-time PCR in a Light Cycler instrument (Roche) using the following primers and probes: forward, 5'-CTCGTGGTGGACTTCTCTC-3', and reverse 5' CAGCAGGATGAAGAGGAA-3'. We also used specific FRET hybridisation probes: 5' CACTCACCAACCTCCTGTCCTCCAA-FL-3', Red640, 5'-TGTCCTGGTTATCGCTGGATGTGTCT-3'. Amplifications were performed as follows: 95 °C for 5 min, followed by 45 cycles at 95 °C for 10 sec, 58 °C for 10 sec, and 72 °C for 20 sec.

3.7.3.8 HBV RNAs and cellular mRNA analysis

Total RNA was extracted from HepG2 cells 48 h after compound treatment, from HepG2-NTCP cells 10 days after treatment and from HepAD38 cells 6 days after treatment using the TRIzol reagent (Invitrogen) as recommended by the manufacturer. The RNA samples were treated with RQ1 RNase-Free DNase (Promega) for 60 min at 37 °C and stored until used. RNA quality and quantity were monitored by ethidium bromide staining and by UV absorbance. For pgRNA analysis, 2 mg of DNase-treated RNA was reverse transcribed and amplified by the ThermoScript RT-PCR System (Invitrogen). Then 1 µL of each cDNA was quantified by real-time PCR analysis (Light Cycler; Roche Diagnostics) using the following pgRNAspecific primers and probes: forward primer, 5'-GCCTTAGAGTCTCCTGAGCA- 3', reverse primer, 5' -GAGGGAGTTCTTCTTCTAGG-3', FRET hybridisation probes, 5'–AGTGTGGATTCGCACTCCTCCAGC-FL-3', and Red640-5'ATAGACCACCAAATGCCCCTATCTTATCAAC-3'. The actin housekeeping gene Light Cycler Set (Roche Diagnostics) was used to normalise the RNA samples.

3.7.3.9 Statistical analysis

P values were determined using the 2-tailed Student's t test. $P < 0.05$ was considered significant.

3.8 Biological evaluation, results and discussion

3.8.1 Enzymatic assays

The final compounds **1b-p** and **1y-z**, obtained by chemical manipulation of **1a** and **1u** working at N1 position of the 1,4 DHP scaffold, were first tested at both 10 and 100 µM against SIRT3 (Fig. 3.11). The two parent compounds **1a** and **1u** were tested against Sirt3, as well.

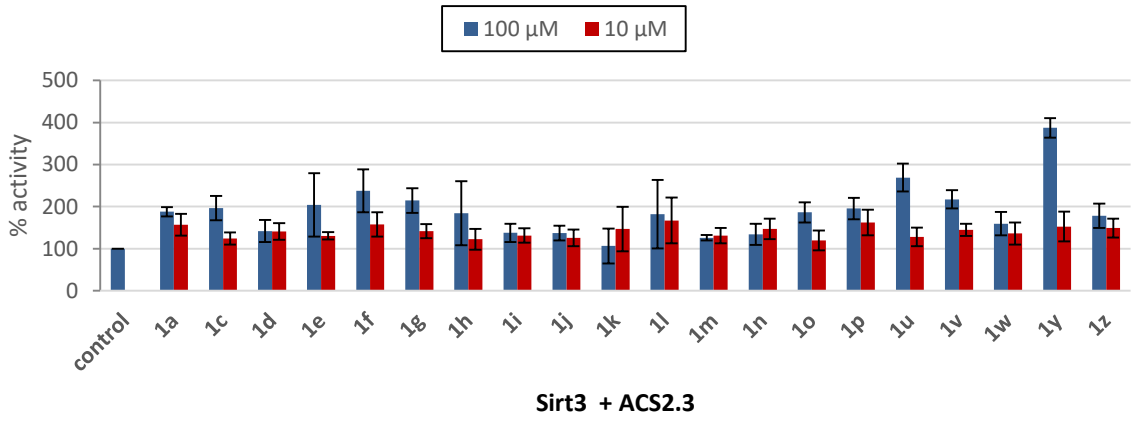

Figure 3.11: SIRT3 activation.

As shown in Fig. 3.11, the parent compounds **1a** and **1u** strongly activate SIRT3 at 100 µM (1.87 ± 0.11 fold activation for **1a** and 2.7 ± 0.33 fold activation for **1u**, respectively) but also discretely activate SIRT3 at 10 µM (1.56 ± 0.25 fold activation for **1a**). For what concerns the lastly synthesized compounds**1b-p** and **1y-z**, despite large errors for some of them, they mostly maintain the activity against SIRT3 and **1y** gives even stronger SIRT3 activation than **1u** (3.87 ± 0.23 fold activation for **1y** at 100 µM) while **1v** gives stronger SIRT3 activation than **1a** (217 ± 0.21 fold activation for **1a** at 100 µM).

Control reactions for compound effects on processing of the Sirtuin product NAM by the coupled enzymes PNCA and GDH showed negligible effects (Fig. 3.12), confirming that the are due to Sirt3 stimulation.

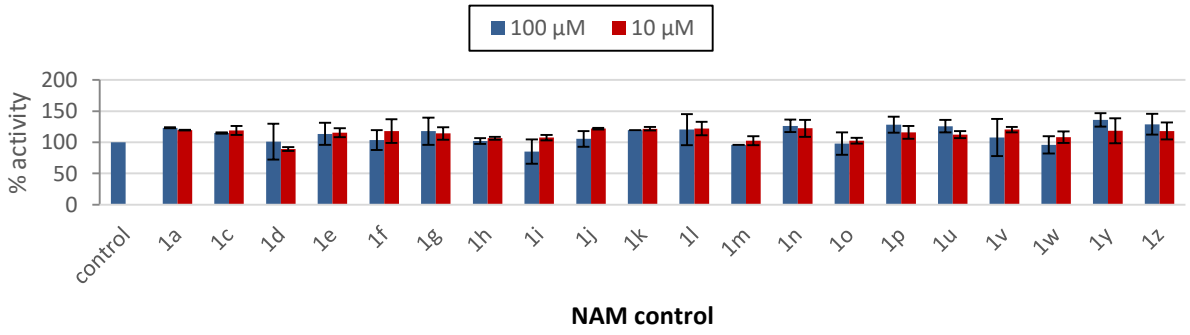

Figure 3.12: NAM control.

Then titration experiments were performed, but it was not possible to get EC_{50} values because of solubility limits of compounds.

The isoform selectivity for the strongest SIRT3 activators **1v** and **1y** was investigated next (Fig. 3.13).

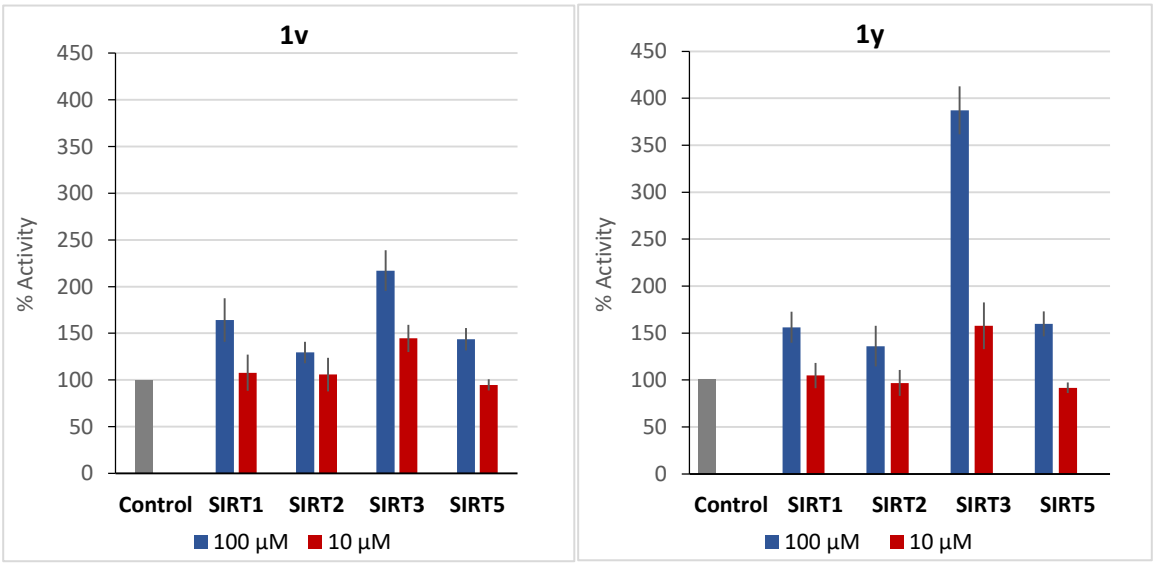

Figure 3.13: Activity of **1v** and **1y** on SIRT1, -2, -3, and -5.

Although **1v** and **1y** seem to be activating other sirtuin isoforms at 100 µM, they selectively activate SIRT3 when used at 10 µM.

SIRT1 activation by resveratrol and other SIRT1 activating compounds is known to be substrate sequence dependent. To test whether Sirt3 activation by **1u** depends on the ACS2-derived substrate peptide employed in our screen, we analyzed **1u** effects on Sirt3-dependent deacetylation of a panel of eleven acetylated peptides (Fig. 3.14).

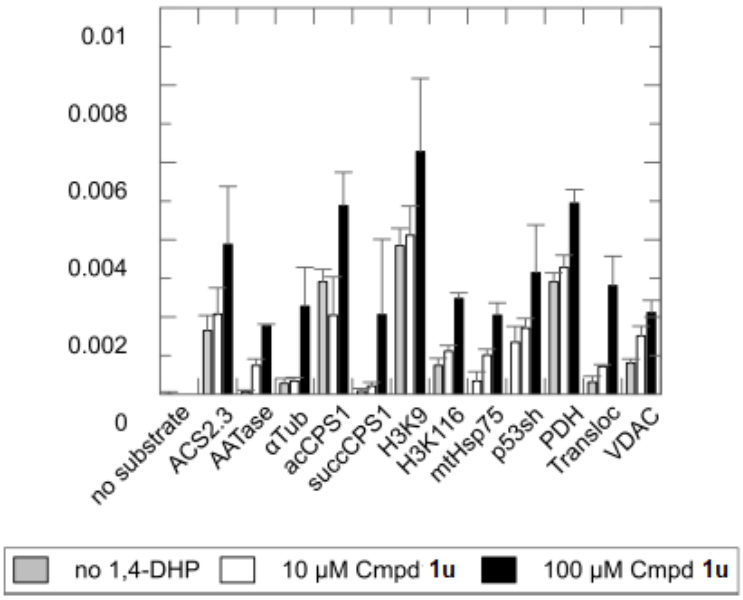

Figure 3.14: SIRT3 activation by **1u** is substrate-independent.

As expected, the enzyme converted the substrates with varying deacetylation rates. However, basal Sirt3-dependent deacetylation of all substrates was stimulated by **1u** weakly at 10 μM and significantly at 100 μM compound. Thus, appears **1u** to enhance Sirt3-dependent deacetylation independent of the substrate sequence.

Based on these results, we next analysed our new series of compounds **1p-u** and **1a'**, **2**, **3**, **4a-m, 5b-c**, **5e**, **5j-k**, **5m-q** and **6**, resulting from chemical manipulation of the two parent compounds **1a** and **1u**, for effects on Sirt1, Sirt2, Sirt3, and Sirt5 activity. However, all the methoxy series **1v-z** was not tested in these assays due to their poor cellular activity (data shown in the paragraph 3.8.2.1). All the newly derivatives exhibited, as expected, poor Sirt1 activation, apart from compounds **5j**, **5k** and **5m** that were able to activate Sirt1 significantly at 100 μM concentration. Additionally, **1s** and **1t** displayed mild Sirt1 activation, while **5p** was found to strongly stimulate all the sirtuins (Fig. 3.15).

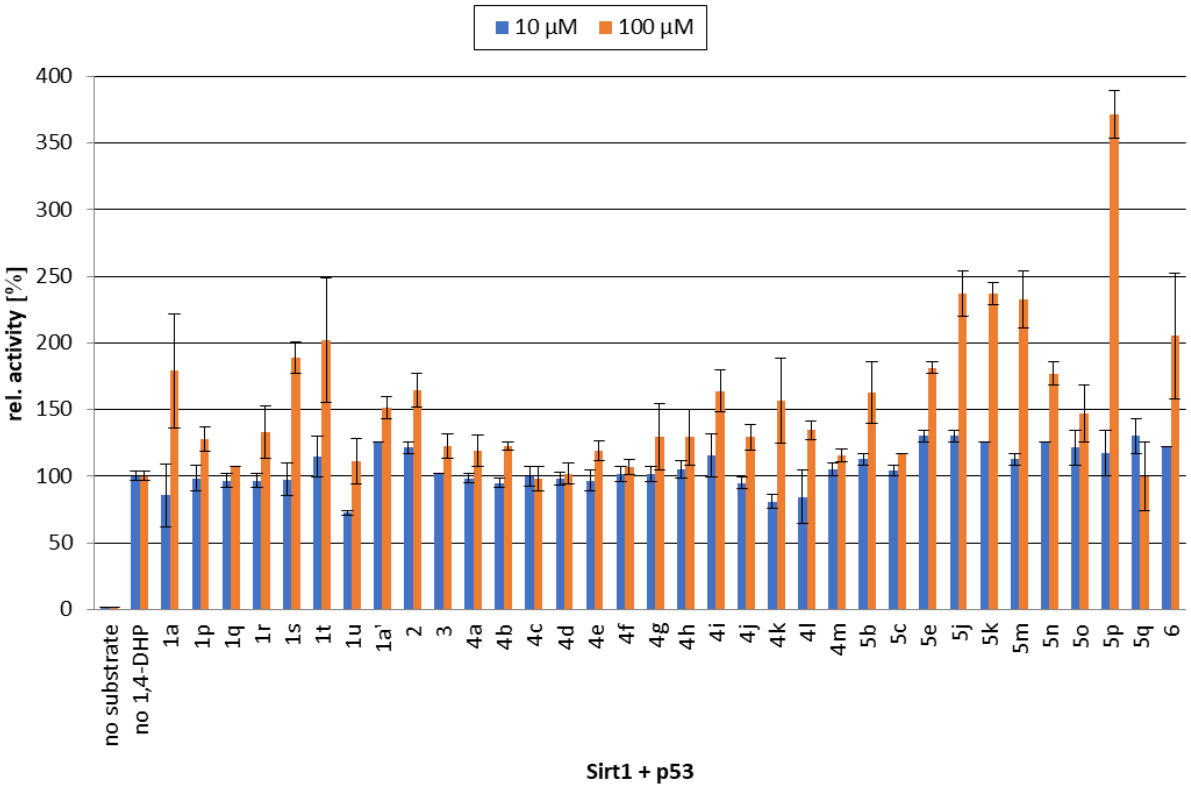

Figure 3.15: Sirt1 activation.

As pan Sirtuin activator, **5p** indeed requires further investigation to assess its potential role in sirtuin biology. Furthermore, the activity of selected compounds against Sirt2 showed that most of them were, however, totally inactive, with the exception of compounds **1s**, **5j** and **5k** (Fig. 3.16).

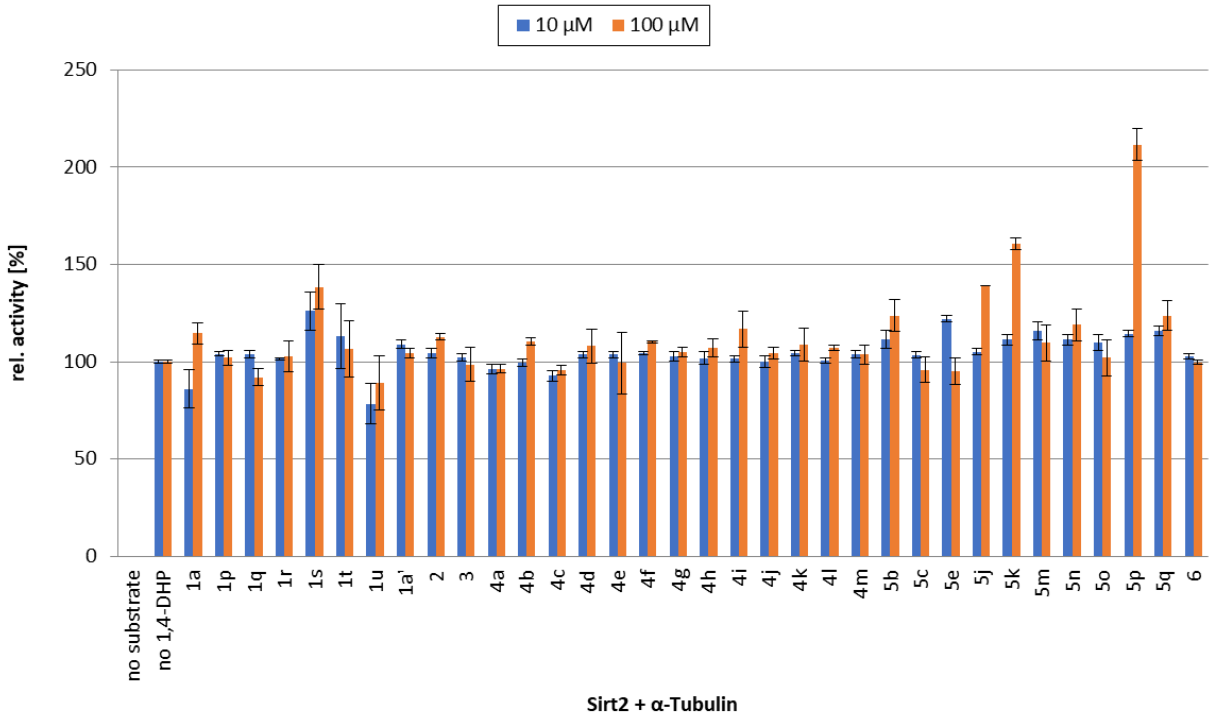

Figure 3.16: Sirt2 activation.

Additionally, testing the novel derivatives at 10 µM or 100 µM yielded no improved Sirt3 activator. However, the most effective compounds in activating Sirt3 were **1s** and **1t**, obtained by inserting at N1 position the 2-naphtyl and 1-quinoxaline rings, respectively (Fig. 3.17).

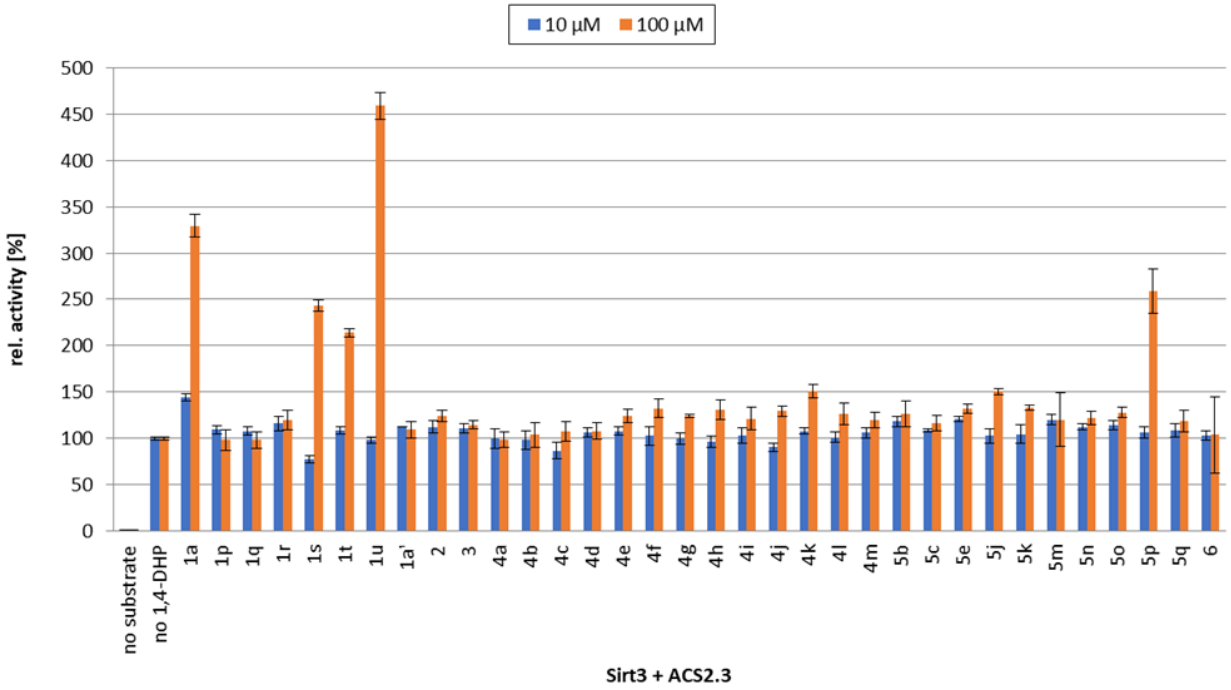

Figure 3.17: Sirt3 activation.

Surprisingly, once tested against Sirt5 (Fig. 3.18), the majority of **1a** derivatives displayed strong and selective Sirt5 activation, whereas only compound **6**, got by chemical manipulation of the **1u** structure by insertion at para position of the C4 phenyl ring a (4-methylpiperazin-1-yl)methyl group as a salifiable function, was able to stimulate Sirt5.

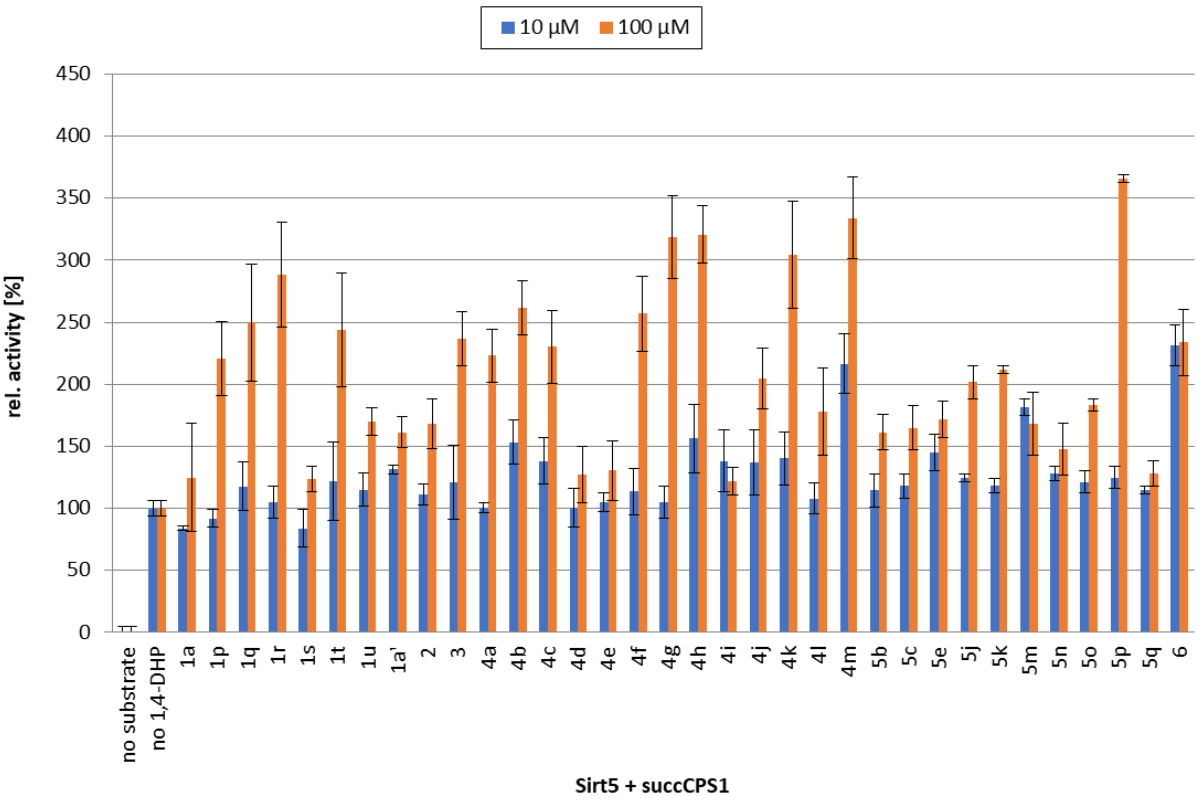

Figure 3.18: Sirt5 activation.

Moreover, compound **1t**, belonging to **1a** analogue series, showed to activate with a comparable potency both Sirt3 and Sirt5. Overall, selective Sirt3, Sirt5 as well as Sirt3/5 activators were discovered and are illustrated in the following table (Table 3.2).

Table 3.2: Sirt3/5 activators.

LAB CODE	COMPOUND	CHEMICAL STRUCTURE	ISOFORM SELECTIVITY
MC2791	**1a**	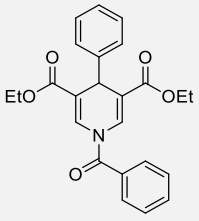	Sirt3a

MC2870	**1q**	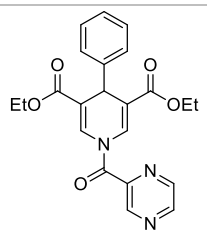	Sirt5a
MC2861	**1r**	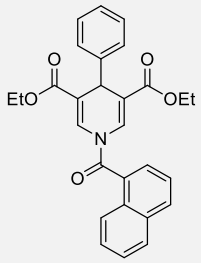	Sirt5a
MC2790	**1s**	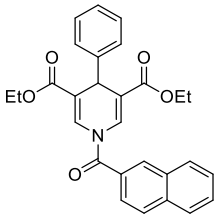	Sirt3a
MC2788	**1t**	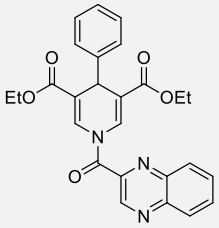	Sirt3/5a
MC2789	**1u**	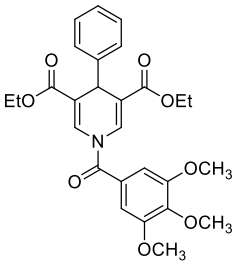	Sirt3a
MC2867	**3**	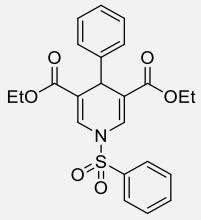	Sirt5a
MC3139	**4a**	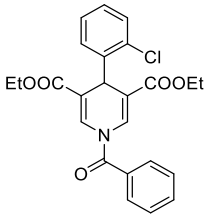	Sirt5a

MC3140	**4b**	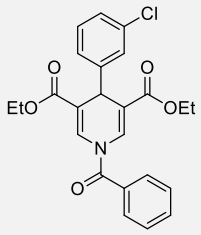	Sirt5a
MC3156	**4c**	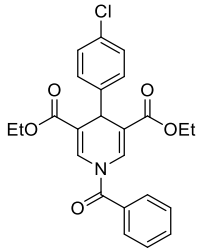	Sirt5a
MC3171	**4f**	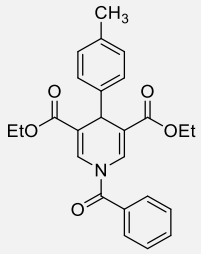	Sirt5a
MC3131	**4g**	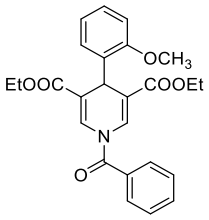	Sirt5a
MC3138	**4h**	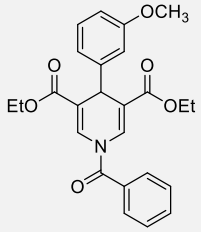	Sirt5a
MC3224	**4k**	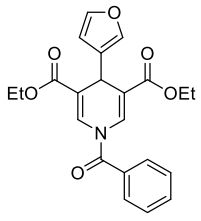	Sirt5a
MC3215	**4m**	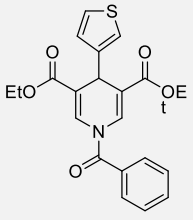	Sirt5a
The isoform selectivity of the strongest compounds was reported in red.			

By means to our SAR investigation into the structure of the two potent Sirt3 activators **1a** and **1u**, novel Sirt3 and Sirt5 activators were identified. More in details, working at the C4 position of **1a** by introducing isosteric rings, provided two potent and selective Sirt5 activators (the 3-furanyl **4k** and the 3-thiophenyl **4m**), thus shifting the activity from Sirt3 to Sirt5. Moreover, by insertion of electron-withdrawing as well as electron-releasing substituents at the C4 position, we found that the *ortho*, *meta* and *para* chloro-phenyl series, **4a**, **4b** and **4c** respectively, as well as the 4-methyl (**4f**) and the 2-methoxy (**4g**) **1a** analogues, exhibited strong isoform selectivity for Sirt5. By contrast, among the N1-aroyl series, compound **1t** was found to activate both Sirt3 and Sirt5 in a similar manner. On the other hand, its closely **1q** simplified analogue, having a pyrazine instead of a quinoxaline ring at N1, was effective against only Sirt5. More importantly, the replacement of the 1-naphthyl ring with 2-naphthyl one at N1, yielded changes into the isoform selectivity, too. Indeed, while the 1-naphthyl **1r** produced a strong Sirt5a activation, the 2-naphtyl **1s** was, instead, selective for Sirt3. Furthermore, in the same series, the phenylsulphonyl derivative **3** showed to preferentially activate Sirt5 rather than Sirt3. Lastly, among the series of **1g** derivatives, any compound proved to selectively activate Sirt5. Overall, several compounds turned out to be specific Sirt5 activators. The strongest effects were, however, observed for **4g** (2-methoxy), **4h** (3-methoxy), **4k** (3-furanyl), and **4m** (3-thiophenyl), with the latter one already activating Sirt5 desuccinylase activity significantly (~2-fold) at 10 μM, and ~3.5-fold at 100 μM.

A titration experiment with **4m** yielded an EC_{50} of ~60 μM and a maximum 5-fold activation of Sirt5 beyond 200 μM compound concentrations (**A**, Fig. 3.19). As for Sirt3 activation by **1u**, MS-based assays confirmed that the activating effects were due to direct Sirt5 stimulation (**B,** Fig. 3.19).

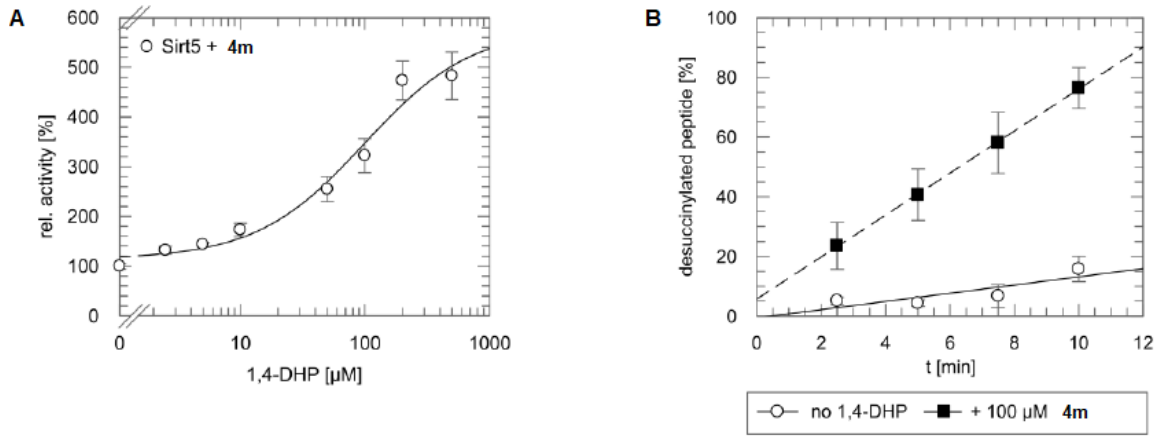

Figure 3.19: A. Titration experiment with **4m**; **B.** Ms-based assays for confirming **4m**-induced Sirt5 activation.

3.8.2 Cell-based assays

Given the excellent results obtained from the enzymatic assays, we next tested the parent compounds **1a** and **1u** together with the more recent -methoxy series **1v-z** in cell-based assays in order to further confirm the SIRT3 activation as well as SARs.

3.8.2.1 GDH activity assay

To test whether our 1,4-DHP based SIRT3 activators can be employed in cellular studies, we analysed the effect of **1a** and whole -methoxy series **1u-z** on the cellular activity of a known SIRT3 substrate, GDH (Fig. 3.20). GDH activity was determined by a coupled enzyme assay in which glutamate is consumed by GDH generating NADH, which reacts with a probe generating a colourimetric (450 nm) product proportional to the GDH activity present. MDA-MB-231 cells were treated with 50 µM compounds and cell lysates were prepared 4h after compound addition.

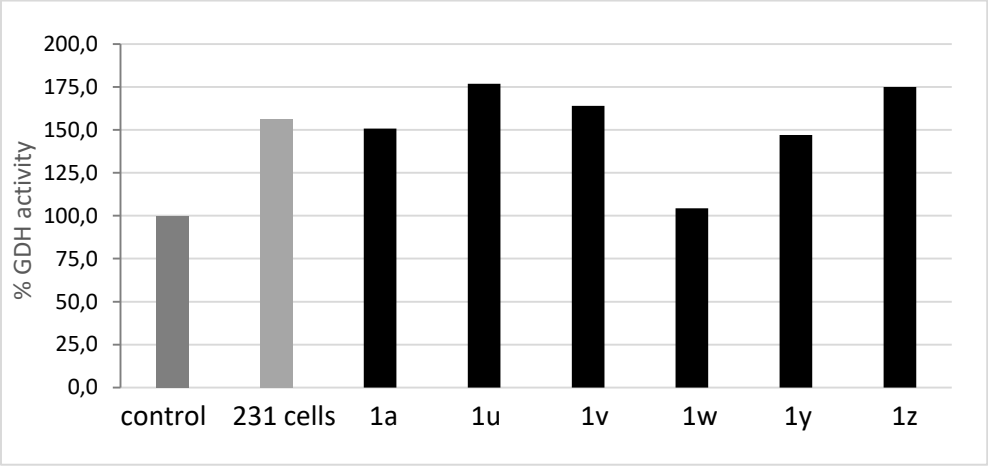

Figure 3.20: GDH activity assay. 231cells SIRT3^{+} = SIRT3 overexpressing cells.

All the compounds activated GDH in this experiment, except *para*-methoxy derivative (**1w**), which also showed a solid decrease in SIRT3 activation in enzyme-based assays compared to the other methoxy derivatives.

3.8.2.2 *MnSOD assay*

To further confirm cellular Sirt3 activation by our compounds, we analysed the deacetylation of MnSOD, another established Sirt3 substrate, in MDA-MB 231 cells that were treated at 8 hours with MC2791 (**1a**) at 50 µM. Results showed an evident increase of the acetylation levels at Lys (K68) of the enzyme MnSOD2; by contrast, in WT 231 cells treated at 16 hours with the same activator, lysine (K68) residue is deacetylated. The deacetylase activity of SIRT3 stimulated by **1a** (MC2791) was confirmed by the absence of deacetylation in 231 cells that do not express SIRT3 (MDA-MB 231 3-). As shown in fig. 3.21,

the expression of SOD2 remains unchanged after treatment with the activator **1a**, which modulates only the acetylation state of the enzyme. Therefore, we can state that **1a** mediates the activation of SIRT3, confirmed by the *in vitro* deacetylation of the SOD2 enzyme at the level of the acetylated lysine residue.

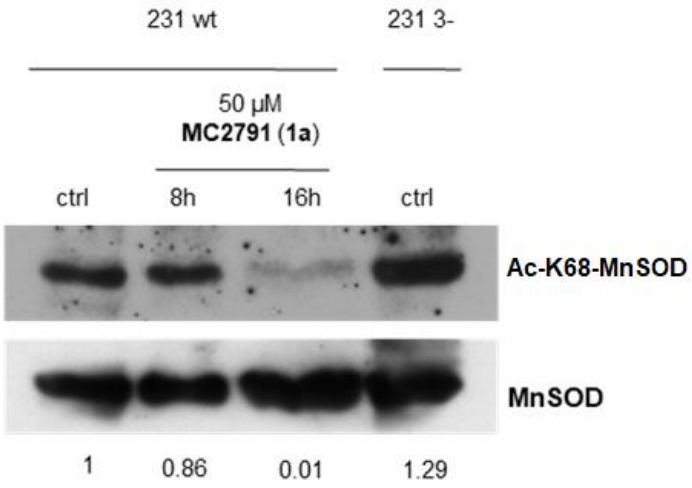

Figure 3.21: Deacetylation activity of **1a** on MnSOD and AcK68-MnSOD in MDA-MB 231 WT and 231 3- cells.

3.8.3 Effects of Sirt3 activation in HBV infection: cellular assays in liver hepatocellular carcinoma HepG2 cells

Very recently, Sirt3 has been described as a protected player against HBx-induced oxidative stress. [459]

Specific Sirt3 activators able to modulate the acetylation status of cccDNA-bound H3/H4 histones, leading to cccDNA transcriptional activity inhibition and silencing of minichromosome activity, provided a novel potential approach for the treatment of chronic HBV infection. [457]

Thus, to gain decreased H3/H4 acetylation in HBV-infected cells, we chose **1a** (MC2791) because in human breast cancer MDA-MB-231 cells it preferentially activates Sirt3 than Sirt1 (Fig.3.22), confirming again its potent and selective Sirt3 activation.

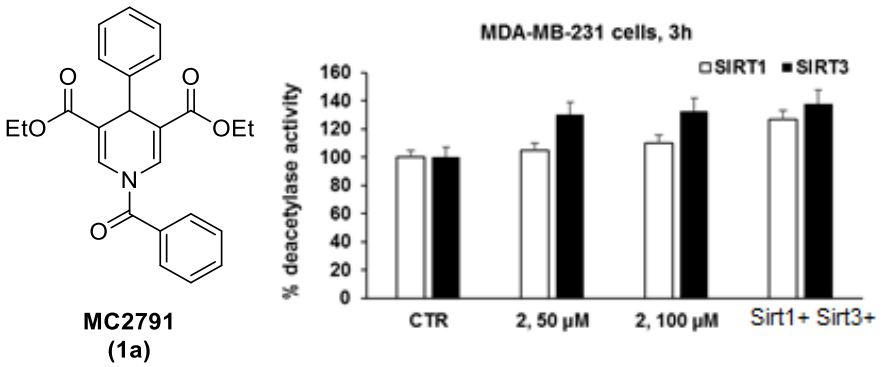

Figure 3.22: Human prostate cancer cells treated with **1a** (MC2791).

3.8.3.1 Gel Electrophoresis and Western Blotting analysis

To evaluate the target modulation exerted by **1a** on host epigenetics, cell proliferation and cell cycle in liver hepatocellular carcinoma HepG2 cells, we used a HepAD38 inducible system, a clone of HepG2 cells. Briefly, after tetracycline induction of HepAD38 in HepG2, cells were treated with compound **1a** at 25 µM for six days. Nuclear protein extracts of harvested cells were analysed by Western blot. Treatment with **1a** lead to a significant reduction in the acetylation level of histone H3 and/or H4 (Fig. 3.23).

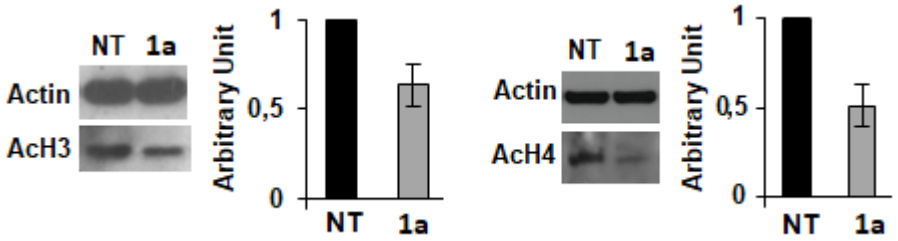

Figure 3.23: Acetylation level of histones H3 and H4 after treatment of **1a** in HepG2 cells.

3.8.3.2 MTT cell proliferation assay

We performed an MTT cell proliferation assay on HepAD38 cells treated for 6 days at 25 µM to test the cytotoxicity of **1a**. Figure 3.24 shows that the fraction of living cells in HepAD38 samples treated with **1a** is not significantly different from the untreated sample, meaning that the tested epigenetic compound does not affect cell viability at the concentration tested. FACS analysis performed on HepAD38 cells treated for 6 days at 25 µM revealed that the fraction of cell populations in G1, G2/M, S and subG1 phase in treated cells was not significantly different from the control, showing that the tested epigenetic compound did not alter the cell cycle progression in this system (data not shown).

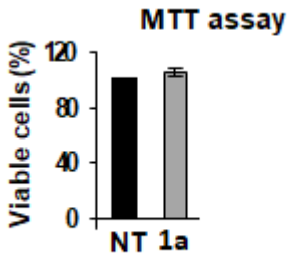

Figure 3.24: MTT cell proliferation assay on HepAD38 cells.

3.8.3.3 HepG2-NTCP infection

The sodium taurocholate cotransporting polypeptide (NTCP) membrane transporter is reported as an HBV entry receptor. HepG2-NTCP cells can be efficiently infected with HBV and recapitulate all the steps of the viral cycle. Infected HepG2-NTCP cells were treated with 25 µM **1a** for ten days following either one, or ten days of infection with HBV, in order to assess the effect of cccDNA accumulation on inhibition (**A**, **B**, Fig. 3.25). Compound treatment did not affect the amount of cccDNA, but significantly decreased the capsid-associated HBV DNA levels (**A** and **B**, left panels) and the pgRNA levels (**A** and **B**, right panels) as indicated by real-time PCR.

Furthermore, after 48 h compound treatment, HepG2 cells were harvested, and capsid-associated (Cp) HBV DNA and pgRNA were extracted. As evidenced by real-time PCR, the treatments lead to a reduction of HBV DNA levels (**C**, left panels) and a substantial reduction in pgRNA levels (**C**, right panels), without altering cccDNA levels.

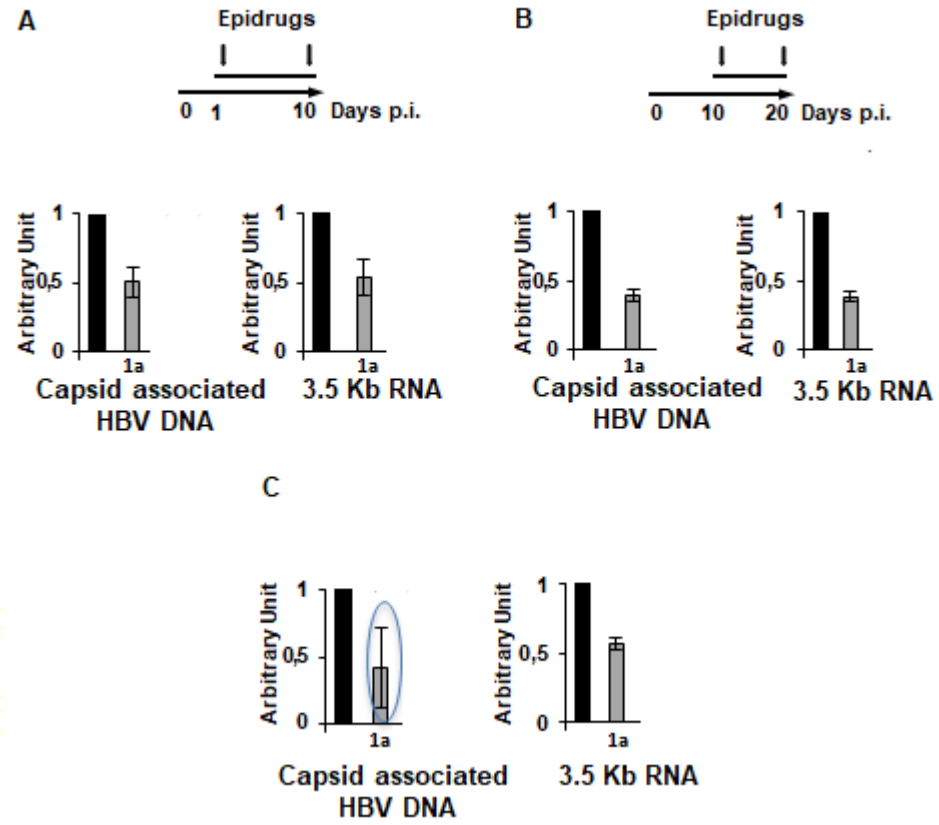

Figure 3.25: Effects of **1a** on capsid-associated HBV DNA levels (**A** and **B**, left panels) and the pgRNA levels (**A** and **B**, right panels).

Together, these results show that alteration of histone PTM status using epigenetic compounds can reduce HBV transcription and replication in both infection and transfection models.

3.8.3.4 HBV RNAs and cellular mRNA analysis

To reduce variability arising from the transfection method, we used HepG2 clones carrying the stably integrated complete HBV genome under the control of a tetracycline (Tet) -off promoter. Cells were incubated in Tet-free medium from 6 to 12 days after which HBV DNA and RNA levels were measured by real-time PCR. After 6 days of integrated HBV genome replication, we added tetracycline in the medium, and we evaluated the amount of HBV replication intermediates (Tet-on system) (**A**, Fig. 3.26). Highly replicating HepAD38 cells were treated with the compounds and harvested after 6 days to isolate capsid-associated HBV DNA. Real-time PCR results show a 40% reduction of HBV DNA levels in cells treated with **1a** (**B**, Fig. 3.26).

To investigate if the reduction in replication is a consequence of a direct epigenetic modulation of minichromosome activity, HepAD38 cells were first allowed to replicate viral DNA for 6 days in a tetracycline-free medium, and then cultured in tetracycline-containing medium and treated for 6 days with **1a** at 25 µM. In this manner, the contribution of the integrated HBV genome to HBV DNA and

pgRNA synthesis is eliminated, and the pool of cccDNA accumulated during stable replication is the only source of pgRNA, independent of cccDNA amount (**C**, Fig. 3.26). Treatment with **1a** reduced pgRNA levels, as assessed by real-time PCR.

These results indicated the ability of **1a** to lower HBV DNA and pgRNA levels in several cellular systems and, importantly, that the transcriptional repression seen as a reduction in pgRNA levels was a direct consequence of epigenetic modulation of cccDNA activity.

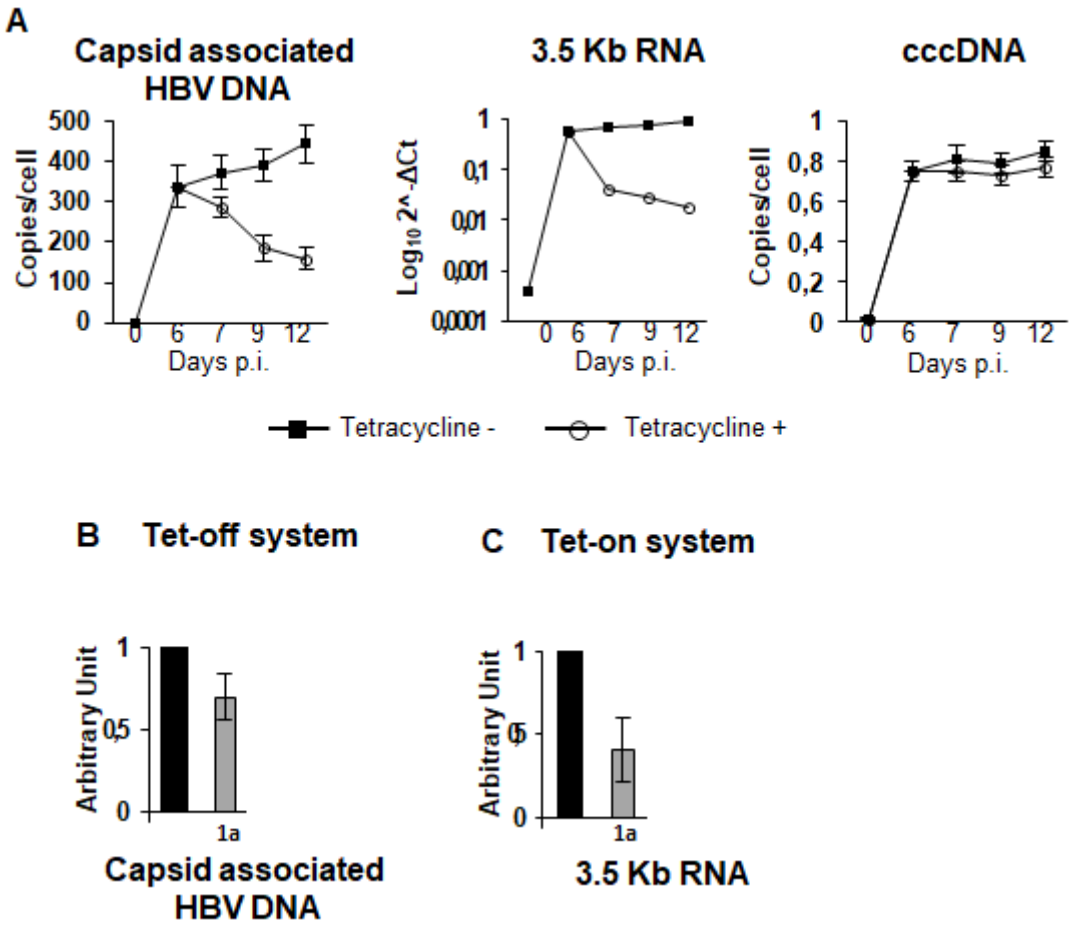

Figure 3.26: A. Cells incubation in Tet-free medium from 6 to 12 days. **B.** Reduction of HBV DNA levels in cells treated with **1a**. **C.** HepAD38 cells treated for 6 days with **1a** at 25 µM.

3.8.3.5 ChIP assays

To determine the effect of the epigenetic compounds on H3/H4 histones associated to the minichromosome, transiently transfected HepG2 and HBV replicating HepAD38 cells were treated with **1a** for 48 h and then harvested at six days post-treatment. Afterwards, cccDNA-ChIP was used to assess histone H3 and H4 acetylation, using specific antibodies for AcH3K9, AcH4K5, -8, -12, and -16. The cells were treated and harvested respectively at 48 h (HepG2) and 6 days (HepAD38) post-treatment, and a specific cccDNA-ChIP assay was performed. First, we found low levels of SIRT3 protein binding the

cccDNA in HepG2 and HBV replicating HepAD38 cells (**A** and **B**, Fig. 3.27). After, treatment with **1a** resulted, as expected, in a significant decrease of acetylated histone H3 and/or H4 levels, both in HepG2 and in HepAD38 cells, (**C** and **D**, Fig. 3.27). These results show the ability of the tested epigenetic compounds to modulate in a strong and specific manner the acetylation status of the cccDNA-bound histones.

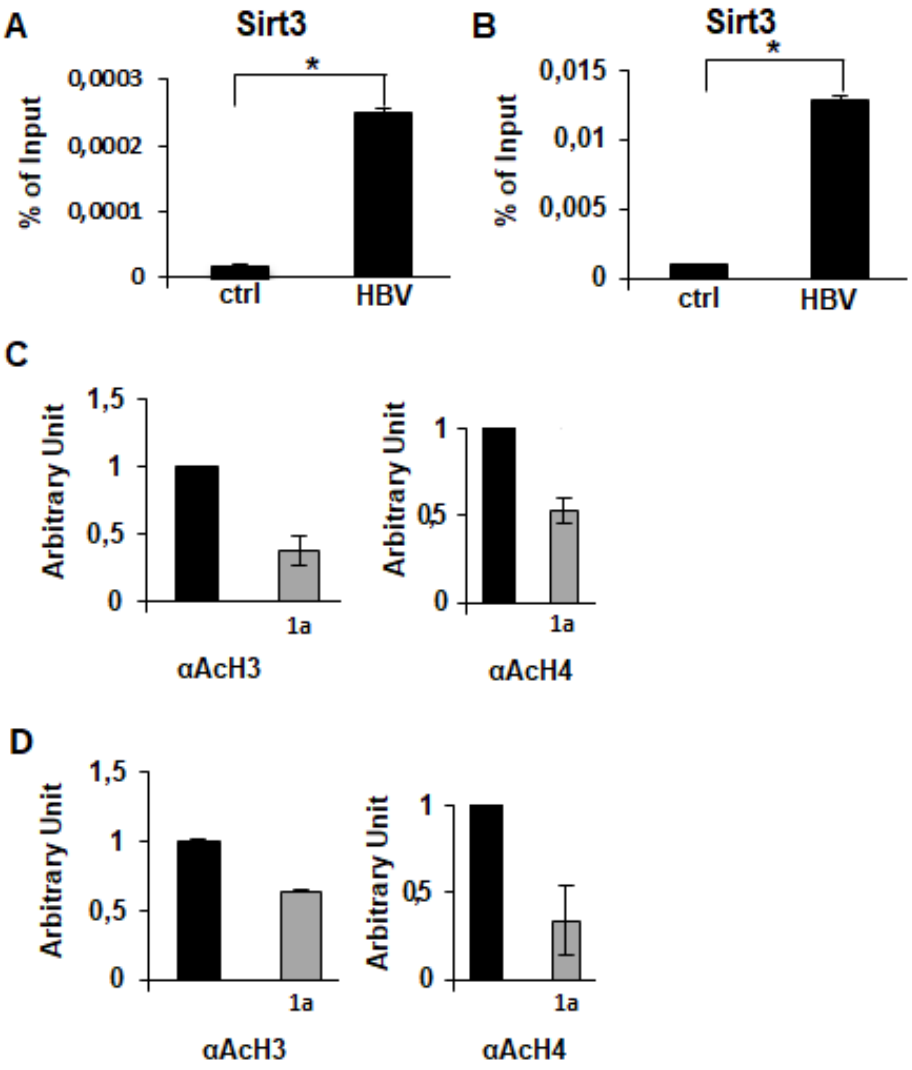

Figure 3.27: A)B) Levels of SIRT3 protein binding the cccDNA in HepG2 and HBV replicating HepAD38 cells. **C)D)** Acetylation histone H3 and/or H4 levels both in HepG2 (**C**) and in HepAD38 cells (**D**) after **1a** treatment.

3.9 Conclusion and Future Perspectives

To conclude, starting from SIRT1-activating 1,4-dihydropyridines, bearing benzyl group at N1, we identified carbonyl group at N1 to be responsible for an increased SIRT3 activation (**1a** and **1u)**. The first set of **1u** related compounds synthesised (**1v**-**a'**) turned out to be able to activate SIRT3, except for the derivative bearing cyano group in *para* which lost the activating activity on SIRT3. Furthermore, the insertion of methoxy substituents on the benzoyl group increases SIRT3 activation. The four strongest SIRT3-activators at 100 μM (**1a**, **1u**, **1y,** and **1z**) revealed to be specific SIRT3 activators when used at 10 μM. Furthermore, **1a** and the whole methoxy series (**1u-z**), activate GDH in a cell-based assay, with the exception of the para methoxy derivative (**1w**). In fact, in the enzyme-based assay, **1w** turned out to be a poor SIRT3 activator. To further confirm cellular Sirt3 activation by our compounds, we also analysed the deacetylation of MnSOD, another established Sirt3 substrate, in MDA-MB-231 cells. MnSOD deacetylation at Lys68 activates the enzyme and can be monitored specifically with a site-specific acetyl-Lys antibody. Sirt3 knock-down caused the expected increase in MnSOD-Lys68 acetylation, whereas treatment with 50 μM MC2791 (**1a**) resulted in a strong increase in MnSOD-Lys68 deacetylation compared to a DMSO control. Thus, we conclude that our DHP-based compounds act as Sirt3 activators in cellular systems.

Moreover, among the second set of **1u** related compounds (**2**, **5b-c**, **5e**, **5j-k**, **5m-q** and **6**), obtained by chemical modification at the C4 position through inserting different substituents (i.e –Cl, -Br, -NO, -NH_2) or replacing the phenyl with isosteric rings (i.e thiophene and furan), compound **6**, tested against other endogenous sirtuin substrates, turned out to preferentially activate Sirt5 over Sirt3. With the same strategy to increase both potency and selectivity of SIRT3 activator, a wider SAR investigation on **1a** structure was carried out. Importantly, the introduction of isosteric rings at the C4 position achieved two potent and selective Sirt5 activators **4k** and **4m**, the 3-furanyl and the 3-thiophenyl derivatives, respectively. In this series, other potent Sirt5 activators arising from **1a** scaffold were identified, such as **4b**, **4f**, and **4g**. On the contrary, looking into the N1-aroyl series, we found that compound **1t**, bearing a quinoxaline ring at N1, displayed comparable inhibition potency against Sirt3 and Sirt5 unlike the pyrazine analogue **1q**, which was found selective for Sirt5. More relevant, the shifting of the naphthyl ring, from 1 to 2 position linked to N1, afforded compounds **1r** and **1s** respectively, showing a different inhibition selectivity *versus* Sirt. In fact, while **1r** was able to induce Sirt3 activation, **1e** was found selective for Sirt5. Lastly, the phenylsulphonyl derivative **3** maintained Sirt3 activation as the parent compound **1a**.

Importantly, pharmacological activation of Sirt3 and Sirt5 is considered attractive for treatment of, e.g., cancer and heart failure. We report here discovery and characterization of potent and specific activators for Sirt3 and Sirt5. The 1,4-DHP-based activators bind to the Sirtuin catalytic core independent of bound substrates and increase the enzyme's turnover. The compounds are selective for Sirt3 or Sirt5 and show

cellular activity. Overall, our results provide a scaffold for potent and specific Sirtuins activation and an activation model for Sirt3 and Sirt5 as a basis for functional studies and further drug development.

Additionally, HBV-infected cells treated with our potent and selective Sirt3 activator MC2791 (**1a**), demonstrated that **1a** regulates the antiviral activity of cccDNA. The treatment of HBV-infected cells with **1a** through SIRT3 stimulation led to histone H3 and/or H4 hypoacetylation and reduction in the transcription from a viral cccDNA template, accompanied by a reduction in HBV replication (Fig. 3.28).

Overall, the results indicate that the Sirt3 activator **1a** can modulate the acetylation status of cccDNA-bound H3/H4 histones, thus providing a novel therapeutic approach for the treatment of chronic HBV infection.

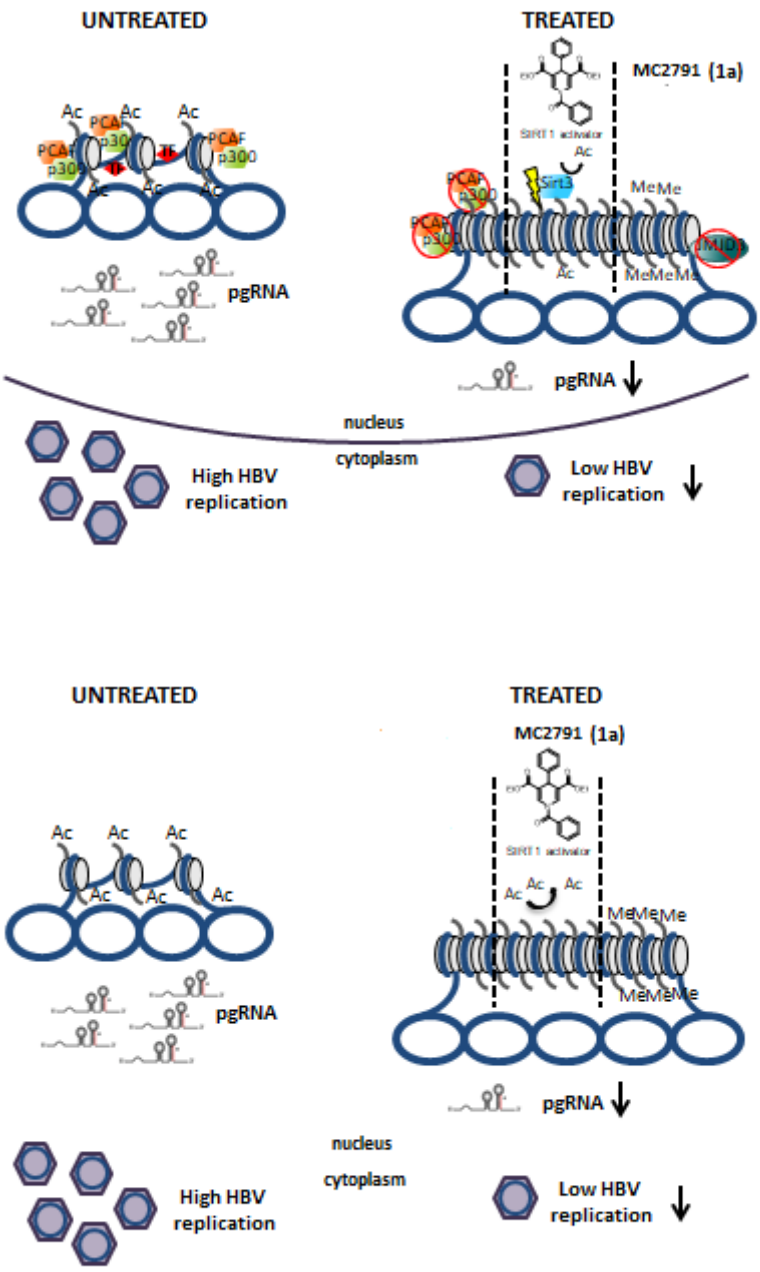

Figure 3.28: Effects of **1a** on HBV-infected cells through SIRT3 stimulation.

4 Design, synthesis and biological evaluation of dual inhibitors of histone deacetylases (HDACs) and methyltransferase (EZH2)

4.1 Dual targeting small molecules in cancer

The development of polypharmacology therapies, able to simultaneously modulate multiple targets involved in the onset of the pathology, is considered an attractive approach to treat multifactorial diseases, such as cancer, neurological and inflammatory disorders. [391] In the last few years, dual targeting small molecules have been developed with the aim to improve their effectiveness and potency as well as to reduce toxicity and any adverse effects. Therefore, the change from the ideology of "one drug target" to "one drug multiple targets" is considered a potential strategy to treat such diseases. Consequently, an effective and successful anticancer treatment should consider the biological system as a whole, owing to the presence of various signal pathways and cross-talk among epigenetic modifications. [371] In this context, the multi-target approach plays a crucial role to drive the research in dual epi-drugs design. However, the most important challenges of polypharmacology lie in the discovery of the target, the identification of the "hit" compound following by the optimisation of its template. [361] The goal of the multi-target approach consists in the design and synthesis of small molecules able to simultaneously and reversibly bind different but specific epi-drugs in order to achieve a final synergistic effect. [460] Multi-target drugs are produced by the connection of two or more molecules individually showing a known activity against specific enzymes. Accordingly, the multi-target approach allows to develop hybrid molecules characterised by the scaffold of an epi-drug fused/linked to another one able to hit a related target. To date, hybrids are emerging molecules scontaining reactive and functional groups that interact with one or more epigenetic targets, thus regulating different pathways involving in the same pathology, such as cancer.

As aforementioned in chapter 2, HDACi are mainly investigated in the design of dual targeting agents due to their wide structural variety and feasibility to host on the surface binding cap a high degree of different chemical structures. Therefore, different chemical entities that inhibit the same or another epi-enzyme can be attached to the ZBG, which plays a crucial role in HDAC inhibition. The combination of two or more distinct moieties in a single hybrid molecule represents, however, the most usual way to build multi-target drugs.

Several studies have already carried out to investigate the effect of dual epigenetic combination in cancer with the aim to achieve potent and beneficial effects.

In the last few years our interest in the design, synthesis and biological evaluation of hybrid compounds able to simultaneously act towards two different epigenetic targets, EZH2 methyltransferase, and HDAC

histone deacetylases, has greatly grown. Prompted by the ideology that the co-inhibition of these enzymes, which overexpression and increased activities are mainly implicated in the onset and progression of cancer, may restore synergically various target genes, including “tumour suppressor” genes. Consequently, dual EZH2/HDAC agents may represent an important strategy to fight cancer due to their already validated anti-cancer activity. Indeed, both enzymes are responsible for mediating the transcriptional silencing of target genes involved in fundamental cellular processes, such as cell cycle regulation, cell fate and differentiation, senescence and cancer. [132, 461-463] HDACs play a crucial role in the remodelling of chromatin and are involved in the epigenetic regulation of gene expression. HDAC can catalyse the removal of the acetyl group on lysine residues of nucleosome histone (i.e. H2A, H2B, H3, and H4) or non-histone proteins, and its role is opposite to the activity of HAT. [464] The balance between the action of HDAC and HAT defines the level of histones acetylation. In the last decade, inhibition of HDACs came out as a target for specific epigenetic changes associated with cancer and other diseases. 11 human zinc-dependent isoforms classified into four families (class I, IIa, IIb and IV) are reported as “classical” HDACs. In addition, another group of deacetylases known as “sirtuins” (class III) is well described which are hydrolysinge acyl-lysines via a NAD dependent mechanism. To date, five known HDACi have been approved by FDA: vorinostat (SAHA), a pan-HDACi and romidepsin, a natural pro-drug HDAC1 inhibitor, both approved in 2006 and 2009 for CTCL respectively, belinostat, a pan-HDACi approved in 2014 for PTCL, panobinostat, a pan-HDACi approved in 2015 for MM and lastly chidamide, HDAC 1/2/3/10 inhibitor only approved in China in 2014 for the treatment of PTCL. On the other hand, the HMT EZH2 is the catalytic subunit of the polycomb repressive complex 2 (PRC2), which induces the methylation of histone H3 on lysine 27 up to its trimethylated form by using SAM as co-substrate. [465] Moreover, EZH2 overexpression and mutations occur in several malignancies and are usually associated with aggressive tumours, drug resistance and poor prognosis. [132, 466] Since 2012, some potent, selective and SAM-competitive small molecules have been reported. [99, 143, 467-469] Actually, GSK2816126, tazemetostat (EPZ005687) and CPI-1205 entered phase I/II clinical trials for the treatment of lymphomas, solid tumours, MM and others tumours. [148, 157, 158] Since EZH2 and HDACs act as gene repressor marks and play a pivotal role in cancer, a dual targeting small molecule may be the best choice to find an adequate and decisive anti-cancer therapy.

4.2 Rational of the project

Following our previous work on the design, synthesis and biological evaluation of EZH2 inhibitors (EZH2i), [470-475] we developed the pyrazole-based small molecule MC3629 (IC_{50}: 5.27÷15.4 μM) as a simplified analog of EPZ005687, modifying the structure of these two known EZH2i by removing the benzene ring from the indazole nucleus, to obtain the pyrazole ring linked through a carboxamide function to the 3-aminomethyl-4,6-dimethyl-2-pyrimidone moiety, known to be crucial for EZH2 inhibition (**A**, Fig. 4.1). [93] Our results showed that the pharmacological inhibition of EZH2 is leading to

the impairment of SHH MB-SLCs cell proliferation and stemness, and the induction of apoptosis *in vitro* and *in vivo*, as well. [476] As a part of our ongoing research to develop inhibitors of histone/MTs, [471, 473, 477-480] through a molecular pruning approach from known inhibitors bearing a bicyclic moiety as a central scaffold, we described novel pyrazole-based EZH2i. All the newly obtained derivatives were tested towards a panel of methyltransferases and four different cancer cell lines (human breast cancer MDA-MB231, myelogenous leukaemia K562, prostate cancer PC3 and neuroblastoma SK-N-BE). Very recently, the most potent compound MC3629 has been reported to arrest cell growth in breast MDA-MB231, leukaemia K562 and neuroblastoma joined to the reduction of H3K27me3 levels and induction of apoptosis and autophagy. [481] In another study, we tried to simplify the structure of GSK126, known EZH2i, to effort a novel series of pyrrole-based EZH2i, tested in a panel of cancer cell lines (breast MDA-MB231, leukaemias SHSY5Y, NB4 and U937, and neuroblastoma KELLY) (**B**, Fig. 4.1). In this study we evaluated the effect of various substituents (alkyl, aryl or different aromatic rings and arylalkyl group) at the N1 or C2/C5 position of the pyrrole and, MC3707 (IC_{50}: 5.78 µM) was identified as a new lead compound.

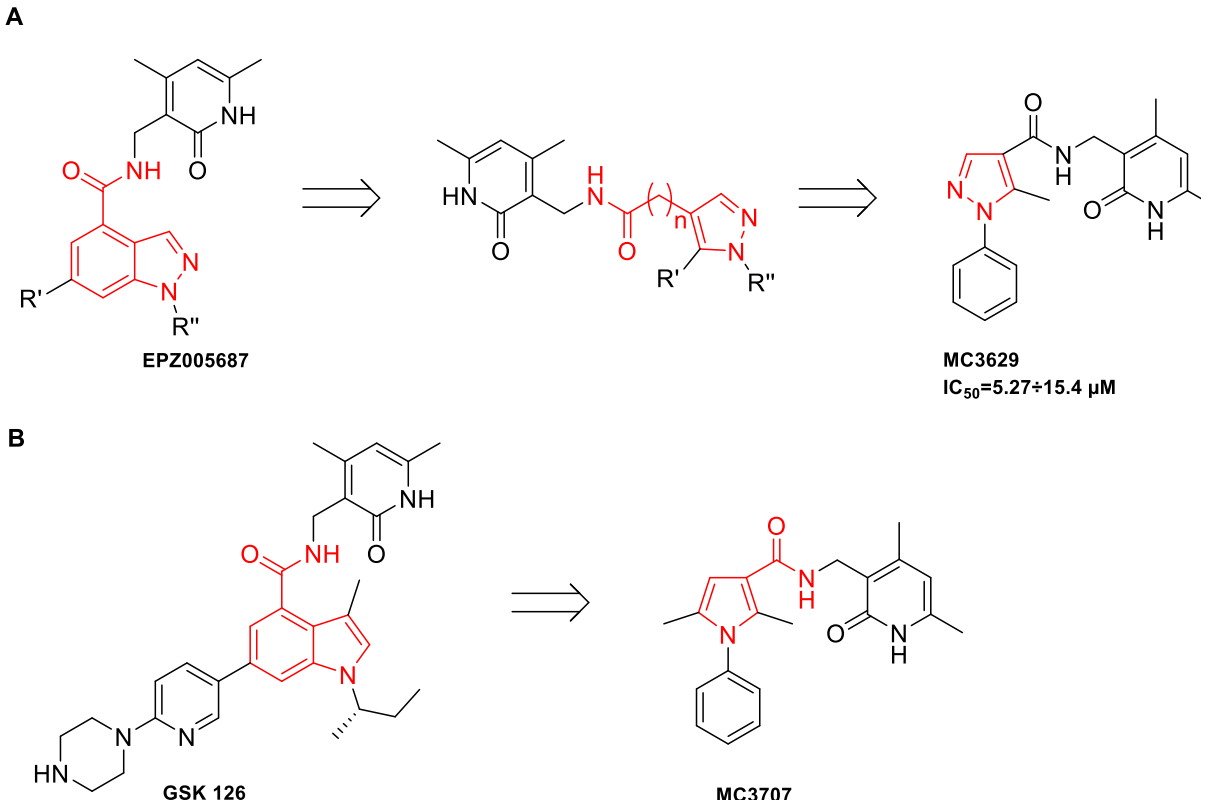

Figure 4.1: Discovery of novel pyrazole-based (**A**, MC3629) and pyrrole-based (**B**, MC3707) EZH2 inhibitors.

On the basis of these evidences, we have designed and synthesised potential dual inhibitors of HDACs (classes I, II) and EZH2, important epigenetic targets overexpressed in cancer and contributing to its initiation and progression. Previous studies (article not yet submitted) suggested the *meta*-position as

the most favourable substitution on phenyl ring bound to the N1-pyrazole/pyrrole thus, we've chosen to link the HDAC targeting scaffolds in that position.

In our first investigation, we combined the *well-known* vorinostat HDACi moiety to the already optimised EZH2i scaffolds MC3629 and MC3707 (Fig. 4.2).

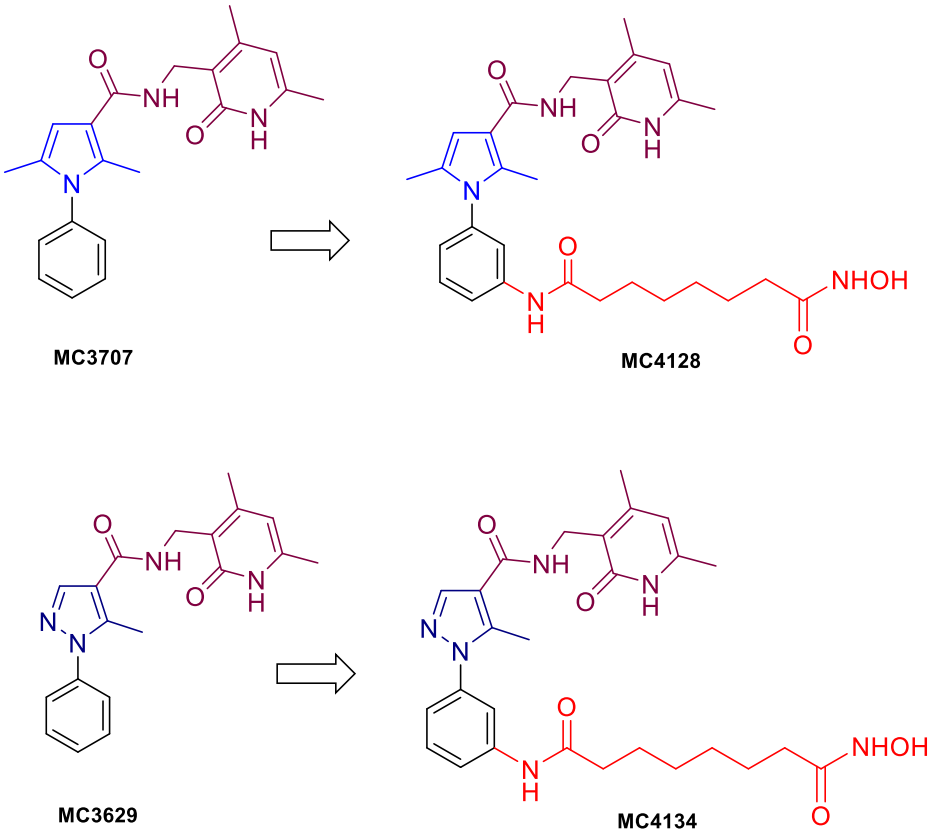

Figure 4.2: First investigation on design of dual inhibitors of HDAC and EZH2.

A first preliminary screening of compounds MC4128 and MC4134 to determine the IC_{50} values against EZH2 and different HDAC isoforms was performed. Data showed that only the pyrrole derivative MC4128 was able to simultaneously inhibit EZH2 and HDAC, also exhibiting an interesting isoform selectivity for HDAC6. Even though MC4134 showed to inhibit HDAC, no inhibition potency against EZH2 was detected, unless at 200 µM.

Compound	EZH2 (IC_{50}, µM)	HDAC isoforms (IC_{50}, µM)						
		1	2	3	4	5	6	8
MC4134	4% inhib. at 100 µM	0.8	2.4	1.5	NA	101	0.01	2.1

MC4128	7.4	0.43	1.3	0.45	36.8	16.6	**0.0054**	1.11

Table 4.1: Biochemical activities against EZH2 and different HDAC isoforms (1, 2, 3, 4, 5, 6 and, 8) of MC4134 and MC4128.

Prompted by these findings, we decided to develop a series of dual inhibitors of EZH2 and HDAC, combining the well-known HDACi moieties to the already optimised EZH2i scaffold MC3707. Therefore, according to the HDACi pharmacophoric model, we have chosen different types of spacer: the aliphatic one (Vorinostat), the benzoic one (Entinostat) and the cinnamic one (Panobinostat and Belinostat). As zinc binding group we used, in turn, a hydroxamic acid or an *ortho*-amino anilide (**8a-g** and **6a-g**, fig. 4.3)

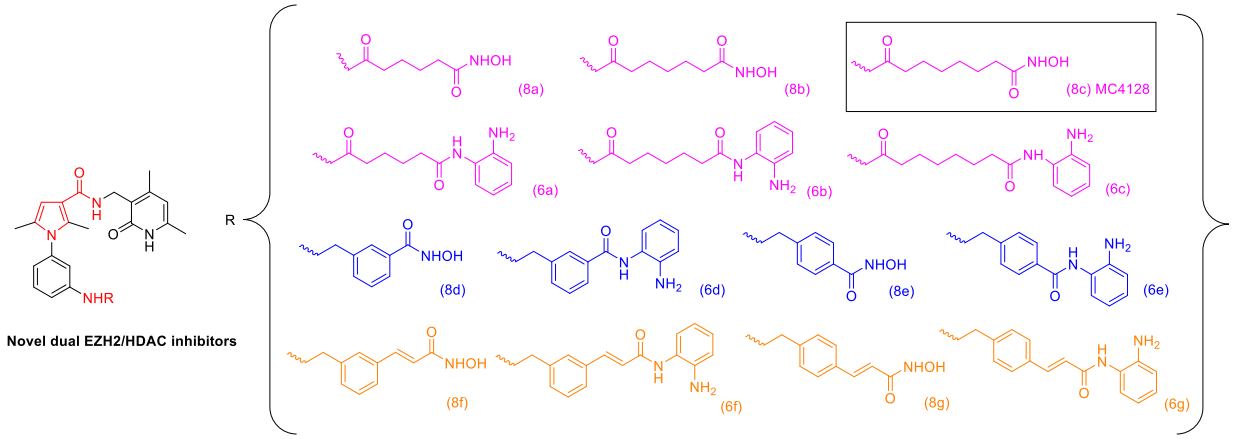

Figure 4.3: Design of novel dual HDAC/EZH2 inhibitors **8a-g** and **6a-g.**

4.3 Chemistry

Scheme 4.1 shows the synthesis of the 3-(aminomethyl)-4,6-dimethylpyridin-2(1H)-one hydrochloride, prepared according to the literature. [481] The cyclocondensation of (3-nitrophenyl)hydrazine chloride with ethyl (Z)-2-((dimethylamino)methylene)-3-oxobutanoate (**1n**) (both commercially available) in dry ethanol at 80 °C provided the pyrazole scaffold of ethyl 5-methyl-1-(3-nitrophenyl)-1H-pyrazole-4-carboxylate **1o** that was hydrolysed with 2N potassium hydroxide in ethanol and tetrahydrofuran giving the carboxylic acid **1p**. The carboxylic acid function was protected as tert-butyl ester **1q** by reaction with *N,N*-dimethylformamide di tert-butyl acetal in dry toluene at 90 °C. The reduction of the nitro group with metal zinc and ammonium chloride in dioxane and water (1:1) at 50 °C gave the amine **1r**, as shown in scheme 4.2. **1r** was acylated by the methyl 8-chloro-8-oxooctanoate obtaining the compound **2h**. The carboxylic acid **3h** was prepared by cleavage of the tert-butyl function with trifluoroacetic acid in dry dichloromethane. The coupling reaction, carried out onto the amine (4,6-dimethyl-2-oxo-1,2-dihydropyridin-3-yl)methanaminium chloride **1i** (prepared according to the literature with O-

benzotriazol-tetramethyluronium tetrafluoroborate (TBTU) and trimethylamine in dry N,N-dimethylformamide, [482]) led to the corresponding amide **4h**. Methyl ester hydrolysis with lithium hydroxide in 1:1 water:tetrahydrofuran mixture gave the acid **5h** which was then converted into the corresponding hydroxamate **8h** by reaction with O-(tetrahydro-2H-pyran-2yl)hydroxylamine (O-THP), O-benzotriazol-tetramethyluronium tetrafluoroborate (TBTU) and trimethylamine in dry *N,N*-dimethylformamide followed by acidic cleavage with 4M hydrogen chloride solution in dioxane (scheme 4.3). Scheme 4.4 shows the synthesis of the pyrrole scaffold of the dimethyl-nitrophenyl-pyrrole **1j**, prepared via a modified procedure described in the literature [483] and followed by a Friedel–Crafts acylation with trichloroacetyl chloride in dry dichloroethane at 70 °C and successive hydrolysis with 2N potassium hydroxide, gave the carboxylic acid **1k**. As previously shown for **1p**, the carboxylic acid function was protected as tert-butyl ester by reaction with *N,N*-dimethylformamide di tert-butyl acetal in dry toluene at 90 °C. The reduction of the nitro group (**1l**) with metal zinc and ammonium chloride in dioxane and water (1:1) at 50 °C gave the amine **1m**. The intermediates **1f** and **1g** were synthesised from the corresponding meta or para benzaldehydes and n-butyl acrylate via Heck reaction performed with triethylamine, triphenylphosphine and palladium (II) acetate under nitrogen condition, as shown in scheme 4.5. Final compounds **6a-c** and **8a-c** were prepared as reported into the scheme 4.6. The amine **1m** underwent to acylation by using various 3-methoxy-3-oxo-carboxylic acids, which differ in the alkyl chain length, to get the corresponding intermediates **2a-c**. The carboxylic acids **3a-c** were prepared by cleavage of the tert-butyl function with trifluoroacetic acid in dry dichloromethane. The coupling reaction with the amine **1i** gave the intermediates **4a-c** which were hydrolysed with lithium hydroxide in 1:1 water: tetrahydrofuran mixture to afford the acids **5a-c**. In the last step, the acid **5a-c** were converted into the final hydroxamates **8a-c** or anilides **6a-c** by reaction with O-THP, TBTU, and trimethylamine in dry *N,N*-dimethylformamide (**7a-c**) followed by acidic cleavages with 4M hydrogen chloride solution in dioxane, or by reaction with *o*-phenylenediamine, trimethylamine, TBTU, and dry *N,N*-dimethylformamide, respectively.

Final compounds **6d-g** and **8d-g** were prepared as reported into the scheme 4.7. The amine **1m** was underwent a reductive amination with the appropriately substituted benzaldehyde to afford the corresponding intermediates **2d-g**. The carboxylic acids **3d-g**, prepared by cleavage of the tert-butyl function with trifluoroacetic acid in dry dichloromethane, underwent the coupling reaction with the amine **1i**, giving the corresponding amides **4d-g**. Ester hydrolysis with lithium hydroxide in 1:1 water:tetrahydrofuran mixture gave the acids **5d-g** which were then converted into the corresponding hydroxamates **8d-g** or anilides **6d-g** by reaction with O-THP, TBTU and trimethylamine in dry *N,N*-dimethylformamide (**7d-g**) followed by an acidic cleavage with 4M hydrogen chloride solution in dioxane, or by reaction with *o*-phenylenediamine, trimethylamine, TBTU and dry *N,N*-dimethylformamide, respectively.

Scheme 4.1

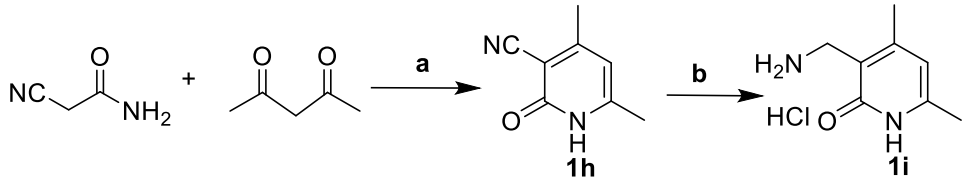

Reagents and conditions: (a) Piperidine, EtOH, reflux; (**b) 1.** H_2, Pd/C, PtO_2, CH_3COOH, 70psi 40°C; **2.** HCl, EtOH.

Scheme 4.2

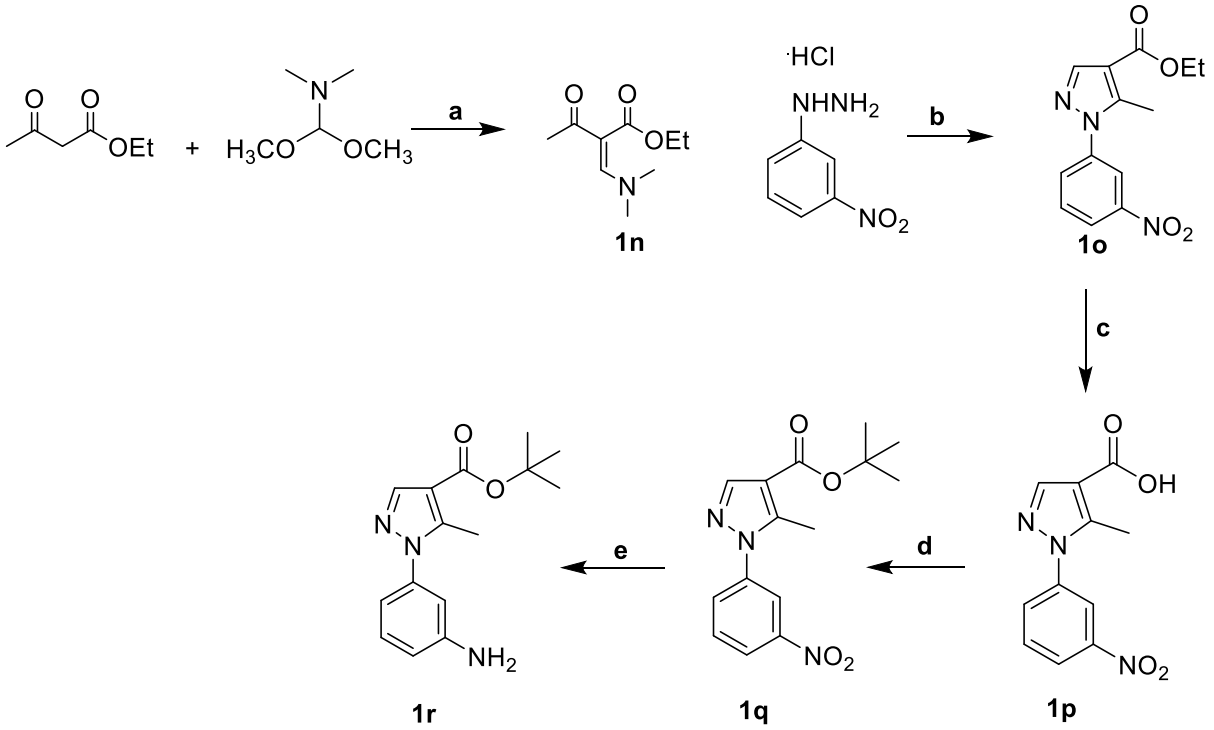

Reagents and conditions: (a) reflux, 110 °C; **(b)** dry EtOH, TEA, 80 °C, reflux; **(c)** 1. 2N KOH, EtOH, THF; 2. 2N HCl; **(d)** *N,N*-dimethylformamide-di-*tert*-butyl acetal, dry Toluene, 90 °C, reflux; **(e)** Zn, NH_4Cl, Dioxane, H_2O, 50 °C.

Scheme 4.3

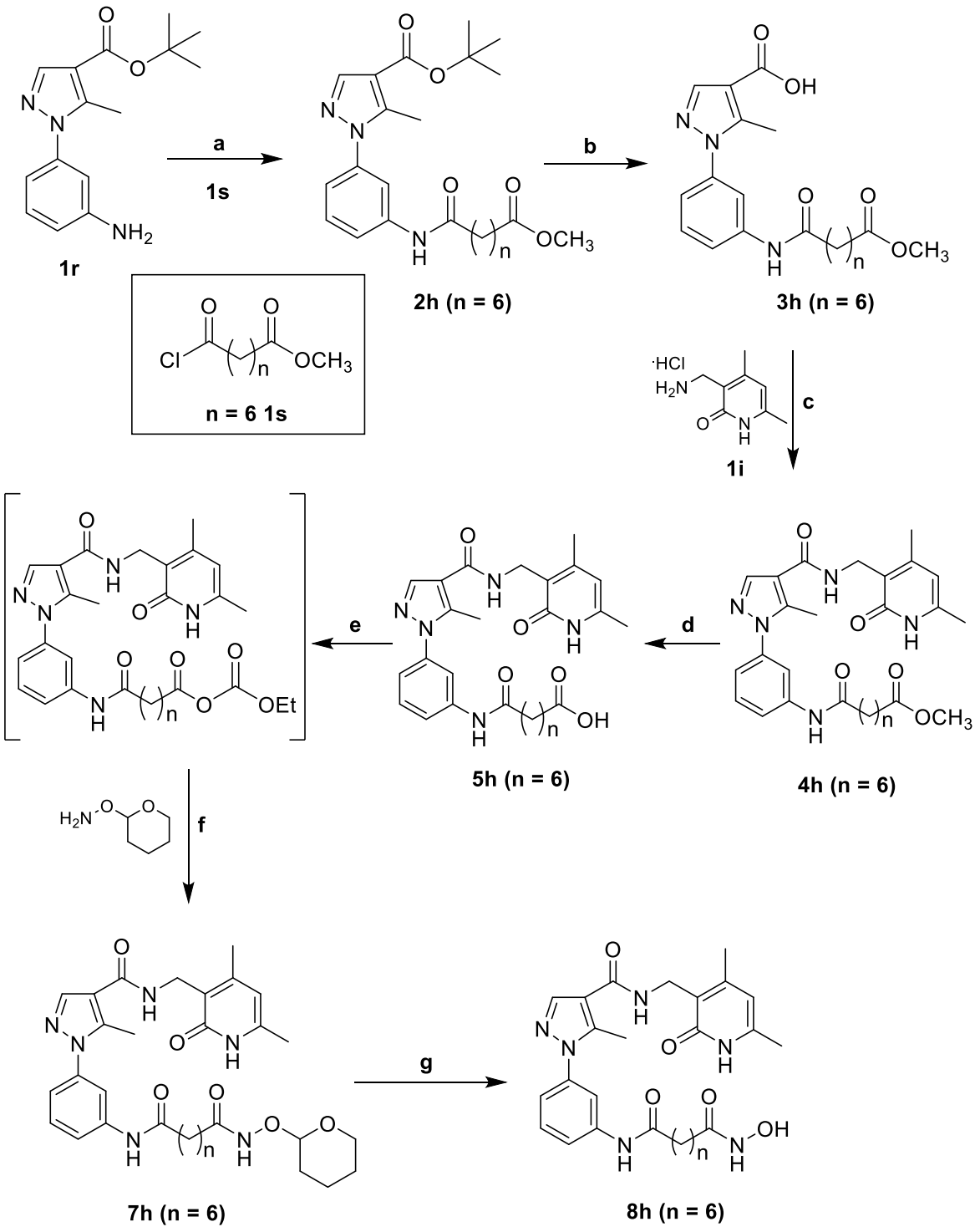

Reagents and conditions: **(a)** dry DCM, TEA, methyl 8-chloro-8-oxooctanoate; **(b)** dry DCM; Trifluoroacetic acid; **(c)** dry DMF; triethylamine; TBTU; N_2; **(d)** H_2O/THF; LiOH; **(e)** THF, ethyl chloroformate, TEA, 0 °C; **(f)** THF, O-(tetrahydro-2H-pyran-2-yl)hydroxylamine; **(g)** dry THF; 4 M HCl in Dioxane.

Scheme 4.4

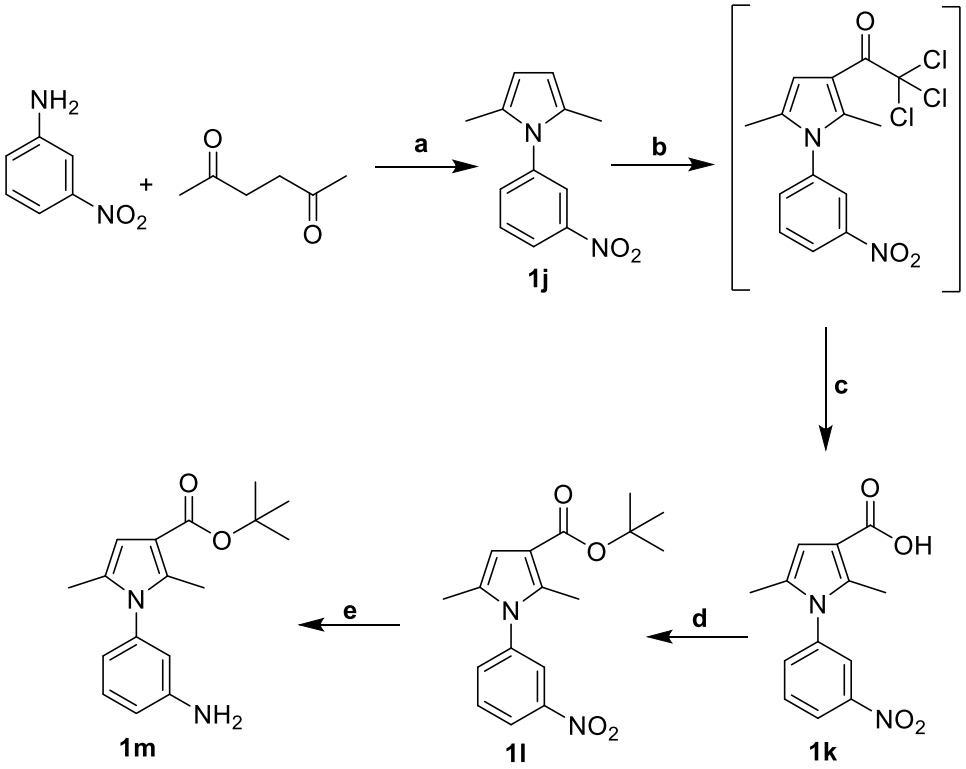

Reagents and conditions: (a) glacial CH_3COOH, $CoCl_2 \times 6H_2O$, 70 °C; **(b)** Trichloroacetyl chloride, dry DCE, 70 °C; **(c)** 1. 2N KOH, EtOH, THF 2. 2N HCl; **(d)** *N,N*-dimethylformamide-di-*tert*-butyl acetal, dry Toluene, 90 °C, reflux**; (e)** Zn, NH_4Cl, Dioxane, H_2O, 50 °C.

Scheme 4.5

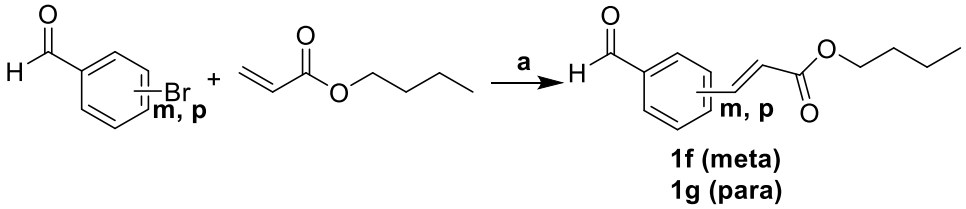

Reagents and conditions: (a) $P(Ph)_3$, $Pd(AcO)_2$, $NaHCO_3$, Triethylamine, dry DMF, 110 °C.

Scheme 4.6

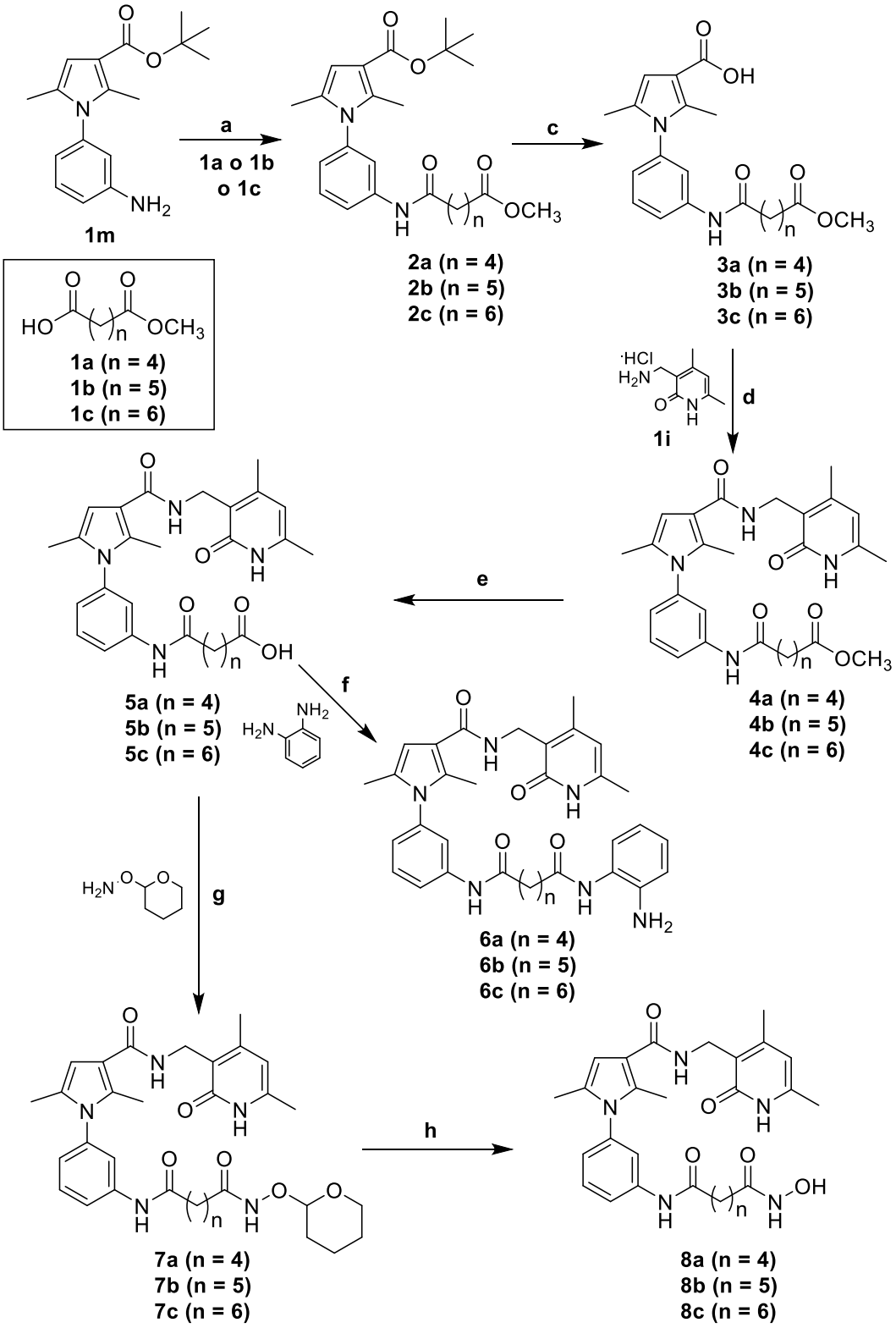

Reagents and conditions: **(a)** 1. $SOCl_2$ 2. Trimethylamine, dry DCM; **(b)** $(CH_3COO)_3BHNa$, dry DCE; **(c)** trifluoroacetic acid, dry DCM; **(d)** Trimethylamine, TBTU, dry DMF, N_2; **(e)** LiOH, H_2O/THF; **(f)** Trimethylamine, TBTU, dry DMF, N_2; **(g)** Trimethylamine, TBTU, dry DMF, N_2; **(h)** 4 M HCl in Dioxane, dry THF.

Scheme 4.7

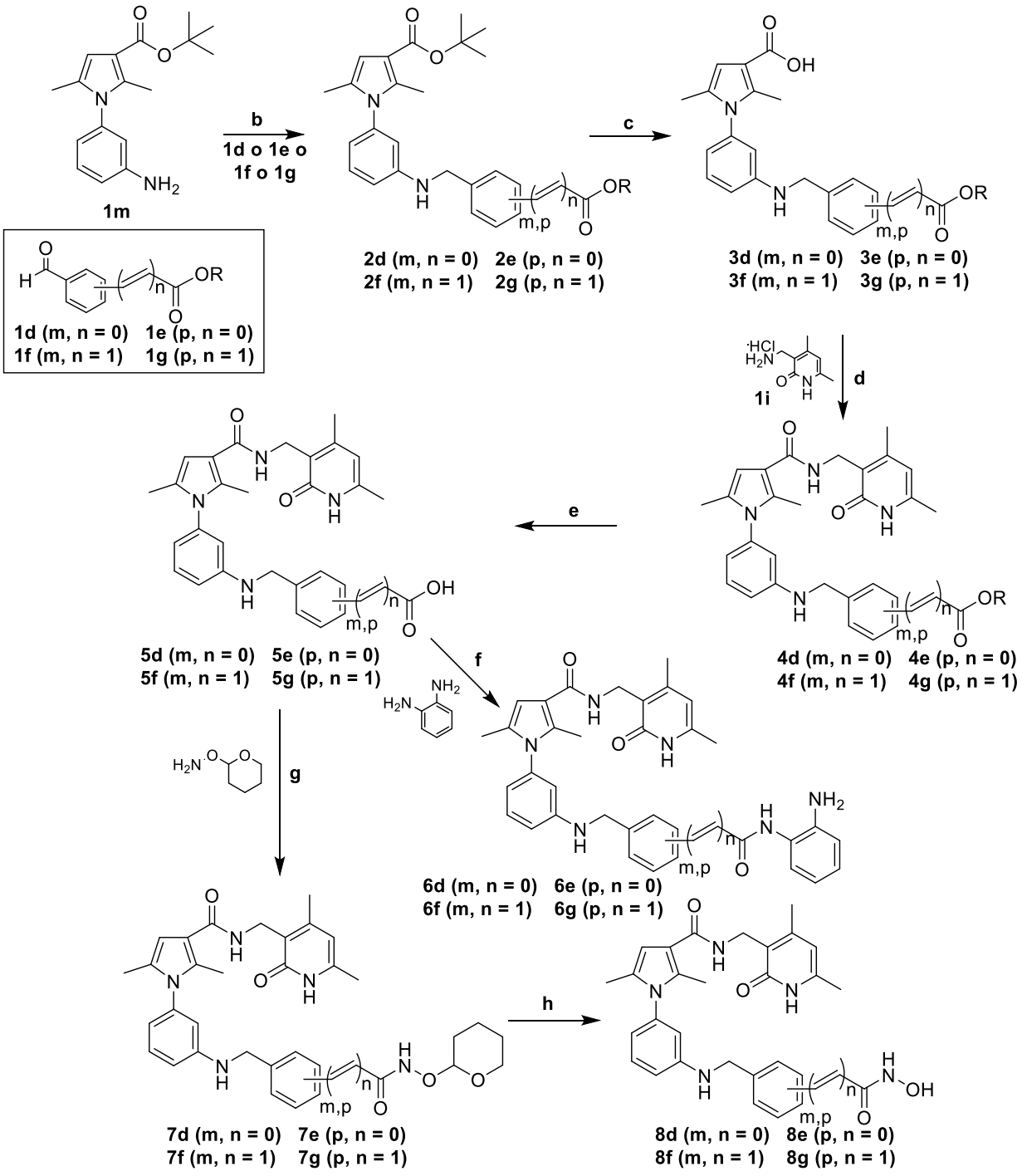

Reagents and conditions: (a) 1. $SOCl_2$ 2. Trimethylamine, dry DCM; **(b)** $(CH_3COO)_3BHNa$, dry DCE; **(c)** trifluoroacetic acid, dry DCM; **(d)** Trimethylamine, TBTU, dry DMF, N_2; **(e)** LiOH, H_2O/THF; **(f)** Trimethylamine, TBTU, dry DMF, N_2; **(g)** Trimethylamine, TBTU, dry DMF, N_2; **(h)** 4 M HCl in Dioxane, dry THF.

Table 4.2: Chemical-Physical Data of Compounds **6a-g** and **8a-g**.

LAB CODE	COMPOUND	CHEMICAL STRUCTURE	M.P.(°C)	YIELD (%)	RECRYSTALLIZATION SOLVENT
MC4255	8a	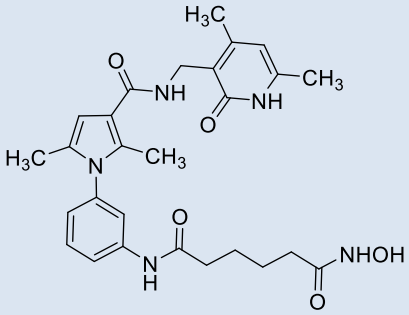	172	60.2	Benzene/Acetonitrile
MC4256	6a	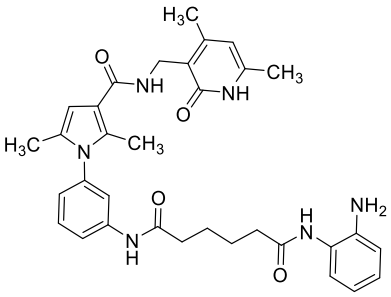	157	38.5	Benzene
MC4243	8b	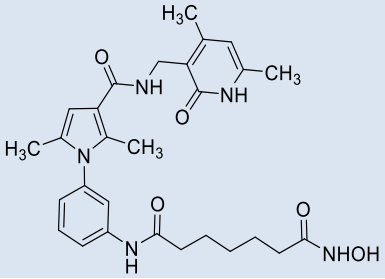	163	86	Benzene/Acetonitrile
MC4240	6b	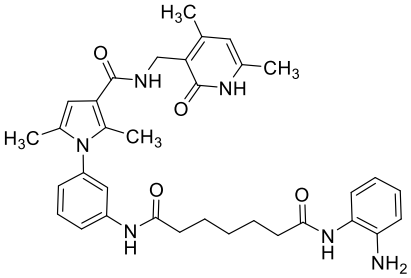	158	77	Benzene
MC4128	8c	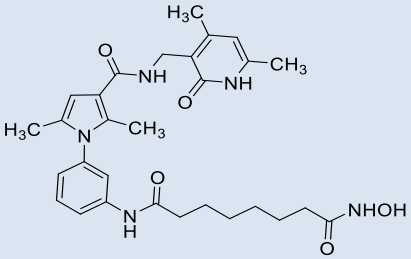	171	69	Benzene/Acetonitrile
MC4213	6c	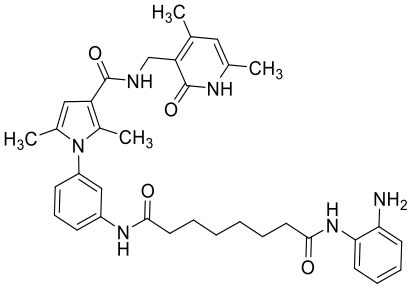	150	73	Benzene

MC4257	**8d**	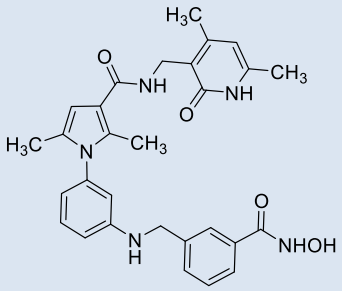	**175**	**72**	**Benzene/Acetonitrile**
MC4258	**6d**	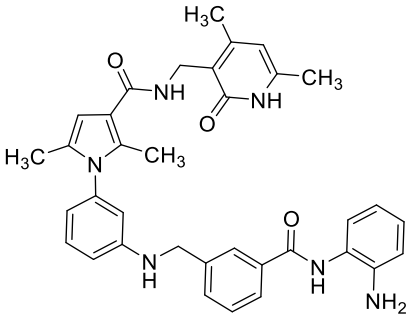	**158**	**34**	**Benzene**
MC4229	**8e**	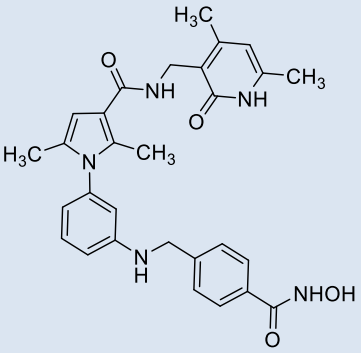	**170**	**60**	**Benzene/Acetonitrile**
MC4227	**6e**	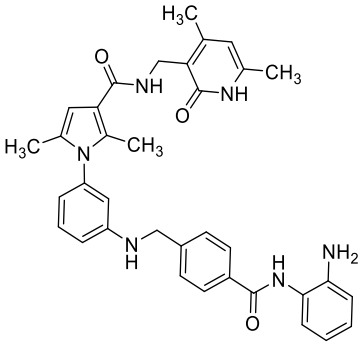	**177**	**42**	**Benzene/Acetonitrile**
MC4242	**8f**	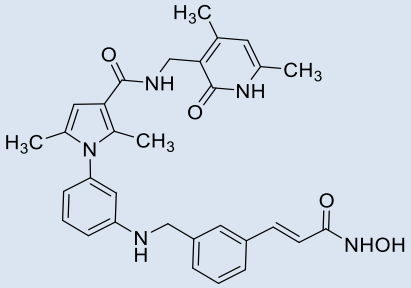	**178**	**83**	**Benzene/Acetonitrile**
MC4271	**6f**	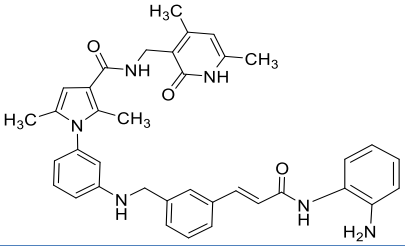	**163**	**56**	**Benzene**

MC4230	**8g**	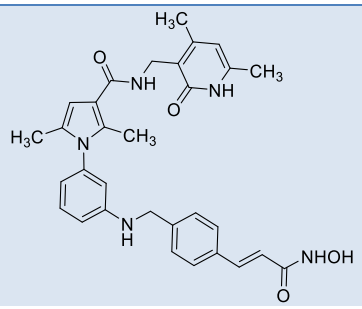	**175**	**55**	**Benzene/Acetonitrile**
MC4272	**6g**	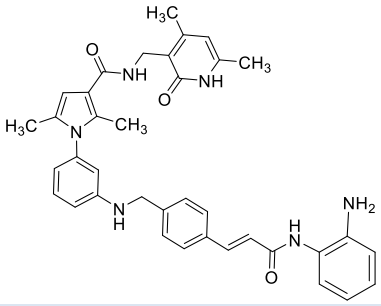	**169**	**59**	**Benzene**
MC4134	**8h**	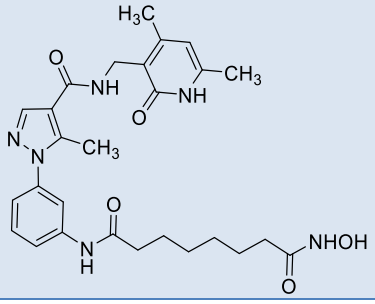	**169**	**68**	**Benzene/Acetonitrile**

4.4 Experimental section

Chemistry. Melting points were determined on a Buchi 530 melting point apparatus and are uncorrected. ^{1}H NMR and ^{13}C NMR spectra were recorded at 400 MHz on a Bruker AC 400 spectrometer; chemical shifts are reported in δ (ppm) units relative to the internal reference tetramethylsilane (Me4Si). EIMS spectra of all compounds were recorded with a Fisons Trio 1000 spectrometer; only molecular ions (M+) and base peaks are given.HR-MS spectra of final compounds were recorded with a ESI Orbitrap spectrometer (capillary temperature:275°C, spray voltage 4,0 kV (ESI +) and 3,8 kV (ESI +), sheath gas: 5, tube lens voltage +/- 90 V). The mass spectrometry samples were solubilized in MeOH + 0,01% HCOOH (10^{-5}M). All compounds were routinely checked by TLC, ^{1}H NMR, and ^{13}C NMR spectra. TLC were performed on aluminum-backed silica gel plates (Merck DC, Alufolien Kieselgel 60 F254) with spots visualised by UV light. All solvents were reagent grade and, when necessary, were purified and dried by standard methods. The concentration of solutions after reactions and extractions involved the use of a rotary evaporator operating at reduced pressure of ca. 20 Torr. Organic solutions were dried over anhydrous sodium sulfate. Elemental analysis has been used to determine the purity of the described compounds, that is, >95%. Analytical results are within ±0.40% of the theoretical values. All chemicals were purchased from Sigma Aldrich, Milan (Italy), or from Alfa Aesar, Karlsruhe (Germany), and were of the highest purity.

Procedure for the synthesis of the ethyl (Z)-2-((dimethylamino)methylene)-3-oxobutanoate (1n).

Ethyl 3-oxobutanoate (12.5 mmol, 1 eq, 1.6 mL,) was reacted with *N, N*-dimethylformamide-dimethylacetal (15 mmol, 1.2 eq, 2 mL) and the resulting mixture was left under stirring at 110 °C (reflux) for an hour and a half. After this time, the reaction was over and the crude product was purified by column chromatography (SiO_2 eluting with pure acetate phase) to afford the desired compound **1n**. (1.05 g; Y = 45.3%). [481]

Mp= 43-45 °C.

Procedure for the synthesis of the ethyl 5-methyl-1-(3-nitrophenyl)-1H-pyrazole-4-carboxylate (1o).

(3-nitrophenyl)hydrazine chloride (5.67 mmol, 1. eq, 1.07 g) and triethylamine (6.24 mmol, 1.1 eq, 0.87 mL) were added to a solution of ethyl (Z)-2-((dimethylamino)methylene)-3-oxobutanoate (5.67 mmol, 1.0 eq, 1.05 g) in dry ethanol (10 mL) and the resulting mixture was heated to 80 °C for 1h. After this time, TLC analysis showed complete conversion of the starting material, therefore, the reaction was quenched with water (50 mL). The precipitated product **1o** was filtered, dried in oven at 60°C and triturated in petroleum ether. (1.36 g; Y = 87 %)

Mp= 97 °C.

^{1}H NMR (400MHz, $CDCl_3$) δ: 1.34 (t, 3H, -$COOCH_2CH_3$), 2.02 (s, 3H, -CH_3 pyrazole), 4.27 (q, 2H, -$COOCH_2CH_3$), 7.65 (t, 1H, aromatic proton), 8.01 (dt, 1H, aromatic proton), 8.15 (s, 1H, pyrazole proton), 8.34 (dt, 1H, aromatic proton), 8.47 (t, 1H, aromatic proton) ppm.

Procedure for the synthesis of the 5-methyl-1-(3-nitrophenyl)-1H-pyrazole-4-carboxylic acid (1p).

2N aqueous solution of KOH (19.8 mmol, 4.0 eq, 1.11 g) was added to a solution of ethyl 5-methyl-1-(3-nitrophenyl)-1*H*-pyrazole-4-carboxylate **1o** (4.94 mmol, 1.0 eq, 1.36 g) in ethanol (5 mL) and the resulting mixture was stirred for 2h at room temperature. After this time, the reaction was judged to be complete by TLC analysis, ethanol was evaporated *in vacuo,* and the carboxylate was titrated with 2N aqueous solution of HCl added at 0 °C dropwise until pH 1. The precipitated acid **1p** was filtered, rinsed several times with distilled water and dried in oven at 60°C. (1.22 g; Y= 99%)

Mp = 115 °C.

^{1}H NMR (400MHz, δ_6-DMSO) δ: 2.51 (s, 3H, CH_3), 7.49 (t, 1H, aromatic proton), 8.25 (m, 2H, aromatic protons), 8.33 (s, 1H, pyrazole proton), 8.35 (m, 1H, aromatic proton), 13.34 (bs, 1H, COO*H*) ppm.

Procedure for the synthesis of the 2,5-dimethyl-1-(3-nitrophenyl)-1H-pyrrole-3-carboxylic acid (1k).

In a sealed tube, 2,5-dimethyl-1-(3-nitrophenyl)-1H-pyrrole (18.6 mmol, 1.0 eq, 4.02 g) was dissolved in dichloroethane (20 mL), and the solution was cooled to 0 °C. Trichloroacetyl chloride (55.8 mmol, 3.0 eq, 6.23 mL) was added dropwise. The solution was stirred at 0 °C for 10 minutes, let warm to room temperature and finally heated to 70 °C for 3 hours. After this time, TLC analysis showed the complete conversion of the starting material. The volatiles were removed *in vacuo*. The residue was dissolved in a 1:1 EtOH: THF mixture. The solution was cooled to 0 °C, and a 2N aqueous solution of KOH (186 mmol,

10 eq, 10.4 g) was added dropwise. The reaction mixture was stirred at room temperature for 1h. After this time, the reaction was judged to be complete by TLC analysis. The organic solvents were removed *in vacuo*. The byproducts were removed by extraction from the basic aqueous layer with ethyl acetate (3 × 20 mL). The aqueous layer was then cooled to 0 °C and acidified till pH 2 by addition of a 2N aqueous solution of HCl. The brownish precipitated solid **1k** was filtered, rinsed several times with distilled water and dried in an oven (60 °C). (2.0 g; Y= 41.3 %).

Mp = 110 °C.

^{1}H NMR (400MHz, d_6-DMSO) δ: 1.96-1.99 (s, 3H, pyrrole C*H*$_3$), 2.23 (s, 3H, pyrrole C*H*$_3$), 6.28 (s, 1H, pyrrole proton), 7.85-7.88 (m, 2H, aromatic protons), 8.18 (m, 1H, aromatic proton), 8.35-8.38 (m, 1H, aromatic proton), 11.78 (bs, 1H, COO*H*) ppm.

General Procedure for the synthesis of the tert-butyl 1-(3-nitrophenyl)-1H-pyrazole/pyrrole-carboxylates (1q, 1l). Example: tert-butyl 2,5-dimethyl-1-(3-nitrophenyl)-1H-pyrrole-3-carboxylate (1l).

N,*N*-Dimethylformamide di-*tert*-butyl acetal (23.1 mmol, 3.0 eq, 5.5 mL,) was added to a solution of 2,5-dimethyl-1-(3-nitrophenyl)-1*H*-pyrrole-3-carboxylic acid **1k** (7.68 mmol, 1.0 eq, 2.0 g) in dry toluene (10 mL). The resulting mixture was stirred at 90 °C for 4h. After this time, the reaction was judged to be complete by TLC analysis therefore the reaction was quenched with brine (20 mL) and extracted with ethyl acetate (3×10mL). The combined organic layers were washed with brine (3×10 mL), dried with sodium sulfate, filtered and evaporated *in vacuo* to obtain the crude product that was purified by column chromatography (SiO_2 eluting with chloroform/methanol 20/1) to give the pure **1l** intermediate. (1.75 g; Y= 72 %)

Mp = 98 °C.

^{1}H NMR (400MHz, $CDCl_3$) δ: 1.59 (s, 9H, COOC(C*H*$_3$)$_3$), 2.02 (s, 3H, pyrrole CH_3), 2.31 (s, 3H, pyrrole CH_3), 6.39 (s, 1H, pyrrole proton), 7.55-7.56 (d, 1H, aromatic proton), 7.71-7.75 (t, 1H, aromatic proton), 8.10-8.11(t, 1H, aromatic proton), 8.35-8.37 (dd, 1H, aromatic proton) ppm.

General procedure for the synthesis of the tert-butyl 1-(3-aminophenyl)-1H-pyrazole/pyrrole-carboxylates (1r, 1m). Example: tert-butyl 1-(3-aminophenyl)-5-methyl-1H-pyrazole-4-carboxylate (1r).

Metallic Zinc (34.2 mmol, 7.25 eq, 2.23 g) and ammonium chloride (9.43 mmol, 2.0 eq, 0.504 g) were added to a solution of *tert*-butyl 5-methyl-1-(3-nitrophenyl)-1*H*-pyrazole-4-carboxylate **1q** (4.71 mmol, 1.0 eq, 1.43 g) in 1:1 dioxane:water mixture. The resulting solution was stirred at 50 °C for 2h. After this time, TLC analysis showed complete conversion of the starting material the reaction was subsequently quenched with a saturated solution of sodium carbonate (20 mL) and extracted with chloroform (3×10 mL). The combined organic phases were washed with brine (3×10 mL), dried with sodium sulfate, filtered and evaporated under reduced pressure to obtain a crude product that was purified by column chromatography (SiO_2 eluting with *n*-Hexane/ethyl acetate 2.5/1) to give the pure **1r** intermediate. (1.13 mg; Y= 87.7 %)

Mp = 109 °C.

^{1}H NMR (400MHz, d_6-DMSO) δ: 1.52 (s, 9H, COOC(CH_3)$_3$), 2.51 (s, 3H, pyrazole CH_3), 5.56 (s, 2H, NH_2), 6.64 (m, 1H, aromatic proton), 7.08 (m, 2H, aromatic proton), 7.26 (m, 1H, aromatic proton), 8.00 (s, 1H, pyrazole proton) ppm.

General procedure for the synthesis of the butyl (E)(3-formylphenyl)acrylates (1f, 1g). Example: butyl (E)-3-(3-formylphenyl)acrylate (1f).

N-butyl acrylate (10.6 mmol, 1 eq, 1.55 mL), $NaHCO_3$ (21.6 mmol, 2 eq, 1.82 g), Triethylamine (24.3 mmol, 2.25 eq, 2.461 g), triphenylphosphine (0.324 mmol, 0.03 eq, 0.073 g) and palladium (II) acetate (0.541 mmol, 0.05 eq, 0.142 g) were added to a solution of 3-bromobenzaldehyde (10.6 mmol, 1 eq, 1.26 mL) in dry DMF. The resulting solution was stirred at 110 °C for 3h. After the completion of the reaction, the solution was quenched with H_20 (20 mL), and the product extracted with AcOEt (4 x 10 mL). The organic phase was then dried over anhydrous sodium sulfate, filtered and evaporated under reduced pressure to give a crude that was purified by silica gel column (SiO_2 eluting with ethyl acetate/*n*-hexane 1/20) to afford the desired intermediate **1f** as a white powder (1.7 g, Y= 67%).

^{1}H NMR (400MHz, $CDCl_3$) δ: 0.99 (t, 3H, -$CH_2CH_2CH_2CH_3$), 1.47 (m, 2H, -$CH_2CH_2CH_2CH_3$), 1.72 (q, 2H, -$CH_2CH_2CH_2CH_3$), 4.25 (t, 2H, -$CH_2CH_2CH_2CH_3$), 6.56 (d, 1H, d, -ArCH=C*H*)**,** 7.59 (t, 1H, aromatic proton), 7.72 (m, 1H, aromatic proton), 7.79 (t, 1H, aromatic proton), 7.91 (d, 1H, -ArC*H*=CH), 8.05 (s, 1H, aromatic proton), 10.1 (s, 1H, -C*H*O) ppm.

General procedure for the synthesis of the tert-butyl 1-(3-(8-methoxy-8-oxooctanamido)phenyl)-1H-pyrazole/pyrrole-carboxylates (2h, 2a-c). Example: tert-butyl 1-(3-(8-methoxy-8-oxooctanamido)phenyl)-2,5-dimethyl-1H-pyrrole-3-carboxylate (2c).

Triethylamine (2.6 mmol, 2.5 eq, 0.36 mL) and methyl 8-chloro-8-oxooctanoate (2.09 mmol, 2.0 eq, 0.3 mL) were added to a solution of *tert*-butyl 1-(3-aminophenyl)-2,5-dimethyl-1*H*-pyrrole-3-carboxylate **1m** (1.05 mmol, 1.0 eq, 300 mg) in dry dichloromethane (7 mL). The resulting mixture was stirred for 3h at room temperature. After this time, the reaction was considered complete according to the TLC analysis, therefore, the reaction was quenched with water (15 mL) and extracted with dichloromethane (3×10 mL). The combined organic layers were washed with a saturated solution of sodium carbonate (3×10 mL), a 2N aqueous solution of HCl (3×10 mL), brine (3×10 mL) and at last dried with sodium sulfate. The crude residue obtained after the evaporation of the solvent *in vacuo* was purified by column chromatography (SiO_2 eluting with ethyl acetate/*n*-hexane 1/2) to give the pure **2c** intermediate that was a dense yellow liquid. (436.7 mg; Y= 91.4 %).

^{1}H NMR (400 MHz, $CDCl_3$) δ: 1.40 (m, 4H, CH_2CH_2), 1.58 (s, 9H, COOC(CH_3)$_3$), 1.66 (m, 2H, CH_2), 1.76 (m, 2H, CH_2) 1.99 (s, 3H, pyrrole CH_3), 2.28 (s, 3H, pyrrole CH_3), 2.34 (t, 2H, CH_2), 2.40 (t, 2H, t, CH_2), 3.68 (s, 3H, COOCH_3), 6.32 (s, 1H, pyrrole proton), 6.91 (d, 1H, aromatic proton), 7.43 (m, 2H, aromatic protons), 7.49 (s, 1H, CON*H*), 7.63 (d, 1H, aromatic proton) ppm.

General procedure for the synthesis of tert-butyl (E)-1-(3-(benzyl)amino)phenyl)-2,5-dimethyl-1H-pyrrole-3-carboxylates (2d-g). Example: tert-butyl (E)-1-(3-((3-(3-methoxy-3-oxoprop-1-en-1-yl)benzyl)amino)phenyl)-2,5-dimethyl-1H-pyrrole-3-carboxylate (2d).

To a mixture of tert-butyl 1-(3-aminophenyl)-2,5-dimethyl-1H-pyrrole-3-carboxylate (**1m**) (1 eq, 0.400 g, 1.40 mmol) in anhydrous dichloroethane were added methyl 3-formylbenzoate (1.2 eq, 0.275 g, 1.68 mmol) and sodium triacetoxyborohydride (2 eq, 0.593 g, 2.8 mmol). The reaction was stirred for 5h at room temperature. After this time, TLC analysis showed complete conversion of the starting material, the reaction was subsequently quenched with H_20 (15 mL) and extracted with chloroform (3×10 mL). The combined organic phases were washed with brine (3×10 mL), dried with sodium sulfate, filtered and evaporated under reduced pressure to obtain a crude product that was purified by column chromatography (SiO_2 eluting with *n*-Hexane/ethyl acetate 6/1) to give the pure **2d** intermediate (490 mg, 80.5%).

^{1}H NMR (400MHz, $CDCl_3$) δ: 1.48 (s, 9H, -COO(C*H*$_3$)$_3$), 1.85 (s, 3H, -COOC*H*$_3$) 2.16 (s, 3H, s, -CH_3 pyrrole), 3.84 (s, 3H, -CH_3 pyrrole), 4.24 (t, 1H, -N*H*CH_2Ph), 4.32 (d, 2H, -C*H*$_2$Ph), 6.20 (m, 1H, pyrrole proton), 6.27 (m, 1H, aromatic proton), 6.42 (m, 1H, aromatic proton), 6.62 (m, 1H, aromatic proton), 7.16 (m, 1H, aromatic proton), 7.35 (m, 1H, aromatic proton), 7.48 (m, 1H, aromatic proton), 7.88 (m, 1H, aromatic proton), 7.96 (m, 1H, aromatic proton) ppm.

General procedure for the synthesis of the 1-(3-(8-methoxy-8-oxooctanamido)phenyl)-1H-pyrazole/pyrrole-4-carboxylic acids (3h, 3a-c). Example: 1-(3-(8-methoxy-8-oxooctanamido)phenyl)-5-methyl-1H-pyrazole-4-carboxylic acid (3h).

The *tert*-butyl 1-(3-(8-methoxy-8-oxooctanamido)phenyl)-5-methyl-1*H*-pyrazole-4-carboxylate **2h** (0.753 mmol, 1.0 eq, 0.334 g) was dissolved in dry dichloromethane (5 mL) and cooled to 0 °C. Trifluoroacetic acid (3.76 mmol 5.0 eq, 0.288 mL) was added slowly, and the resulting solution was first stirred at 0 °C for 10 minutes and then let warm to room temperature. The reaction was monitored, and other little addictions of trifluoroacetic acid have been made at 0 °C (15 eq were added overall). When TLC analysis showed the complete conversion of the starting material, the reaction was quenched with water (15 mL) and extracted by dichloromethane (3×10 mL). The combined organic phases were washed with brine (3×10 mL), dried with sodium sulfate, filtered and evaporated under reduced pressure. Trituration in petroleum ether allowed to obtain the pure acid **3h**. (225 mg; Y= 77 %)

Mp = 127 °C.

^{1}H NMR (400 MHz, d6-DMSO) δ: 1.30 (m, 4H, C*H*$_2$C*H*$_2$), 1.56 (m, 4H, C*H*$_2$C*H*$_2$), 2.32 (m, 4H, C*H*$_2$C*H*$_2$), 2.51 (s, 3H, pyrazole C*H*$_3$), 3.63 (s, 3H, COOC*H*$_3$), 7.19 (d, 1H, aromatic proton), 7.46 (t, 1H, t, aromatic proton), 7.62 (d, 1H, aromatic proton), 7.87 (s, 1H, pyrazole proton), 7.96 (s, 1H, aromatic proton), 10.14 (s, 1H, CON*H*), 12.44 (bs, 1H, COO*H*) ppm.

General procedure for the synthesis of the methyl 8-((3-(((4,6-dimethyl-2-oxo-1,2-dihydropyridin-3-yl)mthyl)carbamoyl)-1H-pyrazole/pyrrole-1-yl-phenyl)amino)-8-oxooctanates (4h, 4a-c). Example:

methyl 8-((3-(3-(((4,6-dimethyl-2-oxo-1,2-dihydropyridin-3-yl)methyl)carbamoyl)-2,5-dimethyl-1H-pyrrol-1-yl)phenyl)amino)-8-oxooctanoate (4c).

The 1-(3-(8-methoxy-8-oxooctanamido)phenyl)-2,5-dimethyl-1*H*-pyrrole-3-carboxylic acid **3c** (0.580 mmol, 1.0 eq, 0.232 g) was dissolved in dry *N*,*N*-dimethylformamide (5 mL). Triethylamine (4.05 mmol, 7.0 eq, 0.57 mL) and 2-(1*H*-Benzotriazole-1-yl)-1,1,3,3-tetramethylaminium tetrafluoroborate (TBTU Reagent) (0.695 mmol, 1.2 eq, 0.223 g) were added under nitrogen atmosphere and the mixture was stirred for 40 minutes. After this time TLC analysis showed a complete conversion of the acid **2f** in the activated form, thus the (4,6-dimethyl-2-oxo-1,2-dihydropyridin-3-yl)methanaminium chloride **3a** (0.638 mmol, 1.1 eq, 0.120 g) was added under nitrogen atmosphere. The resulting solution was stirred at room temperature overnight. The day after, the reaction was considered complete according to the TLC analysis, therefore, the reaction was quenched with brine (10 mL), and the precipitated white solid was filtered, dried in an oven at 60°C and at least purified by column chromatography (SiO_2 eluting with chloroform/methanol 30/1) to give the pure intermediate **4c**. (220.6 mg; Y= 71 %).

Mp = 167 °C.

^{1}H NMR (400MHz, $CDCl_3$)δ: 1.31 (m, 4H, CH_2CH_2), 1.63 (m, 4H, CH_2CH_2), 2.16 (s, 3H, pyrrole CH_3), 2.21 (s, 3H, pyrrole CH_3), 2.22-2.35 (m, 10 H), 3.59 (s, 3H, COOCH_3), 4.42 (s, 1H, CONHCH_2), 5.83 (s, 1H, pyridone C*H*), 5.99 (s, 1H, pyrrole proton), 6.77 (d, 1H, d, aromatic proton), 7.08 (m, 1H, aromatic proton), 7.15 (s, 1H, CON*H*), 7.31 (t, 1H, t, aromatic proton), 7.65 (d, 1H, aromatic proton), 7.85 (s, 1H, CONH), 11.21 (s, 1H, N*H* pyridone) ppm.

General procedure for the synthesis of the 8-((3-(((4,6-dimethyl-2-oxo-1,2-dihydropyridin-3-yl)methyl)carbamoyl)-1H-pyrazole/pyrrole-1-yl-phenyl)amino)-8-oxooctanoic acids (5h, 5a-c). Example: 8-((3-(4-(((4,6-dimethyl-2-oxo-1,2-dihydropyridin-3-yl)methyl)carbamoyl)-5-methyl-1H-pyrazol-1-yl)phenyl)amino)-8-oxooctanoic acid (5h).

A solution of lithium hydroxide monohydrate (0.399 mmol, 2.0 eq, 0.0167 g) in water (3 mL) was added to a solution of methyl 8-((3-(4-(((4,6-dimethyl-2-oxo-1,2-dihydropyridin-3-yl)methyl)carbamoyl)-5-methyl-1*H*-pyrazol-1-yl)phenyl)amino)-8-oxooctanoate **4h** (0.199 mmol, 1.0 eq, 0.104 g) in tetrahydrofuran (3 mL). The resulting mixture was stirred at room temperature overnight. The day after the reaction was judged complete by TLC analysis. The tetrahydrofuran was evaporated *in vacuo* and the HCl 2N aqueous solution was added dropwise at 0 °C until pH 1.0. The white solid product **5h** precipitated was filtered and dried in oven. (0.0506 g; Y= 50.1 %)

Mp = 143 °C.

^{1}H NMR (400MHz, d_6-DMSO) δ: 1.24 (m, 4H, CH_2CH_2), 1.50 (m, 2H, CH_2), 1.59 (m, 2H, CH_2), 2.12 (s, 3H, pyrazole CH_3), 2.32 (t, 2H, CH_2), 2.51 (m, 8H), 4.27 (d, 2H, CH_2), 5.87 (s, 1H, pyridine C*H*), 7.15 (d, 1H, aromatic proton), 7.44 (t, 1H, aromatic proton), 7.60 (d, 1H, aromatic proton), 7.83 (s, 1H, pyrazole proton), 7.97 (m, 1H, aromatic proton), 8.11 (s, 1H, CON*H*CH_2), 10.11 (s, 1H, CON*H*), 11.93 (m, 2H, COO*H*), 12.80 (s, 1H, pyridine N*H*) ppm.

General procedure for the synthesis of the finals compounds N^1-(3-(((4,6-dimethyl-2-oxo-1,2-dihydropyridin-3-yl)methyl)carbamoyl)-1H-pyrazole/pyrrole-1-yl-phenyl)-N^8-hydroxyoctanediamides (8h, 8a-c). Example: N^1-(3-(3-(((4,6-dimethyl-2-oxo-1,2-dihydropyridin-3-yl)methyl)carbamoyl)-2,5-dimethyl-1H-pyrrol-1-yl)phenyl)-N^8-hydroxyoctanediamide (MC4128, 8c).

The 8-((3-(3-(((4,6-dimethyl-2-oxo-1,2-dihydropyridin-3-yl)methyl)carbamoyl)-2,5-dimethyl-1H-pyrrol-1-yl)phenyl)amino)-8-oxooctanoic acid **5c** (0.40 mmol, 1.0 eq, 0.203 g) was dissolved in dry *N*,*N*-dimethylformamide (3 mL). Triethylamine (1.60 mmol, 4.0 eq, 0.22 mL) and 2-(1*H*-Benzotriazole-1-yl)-1,1,3,3-tetramethylaminium tetrafluoroborate (TBTU Reagent) (0.481 mmol, 1.2 eq, 0.154 g) were added under nitrogen atmosphere and the mixture was stirred for 40 minutes. After this time TLC analysis showed a complete conversion of the acid **5c** into the activated form, thus the O-(tetrahydro-2*H*-pyran-2-yl)hydroxylamine (1.20 mmol, 3.0 eq, 0.141 g) was added under nitrogen atmosphere. The resulting solution was stirred at room temperature for 1h. After this time the reaction was considered complete by TLC analysis thus brine (10 mL) was added to the reaction mixture and the white solid of the protect hydroxamate precipitated (**7c**). The solid was filtered, dried in an oven at 60°C and purified by column chromatography (SiO_2 eluting with chloroform/methanol 20/1) to give pure protected hydroxamate. The pure product obtained (1.0 eq, 0.203 g, 0.343 mmol) was dissolved in tetrahydrofuran (3 mL), and the 4M hydrogen chloride solution in dioxane (1.71 mmol, 5.0 eq, 0.43 mL) was added at 0 °C, and the precipitation of a white solid was immediately observed. The resulting mixture was stirred at room temperature, and the reaction was monitored. Other little addictions of the 4M hydrogen chloride solution in dioxane have been made at 0 °C (10 eq added overall). When TLC analysis showed the complete conversion of the starting material, diethyl ether was added, and the solid of the final hydroxamate N^1-(3-(3-(((4,6-dimethyl-2-oxo-1,2-dihydropyridin-3-yl)methyl)carbamoyl)-2,5-dimethyl-*1H*-pyrrol-1-yl)phenyl)-N^8-hydroxyoctanediamide **8c** was filtered and dried in an oven at 60°C. (66 mg; Y= 36 %).

Mp = 171 °C.

^{1}H NMR (400MHz, d_6-DMSO) δ: 1.28 (m, 4H, -CH_2CH_2), 1.49 (m, 2H, CH_2), 1.57 (m, 2H, CH_2), 1.92 (s, 3H, pyrrole CH_3), 1.95 (m, 2H, CH_2), 2.19 (s, 3H, pyrrole CH_3), 2.21 (s, 3H, pyridine CH_3), 2.27 (s, 3H, pyridine CH_3) 2.32 (t, 2H, CH_2), 3.57 (s, 1H, CON*H*CH_2 pyridine), 4.27 (s, 2H, CONHCH_2), 6.10 (s, 1H, pyrrole aromatic proton), 6.34 (s, 1H, pyridine C*H*), 6.93 (d, 1H, aromatic proton), 7.45 (t, 1H, aromatic proton), 7.60 (t, 2H, aromatic protons), 7.90 (bs, 1H, NHO*H*), 10.14 (s, 1H, CON*H*), 10.34 (s, 1H, N*H*OH), 12.11 (s, 1H, pyridine N*H*) ppm. MS (EI): *m/z* $[M]^+$: 535.28.

General procedure for the synthesis of the finals compounds (E)-1-(3-((4-(3-((2-aminophenyl)amino)-3-oxoalken-1-yl)benzyl)amino)phenyl)-N-((4,6-dimethyl-2-oxo-1,2-dihydropyridin-3-yl)methyl)-2,5-dimethyl-1H-pyrrole-3-carboxamides (6d-g). Example: (E)-1-(3-((4-(3-((2-aminophenyl)amino)-3-oxoprop-1-en-1-yl)benzyl)amino)phenyl)-N-((4,6-dimethyl-2-oxo-1,2-dihydropyridin-3-yl)methyl)-2,5-dimethyl-1H-pyrrole-3-carboxamide (MC4227, 6e).

To a solution of (E)-3-(4-(((3-(3-(((4,6-dimethyl-2-oxo-1,2-dihydropyridin-3-yl)methyl)carbamoyl)-2,5-dimethyl-1H-pyrrol-1-yl)phenyl)amino)methyl)phenyl)acrylic acid (**5e**) (1 eq, 0.060 g, 0.000120 mol) in dry *N*,*N*-dimethylformamide (3mL) were added, under nitrogen atmosphere, Triethylamine (4 eq, 0.067 mL, 0.000481 mol) and 2-(1*H*-Benzotriazole-1-yl)-1,1,3,3-tetramethylaminium tetrafluoroborate (TBTU Reagent; 1.2 eq, 0.0464 g, 0.000144 mol) and the reaction was kept under stirring for 20 min. After this time, *o*-phenylendiamine (1.5 eq, 0.0195 g, 0.000181 mol) was added to the reaction mixture which was allowed to cool at room temperature for 2h. The reaction was quenched with saturated NaCl (10 mL) and a white solid precipitate was observed. The crude product was filtered and evaporated to dryness under reduced pressure and purified by column chromatography (SiO_2 eluting with chloroform/methanol 22/1) to afford the pure final compound **6e**. (Y=42%).

^{1}H NMR (400MHz, d_6-DMSO) δ: 1.43 (s, 3H, pyrrole CH_3), 2.11 (s, 3H, pyrrole CH_3), 2.14 (s, 3H, pyridine CH_3), 2.17 (s, 3H, pyridine CH_3), 4.20-4.22 (d, 2H, -CH_2NHPh), 4.38-4.39 (d, 2H, -CH_2NHCO), 4.89 (s, 2H, -NH_2), 5.85 (s, 1H, -C*H* pyridine), 6.21 (s, 1H, pyrrole proton), 6.33-6.36 (m, 2H, aromatic protons), 6.58-6.62 (m, 2H, aromatic protons), 6.77-6.79 (d, 1H, aromatic proton), 6.95-6.99 (t, 1H, -N*H*CH_2Ph), 7.15-7.21 (m, 2H, aromatic protons), 7.36-7.39 (m, 1H, aromatic proton), 7.47-7.49 (d, 2H, aromatic protons), 7.93-7.95 (d, 2H, aromatic protons), 9.62 (s, 1H, -N*HCO*), 11.46 (s, 1H, -N*H*CO) ppm. MS (EI): *m/z* $[M]^+$: 588.28.

^{1}H-NMR and mass spectra of final compounds:

N^1-(3-(3-(((4,6-dimethyl-2-oxo-1,2-dihydropyridin-3-yl)methyl)carbamoyl)-2,5-dimethyl-1H-pyrrol-1-yl)phenyl)-N6-hydroxyadipamide (MC4255, 8a)

^{1}H NMR (400MHz, d_6-DMSO) δ: 1.54 (m, 4H, -CH_2CH_2), 1.93 (s, 3H, pyrrole CH_3), 1.96-1.99 (t, 2H, CH_2), 2.16 (s, 3H, pyrrole CH_3), 2.19 (s, 3H, pyridine CH_3), 2.27 (s, 3H, pyridine CH_3), 2.31-2.33 (s, 2H, -CH_2), 4.27 (s, 2H, -CH_2NHCO), 6.11 (s, 1H, -C*H* pyridine), 6.34 (s, 1H, pyrrole proton), 6.92-6.94 (d, 1H, aromatic proton), 7.44-7.48 (t, 1H, aromatic proton), 7.58-7.62 (t, 2H, aromatic protons), 7.85-7.90 (bs, 1H, -NHO*H*), 10.16 (s, 1H, CON*H*), 10.37 (s, 1H, -N*H*OH), 12.11-12-13 (s, 1H, pyridine N*H*) ppm. MS (EI): *m/z* $[M]^+$: 507.25.

N^1-(2-aminophenyl)-N6-(3-(3-(((4,6-dimethyl-2-oxo-1,2-dihydropyridin-3-yl)methyl)carbamoyl)-2,5-dimethyl-1H-pyrrol-1-yl)phenyl)adipamide (MC4256, 6a)

^{1}H NMR (400MHz, d_6-DMSO) δ: 0.83-0.87 (t, 2H, -CH_2CH_2), 1.25 (m, 2H, CH_2), 1.64 (m, 4H, -CH_2C$H_2$$CH_2$), 1.92 (s, 3H, pyrrole CH_3), 2.09 (s, 3H, pyridine CH_3), 2.18 (s, 3H, pyridine CH_3), 2.20 (s, 3H, pyridine CH_3), 4.22-4.23 (d, 2H, -CH_2NHCO), 4.82 (s, 2H, -NH_2), 5.86 (s, 1H, -C*H* pyridine), 6.29 (s, 1H, pyrrole proton), 6.51-6.55 (t, 1H, -CH_2N*H*CO), 6.70-6.72 (d, 1H, aromatic proton), 6.87-6.93 (dd, 2H, aromatic protons), 7.14-7.16 (d, 1H, aromatic proton), 7.43-7.45 (m, 2H, aromatic protons), 7.56 (m, 1H, aromatic proton),

7.61-7.63 (m, 1H, aromatic proton), 9.11 (s, 1H, -N*HCO*), 10.13 (s, 1H, -CON*H*), 11.42-11.46 (s, 1H, -N*H*CO) ppm. MS (EI): *m/z* $[M]^+$: 582.30.

N^1-(3-(3-(((4,6-dimethyl-2-oxo-1,2-dihydropyridin-3-yl)methyl)carbamoyl)-2,5-dimethyl-1H-pyrrol-1-yl)phenyl)-N7-hydroxyheptanediamide (MC4243, 8b)

^{1}H NMR (400MHz, d_6-DMSO) δ: 1.24-1.31 (m, 2H, -CH_2), 1.47-1.53 (m, 2H, -CH_2), 1.56-1.61 (m, 2H, -CH_2), 1.92 (s, 3H, pyrrole CH_3), 1.97-1.95 (t, 2H, -CH_2), 2.19 (s, 3H, pyrrole CH_3), 2.21 (s, 3H, pyridine CH_3), 2.27 (s, 3H, pyridine CH_3), 3.00-3.34 (t, 2H, -CH_2), 4.27 (s, 2H, -CH_2NHCO), 6.12 (s, 1H, -C*H* pyridine), 6.35 (s, 1H, pyrrole proton), 6.92-6.94 (d, 1H, aromatic proton), 7.43-7.47 (t, 1H, aromatic proton), 7.58-7.62 (t, 2H, aromatic protons), 8.04 (bs, 1H, -NHO*H*), 10.01 (s, 1H, CON*H*), 10.44 (s, 1H, -N*H*OH), 12.13-12-16 (s, 1H, pyridine N*H*) ppm. MS (EI): *m/z* $[M]^+$: 521.26.

N^1-(2-aminophenyl)-N7-(3-(3-(((4,6-dimethyl-2-oxo-1,2-dihydropyridin-3-yl)methyl)carbamoyl)-2,5-dimethyl-1H-pyrrol-1-yl)phenyl)heptanediamide (MC4240, 6b)

^{1}H NMR (400MHz, d_6-DMSO) δ: 1.36-1.38 (m, 2H, -CH_2CH$_2$), 1.63 (m, 4H, -CH_2CH_2), 1.92 (s, 3H, pyrrole CH_3), 2.12 (s, 3H, pyridine CH_3), 2.18 (s, 3H, pyridine CH_3), 2.20 (s, 3H, pyridine CH_3), 2.31-2.34 (m, 4H, -CH$_2$CH_2CH$_2$), 4.22-4.23 (d, 2H, -CH_2NHCO), 4.81 (s, 2H, -NH_2), 5.86 (s, 1H, -C*H* pyridine), 6.29 (s, 1H, pyrrole proton), 6.50-6.53 (t, 1H, -CH$_2$N*H*CO), 6.70-6.72 (d, 1H, aromatic proton), 6.86-6.88 (dd, 2H, aromatic protons), 7.13-7.15 (d, 1H, aromatic proton), 7.45-7.56 (m, 2H, aromatic protons), 7.60-7.62 (m, 2H, aromatic protons), 9.09 (s, 1H, -N*HCO*), 10.11 (s, 1H, -CON*H*), 11.47 (s, 1H, -N*H*CO) ppm. MS (EI): *m/z* $[M]^+$: 596.31.

N^1-(3-(3-(((4,6-dimethyl-2-oxo-1,2-dihydropyridin-3-yl)methyl)carbamoyl)-2,5-dimethyl-1H-pyrrol-1-yl)phenyl)-N^8-hydroxyoctanediamide (MC4128, 8c)

^{1}H NMR (400MHz, d_6-DMSO) δ: 1.28 (m, 4H, -CH_2CH_2), 1.49 (m, 2H, CH_2), 1.57 (m, 2H, CH_2), 1.92 (s, 3H, pyrrole CH_3), 1.95 (m, 2H, CH_2), 2.19 (s, 3H, pyrrole CH_3), 2.21 (s, 3H, pyridine CH_3), 2.27 (s, 3H, pyridine CH_3) 2.32 (t, 2H, CH_2), 3.57 (s, 1H, CON*H*CH$_2$ pyridine), 4.27 (s, 2H, CONHCH_2), 6.10 (s, 1H, pyrrole aromatic proton), 6.34 (s, 1H, pyridine C*H*), 6.93 (d, 1H, aromatic proton), 7.45 (t, 1H, aromatic proton), 7.60 (t, 2H, aromatic protons), 7.90 (bs, 1H, NHO*H*), 10.14 (s, 1H, CON*H*), 10.34 (s, 1H, N*H*OH), 12.11 (s, 1H, pyridine N*H*) ppm. MS (EI): *m/z* $[M]^+$: 535.28.

N^1-(2-aminophenyl)-N8-(3-(3-(((4,6-dimethyl-2-oxo-1,2-dihydropyridin-3-yl)methyl)carbamoyl)-2,5-dimethyl-1H-pyrrol-1-yl)phenyl)octanediamide (MC4213, 6c)

^{1}H NMR (400MHz, d_6-DMSO) δ: 1.35 (m, 4H, -CH_2CH_2), 1.60 (m, 4H, -CH_2CH_2), 1.92 (s, 3H, pyrrole CH_3), 2.12 (s, 3H, pyridine CH_3), 2.18 (s, 3H, pyridine CH_3), 2.20 (s, 3H, pyridine CH_3), 2.29-2.31 (q, 4H, -CH$_2$CH_2CH$_2$), 4.22-4.24 (d, 2H, -CH_2NHCO), 4.80 (s, 2H, -NH_2), 5.86 (s, 1H, -C*H* pyridine), 6.29 (s, 1H,

pyrrole proton), 6.51-6.55 (t, 1H, -CH_2N*H*CO), 6.70-6.72 (d, 1H, aromatic proton), 6.87-6.88 (d, 2H, aromatic protons), 6.91-6.93 (d, 2H, aromatic protons), 7.14-7.15 (d, 1H, aromatic proton), 7.43-7.47 (m, 2H, aromatic protons), 7.55 (s, 1H, aromatic proton), 7.60-7.62 (d, 1H aromatic proton), 9.08 (s, 1H, -N*HCO*), 10.10 (s, 1H, -CON*H*), 11.46 (s, 1H, -N*H*CO) ppm. MS (EI): *m/z* $[M]^+$: 610.33.

N-((4,6-dimethyl-2-oxo-1,2-dihydropyridin-3-yl)methyl)-1-(3-((3 (hydroxycarbamoyl)benzyl)amino)phenyl)-2,5-dimethyl-1H-pyrrole-3-carboxamide (MC4257, 8d)

^{1}H NMR (400MHz, d_6-DMSO) δ: 1.82 (s, 3H, pyrrole CH_3), 2.12 (s, 3H, pyrrole CH_3), 2.18 (s, 3H, pyridine CH_3), 2.25 (s, 3H, pyridine CH_3), 4.25 (s, 2H, - CH_2NHPh), 4.33 (s, 2H, -CH_2NHCO), 6.08 (s, 1H, pyridine -C*H*), 6.25 (s, 1H, pyrrole aromatic proton), 6.27-6.30 (s, 1H, aromatic proton), 6.34-6.36 (d, 1H, aromatic proton), 6.71-6.73 (d, 1H, aromatic proton), 7.17-7.21 (t, 1H, aromatic proton), 7.37-7.41 (t, 1H, aromatic proton), 7.48-7.50 (d, 1H, aromatic proton), 7.59-7.61 (d, 1H, aromatic proton), 7.78 (bs, 2H, NHO*H* and aromatic proton), 11.19 (s, 1H, N*H*OH), 12.03 (s, 1H, pyridine N*H*) ppm. MS (EI): *m/z* $[M]^+$: 513.24.

1-(3-((3-((2-aminophenyl)carbamoyl)benzyl)amino)phenyl)-N-((4,6-dimethyl-2-oxo-1,2-dihydropyridin-3-yl)methyl)-2,5-dimethyl-1H-pyrrole-3-carboxamide (MC4258, 6d)

^{1}H NMR (400MHz, d_6-DMSO) δ: 1.83 (s, 3H, pyrrole CH_3), 2.11 (s, 3H, pyrrole CH_3), 2.13 (s, 3H, pyridine CH_3), 2.17 (s, 3H, pyridine CH_3), 4.20-4.22 (d, 2H, -CH_2NHPh), 4.37-4.38 (d, 2H, -CH_2NHCO), 4.87 (s, 2H, -NH_2), 5.85 (s, 1H, -C*H* pyridine), 6.20 (s, 1H, pyrrole proton), 6.32 (t, 1H, aromatic proton), 6.34-6.36 (m, 1H, aromatic proton), 6.58-6.66 (m, 2H, aromatic protons), 6.72-6.74 (d, 1H, aromatic proton), 6.78-6.80 (d, 1H, aromatic proton), 6.96-7.00 (t, 1H, -N*H*CH_2Ph), 7.15-7.21 (m, 2H, aromatic protons), 7.35-7.37 (m, 1H, aromatic proton), 7.44-7.48 (t, 1H, -CON*H*CH_2), 7.54-7.56 (d, 1H, aromatic proton), 7.85-7.87 (d, 1H aromatic proton), 7.98 (s, 1H, aromatic proton), 9.67 (s, 1H, -N*HCO*), 11.45 (s, 1H, -N*H*CO) ppm. MS (EI): *m/z* $[M]^+$: 588.28.

N-((4,6-dimethyl-2-oxo-1,2-dihydropyridin-3-yl)methyl)-1-(3-((4-(hydroxycarbamoyl)benzyl)amino)phenyl)-2,5-dimethyl-1H-pyrrole-3-carboxamide (MC4229, 8e)

^{1}H NMR (400MHz, d_6-DMSO) δ: 1.76 (s, 3H, pyrrole CH_3), 2.11 (s, 3H, pyrrole CH_3), 2.23 (s, 3H, pyridine CH_3), 2.31 (s, 3H, pyridine CH_3), 4.27 (s, 2H, - CH_2NHPh), 4.35 (s, 2H, -CH_2NHCO), 6.25 (s, 1H, pyridine -C*H*), 6.30 (s, 1H, pyrrole proton), 6.35 (s, 1H, aromatic proton), 6.43-6.46 (s, 1H, aromatic proton), 6.71-6.76 (d, 1H, aromatic proton), 7.18-7.21 (m, 1H, aromatic proton), 7.40-7.42 (d, 1H, aromatic proton), 7.70-7.72 (d, 1H, aromatic proton), 8.14-8.16 (bs, 1H, NHO*H*), 11.54 (s, 1H, N*H*OH) ppm. MS (EI): *m/z* $[M]^+$: 513.24.

1-(3-((4-((2-aminophenyl)carbamoyl)benzyl)amino)phenyl)-N-((4,6-dimethyl-2-oxo-1,2-dihydropyridin-3-yl)methyl)-2,5-dimethyl-1H-pyrrole-3-carboxamide (MC4227, 6e)

^{1}H NMR (400MHz, d_6-DMSO) δ: 1.43 (s, 3H, pyrrole CH_3), 2.11 (s, 3H, pyrrole CH_3), 2.14 (s, 3H, pyridine CH_3), 2.17 (s, 3H, pyridine CH_3), 4.20-4.22 (d, 2H, -CH_2NHPh), 4.38-4.39 (d, 2H, -CH_2NHCO), 4.89 (s, 2H, -NH_2), 5.85 (s, 1H, -C*H* pyridine), 6.21 (s, 1H, pyrrole proton), 6.33-6.36 (m, 2H, aromatic protons), 6.58-

6.62 (m, 2H, aromatic protons), 6.77-6.79 (d, 1H, aromatic proton), 6.95-6.99 (t, 1H, -N*H*CH_2Ph), 7.15-7.21 (m, 2H, aromatic protons), 7.36-7.39 (m, 1H, aromatic proton), 7.47-7.49 (d, 2H, aromatic protons), 7.93-7.95 (d, 2H, aromatic protons), 9.62 (s, 1H, -N*H*CO), 11.46 (s, 1H, -N*H*CO) ppm. MS (EI): *m/z* $[M]^+$: 588.28.

(E)-N-((4,6-dimethyl-2-oxo-1,2-dihydropyridin-3-yl)methyl)-1-(3-((3-(3-(hydroxyamino)-3-oxoprop-1-en-1-yl)benzyl)amino)phenyl)-2,5-dimethyl-1H-pyrrole-3-carboxamide (MC4242, 8f)

^{1}H NMR (400MHz, d_6-DMSO) δ: 1.76 (s, 3H, pyrrole CH_3), 2.09 (s, 3H, pyrrole CH_3), 2.12 (s, 3H, pyridine CH_3), 2.20 (s, 3H, pyridine CH_3), 4.25 (s, 2H, - CH_2NHPh), 4.32 (s, 2H, -CH_2NHCO), 6.15 (s, 1H, pyridine -C*H*), 6.27 (s, 1H, pyrrole proton), 6.30 (s, 1H, aromatic proton), 6.36-6.38 (d, 1H, aromatic proton), 6.42-6.46 (d, 1H, aromatic proton), 6.74-6.76 (d, 1H, aromatic proton), 7.19-7.23 (t, 1H, -CH_2N*H*CO), 7.36-7.54 (m, 5H, aromatic protons), 7.95 (bs, 1H, NHO*H*), 12.3 (s, 1H, N*H*OH) ppm. MS (EI): *m/z* $[M]^+$: 539.25.

(E)-1-(3-((3-(3-((2-aminophenyl)amino)-3-oxoprop-1-en-1-yl)benzyl)amino)phenyl)-N-((4,6-dimethyl-2-oxo-1,2-dihydropyridin-3-yl)methyl)-2,5-dimethyl-1H-pyrrole-3-carboxamide (MC4271, 6f)

^{1}H NMR (400MHz, d_6-DMSO) δ: 1.82 (s, 3H, pyrrole CH_3), 2.11-2.12 (s, 3H, pyrrole CH_3), 2.16 (s, 6H, pyridine CH_3), 4.20-4.21 (s, 2H, -CH_2NHPh), 4.33-4.34 (s, 2H, -CH_2NHCO), 4.96 (s, 2H, NH_2), 5.85 (s, 1H, pyridine -C*H*), 6.20 (s, 1H, pyrrole proton), 6.30 (s, 1H, aromatic proton), 6.35-6.36 (d, 1H, aromatic proton), 6.56-6.60 (m, 2H, aromatic protons), 6.73-6.76 (t, 1H, aromatic proton), 6.87-6.91 (d, 1H, -C*H*=CHCO), 6.92-6.94 (d, 1H, -CH=C*H*CO), 7.18-7.22 (t, 1H, -N*H*CH_2Ph), 7.34-7.43 (m, 4H, aromatic protons), 7.49-7.50 (m, 2H, aromatic protons), 7.61 (s, 1H, aromatic proton), 9.39 (s, 1H, -N*H*CO), 11.47 (s, 1H, -N*H*CO) ppm. MS (EI): *m/z* $[M]^+$: 614.30.

(E)-N-((4,6-dimethyl-2-oxo-1,2-dihydropyridin-3-yl)methyl)-1-(3-((4-(3-(hydroxyamino)-3-oxoprop-1-en-1-yl)benzyl)amino)phenyl)-2,5-dimethyl-1H-pyrrole-3-carboxamide (MC4230, 8g)

^{1}H NMR (400MHz, d_6-DMSO) δ: 1.82 (s, 3H, pyrrole CH_3), 2.12 (s, 3H, pyrrole CH_3), 2.25 (s, 3H, pyridine CH_3), 2.34 (s, 3H, pyridine CH_3), 4.29 (s, 2H, -C*H*=C*H*), 4.32 (s, 4H, 2x -CH_2NHCO), 6.32 (s, 3H, pyrrole proton, -N*H*CO and pyridine -C*H*), 6.37-6.39 (d, 1H, aromatic proton), 6.42-6.46 (d, 1H, aromatic proton), 6.73-6.76 (d, 1H, aromatic proton), 7.19-7.23 (t, 1H, aromatic proton), 7.37-7.44 (m, 3H, aromatic protons), 7.51-7.53 (d, 2H, aromatic protons), 8.31 (bs, 1H, NHO*H*), 12.84 (s, 1H, N*H*OH) ppm. MS (EI): *m/z* $[M]^+$: 539.25.

(E)-1-(3-((4-(3-((2-aminophenyl)amino)-3-oxoprop-1-en-1-yl)benzyl)amino)phenyl)-N-((4,6-dimethyl-2-oxo-1,2-dihydropyridin-3-yl)methyl)-2,5-dimethyl-1H-pyrrole-3-carboxamide (MC4272, 6g)

^{1}H NMR (400MHz, d_6-DMSO) δ: 1.82 (s, 3H, pyrrole CH_3), 2.09 (s, 3H, pyrrole CH_3), 2.11 (s, 3H, pyridine CH_3), 2.17 (s, 3H, pyridine CH_3), 4.20-4.21 (d, 2H, -CH_2NHPh), 4.32-4.34 (d, 2H, -CH_2NHCO), 4.96 (s, 2H, NH_2), 5.85 (s, 1H, pyridine -C*H*), 6.21 (s, 1H, pyrrole proton), 6.29 (s, 1H, aromatic proton), 6.34-6.35 (d, 1H, aromatic proton), 6.56-6.60 (t, 1H, aromatic proton), 6.63-6.65 (m, 1H, aromatic proton), 6.70-6.72 (d, 1H, -C*H*=CHCO), 6.74-6.76 (d, 1H, -CH=C*HCO*), 6.85-6.94 (m, 2H, aromatic protons), 7.17-7.21 (t, 1H, -CH_2N*H*CO), 7.33-7.38 (m, 2H, aromatic protons), 7.41-7.43 (d, 2H, aromatic protons), 7.51 (s, 1H,

aromatic proton), 7.55-7.59 (m, 2H, aromatic protons), 9.38 (s, 1H, -N*HCO*), 11.47 (s, 1H, -N*H*CO) ppm. MS (EI): *m/z* $[M]^+$: 614.30.

N^1-(3-(4-(((4,6-dimethyl-2-oxo-1,2-dihydropyridin-3-yl)methyl)carbamoyl)-5-methyl-1H-pyrazol-1-yl)phenyl)-N8-hydroxyoctanediamide (MC4134, 8h)

^{1}H NMR (400MHz, DMSO-d_6): δ1.23 (m. 4H, -CH_2CH_2), 1.38 (4H, m, CH_2CH_2), 2.27 (m, 10H, 5x -CH_2), 2.38 (s, 3H, pyrazole CH_3), 4.33 (s, 2H, CONHCH_2, CH pyridine, CONH), 5.91 (s, 1H, CONHO*H*), 7.13 (d, 1H, aromatic proton), 7.42 (t, 1H,aromatic proton), 7.68 (t, 1H, t, aromatic proton), 7.88 (s, 1H, pyrazole aromatic proton), 7.69 (m, 1H, aromatic proton), 8.11 (s, 1H, -CON*H*CH_2), 10.51 (s, 1H, -CON*H*OH), 12.80 (s, 1H, pyridine N*H*). MS (EI): *m/z* $[M]^+$: 522.26.

4.5 Methods

4.5.1 Enzymatic assays

All the new synthesised compounds **6a-g** and **8a-g** have been first screened in *in vitro* enzymatic assays to evaluate their ability to inhibit HDAC and EZH2 catalytic activity.

4.5.1.1 EZH2 inhibition assay

Compounds **6a-g** and **8a-g** have been tested against a human five component PRC2 complex, containing EZH2, EED, SUZ12, RbAp48, and AEBP2. The assay was performed using Core Histone as substrate and ^{3}H-SAM as co-substrate. SAH and GSK126 were used as reference compounds (SAH IC_{50} 34.7 μM, GSK126 IC_{50} 0.009 μM). Compounds **6a-g** and **8a-g** have been initially screened at two fixed doses (100 μM and 50 μM). Selected compounds have been further tested in a dose range (10 points) to determine their IC_{50}.

4.5.1.2 HDAC 1-6 and 8 isoforms inhibition assay

Individual IC_{50} values for each HDAC isozyme were measured with the homogeneous fluorescence-release HDAC assay. Purified recombinant enzymes were incubated with serially diluted inhibitors at the indicated concentration. The deacetylase activities of HDACs 1-11 were measured by assaying enzyme activity using AMC-K(Ac)GL substrate or AMCK(TFA)GL substrate. Deacetylated AMC-KGL was sensitive toward lysine peptidase, and free fluorogenic 4-methylcoumarin-7-amide (MCA) was generated, which can be excited at 355 nm and observed at 460 nm (Reactive Biology Corp.). The data were analysed on a plate-to-plate basis in relation to the control and imported into analytical software (GraphPad Prism).

4.5.2 Cell-based assays

4.5.2.1 Cell lines and culture conditions

U937, NB4, and THP1 human acute myeloid leukaemia cell lines, SH-N-SK neuroblastoma, ADF glioblastoma cell lines were maintained in RPMI 1640 medium contained 10% fetal bovine serum (FBS), 2mM L-glutamine and antibiotics in a humidified atmosphere with 5% CO_2 at 37°C. The experiments were performed with early (3-20) cell passages.

4.5.2.2 Cell proliferation assay

The inhibitory effect of different drugs was assessed in a panel of acute myeloid leukaemia and solid tumour cell lines following manufacturer's protocol by quantitation of the ATP present in metabolically active cells using CellTiter-Glo® Luminescent. Data were analysed by the Chou-Talaly method to determine the combination index (CI), a well-established index of the interaction between two drugs. CI values of <1, =1, and >1 indicate synergistic, additive, and antagonistic effects, respectively.

4.5.2.3 Flow cytometric analysis of cell cycle, apoptosis and cell differentiation

Flow cytometric analysis was performed to evaluate cell cycle distribution by propidium iodide (PI) staining, apoptosis by AnnexinV-FITC/PI staining, and to detect cell differentiation by analysis of CD11b expression by using a FITC-CD11b antibody (BD bioscience) as previously described. [484]

4.5.2.4 Western Blot

The effects of different drugs on protein acetylation and methylation mark were assessed by western blot analysis. Cells were lysed, and the total extracts were fractionated by SDS-PAGE, transferred to a nitrocellulose filter, and subjected to immunoblot assay, as previously described. [484] Immunodetection was done using the following antibodies Ac-H3, Hsp70/72 (Millipore), H3(me3K27) (Cell Signaling), Ac-Tubulin (K40) and β-actin (Sigma). Horseradish peroxidase-conjugated secondary antibodies binding was visualised by enhanced chemiluminescence according to manufacturer's specification and recorded on autoradiography film (Amersham Biosciences).

4.6 Biological evaluation, results and discussion

4.6.1 Enzymatic assays

Our final compounds **6a-g** and **8a-g** were tested by Reaction Biology Corporation (PA, USA) against both different HDAC isoforms (HDAC1, 2, 3, 4, 5, 6 and, 8) and EZH2 in order to assess their inhibition potency and isoform selectivity, as well. SAHA and our EZH2 lead compound MC3707 are used as reference compounds to evaluate the meaningfulness of the enzymatic data against HDAC and EZH2, respectively. These results are shown below in table 4.3.

Table 4.3: Enzymatic data of final compounds **6a-g** and **8a-g**.

CPD	LAB CODE	EZH2 (IC_{50}, µM)	HDAC isoforms (IC_{50}, µM)						
			1	2	3	4	5	6	8
8h	**MC4134**	4 % inhib. at 100 µM	0.827	2.36	1.48	NA	101	0.011	2.08
8a	**MC4255**	5.04	0.322	2.03	0.411	145	118	0.039	1.04
8b	**MC4243**	4.57	0.291	0.722	0.212	27.6	4.08	0.004	0.049
8c	**MC4128**	7.37	0.431	1.33	0.454	36.8	16.6	0.005	0.110
6a	**MC4256**	2.01	42.3	18.8	0.925	NA	NA	75.8	NA
6b	**MC4240**	3.30	0.761	2.19	0.622	NA	NA	194	NA
6c	**MC4213**	4.53	31.3	9.10	2.01	NA	NA	NA	26.9
8d	**MC4257**	2.38	98.2	168	128	170	115	5.16	0.795
8e	**MC4229**	3.30	15.4	33.1	16.1	18.8	35.2	0.034	1.20
6d	**MC4258**	4.06	NA	NA	157	NA	NA	NA	NA
6e	**MC4227**	5.25	0.083	0.325	2.02	NA	NA	113	8.13
8f	**MC4242**	1.70	3.76	8.17	4.92	33.1	29.6	0.208	0.797
8g	**MC4230**	2.18	2.46	9.70	2.68	89.3	31.1	0.040	1.03

6f	**MC4271**	ND	NA	169.0	195.0	652.4	NA	NA	389.3
6g	**MC4272**	ND	229.1	99.4	NA	336.5	NA	NA	203.5
-	**MC3707**	5.78							
-	**SAHA**	-	0.068	0.164	0.048	0.101	18.0	0.090	0.152
The values reported in red colour indicate the most interesting results.									

In the biochemical screening, all the compounds showed a comparable inhibition potency against EZH2 (2 μM < IC_{50} < 7 μM), while the inhibition activity on HDAC isoforms 1-6 and 8 proved an interesting isoform selectivity. In particular, the hydroxamic acids **8b** (**MC4243**) and **8c** (**MC4128**) showed a strong selectivity and single-digit nanomolar potency for HDAC6 (IC_{50} = 3.7 nM and IC_{50} = 5.4 nM, respectively) while still able to inhibit EZH2 (IC_{50} = 4.57 μM and IC_{50} = 7.37 μM, respectively). Among the *ortho*-amino anilides, the most potent compound was **6e** (**MC4227**) displaying an IC_{50} of 83 nM against HDAC1, whereas compound **6a** (**MC4256**) displayed the best inhibition value towards HDAC3 (IC_{50} = 0.925 μM).
By contrast, the *ortho*-amino anilides **6f** (**MC4271**) and **6g** (**MC4272**) displayed no inhibition potency against HDACs, while their EZH2 inhibitory activity is still under biochemical evaluation. Overall, the *ortho*-amino anilides follow the inhibition trend of the prototypes Entinostat and Mocetinostat against class I HDAC (HDAC1, 2 and 3), whereas the corresponding hydroxamates show higher isoform selectivity towards HDAC6 and HDAC8.

4.6.2 Cell viability assay

So far, only compound **8c** (**MC4128**), which displayed the most interesting biochemical profile, was subjected to cellular assays, performed by our collaborator Dr. Daniela Trisciuoglio from Sapienza, University of Rome, in order to test its ability to decrease the cell viability of U-937 cancer cell lines. U-937 are monoblastic leukemic cells that under the maturational influence, increase in size, acquire a lobated nucleus, and its cytoplasmic granules are replaced by vacuoles, mimicking the monoblast to monocyte transformation. U-937 cells were isolated for the first time from a previously healthy 37 year old man with a generalised lymphoma. [485] Below, the graphic representation in Fig. 4.4 shows the cell viability for the pharmacological combination between SAHA and the EZH2i MC3707 (ratio: 1:100, 48h), while Fig. 4.5 shows the effect of HDAC/EZH2 dual inhibitor **8c** (**MC4128**) on cell viability, calculated at 48, 72 and 96 hours and at different drug concentrations in U-937 AML cells (5, 10 and 25 μM).

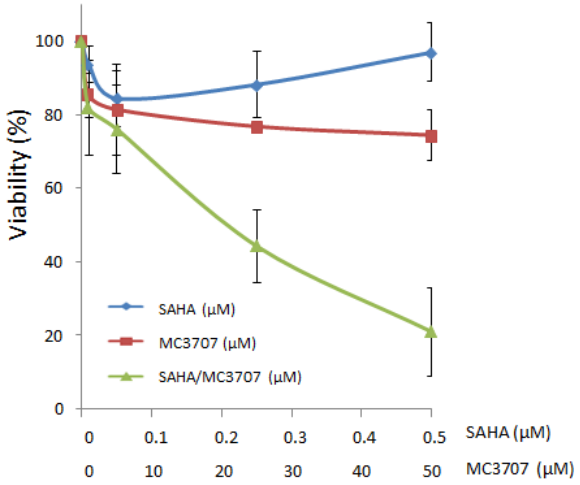

Combination index values at		
ED50	ED75	ED90
0.00031	2.4725e-006	2.7184e-008

Figure 4.4: Graphic representation for the effect of pharmacological combination between SAHA and the EZH2i MC3707 (ratio: 1:100, 48h) on U-937 cell viability.

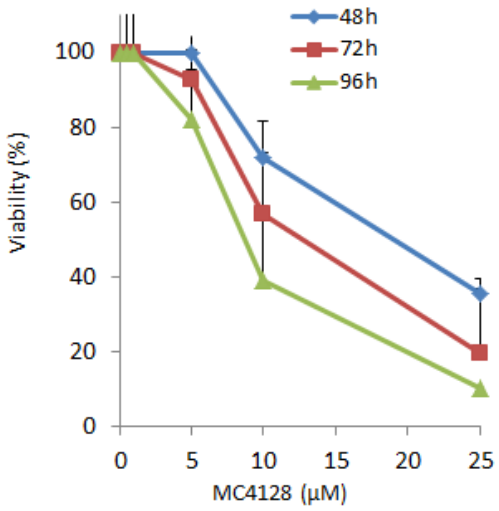

Figure 4.5: Graphic representation for the effect of selected compound **8c** (MC4128) on U-937 cell viability.

In U937 AML cells, **8c** (**MC4128**) impaired cell viability in a dose- and time-dependent manner. In comparison with the pharmacological combination between SAHA and the EZH2i MC3707, **8c** shows an enhanced ability to decrease cell viability. However, the co-treatment with SAHA and MC3707 produced a final synergistic effect as confirmed by the combination value < 0.5, estimated by an accurate algorithm. Moreover, **8c** displayed an improved cellular effect in U-937 cells after 72h of treatment.

4.6.3 Western Blot analysis

As a functional test for HDAC inhibition, Western Blot analyses in human leukaemia U-937 cells were performed to determine the effects on the acetylation levels of histone H3 and α-tubulin for compound

8c (**MC4128**) at 48, 72, 96, 120 and 144 h, using three different drug concentrations (5, 10 and 25 µM). In U-937 AML cells, **8c** (**MC4128**) displayed a dose-dependent α-tubulin and histone H3 hyperacetylation (Fig. 4.6). The decrease of H3K27 tri-methylation is evident only at 144 h, maybe due to the presence of the hydroxamate function, catabolized after 144 h. In fact, this typically leads to increased Lys methylation levels, probably due to inhibition/downregulation of Jumonji demethylases. [486]

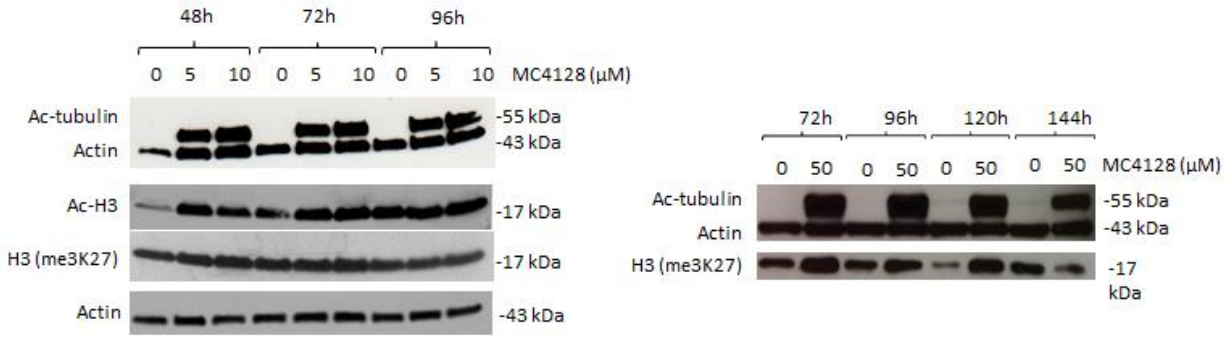

Figure 4.6: Analysis of methylation levels of histone H3 Lysine 27 (H3K27me3) and α-tubulin marks in U-937 AML cells upon treatment with 8c (MC4128).

4.6.4 Cell cycle, apoptosis, and cell differentiation assays

Furthermore, the most biochemically active compound **8c** (**MC4128**) was tested in U-937 AML cell lines to probe its ability to affect cell cycle progression, apoptosis, and cell proliferation, as well. As reference compounds, we used SAHA and our EZH2i MC3707.

In a cell cycle analysis assay the tested **8c** (**MC4128**) displayed a blockage of the cell cycle at G0/G1 phase on U-937 AML cells, as shown in Fig. 4.7.

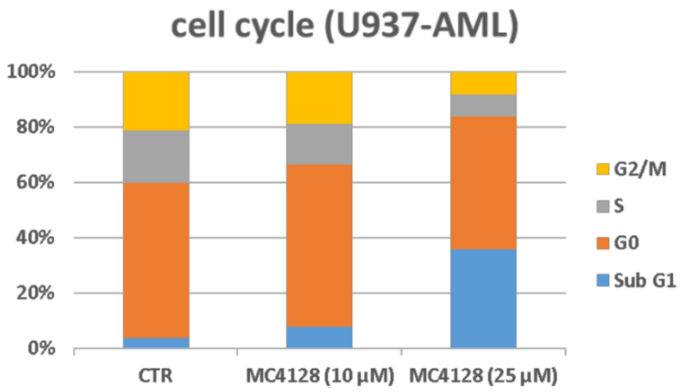

Figure 4.7: Cell cycle effect of **8c** (MC4128) at 10 and 25 µM concentration.

In the same cell lines, **8c** (**MC4128**) displayed an early- and late-apoptosis induction at two different drug concentrations (10 and 25 µM), as suggested by an increase of cell population in the lower left (early-) and in the upper right (late-) of the graph (Fig. 4.8).

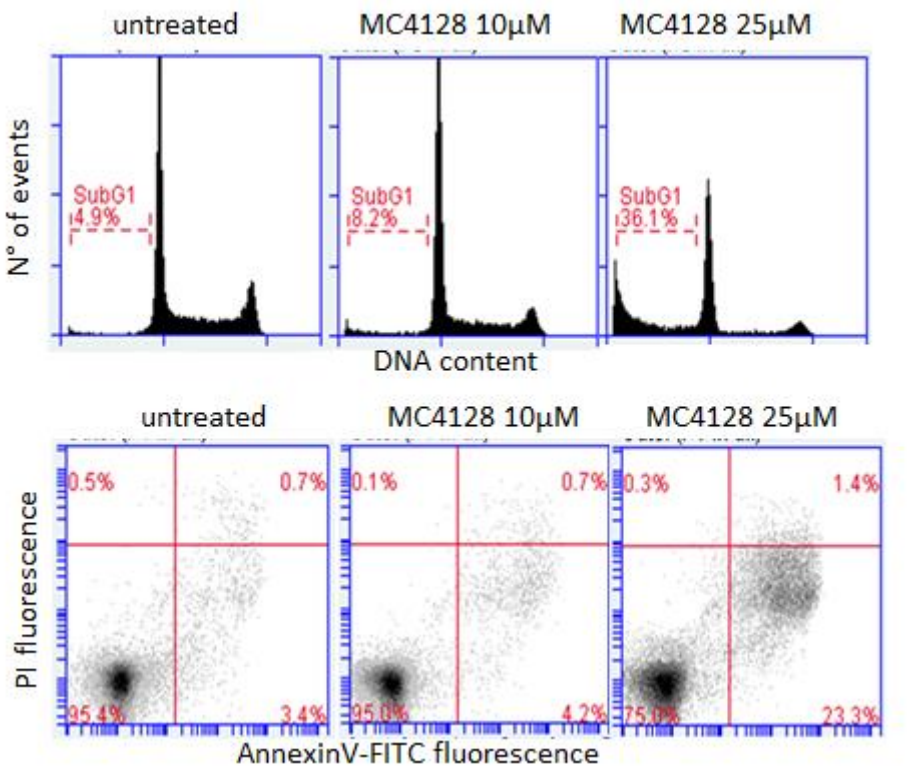

Figure 4.8: Evaluation of apoptosis induced by 8c (MC4128) at both 10 and 25 µM concentration.

Lastly, **8c** (**MC4128**) was tested at 10 and 25 µM to evaluate its effect on cell proliferation, using SAHA and MC3707 as reference drugs. The expression of the surface antigen CD11c in U937 AML cells was used as a marker of granulocytic differentiation. As shown in Fig. 4.8, cells treated with two doses of EZH2i MC3707 were not responsive to the test, whereas those treated with **8c** (**MC4128**) on the left, showed CD11c expression, as confirmed by curve translation compared to K value (in black).

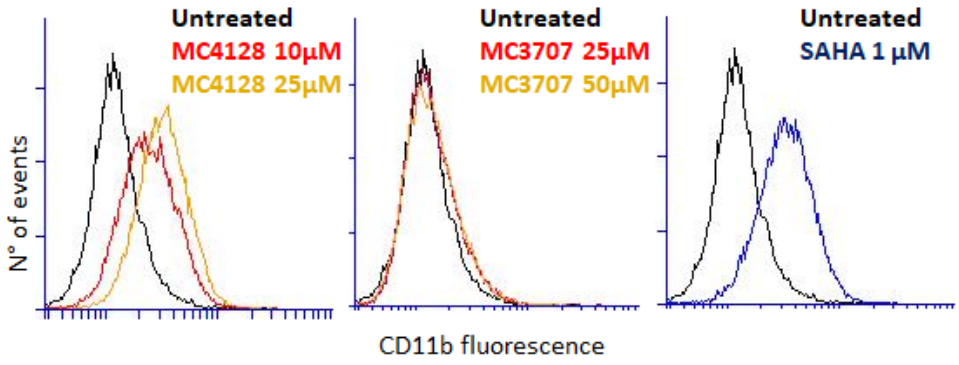

Figure 4.8: Cell proliferation induction in U-937 AML cells.

4.7 Conclusion and Future Perspectives

Overall, compounds **8a-g** and **6a-g** have been confirmed to be dual inhibitors of EZH2 and HDACs *in vitro*, showing an interesting selectivity profile towards HDAC isoforms. In preliminary assays in U-937 AML cells, **8c** (**MC4128**) decreased cell viability and induced apoptosis, with increased levels of acetyl-histone H3 and acetyl-α–tubulin. Based on these evidences, we will evaluate the enzymatic and cellular activities of the other compounds in order to validate their in *vitro* and in vivo activity, as well. Importantly, we expect that our novel HDAC/EZH2 dual inhibitors can display a potent and synergic anti-cancer activity in vivo, thus becoming an attractive therapeutic approach to fight cancer. Furthermore, though a medicinal chemistry optimization of the EZH2i scaffold combined to the already validated HDACi moieties, we plan to develop a novel series of dual HDAC/EZH2 inhibitors that we expect to be more and more potent than the compounds reported in this work.

5 Dissection of epigenetic mechanisms underlying the GAA-mediated FXN silencing in Friedreich's ataxia to identify FXN up-regulating compounds

5.1 Friedreich's ataxia

Friedreich's ataxia (FRDA) is an autosomal recessive neurodegenerative mitochondrial disorder caused by an unstable GAA trinucleotide (TTC) repeat expansion in the first intron of the frataxin gene (*FXN*) located on chromosome 9q21.1. [487] Unaffected individuals have up to 43 GAA repeats, while affected individuals contain 600 to 1700 repeats. [488] However, approximately 4% of patients are compound heterozygous, having one of the two alleles with an activating (or loss-of-function) intragenic mutation, including point mutation [489, 490] or a deletion/duplication [491, 492]. Nowadays, no confirmed FRDA patients have been identified with at least one GAA·TTC repeat expansion. The precise mechanism underlying GAA·TTC is not fully understood, but evidence suggested the involvement of abnormal DNA replication, transcription or repair. [493, 494] In FRDA patients, the expanded GAA·TTC repeats lead to partial transcriptional silencing resulting in expression of structurally and functionally normal frataxin, but at lower levels compared to the normal. [495] The length of the expansion is directly related to the severity of the condition, and inversely related to the age of onset. [496] Therefore, drugs that are able to increase frataxin expression would be, at least, beneficial. Signs and symptoms associated with reduced levels of frataxin protein in FRDA patients, that typically appear between the ages of 5 to 15 years, include: muscle weakness in the arms and legs (stumbling gait and frequent stalling), loss of coordination, vision and hearing impairment, slurred speech, curvature of the spine (scoliosis) and high plantar (arches pes cavus deformity of the foot), as result of progressive spinocerebellar neurodegeneration (Fig. 5.1).

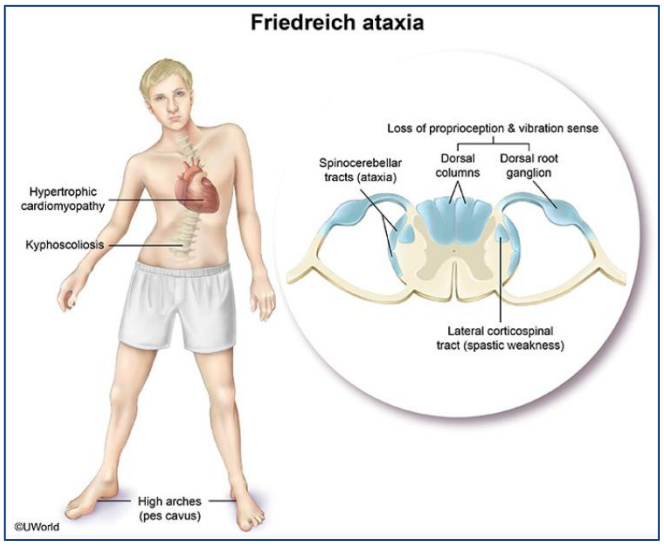

Figure 5.1: Signs and symptoms in FRDA patients.

Indeed, low levels of frataxin protein induce an imbalance or iron-sulfur (Fe-S) cluster biosynthesis [497], mitochondrial iron accumulation in heart, spinal cord, and dental nucleus [498], an increased susceptibility to oxidative stress. [499]

To date, no effective therapy for FRDA have been identified and, therefore, there is a high unmet clinical need to develop a therapy for this devastating disorder. However, FRDA preclinical and clinical trials using antioxidants and iron chelators have been carried out to reduce, at least, secondary disease effects, demonstrating some limited success. [500] An effective FRDA treatment may include drugs targeting the GAA·TTC repeat expansion mutation itself or the mechanism that impairs frataxin expression. Firstly, it has been proposed that the GAA·TTC repeat expansion may adopt abnormal non-B DNA structures (triplexes or "sticky DNA") or DNA·RNA hybrid structures (R loops), which prevent the RNA polymerase process, thus reducing *FXN* gene transcription. [501, 502] Secondly, there is evidence that GAA·TTC repeat expansions can produce heterochromatin-mediated gene silencing effects. [503] According to the latter hypothesis, several FRDA disease-related epigenetic changes have been identified near the expanded GAA·TTC repeats of the *FXN* gene (Fig. 5.2).

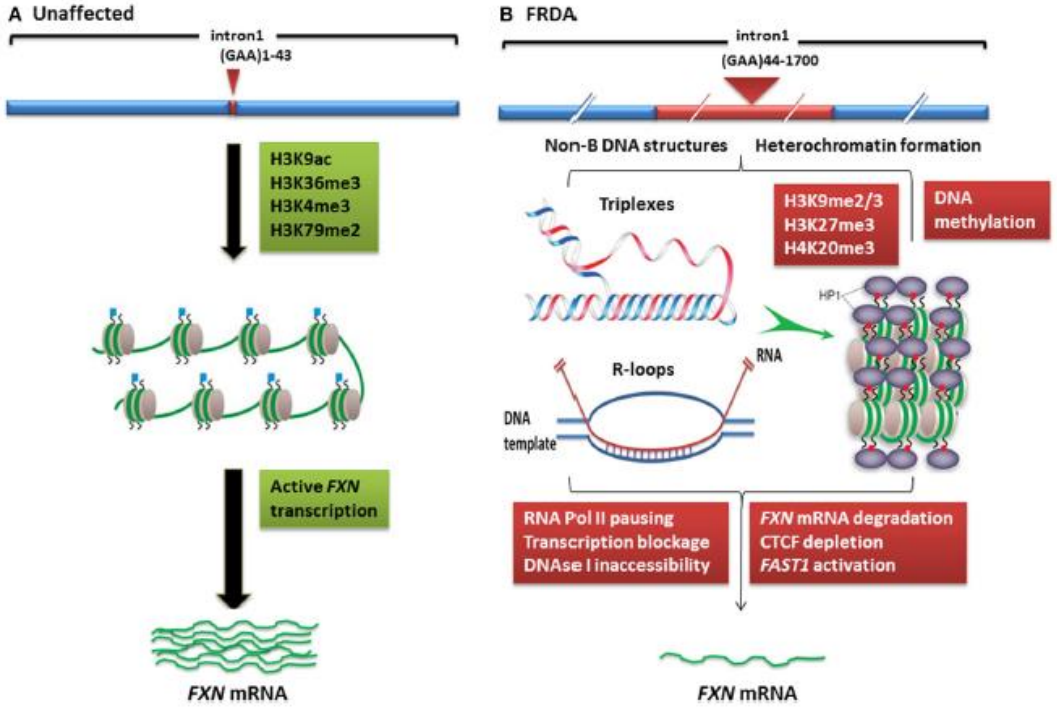

Figure 5.2: Models of *FXN* gene silencing in FRDA. (A) Unaffected individuals, who carry up to 43 GAA•TTC repeats, contain active histone marks of gene transcription initiation and elongation at the *FXN* promoter and intron 1 regions. **(B)** In FRDA patients, the presence of large GAA•TTC repeat expansion leads to *FXN* gene silencing by two potential mechanisms:(i)the GAA•TTC repeat may adopt abnormal non-B DNA structures (triplexes) or DNA•RNA hybrid structures(R loops),which impede the process of RNA polymerase and thus reduce *FXN* gene transcription, (ii) increased levels of DNA methylation and HP1 and significant enrichment of repressive histone marks at the *FXN* gene trigger heterochromatin formation that may lead to more pronounced *FXN* gene silencing. [504]

5.2 Epigenetic changes in FRDA

Epigenetic mechanisms play a key role in silencing or activation of many genes during development. Recognition of the role of epigenetic modifications in human diseases started with oncology and, now it has been extended to other disciplines, such as neurodegenerative disorders, including Alzheimer disease, Parkinson disease, Huntington disease and, FRDA. Epigenetic changes in FXN include increased levels of methylated histones (H3K9me2, H3K9me3, H4K20me3) in regions flanking the GAA repeats, increased DNA methylation at specific CpG sites upstream of the GAA repeats and, reduced acetylation of several H3 and H4 lysine residues (Fig. 5.3). [505-508]

Initially, DNA methylation analysis within *FXN* gene has revealed that hypermethylation of specific CpG sites upstream of the GAA·TTC repeat sequence in FRDA patient-derived lymphoblastoid cells compared to the normal cells. [509] Since FRDA affects different tissues and cell types, in 2008 Al-Mahdwai *et al.* reported significantly increased DNA methylation at the upstream regions of the GAA·TTC repeats in brain, heart and cerebellum tissues. [506] However, in two lines of FRDA YAC transgenic mice (YG8 and YG22), the degree of DNA methylation mice was not as severe as seen in FRDA patients, probably due to the length of the GAA·TTC repeats. [506] In line with the previous studies, the level of DNA methylation was also evaluated in a large cohort of FRDA patients, confirming the increased DNA methylation in FRDA patients, independently from the male or female gender. [510]

Acetylation and methylation of histone modifications at lysine (and arginine) residues are highly dynamic and are involved in several neurological disorders. Transcriptional repression of genes occurs by the deacetylation and the methylation of CpG dinucleotides by DNA methyltransferases (DNMT1, DNMT3a, and DNMT3b), resulting in an increased level of CpG methylation. [511] For many years, researchers have studied the role of epigenetic mechanisms in driving several neurological disorders. Recent studies have indicated that FRDA may also be caused by decreased histone acetylation and increased histone methylation, as well. [507] In FRDA lymphoblastoid cells, Herman D. *et al.* identified, for the first time, histone modifications at the *FXN* locus. They observed reduced levels of several acetylated H3 and H4 lysine residues, together with increased di- and tri-methylation of H3K9 in the upstream GAA·TTC regions. [507] After that, other epigenetic modifications have been identified in FRDA using multiple cell types and animal models. For examples, Greene and co-authors showed increased H3K9me2 levels in the first intron of FXN gene in FRDA lymphoblastoid cells, while Al-Mahdwi *et al.* reported histone modification changes at the promoter, downstream, and upstream of the GAA·TTC repeats in brain tissues and FRDA YAC transgenic mouse model. [506, 509] The latter study also highlighted as several histone protein residues were hypoacetylated close to *FXN* gene with concomitant increased of H3K9 di- and tri-methylation in FRDA brain tissue. Moreover, Biase and collaborators observed higher levels of H3K27me3 and H3K9me3 at FXN 5'-UTR in FRDA patient fibroblasts compared to normal fibroblasts. [512] Other reports showed decreased levels of H3K36me3 and H3K79me3 at the upstream and downstream GAA repeat regions in the *FXN* gene suggesting a

defect in the transcription elongation. [513, 514] Additionally, decreased levels of H3K4me3 have also been identified at the upstream GAA repeat regions, but not at the promoter region. Based on these evidence many efforts have put to identify molecules able to increase frataxin protein expression, although the exact mechanism of transcriptional blockage by GAA repeat expansion remains elusive yet. [515, 516]

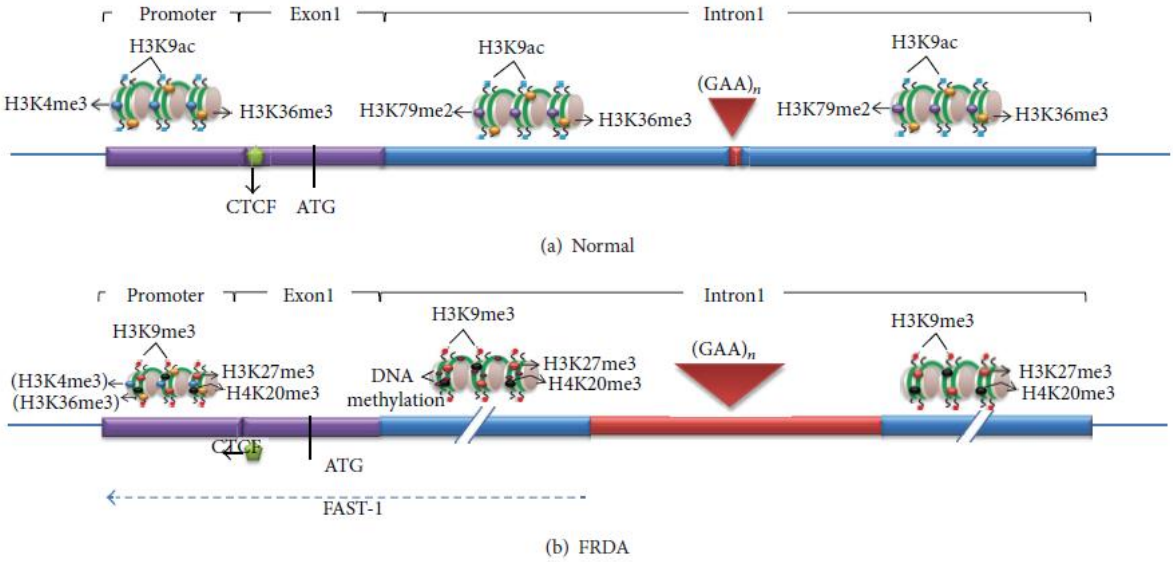

Figure 5.3: The FXN chromatin organisation in normal individuals and FRDA patients. (**a**) In normal individuals, the promoter contains H3K4me3 and H3K36me3, while downstream regions contain H3K79me2 and H3K36me3, marks for transcription initiation and elongation, respectively. All regions contain H3K9ac, a mark for active open chromatin. There is CTCF binding at the 5'-UTR. (**b**) In FRDA, depletion of CTCF may trigger the FAST-1 antisense transcription that may lead to the deacetylation of histones and the increase of H3K9me3 at the promoter and other regions of the gene. However, the levels of H3K4me3 and H3K36me3 are not substantially changed at the promoter (indicated by brackets), suggesting that there may be little deficiency of transcription initiation. The repressive histone marks, H3K27me3, H4K20me3 and H3K9me3, are observed throughout the gene, but most prominently at the upstream GAA repeat region, along with an increased DNA methylation. There are also reduced levels of H3K36me3 and H3K79me2 at the upstream GAA region, indicative of a defect of transcription elongation in FRDA. [505]

Furthermore, since antisense transcription has found to be involved in gene silencing, it may provide further insight into the mechanisms of neurodegenerative disorders, including FRDA. With the aim to identify the presence of any natural antisense transcripts (NATs) in FRDA, De Biase *et al.* revealed an increase in the level of frataxin antisense transcript 1 (*FAST1*) located in the proximity of the transcription start site (TSS) of the *FXN* gene. [512] Additionally, elevated levels of HP1 at this locus in FRDA patient-derived fibroblasts may be correlated with the depletion of CCCTC-binding factor (CTCF), leading to *FXN* gene silencing. CTCF, a highly conserve 11-zinc finger (ZF), is recognised as a transcription factor binding to avian and mammalian *MYC* promoter and is involved in a variety of transcriptional regulatory functions. (91, 92) Recently, CTCF binding sites have been identified in the 5'-UTR region of the *FXN* gene in fibroblasts and cerebellum tissues. [505] DNA methylation of CTCF leads to transcriptional inactivation, thus preventing the binding of CTCF. Even though the 5'-UTR region of the *FXN* gene does not exhibit any significant increase in DNA methylation, the depletion of CTCF has been associated with GAA·TTC repeat expansion in FRDA. [505, 509]

5.3 Potential epigenetic-based therapy for FRDA

FRDA can be considered as an epigenetic disease due to the identification of several associated epigenetic marks. Epi-drugs are being developed to target these epigenetic modifications in attempts to ameliorate the disease phenotype. However, an effective FRDA treatment requires specific epigenetic-based therapy targeting the *FXN* locus to avoid any off-target effects. Although currently no effective therapy for FRDA have yet been identified, many efforts have put in developing epigenetic drugs that slight increase frataxin protein to have a significant clinical effect. So far, it has been proposed the use of DNA demethylating agents, HDM activators, HDAC inhibitors, HAT activators, HMTase inhibitors as well as antigene RNA (agRNAs)-based therapies to treat the afore described disease.

5.3.1 DNA demethylating agents

Since FRDA is associated with increased levels of DNA methylation, DNA demethylating agents have been proposed to potentially activate silenced *FXN* gene. Unfortunately, no DNA demethylating agents have been investigated yet, probably due to the lack of evidence for a causal link between DNA methylation and *FXN* gene silencing. However, the use of DNA demethylating agents, including 5-aza-2'-deoxycytidine (5-aza-CdR or Decitabine), Zebularine and other oligonucleotide antisense inhibitors of DNMT1 such as MG98, may be considered as therapeutic options for FRDA. [517] Recently, Sandi *et al.* studied the effect of several DNMT on FRDA human and transgenic mouse primary fibroblasts using 5-aza-CdR and Zebularine as DNA demethylating agents. They observed an increased *FXN* expression in FRDA transgenic mouse cells and a decreased *FXN* expression in human FRDA cells, suggesting that this discrepancy was maybe due to a difference in the regulatory mechanisms of gene expression between the two species. [518] Further investigations are certainly needed to assess the potential role of DNMT in reducing DNA methylation, thus providing beneficial effects in FRDA patients.

5.3.2 HDAC inhibitors

Alterations in histone acetylation have already been identified in FRDA, so the inhibition of these histone modifications could represent a potential therapeutic approach for FRDA. [507, 519] Initially, the effect of sodium butyrate on increasing frataxin protein expression was evaluated using an EGFR reporter cell line. [520] However, in this study a small increase of *FXN* gene activity was observed. In FRDA lymphoblastoid cells, among a selection of commercially available HDAC inhibitors, only the benzamide compound BML-210 showed a significant increase of *FXN* gene expression. [507] Further studies have been carried out to evaluate the effect of various pimelic o-aminobenzamide compounds as HDACi in FRDA-patient-derived cells and mice and, in particular, compound 109/RG2833 (Fig. 5.4),

discovered by Repligen in 2014, has emerged as the most promising drug for FRDA treatment. [521, 522]

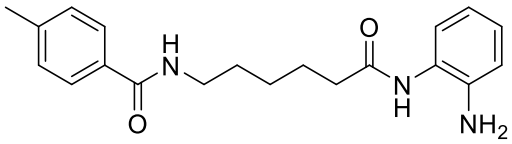

Figure 5.4: Chemical structure of compound 109/RG2833.

Soragni *et al.* showed increased *FXN* mRNA levels and frataxin protein in neuronal cell model after 109/RG2833 treatment, with concomitant changes in the epigenetic state of the gene. [523] Furthermore, they demonstrated that combined HDAC1, 2, and 3 inhibition is required to counteract the epigenetic changes induced by the GAA·TTC repeat expansion, and that H3K9 is a key histone residue whose acetylation/methylation regulates *FXN* expression. Although these results were encouraging, 109/RG2833 suffers from liabilities for chronic use as FRDA therapeutics and, could not advance in clinical trials due to its poor distribution in the brain and spinal cord and its potential to break down into possible toxic or cancer-causing metabolites. In a followed up study, through a medicinal chemistry optimisation of the 109/RG2833 scaffold, new generations of molecules have been synthesised and are now being tested in preclinical studies. [524] Preliminary results showed favourable brain penetration (>0.7 brain/plasma ratio), thus reducing the metabolic liabilities of the lead compound.

In a recent study, the sirtuin inhibitor nicotinamide was found to be effective in restoring *FXN* transcription in peripheral lymphocytes isolated from blood of orally dosed patients although in this trial they used high daily doses. [525, 526] By contrast, benzamide HDACi are effective in the low micromolar range, and the next generation of compounds holds the promise of efficacy in the high nanomolar range, with possibly fewer liabilities for long-term use. Since DNA methylation and histone modifications are both known to act epigenetically, the use of DNA demethylating agents and HDACi together would be a promising therapeutic approach to get a more pronounced synergistic effect on increasing frataxin expression.

5.3.3 HMTase inhibitors

Since HMTase inhibitors are known to induce a more open chromatin structure at the *FXN* gene, they can be considered for FRDA therapy (Fig. 5.5). EZH2, the major component of PRC2 which trimethylates lysine 27 on the tail of histone H3 (H3K27), has been correlated with repression of several genes, thus its inhibition could provide a beneficial therapeutic outcome. Based on these evidence the use of epigenetic drugs able to inhibit H3K27 methylation, such as GSK126, has been proposed for FRDA.

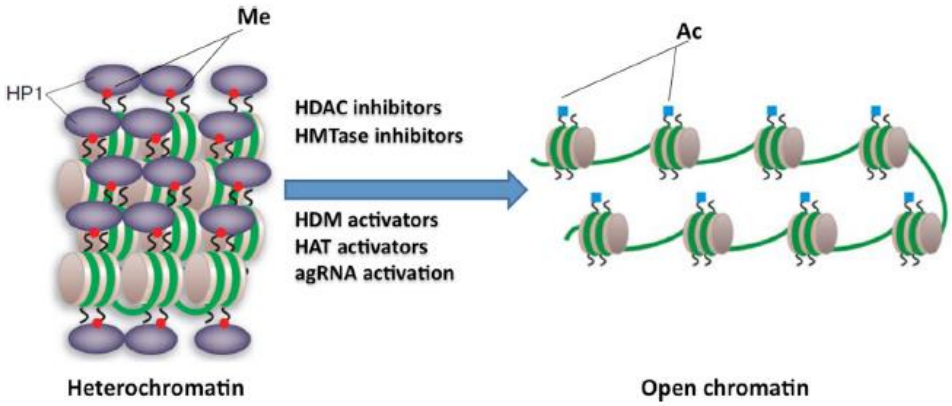

Figure 5.5: Potential epigenetic-based therapies for FRDA. Large GAA•TTC repeats in FRDA patients are associated with heterochromatin mediated FXN gene silencing. The use of specific HDAC inhibitors, HDM activators, HAT activators, HMTase inhibitors, or agRNA activation may reverse the heterochromatin to a more open chromatin structure, and may thus lead to active FXN gene transcription. [504]

Since increased levels of H3K27me3 have been found in FRDA lymphoblastoid and fibroblast cells, GSK126 treatment demonstrated to efficiently reactivate *FXN* gene transcription in these types of cells. [512, 513, 527] Other studies showed that reduced H3K9me2 levels by direct or indirect G9a inhibitors could be an attractive therapeutic option for FRDA, too. Indeed, the use of HMTase inhibitor BIX-01294 in FRDA lymphoblastoid cells revealed a significant reduction of di- and tri-methylation of H3K9 but without increasing the *FXN* mRNA levels. [528] By contrast, in 2013 Chan *et al.* showed that nicotinamide was able to induce the reactivation of the *FXN* gene with concomitant decreased H3K9me3 and H3K27me3. [527]

5.3.4 Antigene RNA-based therapies

AgRNAs are small duplex RNAs of 19bp in length that target gene promoters inducing either gene transcriptional activation or repression, depending on the target sequence and cell type. [529, 530] Since it is possible to modulate agRNAs to activate gene expression, they may represent a valuable option for FRDA. Indeed, reactivation of *FXN* gene by targeting the *FXN* promoter or the *FAST1* transcript could be achieved using agRNAs. Despite the amelioration of FRDA disease by reversing *FXN* gene silencing, currently, no agRNAs have yet been investigated in FRDA.

5.4 Rational of the project

As discussed in chapter 1, increasing evidence indicates that the PKMTs Suv420-h1 and Suv420-h2 are key regulators of genomic integrity. [41] These two highly homologous PKMTs catalyse the di- and tri-methylation of H4K20 ensuring proper chromosome cohesion and compaction, proficient DNA replication and cell cycle progression, efficient NHEJ and telomere lengthening. [38, 44, 54, 531] However, despite the importance of H4K20me in genomic integrity, only a few studies have been carried out to identify Suv420 small-molecule inhibitors. [532, 533]

Very recently, through a high-throughput homogeneous activity-based scintillation proximity assay (SPA), Bromberg *et al.* reported the identification of the first-in-class Suv420 chemical probe A-196 (Fig. 5.6) as a potent, selective and cell active Suv420 inhibitor. [534]

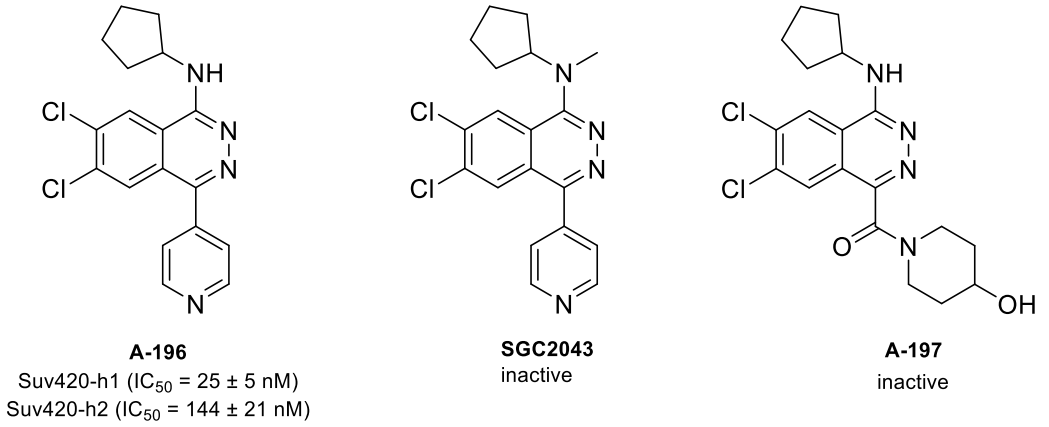

Figure 5.5: Chemical structures of A-196 and its closely inactive analogue SGC2043, and A-197.

A-196 inhibits biochemically both Suv420-h1 (IC_{50} = 25 ± 5 nM) and Suv420-h2 (IC_{50} = 144 ± 21 nM) at 1 and 10 µM concentration. Its closely related analogues **SGC2043**, having a methyl group attached to NH of the cyclopentylamine, and **A-197** are, however, inactive against both Suv420-h1 and Suv420-h2, therefore they were used as negative controls in biochemical, biophysical and cellular assays (Fig. 5.5). Furthermore, A-196 is selective for Suv420 over 29 other methyltransferases. Structural and biophysical studies showed strong cooperativity between the binding of A-196 and SAM to Suv420-h1. Indeed, the IC_{50} values of A-196 increased linearly as the ratio of H4K20me1 peptide/*K*m increased, while the IC_{50} of A-196 remained constant as the ratio of SAM/*K*m increased. These data indicate that A-196 is competitive with the histone peptide substrate but noncompetitive with the cofactor SAM. They also determined the co-crystal structure of Suv420h1 in complex with A-196 and the cofactor SAM to assess the binding-site location and the binding mode of A-196. As shown in figure 5.6, A-196 directly binds within the histone H4 peptide-binding groove of the enzyme blocking the access to the catalytic residue Ser251.

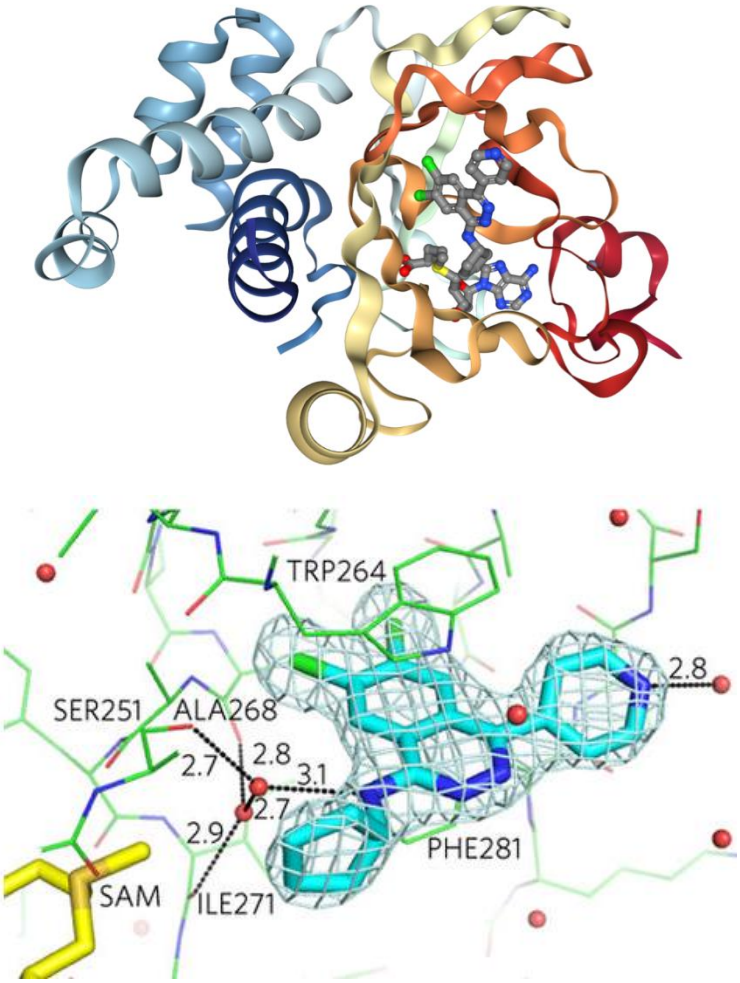

Figure 5.6: Crystal structure of A-196 bound to Suv420-h1 and its binding-site interactions. [534]

Furthermore, phthalazine core is seemingly essential for π-stacking interactions with Trp264 and Phe281 residues in the H4 binding groove. Two notable hydrogen bonds are observed: the first is from the pyridine nitrogen of A-196 to a water (2.8 Å), and the second (perhaps more important) is from the amine to a water (3.1 Å), which also makes hydrogen bond to the catalytic Ser251 and occupies the position where the nitrogen of the methylated lysine substrate would ordinarily be located. Ile231 and Trp264, which move to create a small hydrophobic pocket, accommodate the dichlorophthalazine ring and produce a π sandwich with Trp264 above and Phe281 below the phthalazine ring. Additionally, A-196 was found to attenuate 53BPI foci formation and NHEJ proficiency in human cells by modulating H4K20 methylation. These findings suggest a crucial role of H4K20me2, catalysed by PR-SET7 and Suv420, in 53BPI recruitment and efficient double-strand DNA break repair. Therefore, this chemical probe represents a valuable tool for advancing the understanding of the cellular roles of Suv420 and PKMTs in DNA repair and genomic integrity. Indeed, Suv420-h1 has been reported as an important player and a potential target for FRDA. Preliminary cellular studies in human embryonic cells (HEK) and

in patient fibroblasts revealed that A-196 successfully increases *FXN* levels. In cell-based assays, A-196 inhibits the di- and tri-methylation of H4K20me in multiple cell lines with $IC_{50} < 1\ \mu M$ and it is not toxic. Despite the *in vitro* potency of A-196, confirmed by biochemical and cellular assays, preliminary in vitro metabolic studies in human liver microsomes (HLM) have shown some metabolic liability and potentially low solubility, with a Cl_{int} (µL/min/mg protein) =191 and a $t_{1/2}$ (min)=7.28. Prompted by these findings, a lead chemical optimisation has been carried out during a stay abroad in collaboration with Prof. Brennan with the aim to ameliorate chemical and physical properties of A-196. The co-crystal structure of A-196 and SAM in complex with SUV420-h1, the binding-site location, and the binding mode were taken into account for the development of more potent and metabolically stable A-196 derivatives (Fig. 5.6).

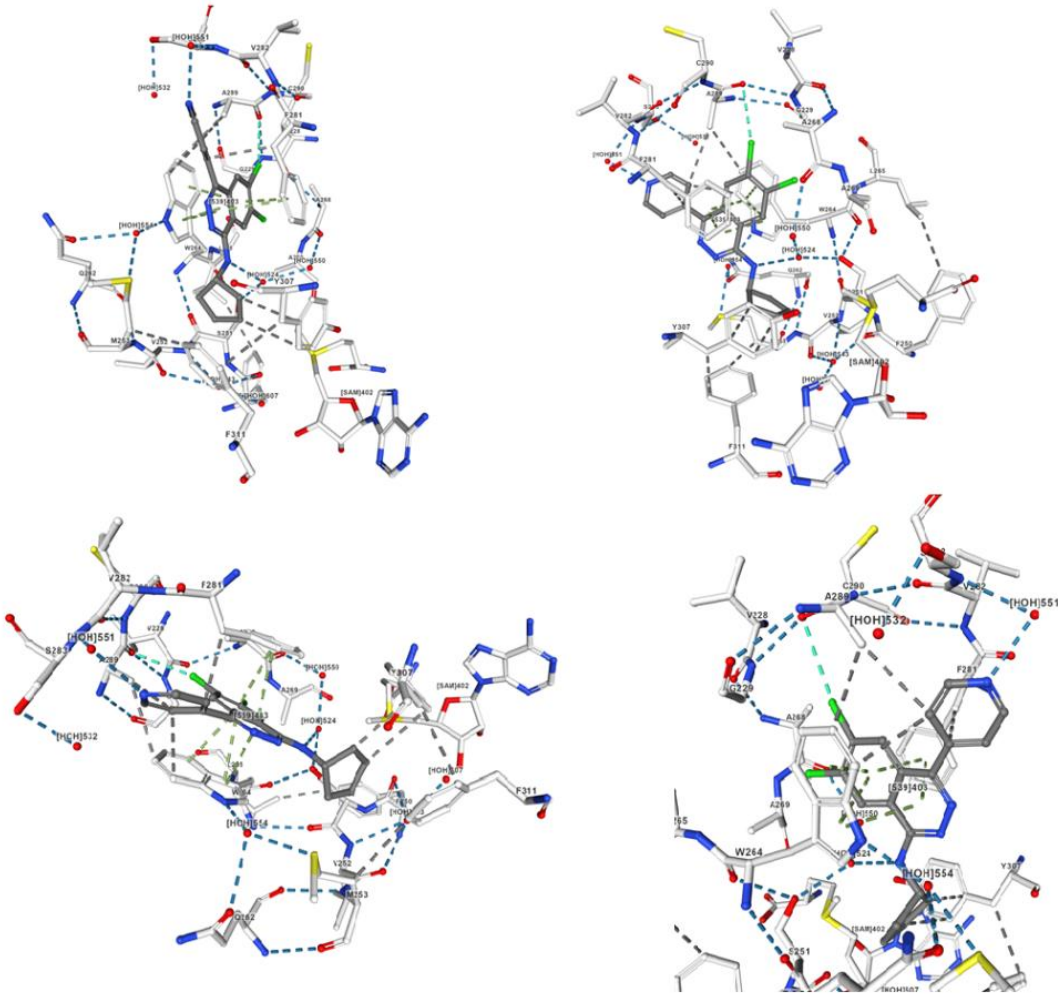

Figure 5.6: Design of new ligands bind to Suv420-h1.

To identify novel epigenetic-based FRDA therapeutic compounds for future testing, we planned to perform an extensive SAR investigation on A-196 scaffold in order to improve its metabolic stability as well as to increase its solubility. Therefore, we applied several structural manipulations working at the

C4 position by insertion of several heterocyclic amines to improve the H-bonding capacity of aniline NH and metabolic stability (5.7).

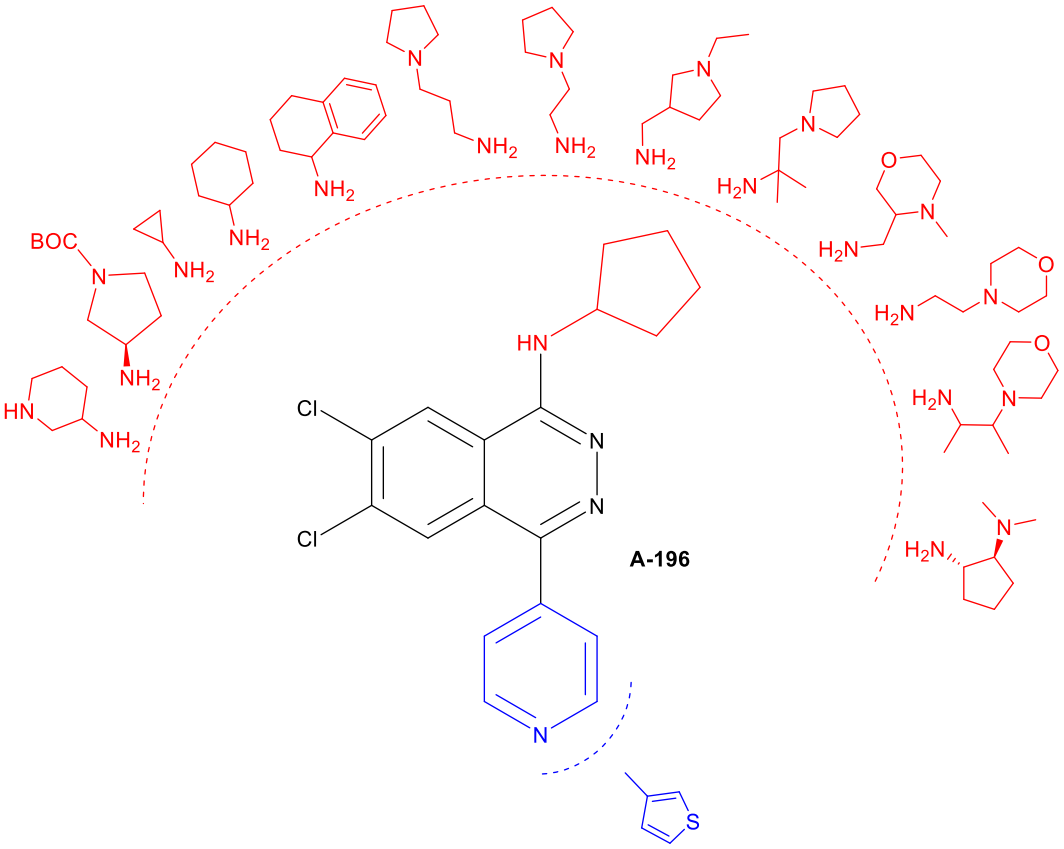

Figure 5.7: Design of novel Suv420 inhibitors.

5.5 Chemistry

Scheme 5.1 shows the synthesis of the final compounds **1a-m** and **2c**. The commercially available 5,6-dichloroisobenzofuran-1,3-dione was cyclised with hydrazine to afford the 6,7-dichloro-2,3-dihydrophthalazine-1,4-dione **5** which was treated with phosphoryl trichloride ($POCl_3$) and *N,N*-diisopropylethylamine (DIPEA) to obtain the 1,4,6,7-tetrachlorophthalazine intermediate **4** which reacted with appropriate amines at the C4 position, giving compounds **3a-l** and **3m**. The **3a-l** derivatives directly underwent a Suzuki-Coupling reaction with the proper arylboronic acid (**1**, **2**) to give final compounds **1a-l** and **2c**, whereas **3m** intermediate was subjected to a prior step of N-BOC cleavage with 4N HCl in 1,4 dioxane in dry THF followed by a Suzuki-Coupling reaction to afford the final compound **1m**. All the final compounds were purified by preparative MS triggered HPLC.

Scheme 5.1

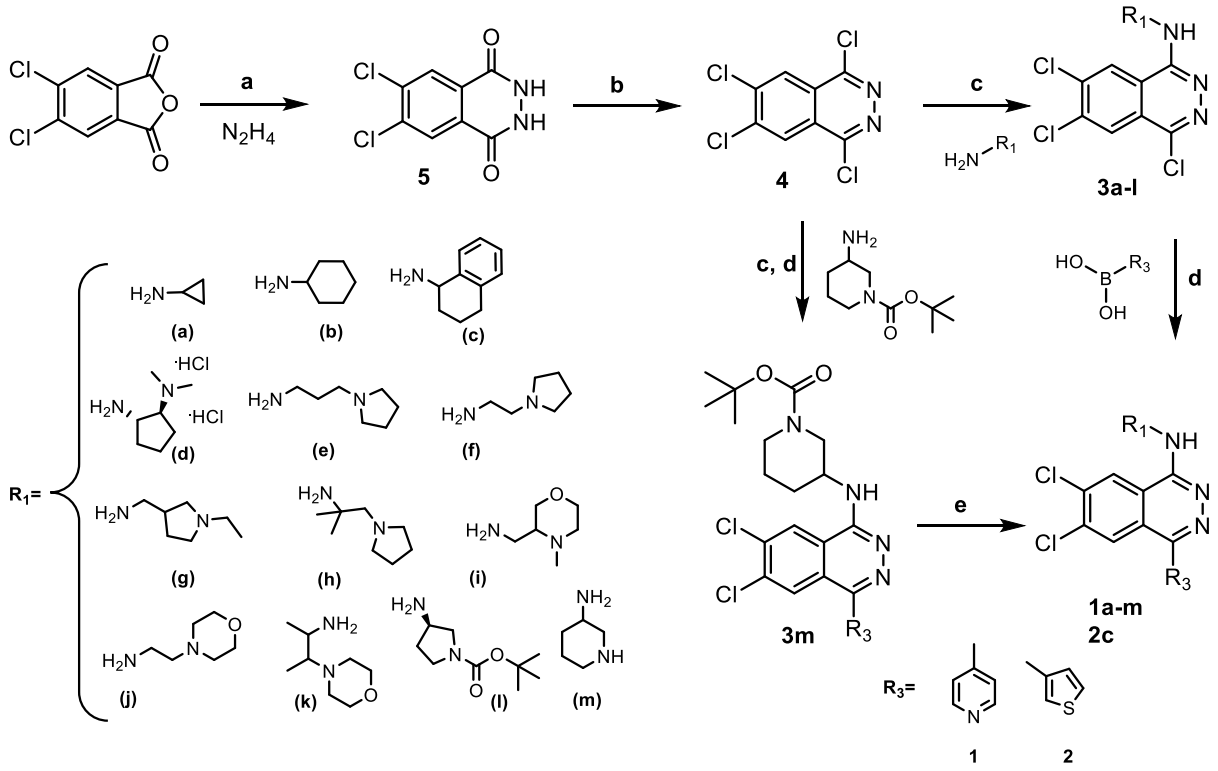

Reagents and conditions: (**a**) AcOH, 70°C, 24h; (**b**) $POCl_3$, DIPEA, 130°C, 24h; (**c**) DIPEA, DMSO, 70°C, 24h; (**d**) 1. $Pd(PPh_3)_4$, K_2CO_3, 2. Dioxane:Water (4:1), 70 °C, 1h; (**e**) 4N HCl in 1,4 dioxane, dry THF, RT⟶40 °C, 24h.

Table 5.1: Chemical structure of the final compounds 1a-m and 2c.

LAB CODE	COMPOUND	CHEMICAL STRUCTURE	MOLECULAR WEIGHT	YIELD (%) after HPLC purification
RM01	**1a**	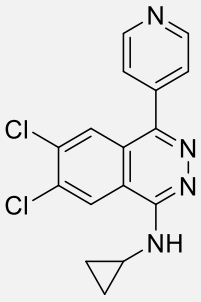	331.20	6.4%

RM02	**1b**	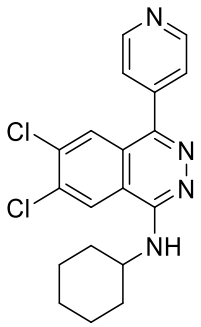	373.28	8.4%
RM03	**1c**	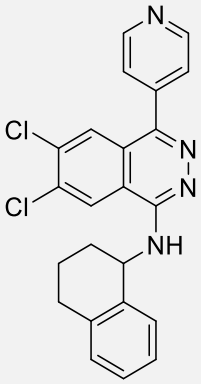	421.33	5.3%
RM04	**2c**	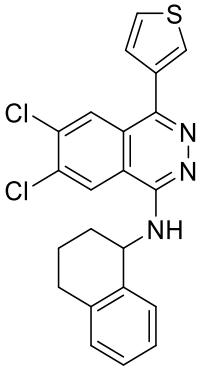	426.36	7.8%
RM05	**1d**	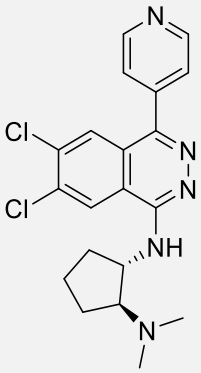	402.32	38.7%

RM06	**1e**	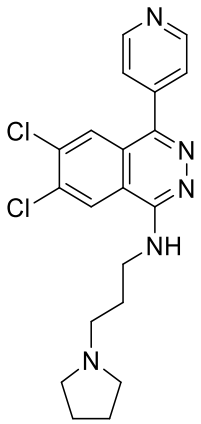	402.32	13%
RM07	**1f**	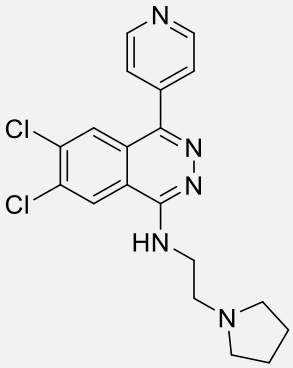	388.30	21%
RM08	**1g**	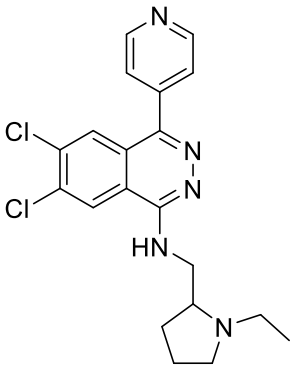	402.32	24.7%
RM09	**1h**	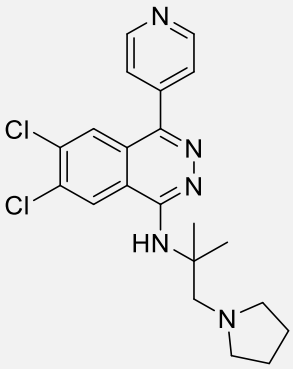	416.35	12.8%

RM010	**1i**	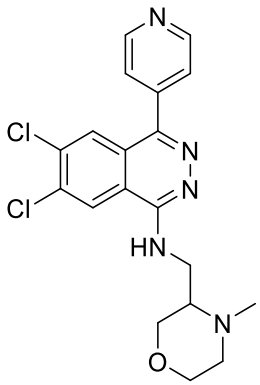	404.30	14%
RM011	**1j**	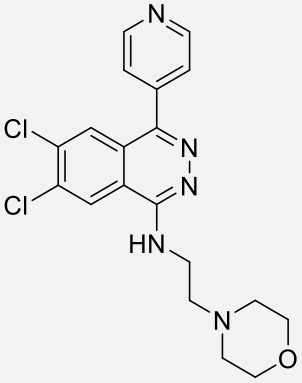	404.30	13.7%
RM012	**1k**	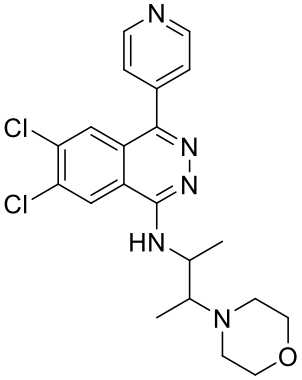	432.35	19.2%
RM013	**1l**	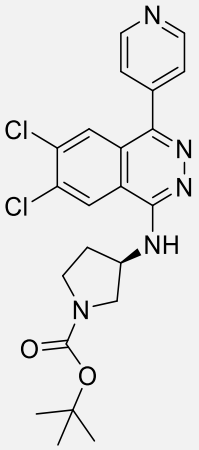	460.36	19.4%

RM014	**1m**	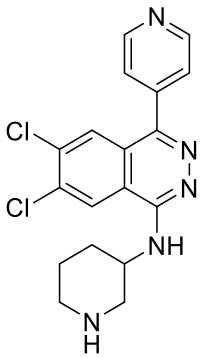	374.27	20.5%

5.6 Experimental section

Chemistry. All solvents were purchased from commercial sources and used without purification (HPLC or analytical grade). Anhydrous solvents were purchased from Acros Organics stored under a nitrogen atmosphere with activated molecular sieves. Standard vacuum line techniques were used and glassware was flame dried prior to use. Deionized water was sourced using an Elga DV 25 system. Organic solvents were dried during work up using anhydrous Na_2SO_4.

NMR spectra were recorded using a Bruker Advance 400 MHz spectrometer using the deuterated solvent stated. Chemical shifts (δ) quoted in parts per million (ppm) and referenced to the residual solvent peak. Multiplicities are denoted as s- singlet, d- doublet, t- triplet, q- quartet and quin- quintet and derivatives thereof (br denotes a broad resonance peak). Coupling constants recorded as Hz and round to the nearest 0.1 Hz. Two-dimensional NMR experiments (COSY, HSQC, HMBC) were used to aid the assignment of 1H and 13C spectra. Low Resolution mass spectra were recorded on a Waters SQ Detector 2 (LC-MS).

Thin Layer Chromatography (TLC) was carried out using aluminium plates coated with 60 F254 silica gel. Plates were visualised using UV light (254 or 365 nm) or staining with Ninhydrin (1 M, EtOH) or 1% aq. KMnO4. Normal-phase silica gel chromatography was carried out using Biotage Isolera One flash column chromatography system (LPLC). Reverse-phase high-pressure liquid chromatography (RP-HPLC) was performed using a Waters system equipped with a Waters 2545 Binary Gradient Module, a SecurityGuard™ ULTRA cartridges for EVO-C18 UHPLC HPLC, Kinetex 5 µM EVO C18 100 Å 100 x 3.0 mm column and a Waters SQ Detector 2 using the stated eluent system.

Procedure for the synthesis of 6,7-dichloro-2,3-dihydrophthalazine-1,4-dione (5)

To a solution of 5,6 dichloroisobenzofuran-1,3-dione (1 eq, 8.8 g, 40.6 mmol) in acetic acid (40 mL), hydrazine (1.2 eq, 1.886 mL, 48.7 mmol) was added carefully at room temperature. The mixture was stirred at 70°C overnight under nitrogen. The reaction mixture was cooled, and the solid material was collected to give the title compound **5**, which was used without further purification (8.9 g, Y= 90%).

^{1}H NMR (400MHz, d_6-DMSO) δ: 8.18 (s, 2H, aromatic protons), 11.88 (s, 2H, 2x N*H*) ppm. MS (EI): *m/z* $[M]^+$: 231.7.

Procedure for the synthesis of 1,4,6,7-tetrachlorophthalazine (4)

To a mixture of **5** (1 eq, 4.0 g, 17.31 mmol) in $POCl_3$ (10 eq, 16.14 mL, 173 mmol) in a 250 mL round-bottomed flask diisopropylethylamine (1 eq, 3.02 mL, 17.31 mmol) was added dropwise. The mixture was heated at 130°C overnight. After cooling to room temperature, the mixture was slowly poured into ice-water (500 mL) and stirred for 1 hour. The solid was collected by filtration and re-dissolved in dichloroethane (200 mL). The organic solution was washed with brine (3x10 mL) dried with anhydrous sodium sulfate and filtered. The filtrate was concentrated under reduced pressure to give the crude product which was purified by column chromatography (SiO2 eluting with EtOAc:Cyclohex=1:20) to afford the title compound **4** as a yellow solid (4.0 g, Y= 70%).

MS (EI): *m/z* $[M]^+$: 266.8.

General procedure for the synthesis of 4,6,7-trichloro-N-cycloarylalkylphthalazin-1-amines (3a-l). Example 4,6,7-trichloro-N-(3-(pyrrolidin-1-yl)propyl)phthalazin-1-amine (3e).

A mixture of **4** (1 eq, 0.1 g, 0.373 mmol) and diisopropylethylamine (1.2 eq, 0.058 g, 0.448 mmol) in dimethylsulfoxide (2 mL) in a 100 mL round-bottomed flask was heated to 80°C and then a solution of 3-(pyrrolidin-1-yl)propan-1-amine (1 eq, 0.048 g, 0.373 mmol) in dimethylsulfoxide (2 mL) was added drop wise. The mixture was stirred at 80°C for about 2h and then at room temperature overnight. The reaction was quenched by H_20 and extracted with ethyl acetate (5 x 6 mL), dried over magnesium sulfate and concentrated *in vacuo.* The resultant crude product was purified by column chromatography (SiO_2 eluting with DCM/MeOH 5%) to afford the desired product **3e** (0.0388g, Y=29%).

^{1}H NMR (400MHz, DMSO) δ: 1.68-1.72 (m, 4H, -CH_2CH_2 pyrrolidine), 1.82-1.89 (m, 2H, -CH_2C$H_2$$CH_2$), 2.44-2.47 (td, 4H, 2x CH_2 pyrrolidine), 3.53-3.58 (q, 2H, -CH_2CH_2 pyrrolidine), 7.96 (t, 1H, N*H*), 8.23 (s, 1H, aromatic proton), 8.69 (s, 1H, aromatic proton) ppm. MS (EI): *m/z* $[M]^+$: 358.05.

General procedure for the synthesis of the final compounds 6,7-dichloro-4-(pyridin-4-yl)-N-cycloarylalkylphthalazin-1-amines (1a-l). Example 6,7-dichloro-N-cyclohexyl-4-(pyridin-4-yl)phthalazin-1-amine (1b).

A mixture of **3b** (1 eq, 0.0474 g, 0.143 mmol), pyridin-4ylboronic acid (1 eq, 0.0176 g, 0.143 mmol), tetrakis (triphenylphosphine) palladium (0) (0.1 eq, 0.0166 g, 0.0143 mmol) and K_2CO_3 (3 eq, 0.0594 g, 0.430 mmol) in 1,4 dioxane in water (ratio: 4:1, 3.13 mL) was stirred at 80 °C for 5 hours. The palladium was removed by filtering through celite and the reaction was extracted with EtOAc (3 x 10 mL). The combined organic phases were washed with water (3 x 10 mL) and dried over sodium sulfate. The

remaining solvent was removed *in vacuo* and the resultant crude product purified by HPLC. (0.0045 g, Y= 8.4%).

^{1}H NMR (400MHz, $CDCl_3$) δ: 1.18-1.32 (m, 8H, -CH_2CH_2CH_2CH_2 cyclohexane), 1.40-1.43 (m, 2H, -CH_2 cyclohexane), 1.66 (m, 1H, -C*H* cyclohexane), 4.93 (d, 1H, N*H*), 7.55 (d, 2H, pyridine protons), 7.85 (s, 1H, aromatic proton), 7.95 (d, 2H, pyridine protons), 8.73 (s, 1H, aromatic proton) ppm. MS (EI): *m/z* $[M]^+$: 372.09.

Procedure for the synthesis of the final compound 6,7-dichloro-N-(piperidin-3-yl)-4-(pyridin-4-yl)phthalazin-1-amine (1m)

To a solution of **3m** (1 eq, 0.1 g, 0.211 mmol) in dry THF (2 mL), 4N hydrogen chloride in 1,4 dioxane (5eq, 0.035 mL, 1.05 mmol) was added dropwise at 0° C. The resulting mixture was stirred at room temperature for about 1 hour and then at 40 °C overnight. After this time, the reaction was cooled to room temperature, the precipitate was collected by filtration and washed with dry THF (3 x 3 mL), and dried *in vacuo* to give the title compound **1m** as a white pure solid (0.0162 g, Y= 20.5%).

^{1}H NMR (400MHz, $CDCl_3$) δ: 1.75-1.81 (m, 2H, CH_2 piperidine), 2.04 (m, 4H, 2x CH_2 piperidine), 2.19 (m, 2H, CH_2 piperidine), 2.88 (td, 1H, -C*H* piperidine), 3.48 (m, 1H, N*H* piperidine), 5.04 (d, 1H, N*H*), 7.54 (d, 2H, pyridine protons), 7.90 (s, 1H, aromatic proton), 8.74 (d, 2H, pyridine protons), 8.81 (s, 1H, aromatic proton) ppm. MS (EI): *m/z* $[M]^+$: 372.09.

^{1}H-NMR and mass spectra of final compounds:

6,7-dichloro-N-cyclopropyl-4-(pyridin-4-yl)phthalazin-1-amine (RM01, 1a)

^{1}H NMR (400MHz, $CDCl_3$) δ: 1.66-1.71 (m, 2H, -CH_2 cyclopropane), 1.73-1.78 (m, 2H, -CH_2 cyclopropane), 1.85-1.93 (m, 1H, -C*H* cyclopropane), 5.32 (m, 1H, N*H*), 7.45 (s, 1H, aromatic proton), 7.71 (d, 2H, pyridine protons), 7.72 (d, 2H, pyridine protons), 8.63 (s, 1H, aromatic proton) ppm. MS (EI): *m/z* $[M]^+$: 330.04.

6,7-dichloro-N-cyclohexyl-4-(pyridin-4-yl)phthalazin-1-amine (RM02, 1b).

^{1}H NMR (400MHz, $CDCl_3$) δ: 1.18-1.32 (m, 8H, -CH_2CH_2CH_2CH_2 cyclohexane), 1.40-1.43 (m, 2H, -CH_2 cyclohexane), 1.66 (m, 1H, -C*H* cyclohexane), 4.93 (d, 1H, N*H*), 7.55 (s, 1H, aromatic proton), 7.85 (d, 2H, pyridine protons), 7.95 (s, 1H, aromatic proton), 8.73 (d, 2H, pyridine protons) ppm. MS (EI): *m/z* $[M]^+$: 372.09.

6,7-dichloro-4-(pyridin-4-yl)-N-(1,2,3,4-tetrahydronaphthalen-1-yl)phthalazin-1-amine (RM03, 1c)

^{1}H NMR (400MHz, $CDCl_3$) δ: 1.86 (m, 2H, -CH_2 naphthalene), 2.15 (m, 2H, -CH_2 naphthalene), 2.83 (m, 2H, -CH_2 naphthalene), 5.30 (d, 1H, N*H*), 5.80 (m, 1H, -C*H* naphthalene), 7.13-7.17 (m, 3H, aromatic

protons), 7.36 (m, 1H, aromatic proton), 7.58 (d, 2H, pyridine protons), 7.82 (s, 1H, aromatic proton), 7.97 (s, 1H, aromatic proton), 8.75 (d, 2H, pyridine protons) ppm. MS (EI): *m/z* $[M]^+$: 420.09.

6,7-dichloro-N-(1,2,3,4-tetrahydronaphthalen-1-yl)-4-(thiophen-3-yl)phthalazin-1-amine (RM04, 2c)

^{1}H NMR (400MHz, $CDCl_3$) δ: 2.11 (m, 2H, -C*H*$_2$ naphthalene), 2.18 (m, 2H, -C*H*$_2$ naphthalene), 2.82 (m, 2H, -C*H*$_2$ naphthalene), 5.16 (s, 1H, N*H*), 5.77 (m, 1H, -C*H* naphthalene), 7.13-7.19 (m, 4H, aromatic protons), 7.44 (m, 3H, thiophene protons), 7.58 (d, 2H, pyridine protons), 7.82 (s, 1H, aromatic proton), 7.97 (s, 1H, aromatic proton), 8.75 (d, 2H, pyridine protons) ppm. MS (EI): *m/z* $[M]^+$: 425.05.

(1S,2S)-N1-(6,7-dichloro-4-(pyridin-4-yl)phthalazin-1-yl)-N2,N2-dimethylcyclopentane-1,2-diamine (RM05, 1d)

^{1}H NMR (400MHz, $CDCl_3$) δ: 1.22 (m, 4H, 2x -C*H*$_2$ cyclopentane), 1.60 (m, 2H, -C*H*$_2$ cyclopentane), 2.27 (m, 2H, 2x –C*H* cyclopentane), 2.92 (s, 6H, 2x –C*H*$_3$), 5.25 (d, 1H, N*H*), 7.79 (s, 1H, aromatic proton), 7.93 (s, 1H, aromatic proton), 8.26 (d, 2H, pyridine protons), 8.47 (d, 2H, pyridine protons) ppm. MS (EI): *m/z* $[M]^+$: 401.12.

6,7-dichloro-4-(pyridin-4-yl)-N-(3-(pyrrolidin-1-yl)propyl)phthalazin-1-amine (RM06, 1e)

^{1}H NMR (400MHz, $CDCl_3$) δ: 1.18 (m, 4H, 2x -C*H*$_2$ pyrrolidine), 2.11 (m, 4H, 2x -C*H*$_2$ pyrrolidine), 3.06 (m, 4H, -C*H*$_2$C*H*$_2$), 3.78 (m, 2H, -C*H*$_2$), 5.23 (m, 1H, N*H*), 7.55 (s, 1H, aromatic proton), 7.89 (s, 1H, aromatic proton), 8.63 (d, 2H, pyridine protons), 8.62 (d, 2H, pyridine protons) ppm. MS (EI): *m/z* $[M]^+$: 401.12.

6,7-dichloro-4-(pyridin-4-yl)-N-(2-(pyrrolidin-1-yl)ethyl)phthalazin-1-amine (RM07, 1f)

^{1}H NMR (400MHz, $CDCl_3$) δ: 1.99 (m, 4H, 2x -C*H*$_2$ pyrrolidine), 3.06 (m, 4H, 2x -C*H*$_2$ pyrrolidine), 3.26 (m, 2H, , -C*H*$_2$), 4.01 (m, 2H, , -C*H*$_2$), 4.94 (s, 1H, N*H*), 7.54 (s, 1H, aromatic proton), 7.89 (d, 2H, pyridine protons), 8.38 (s, 1H, aromatic proton), 8.73 (d, 2H, pyridine protons) ppm. MS (EI): *m/z* $[M]^+$: 387.10.

6,7-dichloro-N-((1-ethylpyrrolidin-2-yl)methyl)-4-(pyridin-4-yl)phthalazin-1-amine (RM08, 1g)

^{1}H NMR (400MHz, $CDCl_3$) δ: 1.17 (t, 3H, -CH_2CH_3), 1.94 (q, 2H, -C*H*$_2$$CH_3$), 2.23 (m, 2H, -C*H*$_2$ pyrrolidine), 3.17 (m, 2H, -C*H*$_2$ pyrrolidine), 3.75 (m, 2H, -C*H*$_2$ pyrrolidine), 3.92 (m, 2H, -C*H*$_2$ pyrrolidine), 4.21 (d, 2H, -C*H*$_2$NH), 4.61 (t, 1H, -CH_2N*H*), 7.57 (d, 2H, pyridine protons), 7.89 (s, 1H, aromatic proton), 8.61 (s, 1H, aromatic proton), 8.74 (d, 2H, pyridine protons) ppm. MS (EI): *m/z* $[M]^+$: 401.12.

6,7-dichloro-N-(2-methyl-1-(pyrrolidin-1-yl)propan-2-yl)-4-(pyridin-4-yl)phthalazin-1-amine (RM09, 1h)

^{1}H NMR (400MHz, $CDCl_3$) δ: 1.18 (s, 6H, 2x –C*H*$_3$), 1.94 (m, 4H, 2x –C*H*$_2$ pyrrolidine), 2.03 (m, 2H, –C*H*$_2$ pyrrolidine), 2.15 (m, 2H, –C*H*$_2$ pyrrolidine), 2.47 (s, 2H, -C*H*$_2$-Pyr), 5.28 (s, 1H, N*H*), 7.88 (s, 2h, aromatic protons), 7.99 (d, 2H, pyridine protons), 8.75 (d, 2H, pyridine protons) ppm. MS (EI): *m/z* $[M]^+$: 415.13.

6,7-dichloro-N-((4-methylmorpholin-3-yl)methyl)-4-(pyridin-4-yl)phthalazin-1-amine (RM010, 1i)

^{1}H NMR (400MHz, $CDCl_3$) δ: 2.36 (s, 3H, -CH_3), 2.46 (m, 2H, –CH_2 morpholine), 2.57 (m, 2H, –CH_2 morpholine), 2.81 (d, 2H, –CH_2 morpholine), 3.65 (t, 2H, -CH_2NH), 6.14 (s, 1H, N*H*), 7.54 (s, 2H, aromatic protons), 7.94 (d, 2H, pyridine protons), 8.74 (d, 2H, pyridine protons) ppm. MS (EI): *m/z* $[M]^+$: 403.10.

6,7-dichloro-N-(2-morpholinoethyl)-4-(pyridin-4-yl)phthalazin-1-amine (RM011, 1j)

^{1}H NMR (400MHz, $CDCl_3$) δ: 2.53 (m, 4H,2x -CH_2 morpholine), 2.74 (m, 4H,2x -CH_2 morpholine), 3.75 (dt, 4H, -CH_2CH_2), 6.15 (s, 1H, N*H*), 7.54 (s, 2H, aromatic protons), 7.93 (d, 2H, pyridine protons), 8.74 (d, 2H, pyridine protons) ppm. MS (EI): *m/z* $[M]^+$: 403.10.

6,7-dichloro-N-(3-morpholinobutan-2-yl)-4-(pyridin-4-yl)phthalazin-1-amine (RM012, 1k)

^{1}H NMR (400MHz, $CDCl_3$) δ: 1.13 (d, 3H, -CH_3), 1.44 (d, 3H, -CH_3), 2.04 (s, 1H, -C*H*), 2.69 (s, 1H, -C*H*), 3.58 (m, 2H, -CH_2CH_2 morpholine), 3.67 (m, 4H, -CH_2CH_2 morpholine), 3.86 (m, 2H, -CH_2CH_2 morpholine), 5.28 (s, 1H, N*H*), 7.57 (d, 2H, pyridine protons), 7.97 (s, 2H, aromatic protons), 8.74 (d, 2H, pyridine protons) ppm. MS (EI): *m/z* $[M]^+$: 431.13.

tert-butyl (R)-3-((6,7-dichloro-4-(pyridin-4-yl)phthalazin-1-yl)amino)pyrrolidine-1-carboxylate (RM013, 1l)

^{1}H NMR (400MHz, $CDCl_3$) δ: 1.41 (s, 9H, 3x -CH_3), 2.34 (m, 2H, -CH_2 pyrrolidine), 3.53 (m, 2H, -CH_2 pyrrolidine), 4.94 (s, 2H, -CH_2 pyrrolidine) 5.49 (s, 1H, N*H*), 7.55 (d, 2H, pyridine protons), 8.04 (s, 2H, aromatic protons), 8.75 (d, 2H, pyridine protons) ppm. MS (EI): *m/z* $[M]^+$: 459.12.

6,7-dichloro-N-(piperidin-3-yl)-4-(pyridin-4-yl)phthalazin-1-amine (RM014, 1m)

^{1}H NMR (400MHz, $CDCl_3$) δ: 1.75-1.81 (m, 2H, CH_2 piperidine), 2.04 (m, 4H, 2x CH_2 piperidine), 2.19 (m, 2H, CH_2 piperidine), 2.88 (td, 1H, -C*H* piperidine), 3.48 (m, 1H, N*H* piperidine), 5.04 (d, 1H, N*H*), 7.54 (d, 2H, pyridine protons), 7.90 (s, 1H, aromatic proton), 8.74 (d, 2H, pyridine protons), 8.81 (s, 1H, aromatic proton) ppm. MS (EI): *m/z* $[M]^+$: 372.09.

5.7 Methods

5.7.1 Gene expression (luciferase expression)

HEK293 cell model of FRDA present two variants:

1) A wild-type (WT) model that is a mimic of a healthy patient with normal levels of frataxin. This model was achieved by transforming the cells with a pBac-FXN-Luc fusion vector with 6 GAA repeats;

2) A disease model, where the cells were transformed with a pBac-FXN-Luc fusion vector with 310 GAA repeats. This was done in order to mimic the repeat expansion observed in FRDA (Fig. 5.8).

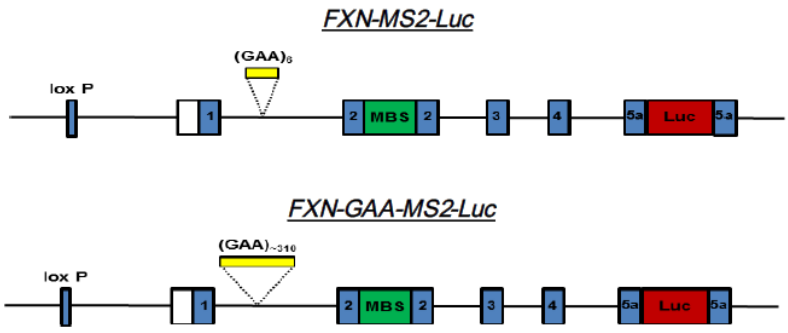

Figure 5.8: The FXN-MS2-Luc cell lines built in a HEK 293 background express a human pBAC-FXN-Luc fusion vector with either 6 GAA repeats (FXN-MS2-Luc) or 310 GAA repeats (FXN-GAA-MS2-Luc). [535]

These cells expressed a modified frataxin-luciferase fusion protein, and obviously the WT cells express normal levels of FXN and the diseased cells expressing significantly reduced levels. These levels were measured as a function of luciferase expression, as this is directly correlated to the amount of frataxin expression. A-196 was the positive control, and SGC2043 (A-197) was the negative control.

In detail, to assay luciferase expression, 1.5 × 106 cells of FXN-MS2-Luc and FXN-GAA-MS2-Luc clonal cell lines were used as described in the literature. [536] Cells were seeded in 6-well plates, washed in phosphate-buffered saline (PBS) and lysed in lysis buffer (25 mM Tris–PO_4, pH 7.8, 2 mM CDTA, 10% glycerol and 1% Triton-X 100) for 20 min at 4°C. Seventy-five microlitres of lysates were mixed with 100 µl of luciferase assay buffer (15 mM $MgSO_4$, 15 mM KPO_4, pH 7.8, 4 mM ethylene glycol tetraacetic acid, pH 7.8, 2 mM adenosine 5′-triphosphate and 2 mM dithiothreitol) and 50 µl of D-luciferin (0.3 mg/ml). The relative light units of luciferase of each cell line were determined using the Dynex MLX 96 Well Plate Luminometer and were normalised by total protein concentration, determined using bicinchoninic acid solution (BCA, Sigma). [535]

5.8 Biological evaluation, results, and discussion

The final compounds **1a-m** and **2c** were tested against a HEK293 cell model of FRDA. Therefore, the ability of potentially Suv420 inhibitors to reactivate gene expression was tested on a gene reporter model containing a modified frataxin-luciferase fusion protein. The Luciferase signal is measured in the cells incubated over 6 days in the presence of the inhibitor at 5 µM and normalised with the value of the signal from untreated cells. The measured signal is expressed in terms of “fold induction”, that is the ratio between the fluorescence signal coming from the tested compounds and the signal coming from the control. The fluorescence was normalised to total protein concentration as determined by Bicinchoninic acid (BCA) assay. The lead compound A-196 and the inhibitor SGC2043 are used as reference compounds. Frataxin expression was measured as a function of relative luciferase expression, with the WT at 1.0, and the vehicle (DMSO) at 0.6.

Table 5.2: Luciferase reactivation fold (RF) in HEK293 cell model of FRDA after 6 days treatment [a]

Lab code	Compound	Chemical structure	Reactivation fold of luciferase gene reporter (RF)
SGC2043	-	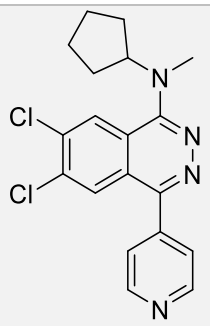	0.65
-	**A-196**	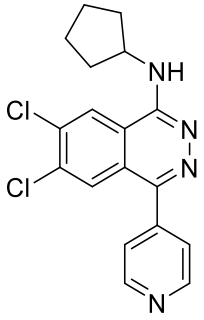	1.15
RM01	**1a**	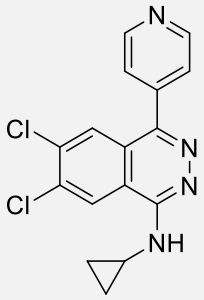	ND
RM02	**1b**	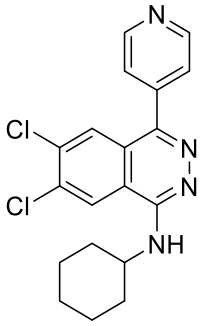	1.20

RM03	**1c**	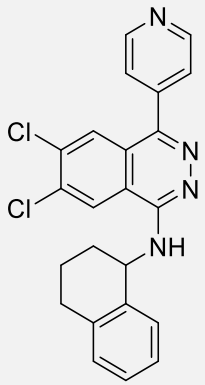	0.65
RM04	**2c**	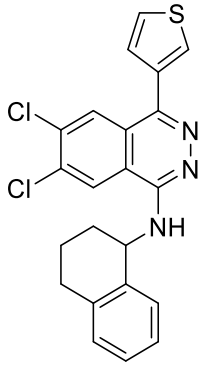	ND
RM05	**1d**	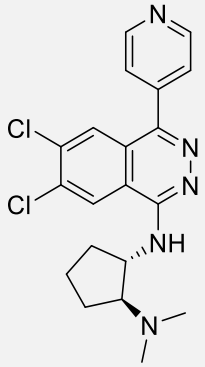	ND
RM06	**1e**	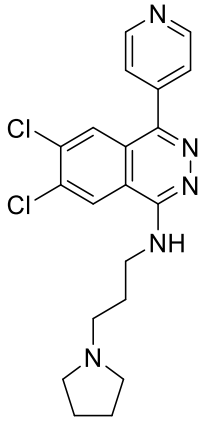	0.50

RM07	**1f**	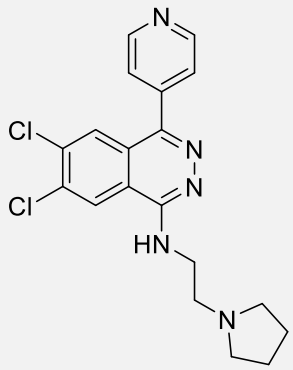	0.45
RM08	**1g**	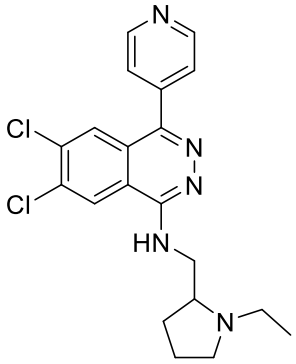	0.45
RM09	**1h**	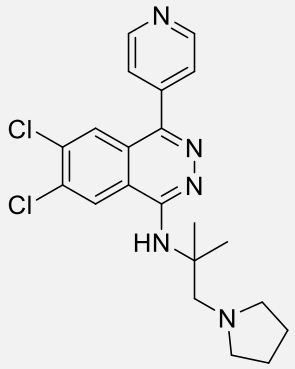	ND
RM010	**1i**	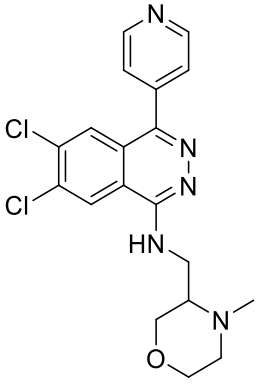	0.50

RM011	**1j**	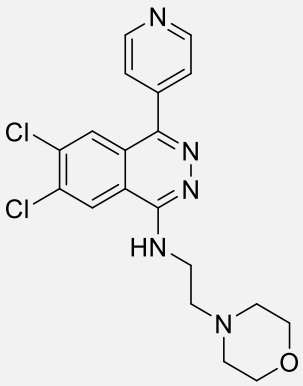	0.50
RM012	**1k**	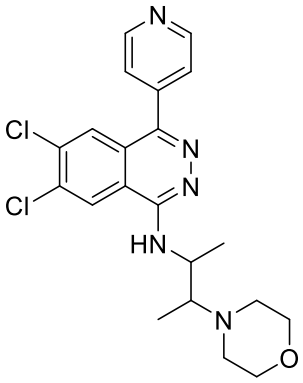	0.45
RM013	**1l**	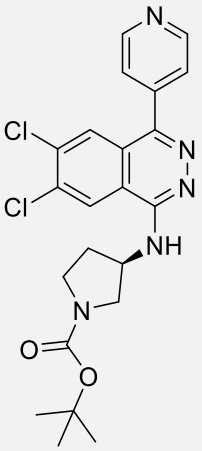	0.70
RM014	**1m**	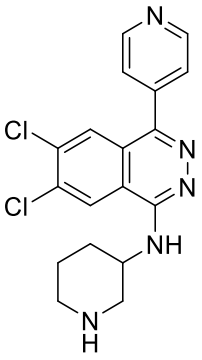	0.50
[a] **: The value reported in red colour indicate the most interesting result.**			

These results can be interpreted by comparing the values relative to the newly synthesised compounds with the data for the lead compound **A-196** and **SGC2043**. Among the tested compounds, only **1b** (**RM02**) demonstrated to be more effective than the reference compound A-196 at the concentration of

5 µM after 6 days of treatment with a luciferase fold reactivation of 1.20. The other compounds, unfortunately, showed no increase in frataxin expression beyond that one induced by the vehicle DMSO. Preliminary data for the evaluation of the cytotoxicity (adenylate kinase scores) showed that our compounds are probable non-toxic to the cells. However, no final and presentable data are available yet.

5.9 Conclusion and Future Perspectives

SGC in Toronto is still evaluating the *in vitro* inhibitory activity of our newly synthesized compounds on Suv420. Afterwards, our collaborators at the Department of Physiology, Anatomy, and Genetics at the University of Oxford, will assess the activity of our compounds regarding their potential to lead to increased FXN levels in patient-derived cell assays. However, among the newly synthesised A-196 derivatives tested by luciferase assay, only compound **1b (RM02)** was found to reactivate FXN gene expression, thus increasing frataxin protein levels.

Our future plans to continue to work at the C4 position of the phthalazine ring by insertion of fluorinated or spirocyclic or more stable amines to improve the metabolic stability and H-bonding capacity of aniline NH, thus ameliorating the pharmacokinetic and pharmacodynamic parameters of the lead compound A-196 (Fig. 5.9).

The discovery of a potent and selective Suv420 inhibitor would be a useful tool to understand better the potential biological role of Suv420me in genomic integrity and in neurological disorders. Therefore, we expected that our study will provide new insights into the pathogenesis of FRDA, helping the research in the discovery of an effective treatment for FRDA disorder.

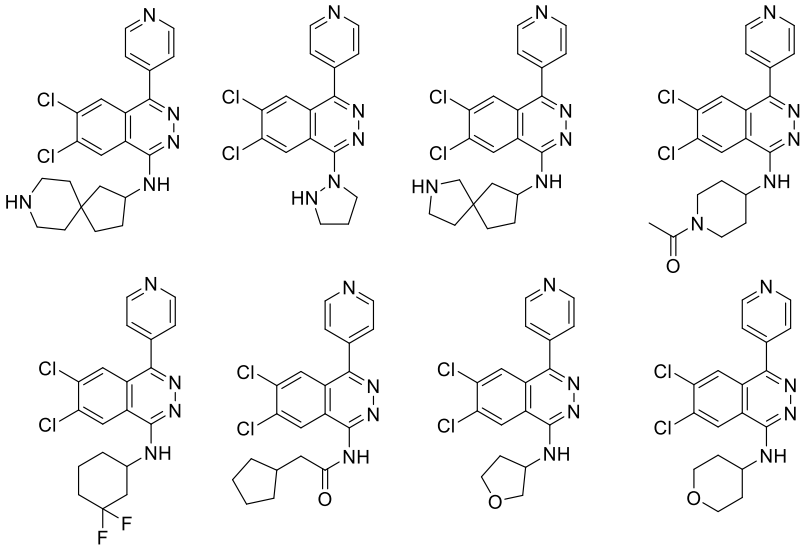

Figure 5.9: Development of novel A-196 derivatives as Suv420 inhibitors.

Bibliography

1. Goldberg, A.D., C.D. Allis, and E. Bernstein, *Epigenetics: a landscape takes shape.* Cell, 2007. **128**(4): p. 635-8.
2. Kouzarides, T., *Chromatin modifications and their function.* Cell, 2007. **128**(4): p. 693-705.
3. Rothbart, S.B. and B.D. Strahl, *Interpreting the language of histone and DNA modifications.* Biochim Biophys Acta, 2014. **1839**(8): p. 627-43.
4. Koh, K.P. and A. Rao, *DNA methylation and methylcytosine oxidation in cell fate decisions.* Curr Opin Cell Biol, 2013. **25**(2): p. 152-61.
5. Biterge, B. and R. Schneider, *Histone variants: key players of chromatin.* Cell Tissue Res, 2014. **356**(3): p. 457-66.
6. Hargreaves, D.C. and G.R. Crabtree, *ATP-dependent chromatin remodeling: genetics, genomics and mechanisms.* Cell Res, 2011. **21**(3): p. 396-420.
7. Wilusz, J.E., H. Sunwoo, and D.L. Spector, *Long noncoding RNAs: functional surprises from the RNA world.* Genes Dev, 2009. **23**(13): p. 1494-504.
8. Meaney, M.J., *Epigenetics and the biological definition of gene x environment interactions.* Child Dev, 2010. **81**(1): p. 41-79.
9. Langevin, S.M., et al., *The influence of aging, environmental exposures and local sequence features on the variation of DNA methylation in blood.* Epigenetics, 2011. **6**(7): p. 908-19.
10. Niculescu, M.D. and S.H. Zeisel, *Diet, methyl donors and DNA methylation: interactions between dietary folate, methionine and choline.* J Nutr, 2002. **132**(8 Suppl): p. 2333S-2335S.
11. Jenuwein, T. and C.D. Allis, *Translating the histone code.* Science, 2001. **293**(5532): p. 1074-80.
12. Kebede, A.F., R. Schneider, and S. Daujat, *Novel types and sites of histone modifications emerge as players in the transcriptional regulation contest.* FEBS J, 2015. **282**(9): p. 1658-74.
13. Lawrence, M., S. Daujat, and R. Schneider, *Lateral Thinking: How Histone Modifications Regulate Gene Expression.* Trends Genet, 2016. **32**(1): p. 42-56.
14. Helin, K. and D. Dhanak, *Chromatin proteins and modifications as drug targets.* Nature, 2013. **502**(7472): p. 480-8.
15. Marfella, C.G. and A.N. Imbalzano, *The Chd family of chromatin remodelers.* Mutat Res, 2007. **618**(1-2): p. 30-40.
16. Lessard, J., et al., *An essential switch in subunit composition of a chromatin remodeling complex during neural development.* Neuron, 2007. **55**(2): p. 201-15.
17. Boyer, L.A., R.R. Latek, and C.L. Peterson, *The SANT domain: a unique histone-tail-binding module?* Nat Rev Mol Cell Biol, 2004. **5**(2): p. 158-63.
18. Bao, Y. and X. Shen, *INO80 subfamily of chromatin remodeling complexes.* Mutat Res, 2007. **618**(1-2): p. 18-29.
19. Clapier, C.R. and B.R. Cairns, *The biology of chromatin remodeling complexes.* Annu Rev Biochem, 2009. **78**: p. 273-304.
20. Allfrey, V.G., R. Faulkner, and A.E. Mirsky, *Acetylation and Methylation of Histones and Their Possible Role in the Regulation of Rna Synthesis.* Proc Natl Acad Sci U S A, 1964. **51**: p. 786-94.
21. Luger, K., et al., *Crystal structure of the nucleosome core particle at 2.8 A resolution.* Nature, 1997. **389**(6648): p. 251-60.
22. Kleefstra, T., et al., *Disruption of an EHMT1-associated chromatin-modification module causes intellectual disability.* Am J Hum Genet, 2012. **91**(1): p. 73-82.
23. Hecht, A., et al., *Histone H3 and H4 N-termini interact with SIR3 and SIR4 proteins: a molecular model for the formation of heterochromatin in yeast.* Cell, 1995. **80**(4): p. 583-92.
24. Sterner, D.E. and S.L. Berger, *Acetylation of histones and transcription-related factors.* Microbiol Mol Biol Rev, 2000. **64**(2): p. 435-59.
25. Rossetto, D., N. Avvakumov, and J. Cote, *Histone phosphorylation: a chromatin modification involved in diverse nuclear events.* Epigenetics, 2012. **7**(10): p. 1098-108.

26. Lau, P.N. and P. Cheung, *Elucidating combinatorial histone modifications and crosstalks by coupling histone-modifying enzyme with biotin ligase activity.* Nucleic Acids Res, 2013. **41**(3): p. e49.
27. Shi, Y., et al., *Histone demethylation mediated by the nuclear amine oxidase homolog LSD1.* Cell, 2004. **119**(7): p. 941-53.
28. Biggar, K.K. and S.S. Li, *Non-histone protein methylation as a regulator of cellular signalling and function.* Nat Rev Mol Cell Biol, 2015. **16**(1): p. 5-17.
29. Rea, S., et al., *Regulation of chromatin structure by site-specific histone H3 methyltransferases.* Nature, 2000. **406**(6796): p. 593-9.
30. McGrath, J. and P. Trojer, *Targeting histone lysine methylation in cancer.* Pharmacol Ther, 2015. **150**: p. 1-22.
31. Fischle, W., Y. Wang, and C.D. Allis, *Binary switches and modification cassettes in histone biology and beyond.* Nature, 2003. **425**(6957): p. 475-9.
32. Lachner, M., R.J. O'Sullivan, and T. Jenuwein, *An epigenetic road map for histone lysine methylation.* J Cell Sci, 2003. **116**(Pt 11): p. 2117-24.
33. Vaquero, A., A. Loyola, and D. Reinberg, *The constantly changing face of chromatin.* Sci Aging Knowledge Environ, 2003. **2003**(14): p. RE4.
34. Plath, K., et al., *Role of histone H3 lysine 27 methylation in X inactivation.* Science, 2003. **300**(5616): p. 131-5.
35. Peters, A.H., et al., *Partitioning and plasticity of repressive histone methylation states in mammalian chromatin.* Mol Cell, 2003. **12**(6): p. 1577-89.
36. Schotta, G., et al., *A silencing pathway to induce H3-K9 and H4-K20 trimethylation at constitutive heterochromatin.* Genes Dev, 2004. **18**(11): p. 1251-62.
37. Fraga, M.F., et al., *Loss of acetylation at Lys16 and trimethylation at Lys20 of histone H4 is a common hallmark of human cancer.* Nat Genet, 2005. **37**(4): p. 391-400.
38. Nishioka, K., et al., *PR-Set7 is a nucleosome-specific methyltransferase that modifies lysine 20 of histone H4 and is associated with silent chromatin.* Mol Cell, 2002. **9**(6): p. 1201-13.
39. Fang, J., et al., *Purification and functional characterization of SET8, a nucleosomal histone H4-lysine 20-specific methyltransferase.* Curr Biol, 2002. **12**(13): p. 1086-99.
40. Hahn, M., et al., *Suv4-20h2 mediates chromatin compaction and is important for cohesin recruitment to heterochromatin.* Genes Dev, 2013. **27**(8): p. 859-72.
41. Jorgensen, S., G. Schotta, and C.S. Sorensen, *Histone H4 lysine 20 methylation: key player in epigenetic regulation of genomic integrity.* Nucleic Acids Res, 2013. **41**(5): p. 2797-806.
42. Nishioka, K., et al., *Set9, a novel histone H3 methyltransferase that facilitates transcription by precluding histone tail modifications required for heterochromatin formation.* Genes Dev, 2002. **16**(4): p. 479-89.
43. Tsang, L.W., N. Hu, and D.A. Underhill, *Comparative analyses of SUV420H1 isoforms and SUV420H2 reveal differences in their cellular localization and effects on myogenic differentiation.* PLoS One, 2010. **5**(12): p. e14447.
44. Yang, H., et al., *Preferential dimethylation of histone H4 lysine 20 by Suv4-20.* J Biol Chem, 2008. **283**(18): p. 12085-92.
45. Sarg, B., et al., *Postsynthetic trimethylation of histone H4 at lysine 20 in mammalian tissues is associated with aging.* J Biol Chem, 2002. **277**(42): p. 39195-201.
46. Wu, H., et al., *Crystal structures of the human histone H4K20 methyltransferases SUV420H1 and SUV420H2.* FEBS Lett, 2013. **587**(23): p. 3859-68.
47. Dillon, S.C., et al., *The SET-domain protein superfamily: protein lysine methyltransferases.* Genome Biol, 2005. **6**(8): p. 227.
48. Oda, H., et al., *Monomethylation of histone H4-lysine 20 is involved in chromosome structure and stability and is essential for mouse development.* Mol Cell Biol, 2009. **29**(8): p. 2278-95.
49. Huen, M.S., et al., *Direct interaction between SET8 and proliferating cell nuclear antigen couples H4-K20 methylation with DNA replication.* J Biol Chem, 2008. **283**(17): p. 11073-7.
50. Sakaguchi, A. and R. Steward, *Aberrant monomethylation of histone H4 lysine 20 activates the DNA damage checkpoint in Drosophila melanogaster.* J Cell Biol, 2007. **176**(2): p. 155-62.

51. Tardat, M., et al., *PR-Set7-dependent lysine methylation ensures genome replication and stability through S phase.* J Cell Biol, 2007. **179**(7): p. 1413-26.
52. Houston, S.I., et al., *Catalytic function of the PR-Set7 histone H4 lysine 20 monomethyltransferase is essential for mitotic entry and genomic stability.* J Biol Chem, 2008. **283**(28): p. 19478-88.
53. Jorgensen, S., et al., *The histone methyltransferase SET8 is required for S-phase progression.* J Cell Biol, 2007. **179**(7): p. 1337-45.
54. Schotta, G., et al., *A chromatin-wide transition to H4K20 monomethylation impairs genome integrity and programmed DNA rearrangements in the mouse.* Genes Dev, 2008. **22**(15): p. 2048-61.
55. Abbas, T., et al., *CRL4(Cdt2) regulates cell proliferation and histone gene expression by targeting PR-Set7/Set8 for degradation.* Mol Cell, 2010. **40**(1): p. 9-21.
56. Centore, R.C., et al., *CRL4(Cdt2)-mediated destruction of the histone methyltransferase Set8 prevents premature chromatin compaction in S phase.* Mol Cell, 2010. **40**(1): p. 22-33.
57. Jorgensen, S., et al., *SET8 is degraded via PCNA-coupled CRL4(CDT2) ubiquitylation in S phase and after UV irradiation.* J Cell Biol, 2011. **192**(1): p. 43-54.
58. Trojer, P., et al., *L3MBTL1, a histone-methylation-dependent chromatin lock.* Cell, 2007. **129**(5): p. 915-28.
59. Liu, W., et al., *PHF8 mediates histone H4 lysine 20 demethylation events involved in cell cycle progression.* Nature, 2010. **466**(7305): p. 508-12.
60. Gurvich, N., et al., *L3MBTL1 polycomb protein, a candidate tumor suppressor in del(20q12) myeloid disorders, is essential for genome stability.* Proc Natl Acad Sci U S A, 2010. **107**(52): p. 22552-7.
61. Lu, X., et al., *The effect of H3K79 dimethylation and H4K20 trimethylation on nucleosome and chromatin structure.* Nat Struct Mol Biol, 2008. **15**(10): p. 1122-4.
62. Wu, S., et al., *Dynamic regulation of the PR-Set7 histone methyltransferase is required for normal cell cycle progression.* Genes Dev, 2010. **24**(22): p. 2531-42.
63. Kuo, A.J., et al., *The BAH domain of ORC1 links H4K20me2 to DNA replication licensing and Meier-Gorlin syndrome.* Nature, 2012. **484**(7392): p. 115-9.
64. Tardat, M., et al., *The histone H4 Lys 20 methyltransferase PR-Set7 regulates replication origins in mammalian cells.* Nat Cell Biol, 2010. **12**(11): p. 1086-93.
65. Bouwman, P., et al., *53BP1 loss rescues BRCA1 deficiency and is associated with triple-negative and BRCA-mutated breast cancers.* Nat Struct Mol Biol, 2010. **17**(6): p. 688-95.
66. Densham, R.M., et al., *Human BRCA1-BARD1 ubiquitin ligase activity counteracts chromatin barriers to DNA resection.* Nat Struct Mol Biol, 2016. **23**(7): p. 647-55.
67. Simonetta, M., et al., *H4K20me2 distinguishes pre-replicative from post-replicative chromatin to appropriately direct DNA repair pathway choice by 53BP1-RIF1-MAD2L2.* Cell Cycle, 2018. **17**(1): p. 124-136.
68. Eliezer, Y., et al., *The direct interaction between 53BP1 and MDC1 is required for the recruitment of 53BP1 to sites of damage.* J Biol Chem, 2009. **284**(1): p. 426-35.
69. Wang, B., et al., *53BP1, a mediator of the DNA damage checkpoint.* Science, 2002. **298**(5597): p. 1435-8.
70. Ward, I.M., et al., *Accumulation of checkpoint protein 53BP1 at DNA breaks involves its binding to phosphorylated histone H2AX.* J Biol Chem, 2003. **278**(22): p. 19579-82.
71. Benetti, R., et al., *Suv4-20h deficiency results in telomere elongation and derepression of telomere recombination.* J Cell Biol, 2007. **178**(6): p. 925-36.
72. Paquin, K.L. and N.G. Howlett, *Understanding the Histone DNA Repair Code: H4K20me2 Makes Its Mark.* Mol Cancer Res, 2018.
73. Pellegrino, S., et al., *Replication-Coupled Dilution of H4K20me2 Guides 53BP1 to Pre-replicative Chromatin.* Cell Rep, 2017. **19**(9): p. 1819-1831.
74. Saredi, G., et al., *H4K20me0 marks post-replicative chromatin and recruits the TONSL-MMS22L DNA repair complex.* Nature, 2016. **534**(7609): p. 714-718.

75. Pryde, F., et al., *53BP1 exchanges slowly at the sites of DNA damage and appears to require RNA for its association with chromatin.* J Cell Sci, 2005. **118**(Pt 9): p. 2043-55.
76. Fu, H., et al., *Methylation of histone H3 on lysine 79 associates with a group of replication origins and helps limit DNA replication once per cell cycle.* PLoS Genet, 2013. **9**(6): p. e1003542.
77. O'Sullivan, R.J., et al., *Reduced histone biosynthesis and chromatin changes arising from a damage signal at telomeres.* Nat Struct Mol Biol, 2010. **17**(10): p. 1218-25.
78. Margueron, R. and D. Reinberg, *The Polycomb complex PRC2 and its mark in life.* Nature, 2011. **469**(7330): p. 343-9.
79. Shaver, S., et al., *Origin of the polycomb repressive complex 2 and gene silencing by an E(z) homolog in the unicellular alga Chlamydomonas.* Epigenetics, 2010. **5**(4): p. 301-12.
80. Scheuermann, J.C., et al., *Histone H2A deubiquitinase activity of the Polycomb repressive complex PR-DUB.* Nature, 2010. **465**(7295): p. 243-7.
81. Klymenko, T., et al., *A Polycomb group protein complex with sequence-specific DNA-binding and selective methyl-lysine-binding activities.* Genes Dev, 2006. **20**(9): p. 1110-22.
82. Czermin, B., et al., *Drosophila enhancer of Zeste/ESC complexes have a histone H3 methyltransferase activity that marks chromosomal Polycomb sites.* Cell, 2002. **111**(2): p. 185-96.
83. Cao, R., et al., *Role of histone H3 lysine 27 methylation in Polycomb-group silencing.* Science, 2002. **298**(5595): p. 1039-43.
84. Muller, J., et al., *Histone methyltransferase activity of a Drosophila Polycomb group repressor complex.* Cell, 2002. **111**(2): p. 197-208.
85. Herz, H.M., A. Garruss, and A. Shilatifard, *SET for life: biochemical activities and biological functions of SET domain-containing proteins.* Trends Biochem Sci, 2013. **38**(12): p. 621-39.
86. Cao, R. and Y. Zhang, *SUZ12 is required for both the histone methyltransferase activity and the silencing function of the EED-EZH2 complex.* Mol Cell, 2004. **15**(1): p. 57-67.
87. Kaneko, S., et al., *Interactions between JARID2 and noncoding RNAs regulate PRC2 recruitment to chromatin.* Mol Cell, 2014. **53**(2): p. 290-300.
88. Kim, H., K. Kang, and J. Kim, *AEBP2 as a potential targeting protein for Polycomb Repression Complex PRC2.* Nucleic Acids Res, 2009. **37**(9): p. 2940-50.
89. Schmitges, F.W., et al., *Histone methylation by PRC2 is inhibited by active chromatin marks.* Mol Cell, 2011. **42**(3): p. 330-41.
90. Danishuddin, et al., *Polycomb repressive complex 2 inhibitors: emerging epigenetic modulators.* Drug Discov Today, 2018.
91. Ciferri, C., et al., *Molecular architecture of human polycomb repressive complex 2.* Elife, 2012. **1**: p. e00005.
92. Jiao, L. and X. Liu, *Structural basis of histone H3K27 trimethylation by an active polycomb repressive complex 2.* Science, 2015. **350**(6258): p. aac4383.
93. Brooun, A., et al., *Polycomb repressive complex 2 structure with inhibitor reveals a mechanism of activation and drug resistance.* Nat Commun, 2016. **7**: p. 11384.
94. Margueron, R., et al., *Ezh1 and Ezh2 maintain repressive chromatin through different mechanisms.* Mol Cell, 2008. **32**(4): p. 503-18.
95. Justin, N., et al., *Structural basis of oncogenic histone H3K27M inhibition of human polycomb repressive complex 2.* Nat Commun, 2016. **7**: p. 11316.
96. Han, Z., et al., *Structural basis of EZH2 recognition by EED.* Structure, 2007. **15**(10): p. 1306-15.
97. Moritz, L.E. and R.C. Trievel, *Structure, mechanism, and regulation of polycomb repressive complex 2.* J Biol Chem, 2017.
98. Graham, S.E., S.E. Tweedy, and H.A. Carlson, *Dynamic behavior of the post-SET loop region of NSD1: Implications for histone binding and drug development.* Protein Sci, 2016. **25**(5): p. 1021-9.
99. Kim, K.H. and C.W. Roberts, *Targeting EZH2 in cancer.* Nat Med, 2016. **22**(2): p. 128-34.
100. Xu, C. and J. Min, *Structure and function of WD40 domain proteins.* Protein Cell, 2011. **2**(3): p. 202-14.

101. Margueron, R., et al., *Role of the polycomb protein EED in the propagation of repressive histone marks.* Nature, 2009. **461**(7265): p. 762-7.
102. Yun, M., et al., *Readers of histone modifications.* Cell Res, 2011. **21**(4): p. 564-78.
103. Adams-Cioaba, M.A. and J. Min, *Structure and function of histone methylation binding proteins.* Biochem Cell Biol, 2009. **87**(1): p. 93-105.
104. Jacobs, S.A. and S. Khorasanizadeh, *Structure of HP1 chromodomain bound to a lysine 9-methylated histone H3 tail.* Science, 2002. **295**(5562): p. 2080-3.
105. Xu, C., et al., *Binding of different histone marks differentially regulates the activity and specificity of polycomb repressive complex 2 (PRC2).* Proc Natl Acad Sci U S A, 2010. **107**(45): p. 19266-71.
106. Ketel, C.S., et al., *Subunit contributions to histone methyltransferase activities of fly and worm polycomb group complexes.* Mol Cell Biol, 2005. **25**(16): p. 6857-68.
107. Rai, A.N., et al., *Elements of the polycomb repressor SU(Z)12 needed for histone H3-K27 methylation, the interface with E(Z), and in vivo function.* Mol Cell Biol, 2013. **33**(24): p. 4844-56.
108. Score, J., et al., *Inactivation of polycomb repressive complex 2 components in myeloproliferative and myelodysplastic/myeloproliferative neoplasms.* Blood, 2012. **119**(5): p. 1208-13.
109. Veneti, Z., K.K. Gkouskou, and A.G. Eliopoulos, *Polycomb Repressor Complex 2 in Genomic Instability and Cancer.* Int J Mol Sci, 2017. **18**(8).
110. Zhang, Y., et al., *Comment on "Structural basis of histone H3K27 trimethylation by an active polycomb repressive complex 2".* Science, 2016. **354**(6319): p. 1543.
111. Varambally, S., et al., *The polycomb group protein EZH2 is involved in progression of prostate cancer.* Nature, 2002. **419**(6907): p. 624-9.
112. Han Li, C. and Y. Chen, *Targeting EZH2 for cancer therapy: progress and perspective.* Curr Protein Pept Sci, 2015. **16**(6): p. 559-70.
113. Suva, M.L., et al., *EZH2 is essential for glioblastoma cancer stem cell maintenance.* Cancer Res, 2009. **69**(24): p. 9211-8.
114. Chang, C.J., et al., *EZH2 promotes expansion of breast tumor initiating cells through activation of RAF1-beta-catenin signaling.* Cancer Cell, 2011. **19**(1): p. 86-100.
115. Lee, J., et al., *Epigenetic-mediated dysfunction of the bone morphogenetic protein pathway inhibits differentiation of glioblastoma-initiating cells.* Cancer Cell, 2008. **13**(1): p. 69-80.
116. Morin, R.D., et al., *Somatic mutations altering EZH2 (Tyr641) in follicular and diffuse large B-cell lymphomas of germinal-center origin.* Nat Genet, 2010. **42**(2): p. 181-5.
117. Sneeringer, C.J., et al., *Coordinated activities of wild-type plus mutant EZH2 drive tumor-associated hypertrimethylation of lysine 27 on histone H3 (H3K27) in human B-cell lymphomas.* Proc Natl Acad Sci U S A, 2010. **107**(49): p. 20980-5.
118. Beguelin, W., et al., *EZH2 is required for germinal center formation and somatic EZH2 mutations promote lymphoid transformation.* Cancer Cell, 2013. **23**(5): p. 677-92.
119. Majer, C.R., et al., *A687V EZH2 is a gain-of-function mutation found in lymphoma patients.* FEBS Lett, 2012. **586**(19): p. 3448-51.
120. McCabe, M.T., et al., *Mutation of A677 in histone methyltransferase EZH2 in human B-cell lymphoma promotes hypertrimethylation of histone H3 on lysine 27 (H3K27).* Proc Natl Acad Sci U S A, 2012. **109**(8): p. 2989-94.
121. Lewis, P.W., et al., *Inhibition of PRC2 activity by a gain-of-function H3 mutation found in pediatric glioblastoma.* Science, 2013. **340**(6134): p. 857-61.
122. Bender, S., et al., *Reduced H3K27me3 and DNA hypomethylation are major drivers of gene expression in K27M mutant pediatric high-grade gliomas.* Cancer Cell, 2013. **24**(5): p. 660-72.
123. Chan, K.M., et al., *The histone H3.3K27M mutation in pediatric glioma reprograms H3K27 methylation and gene expression.* Genes Dev, 2013. **27**(9): p. 985-90.
124. Alford, S.H., et al., *Increased risk for distant metastasis in patients with familial early-stage breast cancer and high EZH2 expression.* Breast Cancer Res Treat, 2012. **132**(2): p. 429-37.
125. Behrens, C., et al., *EZH2 protein expression associates with the early pathogenesis, tumor progression, and prognosis of non-small cell lung carcinoma.* Clin Cancer Res, 2013. **19**(23): p. 6556-65.

126. Yamada, A., et al., *Aberrant expression of EZH2 is associated with a poor outcome and P53 alteration in squamous cell carcinoma of the esophagus.* Int J Oncol, 2011. **38**(2): p. 345-53.
127. Rao, Z.Y., et al., *EZH2 supports ovarian carcinoma cell invasion and/or metastasis via regulation of TGF-beta1 and is a predictor of outcome in ovarian carcinoma patients.* Carcinogenesis, 2010. **31**(9): p. 1576-83.
128. Lee, H.W. and M. Choe, *Expression of EZH2 in renal cell carcinoma as a novel prognostic marker.* Pathol Int, 2012. **62**(11): p. 735-41.
129. Kondo, Y., et al., *Alterations of DNA methylation and histone modifications contribute to gene silencing in hepatocellular carcinomas.* Hepatol Res, 2007. **37**(11): p. 974-83.
130. Matsukawa, Y., et al., *Expression of the enhancer of zeste homolog 2 is correlated with poor prognosis in human gastric cancer.* Cancer Sci, 2006. **97**(6): p. 484-91.
131. Raman, J.D., et al., *Increased expression of the polycomb group gene, EZH2, in transitional cell carcinoma of the bladder.* Clin Cancer Res, 2005. **11**(24 Pt 1): p. 8570-6.
132. Bachmann, I.M., et al., *EZH2 expression is associated with high proliferation rate and aggressive tumor subgroups in cutaneous melanoma and cancers of the endometrium, prostate, and breast.* J Clin Oncol, 2006. **24**(2): p. 268-73.
133. Crea, F., et al., *Pharmacologic disruption of Polycomb Repressive Complex 2 inhibits tumorigenicity and tumor progression in prostate cancer.* Mol Cancer, 2011. **10**: p. 40.
134. Tong, Z.T., et al., *EZH2 supports nasopharyngeal carcinoma cell aggressiveness by forming a co-repressor complex with HDAC1/HDAC2 and Snail to inhibit E-cadherin.* Oncogene, 2012. **31**(5): p. 583-94.
135. Smits, M., et al., *miR-101 is down-regulated in glioblastoma resulting in EZH2-induced proliferation, migration, and angiogenesis.* Oncotarget, 2010. **1**(8): p. 710-20.
136. Gonzalez, M.E., et al., *EZH2 expands breast stem cells through activation of NOTCH1 signaling.* Proc Natl Acad Sci U S A, 2014. **111**(8): p. 3098-103.
137. Li, X., et al., *Targeted overexpression of EZH2 in the mammary gland disrupts ductal morphogenesis and causes epithelial hyperplasia.* Am J Pathol, 2009. **175**(3): p. 1246-54.
138. Ernst, T., et al., *Inactivating mutations of the histone methyltransferase gene EZH2 in myeloid disorders.* Nat Genet, 2010. **42**(8): p. 722-6.
139. Nikoloski, G., et al., *Somatic mutations of the histone methyltransferase gene EZH2 in myelodysplastic syndromes.* Nat Genet, 2010. **42**(8): p. 665-7.
140. Ntziachristos, P., et al., *Genetic inactivation of the polycomb repressive complex 2 in T cell acute lymphoblastic leukemia.* Nat Med, 2012. **18**(2): p. 298-301.
141. Simon, C., et al., *A key role for EZH2 and associated genes in mouse and human adult T-cell acute leukemia.* Genes Dev, 2012. **26**(7): p. 651-6.
142. Mallen-St Clair, J., et al., *EZH2 couples pancreatic regeneration to neoplastic progression.* Genes Dev, 2012. **26**(5): p. 439-44.
143. Tan, J., et al., *Pharmacologic disruption of Polycomb-repressive complex 2-mediated gene repression selectively induces apoptosis in cancer cells.* Genes Dev, 2007. **21**(9): p. 1050-63.
144. Sun, F., et al., *Preclinical pharmacokinetic studies of 3-deazaneplanocin A, a potent epigenetic anticancer agent, and its human pharmacokinetic prediction using GastroPlus.* Eur J Pharm Sci, 2015. **77**: p. 290-302.
145. Hayden, A., et al., *S-adenosylhomocysteine hydrolase inhibition by 3-deazaneplanocin A analogues induces anti-cancer effects in breast cancer cell lines and synergy with both histone deacetylase and HER2 inhibition.* Breast Cancer Res Treat, 2011. **127**(1): p. 109-19.
146. Miranda, T.B., et al., *DZNep is a global histone methylation inhibitor that reactivates developmental genes not silenced by DNA methylation.* Mol Cancer Ther, 2009. **8**(6): p. 1579-88.
147. Knutson, S.K., et al., *A selective inhibitor of EZH2 blocks H3K27 methylation and kills mutant lymphoma cells.* Nat Chem Biol, 2012. **8**(11): p. 890-6.
148. McCabe, M.T., et al., *EZH2 inhibition as a therapeutic strategy for lymphoma with EZH2-activating mutations.* Nature, 2012. **492**(7427): p. 108-12.
149. Morera, L., M. Lubbert, and M. Jung, *Targeting histone methyltransferases and demethylases in clinical trials for cancer therapy.* Clin Epigenetics, 2016. **8**: p. 57.

150. Chen, Y.T., et al., *The novel EZH2 inhibitor, GSK126, suppresses cell migration and angiogenesis via down-regulating VEGF-A.* Cancer Chemother Pharmacol, 2016. **77**(4): p. 757-65.
151. Yu, T., et al., *The EZH2 inhibitor GSK343 suppresses cancer stem-like phenotypes and reverses mesenchymal transition in glioma cells.* Oncotarget, 2017. **8**(58): p. 98348-98359.
152. Qi, W., et al., *Selective inhibition of Ezh2 by a small molecule inhibitor blocks tumor cells proliferation.* Proc Natl Acad Sci U S A, 2012. **109**(52): p. 21360-5.
153. Konze, K.D., et al., *An orally bioavailable chemical probe of the Lysine Methyltransferases EZH2 and EZH1.* ACS Chem Biol, 2013. **8**(6): p. 1324-34.
154. Xu, B., et al., *Selective inhibition of EZH2 and EZH1 enzymatic activity by a small molecule suppresses MLL-rearranged leukemia.* Blood, 2015. **125**(2): p. 346-57.
155. Knutson, S.K., et al., *Selective inhibition of EZH2 by EPZ-6438 leads to potent antitumor activity in EZH2-mutant non-Hodgkin lymphoma.* Mol Cancer Ther, 2014. **13**(4): p. 842-54.
156. Kurmasheva, R.T., et al., *Initial testing (stage 1) of tazemetostat (EPZ-6438), a novel EZH2 inhibitor, by the Pediatric Preclinical Testing Program.* Pediatr Blood Cancer, 2017. **64**(3).
157. Nasveschuk, C.G., et al., *Discovery and Optimization of Tetramethylpiperidinyl Benzamides as Inhibitors of EZH2.* ACS Med Chem Lett, 2014. **5**(4): p. 378-83.
158. Vaswani, R.G., et al., *Identification of (R)-N-((4-Methoxy-6-methyl-2-oxo-1,2-dihydropyridin-3-yl)methyl)-2-methyl-1-(1-(1 -(2,2,2-trifluoroethyl)piperidin-4-yl)ethyl)-1H-indole-3-carboxamide (CPI-1205), a Potent and Selective Inhibitor of Histone Methyltransferase EZH2, Suitable for Phase I Clinical Trials for B-Cell Lymphomas.* J Med Chem, 2016. **59**(21): p. 9928-9941.
159. Chen, H., et al., *Wedelolactone disrupts the interaction of EZH2-EED complex and inhibits PRC2-dependent cancer.* Oncotarget, 2015. **6**(15): p. 13049-59.
160. Kong, X., et al., *Astemizole arrests the proliferation of cancer cells by disrupting the EZH2-EED interaction of polycomb repressive complex 2.* J Med Chem, 2014. **57**(22): p. 9512-21.
161. Li, L., et al., *Discovery and Molecular Basis of a Diverse Set of Polycomb Repressive Complex 2 Inhibitors Recognition by EED.* PLoS One, 2017. **12**(1): p. e0169855.
162. Huang, Y., et al., *Discovery of First-in-Class, Potent, and Orally Bioavailable Embryonic Ectoderm Development (EED) Inhibitor with Robust Anticancer Efficacy.* J Med Chem, 2017. **60**(6): p. 2215-2226.
163. Qi, W., et al., *An allosteric PRC2 inhibitor targeting the H3K27me3 binding pocket of EED.* Nat Chem Biol, 2017. **13**(4): p. 381-388.
164. Lingel, A., et al., *Structure-Guided Design of EED Binders Allosterically Inhibiting the Epigenetic Polycomb Repressive Complex 2 (PRC2) Methyltransferase.* J Med Chem, 2017. **60**(1): p. 415-427.
165. He, Y., et al., *The EED protein-protein interaction inhibitor A-395 inactivates the PRC2 complex.* Nat Chem Biol, 2017. **13**(4): p. 389-395.
166. Barnash, K.D., et al., *Discovery of Peptidomimetic Ligands of EED as Allosteric Inhibitors of PRC2.* ACS Comb Sci, 2017. **19**(3): p. 161-172.
167. Marmorstein, R. and M.M. Zhou, *Writers and readers of histone acetylation: structure, mechanism, and inhibition.* Cold Spring Harb Perspect Biol, 2014. **6**(7): p. a018762.
168. Schneider, A., et al., *Acetyltransferases (HATs) as targets for neurological therapeutics.* Neurotherapeutics, 2013. **10**(4): p. 568-88.
169. Hong, L., et al., *Studies of the DNA binding properties of histone H4 amino terminus. Thermal denaturation studies reveal that acetylation markedly reduces the binding constant of the H4 "tail" to DNA.* J Biol Chem, 1993. **268**(1): p. 305-14.
170. Vettese-Dadey, M., et al., *Acetylation of histone H4 plays a primary role in enhancing transcription factor binding to nucleosomal DNA in vitro.* EMBO J, 1996. **15**(10): p. 2508-18.
171. Davie, J.R., *Covalent modifications of histones: expression from chromatin templates.* Curr Opin Genet Dev, 1998. **8**(2): p. 173-8.
172. Turner, B.M., *Histone acetylation and an epigenetic code.* Bioessays, 2000. **22**(9): p. 836-45.
173. Zeng, L. and M.M. Zhou, *Bromodomain: an acetyl-lysine binding domain.* FEBS Lett, 2002. **513**(1): p. 124-8.
174. Brownell, J.E., et al., *Tetrahymena histone acetyltransferase A: a homolog to yeast Gcn5p linking histone acetylation to gene activation.* Cell, 1996. **84**(6): p. 843-51.

175. Kleff, S., et al., *Identification of a gene encoding a yeast histone H4 acetyltransferase.* J Biol Chem, 1995. **270**(42): p. 24674-7.
176. Parthun, M.R., J. Widom, and D.E. Gottschling, *The major cytoplasmic histone acetyltransferase in yeast: links to chromatin replication and histone metabolism.* Cell, 1996. **87**(1): p. 85-94.
177. Choudhary, C., et al., *Lysine acetylation targets protein complexes and co-regulates major cellular functions.* Science, 2009. **325**(5942): p. 834-40.
178. You, L., et al., *Lysine acetylation: enzymes, bromodomains and links to different diseases.* Essays Biochem, 2012. **52**: p. 1-12.
179. Livengood, J.A., et al., *p53 Transcriptional activity is mediated through the SRC1-interacting domain of CBP/p300.* J Biol Chem, 2002. **277**(11): p. 9054-61.
180. Sanjuan, R. and I. Marin, *Tracing the origin of the compensasome: evolutionary history of DEAH helicase and MYST acetyltransferase gene families.* Mol Biol Evol, 2001. **18**(3): p. 330-43.
181. Heery, D.M. and P.M. Fischer, *Pharmacological targeting of lysine acetyltransferases in human disease: a progress report.* Drug Discov Today, 2007. **12**(1-2): p. 88-99.
182. Renthal, W. and E.J. Nestler, *Histone acetylation in drug addiction.* Semin Cell Dev Biol, 2009. **20**(4): p. 387-94.
183. Haberland, M., R.L. Montgomery, and E.N. Olson, *The many roles of histone deacetylases in development and physiology: implications for disease and therapy.* Nat Rev Genet, 2009. **10**(1): p. 32-42.
184. Dokmanovic, M., C. Clarke, and P.A. Marks, *Histone deacetylase inhibitors: overview and perspectives.* Mol Cancer Res, 2007. **5**(10): p. 981-9.
185. Seto, E. and M. Yoshida, *Erasers of histone acetylation: the histone deacetylase enzymes.* Cold Spring Harb Perspect Biol, 2014. **6**(4): p. a018713.
186. Bjerling, P., et al., *Functional divergence between histone deacetylases in fission yeast by distinct cellular localization and in vivo specificity.* Mol Cell Biol, 2002. **22**(7): p. 2170-81.
187. Gao, L., et al., *Cloning and functional characterization of HDAC11, a novel member of the human histone deacetylase family.* J Biol Chem, 2002. **277**(28): p. 25748-55.
188. Buggy, J.J., et al., *Cloning and characterization of a novel human histone deacetylase, HDAC8.* Biochem J, 2000. **350 Pt 1**: p. 199-205.
189. Galasinski, S.C., et al., *Phosphatase inhibition leads to histone deacetylases 1 and 2 phosphorylation and disruption of corepressor interactions.* J Biol Chem, 2002. **277**(22): p. 19618-26.
190. Zhang, Y., et al., *Analysis of the NuRD subunits reveals a histone deacetylase core complex and a connection with DNA methylation.* Genes Dev, 1999. **13**(15): p. 1924-35.
191. Ashburner, B.P., S.D. Westerheide, and A.S. Baldwin, Jr., *The p65 (RelA) subunit of NF-kappaB interacts with the histone deacetylase (HDAC) corepressors HDAC1 and HDAC2 to negatively regulate gene expression.* Mol Cell Biol, 2001. **21**(20): p. 7065-77.
192. Yoshida, M., et al., *Histone deacetylase as a new target for cancer chemotherapy.* Cancer Chemother Pharmacol, 2001. **48 Suppl 1**: p. S20-6.
193. Kao, H.Y., et al., *Isolation of a novel histone deacetylase reveals that class I and class II deacetylases promote SMRT-mediated repression.* Genes Dev, 2000. **14**(1): p. 55-66.
194. Li, J., et al., *Specific targeting and constitutive association of histone deacetylase complexes during transcriptional repression.* Genes Dev, 2002. **16**(6): p. 687-92.
195. Nair, A.R., et al., *Paradoxical effects of trichostatin A: inhibition of NF-Y-associated histone acetyltransferase activity, phosphorylation of hGCN5 and downregulation of cyclin A and B1 mRNA.* Cancer Lett, 2001. **166**(1): p. 55-64.
196. Yang, W.M., et al., *Isolation and characterization of cDNAs corresponding to an additional member of the human histone deacetylase gene family.* J Biol Chem, 1997. **272**(44): p. 28001-7.
197. Hu, E., et al., *Cloning and characterization of a novel human class I histone deacetylase that functions as a transcription repressor.* J Biol Chem, 2000. **275**(20): p. 15254-64.
198. Guenther, M.G., O. Barak, and M.A. Lazar, *The SMRT and N-CoR corepressors are activating cofactors for histone deacetylase 3.* Mol Cell Biol, 2001. **21**(18): p. 6091-101.

199. Grozinger, C.M., C.A. Hassig, and S.L. Schreiber, *Three proteins define a class of human histone deacetylases related to yeast Hda1p.* Proc Natl Acad Sci U S A, 1999. **96**(9): p. 4868-73.
200. Hubbert, C., et al., *HDAC6 is a microtubule-associated deacetylase.* Nature, 2002. **417**(6887): p. 455-8.
201. Van den Wyngaert, I., et al., *Cloning and characterization of human histone deacetylase 8.* FEBS Lett, 2000. **478**(1-2): p. 77-83.
202. Bertos, N.R., A.H. Wang, and X.J. Yang, *Class II histone deacetylases: structure, function, and regulation.* Biochem Cell Biol, 2001. **79**(3): p. 243-52.
203. Zhou, X., et al., *Cloning and characterization of a histone deacetylase, HDAC9.* Proc Natl Acad Sci U S A, 2001. **98**(19): p. 10572-7.
204. Zhou, X., et al., *Identification of a transcriptional repressor related to the noncatalytic domain of histone deacetylases 4 and 5.* Proc Natl Acad Sci U S A, 2000. **97**(3): p. 1056-61.
205. Guardiola, A.R. and T.P. Yao, *Molecular cloning and characterization of a novel histone deacetylase HDAC10.* J Biol Chem, 2002. **277**(5): p. 3350-6.
206. Tong, J.J., et al., *Identification of HDAC10, a novel class II human histone deacetylase containing a leucine-rich domain.* Nucleic Acids Res, 2002. **30**(5): p. 1114-23.
207. Kao, H.Y., et al., *Isolation and characterization of mammalian HDAC10, a novel histone deacetylase.* J Biol Chem, 2002. **277**(1): p. 187-93.
208. Glozak, M.A. and E. Seto, *Acetylation/deacetylation modulates the stability of DNA replication licensing factor Cdt1.* J Biol Chem, 2009. **284**(17): p. 11446-53.
209. Brachmann, C.B., et al., *The SIR2 gene family, conserved from bacteria to humans, functions in silencing, cell cycle progression, and chromosome stability.* Genes Dev, 1995. **9**(23): p. 2888-902.
210. Frye, R.A., *Characterization of five human cDNAs with homology to the yeast SIR2 gene: Sir2-like proteins (sirtuins) metabolize NAD and may have protein ADP-ribosyltransferase activity.* Biochem Biophys Res Commun, 1999. **260**(1): p. 273-9.
211. Du, J., et al., *Sirt5 is a NAD-dependent protein lysine demalonylase and desuccinylase.* Science, 2011. **334**(6057): p. 806-9.
212. Carafa, V., et al., *Sirtuin functions and modulation: from chemistry to the clinic.* Clin Epigenetics, 2016. **8**: p. 61.
213. Das, C., et al., *CBP/p300-mediated acetylation of histone H3 on lysine 56.* Nature, 2009. **459**(7243): p. 113-7.
214. Vaquero, A., R. Sternglanz, and D. Reinberg, *NAD+-dependent deacetylation of H4 lysine 16 by class III HDACs.* Oncogene, 2007. **26**(37): p. 5505-20.
215. Kauppinen, A., et al., *Antagonistic crosstalk between NF-kappaB and SIRT1 in the regulation of inflammation and metabolic disorders.* Cell Signal, 2013. **25**(10): p. 1939-48.
216. Yang, Y., et al., *Suppression of FOXO1 activity by FHL2 through SIRT1-mediated deacetylation.* EMBO J, 2005. **24**(5): p. 1021-32.
217. van der Horst, A., et al., *FOXO4 is acetylated upon peroxide stress and deacetylated by the longevity protein hSir2(SIRT1).* J Biol Chem, 2004. **279**(28): p. 28873-9.
218. Pruitt, K., et al., *Inhibition of SIRT1 reactivates silenced cancer genes without loss of promoter DNA hypermethylation.* PLoS Genet, 2006. **2**(3): p. e40.
219. Jeong, J., et al., *SIRT1 promotes DNA repair activity and deacetylation of Ku70.* Exp Mol Med, 2007. **39**(1): p. 8-13.
220. Heltweg, B., et al., *Antitumor activity of a small-molecule inhibitor of human silent information regulator 2 enzymes.* Cancer Res, 2006. **66**(8): p. 4368-77.
221. Lain, S., et al., *Discovery, in vivo activity, and mechanism of action of a small-molecule p53 activator.* Cancer Cell, 2008. **13**(5): p. 454-63.
222. Bereshchenko, O.R., W. Gu, and R. Dalla-Favera, *Acetylation inactivates the transcriptional repressor BCL6.* Nat Genet, 2002. **32**(4): p. 606-13.
223. Lin, Y.H., et al., *KAP1 Deacetylation by SIRT1 Promotes Non-Homologous End-Joining Repair.* PLoS One, 2015. **10**(4): p. e0123935.
224. Deng, C.X., *SIRT1, is it a tumor promoter or tumor suppressor?* Int J Biol Sci, 2009. **5**(2): p. 147-52.

225. Bordone, L., et al., *SIRT1 transgenic mice show phenotypes resembling calorie restriction.* Aging Cell, 2007. **6**(6): p. 759-67.
226. Hara, F., et al., *Molecular Hydrogen Alleviates Cellular Senescence in Endothelial Cells.* Circ J, 2016. **80**(9): p. 2037-46.
227. Li, D.J., et al., *alpha7 Nicotinic Acetylcholine Receptor Relieves Angiotensin II-Induced Senescence in Vascular Smooth Muscle Cells by Raising Nicotinamide Adenine Dinucleotide-Dependent SIRT1 Activity.* Arterioscler Thromb Vasc Biol, 2016. **36**(8): p. 1566-76.
228. de Picciotto, N.E., et al., *Nicotinamide mononucleotide supplementation reverses vascular dysfunction and oxidative stress with aging in mice.* Aging Cell, 2016. **15**(3): p. 522-30.
229. Hallows, W.C., S. Lee, and J.M. Denu, *Sirtuins deacetylate and activate mammalian acetyl-CoA synthetases.* Proc Natl Acad Sci U S A, 2006. **103**(27): p. 10230-10235.
230. Li, X., et al., *SIRT1 deacetylates and positively regulates the nuclear receptor LXR.* Mol Cell, 2007. **28**(1): p. 91-106.
231. Qiao, L. and J. Shao, *SIRT1 regulates adiponectin gene expression through Foxo1-C/enhancer-binding protein alpha transcriptional complex.* J Biol Chem, 2006. **281**(52): p. 39915-24.
232. Bordone, L., et al., *Correction: Sirt1 Regulates Insulin Secretion by Repressing UCP2 in Pancreatic beta Cells.* PLoS Biol, 2015. **13**(12): p. e1002346.
233. Nemoto, S., M.M. Fergusson, and T. Finkel, *SIRT1 functionally interacts with the metabolic regulator and transcriptional coactivator PGC-1{alpha}.* J Biol Chem, 2005. **280**(16): p. 16456-60.
234. Rodgers, J.T., et al., *Nutrient control of glucose homeostasis through a complex of PGC-1alpha and SIRT1.* Nature, 2005. **434**(7029): p. 113-8.
235. Lee, I.H., et al., *A role for the NAD-dependent deacetylase Sirt1 in the regulation of autophagy.* Proc Natl Acad Sci U S A, 2008. **105**(9): p. 3374-9.
236. Morselli, E., et al., *Caloric restriction and resveratrol promote longevity through the Sirtuin-1-dependent induction of autophagy.* Cell Death Dis, 2010. **1**: p. e10.
237. Yang, Y., et al., *SIRT1 sumoylation regulates its deacetylase activity and cellular response to genotoxic stress.* Nat Cell Biol, 2007. **9**(11): p. 1253-62.
238. Verdin, E., *AROuSing SIRT1: identification of a novel endogenous SIRT1 activator.* Mol Cell, 2007. **28**(3): p. 354-6.
239. Jeong, H., et al., *Sirt1 mediates neuroprotection from mutant huntingtin by activation of the TORC1 and CREB transcriptional pathway.* Nat Med, 2011. **18**(1): p. 159-65.
240. Sussmuth, S.D., et al., *An exploratory double-blind, randomized clinical trial with selisistat, a SirT1 inhibitor, in patients with Huntington's disease.* Br J Clin Pharmacol, 2015. **79**(3): p. 465-76.
241. Westerberg, G., et al., *Safety, pharmacokinetics, pharmacogenomics and QT concentration-effect modelling of the SirT1 inhibitor selisistat in healthy volunteers.* Br J Clin Pharmacol, 2015. **79**(3): p. 477-91.
242. North, B.J., et al., *The human Sir2 ortholog, SIRT2, is an NAD+-dependent tubulin deacetylase.* Mol Cell, 2003. **11**(2): p. 437-44.
243. Palazzo, A., B. Ackerman, and G.G. Gundersen, *Cell biology: Tubulin acetylation and cell motility.* Nature, 2003. **421**(6920): p. 230.
244. Kim, H.S., et al., *SIRT2 maintains genome integrity and suppresses tumorigenesis through regulating APC/C activity.* Cancer Cell, 2011. **20**(4): p. 487-99.
245. Vaquero, A., et al., *SirT2 is a histone deacetylase with preference for histone H4 Lys 16 during mitosis.* Genes Dev, 2006. **20**(10): p. 1256-61.
246. Serrano, L., et al., *The tumor suppressor SirT2 regulates cell cycle progression and genome stability by modulating the mitotic deposition of H4K20 methylation.* Genes Dev, 2013. **27**(6): p. 639-53.
247. Yang, M.H., et al., *HDAC6 and SIRT2 regulate the acetylation state and oncogenic activity of mutant K-RAS.* Mol Cancer Res, 2013. **11**(9): p. 1072-7.
248. Jin, Y.H., et al., *Sirt2 interacts with 14-3-3 beta/gamma and down-regulates the activity of p53.* Biochem Biophys Res Commun, 2008. **368**(3): p. 690-5.
249. He, X., et al., *SIRT2 activity is required for the survival of C6 glioma cells.* Biochem Biophys Res Commun, 2012. **417**(1): p. 468-72.

250. Rothgiesser, K.M., et al., *SIRT2 regulates NF-kappaB dependent gene expression through deacetylation of p65 Lys310.* J Cell Sci, 2010. **123**(Pt 24): p. 4251-8.
251. Wang, F., et al., *SIRT2 deacetylates FOXO3a in response to oxidative stress and caloric restriction.* Aging Cell, 2007. **6**(4): p. 505-14.
252. Pais, T.F., et al., *The NAD-dependent deacetylase sirtuin 2 is a suppressor of microglial activation and brain inflammation.* EMBO J, 2013. **32**(19): p. 2603-16.
253. Lee, A.S., et al., *SIRT2 ameliorates lipopolysaccharide-induced inflammation in macrophages.* Biochem Biophys Res Commun, 2014. **450**(4): p. 1363-9.
254. Jiang, W., et al., *Acetylation regulates gluconeogenesis by promoting PEPCK1 degradation via recruiting the UBR5 ubiquitin ligase.* Mol Cell, 2011. **43**(1): p. 33-44.
255. Maxwell, M.M., et al., *The Sirtuin 2 microtubule deacetylase is an abundant neuronal protein that accumulates in the aging CNS.* Hum Mol Genet, 2011. **20**(20): p. 3986-96.
256. Outeiro, T.F., et al., *Sirtuin 2 inhibitors rescue alpha-synuclein-mediated toxicity in models of Parkinson's disease.* Science, 2007. **317**(5837): p. 516-9.
257. Eskandarian, H.A., et al., *A role for SIRT2-dependent histone H3K18 deacetylation in bacterial infection.* Science, 2013. **341**(6145): p. 1238858.
258. Schwer, B., et al., *Reversible lysine acetylation controls the activity of the mitochondrial enzyme acetyl-CoA synthetase 2.* Proc Natl Acad Sci U S A, 2006. **103**(27): p. 10224-10229.
259. Lombard, D.B., et al., *Mammalian Sir2 homolog SIRT3 regulates global mitochondrial lysine acetylation.* Mol Cell Biol, 2007. **27**(24): p. 8807-14.
260. Schlicker, C., et al., *Substrates and regulation mechanisms for the human mitochondrial sirtuins Sirt3 and Sirt5.* J Mol Biol, 2008. **382**(3): p. 790-801.
261. Sundaresan, N.R., et al., *SIRT3 is a stress-responsive deacetylase in cardiomyocytes that protects cells from stress-mediated cell death by deacetylation of Ku70.* Mol Cell Biol, 2008. **28**(20): p. 6384-401.
262. Tseng, A.H., S.S. Shieh, and D.L. Wang, *SIRT3 deacetylates FOXO3 to protect mitochondria against oxidative damage.* Free Radic Biol Med, 2013. **63**: p. 222-34.
263. Lu, Z., et al., *Prolonged fasting identifies heat shock protein 10 as a Sirtuin 3 substrate: elucidating a new mechanism linking mitochondrial protein acetylation to fatty acid oxidation enzyme folding and function.* J Biol Chem, 2015. **290**(4): p. 2466-76.
264. Sundaresan, N.R., et al., *SIRT3 Blocks Aging-Associated Tissue Fibrosis in Mice by Deacetylating and Activating Glycogen Synthase Kinase 3beta.* Mol Cell Biol, 2015. **36**(5): p. 678-92.
265. He, X., H. Zeng, and J.X. Chen, *Ablation of SIRT3 causes coronary microvascular dysfunction and impairs cardiac recovery post myocardial ischemia.* Int J Cardiol, 2016. **215**: p. 349-57.
266. Lu, Y., et al., *SIRT3 in cardiovascular diseases: Emerging roles and therapeutic implications.* Int J Cardiol, 2016. **220**: p. 700-5.
267. Bellizzi, D., et al., *A novel VNTR enhancer within the SIRT3 gene, a human homologue of SIR2, is associated with survival at oldest ages.* Genomics, 2005. **85**(2): p. 258-63.
268. Kim, H.S., et al., *SIRT3 is a mitochondria-localized tumor suppressor required for maintenance of mitochondrial integrity and metabolism during stress.* Cancer Cell, 2010. **17**(1): p. 41-52.
269. Alhazzazi, T.Y., et al., *SIRT3 and cancer: tumor promoter or suppressor?* Biochim Biophys Acta, 2011. **1816**(1): p. 80-8.
270. Wei, L., et al., *Oroxylin A induces dissociation of hexokinase II from the mitochondria and inhibits glycolysis by SIRT3-mediated deacetylation of cyclophilin D in breast carcinoma.* Cell Death Dis, 2013. **4**: p. e601.
271. Hirschey, M.D., et al., *SIRT3 regulates mitochondrial fatty-acid oxidation by reversible enzyme deacetylation.* Nature, 2010. **464**(7285): p. 121-5.
272. Shimazu, T., et al., *SIRT3 deacetylates mitochondrial 3-hydroxy-3-methylglutaryl CoA synthase 2 and regulates ketone body production.* Cell Metab, 2010. **12**(6): p. 654-61.
273. Hallows, W.C., et al., *Sirt3 promotes the urea cycle and fatty acid oxidation during dietary restriction.* Mol Cell, 2011. **41**(2): p. 139-49.
274. Yang, Y., et al., *NAD+-dependent deacetylase SIRT3 regulates mitochondrial protein synthesis by deacetylation of the ribosomal protein MRPL10.* J Biol Chem, 2010. **285**(10): p. 7417-29.

275. Ahn, B.H., et al., *A role for the mitochondrial deacetylase Sirt3 in regulating energy homeostasis.* Proc Natl Acad Sci U S A, 2008. **105**(38): p. 14447-52.
276. Finley, L.W., et al., *Succinate dehydrogenase is a direct target of sirtuin 3 deacetylase activity.* PLoS One, 2011. **6**(8): p. e23295.
277. Cimen, H., et al., *Regulation of succinate dehydrogenase activity by SIRT3 in mammalian mitochondria.* Biochemistry, 2010. **49**(2): p. 304-11.
278. Bao, J., et al., *SIRT3 is regulated by nutrient excess and modulates hepatic susceptibility to lipotoxicity.* Free Radic Biol Med, 2010. **49**(7): p. 1230-7.
279. Someya, S., et al., *Sirt3 mediates reduction of oxidative damage and prevention of age-related hearing loss under caloric restriction.* Cell, 2010. **143**(5): p. 802-12.
280. Sundaresan, N.R., et al., *Sirt3 blocks the cardiac hypertrophic response by augmenting Foxo3a-dependent antioxidant defense mechanisms in mice.* J Clin Invest, 2009. **119**(9): p. 2758-71.
281. van de Ven, R.A.H., D. Santos, and M.C. Haigis, *Mitochondrial Sirtuins and Molecular Mechanisms of Aging.* Trends Mol Med, 2017. **23**(4): p. 320-331.
282. Tao, R., et al., *Sirt3-mediated deacetylation of evolutionarily conserved lysine 122 regulates MnSOD activity in response to stress.* Mol Cell, 2010. **40**(6): p. 893-904.
283. Signorile, A., et al., *Mitochondrial cAMP prevents apoptosis modulating Sirt3 protein level and OPA1 processing in cardiac myoblast cells.* Biochim Biophys Acta, 2017. **1864**(2): p. 355-366.
284. Samant, S.A., et al., *SIRT3 deacetylates and activates OPA1 to regulate mitochondrial dynamics during stress.* Mol Cell Biol, 2014. **34**(5): p. 807-19.
285. Sun, W., et al., *SIRT3: A New Regulator of Cardiovascular Diseases.* Oxid Med Cell Longev, 2018. **2018**: p. 7293861.
286. Hirschey, M.D., et al., *SIRT3 deficiency and mitochondrial protein hyperacetylation accelerate the development of the metabolic syndrome.* Mol Cell, 2011. **44**(2): p. 177-90.
287. Paulin, R., et al., *Sirtuin 3 deficiency is associated with inhibited mitochondrial function and pulmonary arterial hypertension in rodents and humans.* Cell Metab, 2014. **20**(5): p. 827-839.
288. Brown, K., et al., *SIRT3 reverses aging-associated degeneration.* Cell Rep, 2013. **3**(2): p. 319-27.
289. Morigi, M., et al., *Sirtuin 3-dependent mitochondrial dynamic improvements protect against acute kidney injury.* J Clin Invest, 2015. **125**(2): p. 715-26.
290. Winnik, S., et al., *Mild endothelial dysfunction in Sirt3 knockout mice fed a high-cholesterol diet: protective role of a novel C/EBP-beta-dependent feedback regulation of SOD2.* Basic Res Cardiol, 2016. **111**(3): p. 33.
291. Disch, J.S., et al., *Discovery of thieno[3,2-d]pyrimidine-6-carboxamides as potent inhibitors of SIRT1, SIRT2, and SIRT3.* J Med Chem, 2013. **56**(9): p. 3666-79.
292. Dai, H., et al., *Crystallographic structure of a small molecule SIRT1 activator-enzyme complex.* Nat Commun, 2015. **6**: p. 7645.
293. Nguyen, G.T., et al., *Structures of human sirtuin 3 complexes with ADP-ribose and with carba-NAD+ and SRT1720: binding details and inhibition mechanism.* Acta Crystallogr D Biol Crystallogr, 2013. **69**(Pt 8): p. 1423-32.
294. Haigis, M.C., et al., *SIRT4 inhibits glutamate dehydrogenase and opposes the effects of calorie restriction in pancreatic beta cells.* Cell, 2006. **126**(5): p. 941-54.
295. Rauh, D., et al., *An acetylome peptide microarray reveals specificities and deacetylation substrates for all human sirtuin isoforms.* Nat Commun, 2013. **4**: p. 2327.
296. Laurent, G., et al., *SIRT4 represses peroxisome proliferator-activated receptor alpha activity to suppress hepatic fat oxidation.* Mol Cell Biol, 2013. **33**(22): p. 4552-61.
297. Jeong, S.M., et al., *SIRT4 protein suppresses tumor formation in genetic models of Myc-induced B cell lymphoma.* J Biol Chem, 2014. **289**(7): p. 4135-44.
298. Nakahara, Y., et al., *Downregulation of SIRT4 Expression Is Associated with Poor Prognosis in Esophageal Squamous Cell Carcinoma.* Oncology, 2016. **90**(6): p. 347-55.
299. Mathias, R.A., et al., *Sirtuin 4 is a lipoamidase regulating pyruvate dehydrogenase complex activity.* Cell, 2014. **159**(7): p. 1615-25.
300. Tan, M., et al., *Lysine glutarylation is a protein posttranslational modification regulated by SIRT5.* Cell Metab, 2014. **19**(4): p. 605-17.

301. Nakagawa, T., et al., *SIRT5 Deacetylates carbamoyl phosphate synthetase 1 and regulates the urea cycle.* Cell, 2009. **137**(3): p. 560-70.
302. Lin, Z.F., et al., *SIRT5 desuccinylates and activates SOD1 to eliminate ROS.* Biochem Biophys Res Commun, 2013. **441**(1): p. 191-5.
303. Rardin, M.J., et al., *SIRT5 regulates the mitochondrial lysine succinylome and metabolic networks.* Cell Metab, 2013. **18**(6): p. 920-33.
304. Nakamura, Y., et al., *SIRT5 deacetylates and activates urate oxidase in liver mitochondria of mice.* FEBS Lett, 2012. **586**(23): p. 4076-81.
305. Zhang, Y., et al., *SIRT3 and SIRT5 regulate the enzyme activity and cardiolipin binding of very long-chain acyl-CoA dehydrogenase.* PLoS One, 2015. **10**(3): p. e0122297.
306. Yu, J., et al., *Metabolic characterization of a Sirt5 deficient mouse model.* Sci Rep, 2013. **3**: p. 2806.
307. Sadhukhan, S., et al., *Metabolomics-assisted proteomics identifies succinylation and SIRT5 as important regulators of cardiac function.* Proc Natl Acad Sci U S A, 2016. **113**(16): p. 4320-5.
308. Schuetz, A., et al., *Structural basis of inhibition of the human NAD+-dependent deacetylase SIRT5 by suramin.* Structure, 2007. **15**(3): p. 377-89.
309. Peng, C., et al., *The first identification of lysine malonylation substrates and its regulatory enzyme.* Mol Cell Proteomics, 2011. **10**(12): p. M111 012658.
310. Park, J., et al., *SIRT5-mediated lysine desuccinylation impacts diverse metabolic pathways.* Mol Cell, 2013. **50**(6): p. 919-30.
311. Maurer, B., et al., *Inhibitors of the NAD(+)-Dependent Protein Desuccinylase and Demalonylase Sirt5.* ACS Med Chem Lett, 2012. **3**(12): p. 1050-3.
312. Fischer, F., et al., *Sirt5 deacylation activities show differential sensitivities to nicotinamide inhibition.* PLoS One, 2012. **7**(9): p. e45098.
313. Roessler, C., et al., *Chemical probing of the human sirtuin 5 active site reveals its substrate acyl specificity and peptide-based inhibitors.* Angew Chem Int Ed Engl, 2014. **53**(40): p. 10728-32.
314. Michishita, E., et al., *Cell cycle-dependent deacetylation of telomeric histone H3 lysine K56 by human SIRT6.* Cell Cycle, 2009. **8**(16): p. 2664-6.
315. Jiang, H., et al., *SIRT6 regulates TNF-alpha secretion through hydrolysis of long-chain fatty acyl lysine.* Nature, 2013. **496**(7443): p. 110-3.
316. Liszt, G., et al., *Mouse Sir2 homolog SIRT6 is a nuclear ADP-ribosyltransferase.* J Biol Chem, 2005. **280**(22): p. 21313-20.
317. Van Meter, M., et al., *SIRT6 represses LINE1 retrotransposons by ribosylating KAP1 but this repression fails with stress and age.* Nat Commun, 2014. **5**: p. 5011.
318. Yang, B., et al., *The sirtuin SIRT6 deacetylates H3 K56Ac in vivo to promote genomic stability.* Cell Cycle, 2009. **8**(16): p. 2662-3.
319. Kawahara, T.L., et al., *SIRT6 links histone H3 lysine 9 deacetylation to NF-kappaB-dependent gene expression and organismal life span.* Cell, 2009. **136**(1): p. 62-74.
320. Lee, H.S., et al., *Overexpression of sirtuin 6 suppresses inflammatory responses and bone destruction in mice with collagen-induced arthritis.* Arthritis Rheum, 2013. **65**(7): p. 1776-85.
321. Ford, E., et al., *Mammalian Sir2 homolog SIRT7 is an activator of RNA polymerase I transcription.* Genes Dev, 2006. **20**(9): p. 1075-80.
322. Chen, S., et al., *Repression of RNA polymerase I upon stress is caused by inhibition of RNA-dependent deacetylation of PAF53 by SIRT7.* Mol Cell, 2013. **52**(3): p. 303-13.
323. Barber, M.F., et al., *SIRT7 links H3K18 deacetylation to maintenance of oncogenic transformation.* Nature, 2012. **487**(7405): p. 114-8.
324. Kim, J.K., et al., *Sirtuin7 oncogenic potential in human hepatocellular carcinoma and its regulation by the tumor suppressors MiR-125a-5p and MiR-125b.* Hepatology, 2013. **57**(3): p. 1055-67.
325. Yu, H., et al., *Overexpression of sirt7 exhibits oncogenic property and serves as a prognostic factor in colorectal cancer.* Clin Cancer Res, 2014. **20**(13): p. 3434-45.
326. Ryu, D., et al., *A SIRT7-dependent acetylation switch of GABPbeta1 controls mitochondrial function.* Cell Metab, 2014. **20**(5): p. 856-869.

327. Vakhrusheva, O., et al., *Sirt7 increases stress resistance of cardiomyocytes and prevents apoptosis and inflammatory cardiomyopathy in mice.* Circ Res, 2008. **102**(6): p. 703-10.
328. Tong, Z., et al., *SIRT7 Is Activated by DNA and Deacetylates Histone H3 in the Chromatin Context.* ACS Chem Biol, 2016. **11**(3): p. 742-7.
329. Hull, E.E., M.R. Montgomery, and K.J. Leyva, *HDAC Inhibitors as Epigenetic Regulators of the Immune System: Impacts on Cancer Therapy and Inflammatory Diseases.* Biomed Res Int, 2016. **2016**: p. 8797206.
330. Furumai, R., et al., *FK228 (depsipeptide) as a natural prodrug that inhibits class I histone deacetylases.* Cancer Res, 2002. **62**(17): p. 4916-21.
331. Lavu, S., et al., *Sirtuins--novel therapeutic targets to treat age-associated diseases.* Nat Rev Drug Discov, 2008. **7**(10): p. 841-53.
332. Afifi, S., et al., *Role of Histone Deacetylase Inhibitors in Relapsed Refractory Multiple Myeloma: A Focus on Vorinostat and Panobinostat.* Pharmacotherapy, 2015. **35**(12): p. 1173-88.
333. Woan, K.V., et al., *Targeting histone deacetylase 6 mediates a dual anti-melanoma effect: Enhanced antitumor immunity and impaired cell proliferation.* Mol Oncol, 2015. **9**(7): p. 1447-1457.
334. Dawson, M.A. and T. Kouzarides, *Cancer epigenetics: from mechanism to therapy.* Cell, 2012. **150**(1): p. 12-27.
335. Kretsovali, A., C. Hadjimichael, and N. Charmpilas, *Histone deacetylase inhibitors in cell pluripotency, differentiation, and reprogramming.* Stem Cells Int, 2012. **2012**: p. 184154.
336. Yoshida, M., *[Potent and specific inhibition of mammalian histone deacetylase both in vivo and in vitro by trichostatin A].* Tanpakushitsu Kakusan Koso, 2007. **52**(13 Suppl): p. 1788-9.
337. Richon, V.M., et al., *A class of hybrid polar inducers of transformed cell differentiation inhibits histone deacetylases.* Proc Natl Acad Sci U S A, 1998. **95**(6): p. 3003-7.
338. Richon, V.M., et al., *Histone deacetylase inhibitor selectively induces p21WAF1 expression and gene-associated histone acetylation.* Proc Natl Acad Sci U S A, 2000. **97**(18): p. 10014-9.
339. Sandor, V., et al., *P21-dependent g(1)arrest with downregulation of cyclin D1 and upregulation of cyclin E by the histone deacetylase inhibitor FR901228.* Br J Cancer, 2000. **83**(6): p. 817-25.
340. Eckschlager, T., et al., *Histone Deacetylase Inhibitors as Anticancer Drugs.* Int J Mol Sci, 2017. **18**(7).
341. Minucci, S. and P.G. Pelicci, *Histone deacetylase inhibitors and the promise of epigenetic (and more) treatments for cancer.* Nat Rev Cancer, 2006. **6**(1): p. 38-51.
342. Zhang, Y., et al., *Bmf is a possible mediator in histone deacetylase inhibitors FK228 and CBHA-induced apoptosis.* Cell Death Differ, 2006. **13**(1): p. 129-40.
343. Zhao, Y., et al., *Inhibitors of histone deacetylases target the Rb-E2F1 pathway for apoptosis induction through activation of proapoptotic protein Bim.* Proc Natl Acad Sci U S A, 2005. **102**(44): p. 16090-5.
344. Zhu, P., et al., *Induction of HDAC2 expression upon loss of APC in colorectal tumorigenesis.* Cancer Cell, 2004. **5**(5): p. 455-63.
345. Xu, Y., *Regulation of p53 responses by post-translational modifications.* Cell Death Differ, 2003. **10**(4): p. 400-3.
346. Yano, T., et al., *The RUNX3 tumor suppressor upregulates Bim in gastric epithelial cells undergoing transforming growth factor beta-induced apoptosis.* Mol Cell Biol, 2006. **26**(12): p. 4474-88.
347. Chi, X.Z., et al., *RUNX3 suppresses gastric epithelial cell growth by inducing p21(WAF1/Cip1) expression in cooperation with transforming growth factor {beta}-activated SMAD.* Mol Cell Biol, 2005. **25**(18): p. 8097-107.
348. Jeong, J.W., et al., *Regulation and destabilization of HIF-1alpha by ARD1-mediated acetylation.* Cell, 2002. **111**(5): p. 709-20.
349. Deroanne, C.F., et al., *Histone deacetylases inhibitors as anti-angiogenic agents altering vascular endothelial growth factor signaling.* Oncogene, 2002. **21**(3): p. 427-36.
350. Rosato, R.R., J.A. Almenara, and S. Grant, *The histone deacetylase inhibitor MS-275 promotes differentiation or apoptosis in human leukemia cells through a process regulated by generation*

of reactive oxygen species and induction of p21CIP1/WAF1 1. Cancer Res, 2003. **63**(13): p. 3637-45.
351. Bali, P., et al., *Inhibition of histone deacetylase 6 acetylates and disrupts the chaperone function of heat shock protein 90: a novel basis for antileukemia activity of histone deacetylase inhibitors.* J Biol Chem, 2005. **280**(29): p. 26729-34.
352. Liu, Y.L., et al., *Autophagy potentiates the anti-cancer effects of the histone deacetylase inhibitors in hepatocellular carcinoma.* Autophagy, 2010. **6**(8): p. 1057-65.
353. Frohlich, L.F., et al., *Molecular mechanism leading to SAHA-induced autophagy in tumor cells: evidence for a p53-dependent pathway.* Cancer Cell Int, 2016. **16**(1): p. 68.
354. Higuchi, A., et al., *Generation of pluripotent stem cells without the use of genetic material.* Lab Invest, 2015. **95**(1): p. 26-42.
355. Burba, I., et al., *Histone deacetylase inhibition enhances self renewal and cardioprotection by human cord blood-derived CD34 cells.* PLoS One, 2011. **6**(7): p. e22158.
356. Khalil, M.A., et al., *Valproic Acid Increases CD133 Positive Cells that Show Low Sensitivity to Cytostatics in Neuroblastoma.* PLoS One, 2016. **11**(9): p. e0162916.
357. Zhan, P., et al., *Strategies for the Discovery of Target-Specific or Isoform-Selective Modulators.* J Med Chem, 2015. **58**(19): p. 7611-33.
358. Franci, G., M. Miceli, and L. Altucci, *Targeting epigenetic networks with polypharmacology: a new avenue to tackle cancer.* Epigenomics, 2010. **2**(6): p. 731-42.
359. Cavalli, A., et al., *Multi-target-directed ligands to combat neurodegenerative diseases.* J Med Chem, 2008. **51**(3): p. 347-72.
360. Medina-Franco, J.L., et al., *Shifting from the single to the multitarget paradigm in drug discovery.* Drug Discov Today, 2013. **18**(9-10): p. 495-501.
361. Anighoro, A., J. Bajorath, and G. Rastelli, *Polypharmacology: challenges and opportunities in drug discovery.* J Med Chem, 2014. **57**(19): p. 7874-87.
362. Ramsay, R.R., et al., *A perspective on multi-target drug discovery and design for complex diseases.* Clin Transl Med, 2018. **7**(1): p. 3.
363. Merino, A., et al., *Drug profiling: knowing where it hits.* Drug Discov Today, 2010. **15**(17-18): p. 749-56.
364. Langedijk, J., et al., *Drug repositioning and repurposing: terminology and definitions in literature.* Drug Discov Today, 2015. **20**(8): p. 1027-34.
365. Mendez-Lucio, O., et al., *Toward drug repurposing in epigenetics: olsalazine as a hypomethylating compound active in a cellular context.* ChemMedChem, 2014. **9**(3): p. 560-5.
366. Szyf, M., *Epigenetics, DNA methylation, and chromatin modifying drugs.* Annu Rev Pharmacol Toxicol, 2009. **49**: p. 243-63.
367. Candelaria, M., et al., *A phase II study of epigenetic therapy with hydralazine and magnesium valproate to overcome chemotherapy resistance in refractory solid tumors.* Ann Oncol, 2007. **18**(9): p. 1529-38.
368. Brueckner, B. and F. Lyko, *DNA methyltransferase inhibitors: old and new drugs for an epigenetic cancer therapy.* Trends Pharmacol Sci, 2004. **25**(11): p. 551-4.
369. Rotili, D., et al., *Pan-histone demethylase inhibitors simultaneously targeting Jumonji C and lysine-specific demethylases display high anticancer activities.* J Med Chem, 2014. **57**(1): p. 42-55.
370. Valente, S., et al., *Pure Diastereomers of a Tranylcypromine-Based LSD1 Inhibitor: Enzyme Selectivity and In-Cell Studies.* ACS Med Chem Lett, 2015. **6**(2): p. 173-7.
371. Benedetti, R., et al., *Epigenetic-based therapy: From single- to multi-target approaches.* Int J Biochem Cell Biol, 2015. **69**: p. 121-31.
372. Tambunan, U.S. and E.K. Wulandari, *Identification of a better Homo sapiens Class II HDAC inhibitor through binding energy calculations and descriptor analysis.* BMC Bioinformatics, 2010. **11 Suppl 7**: p. S16.
373. Wilting, R.H., et al., *Overlapping functions of Hdac1 and Hdac2 in cell cycle regulation and haematopoiesis.* EMBO J, 2010. **29**(15): p. 2586-97.

374. Dovey, O.M., C.T. Foster, and S.M. Cowley, *Histone deacetylase 1 (HDAC1), but not HDAC2, controls embryonic stem cell differentiation.* Proc Natl Acad Sci U S A, 2010. **107**(18): p. 8242-7.
375. Van Aller, G.S., et al., *Long residence time inhibition of EZH2 in activated polycomb repressive complex 2.* ACS Chem Biol, 2014. **9**(3): p. 622-9.
376. Kim, E., et al., *Phosphorylation of EZH2 activates STAT3 signaling via STAT3 methylation and promotes tumorigenicity of glioblastoma stem-like cells.* Cancer Cell, 2013. **23**(6): p. 839-52.
377. Grant, S. and Y. Dai, *Histone deacetylase inhibitors and rational combination therapies.* Adv Cancer Res, 2012. **116**: p. 199-237.
378. Bots, M. and R.W. Johnstone, *Rational combinations using HDAC inhibitors.* Clin Cancer Res, 2009. **15**(12): p. 3970-7.
379. Ornstein, M.C., S. Mukherjee, and M.A. Sekeres, *More is better: combination therapies for myelodysplastic syndromes.* Best Pract Res Clin Haematol, 2015. **28**(1): p. 22-31.
380. Bu, Q., et al., *SAHA and S116836, a novel tyrosine kinase inhibitor, synergistically induce apoptosis in imatinib-resistant chronic myelogenous leukemia cells.* Cancer Biol Ther, 2014. **15**(7): p. 951-62.
381. Matei, D., et al., *Epigenetic resensitization to platinum in ovarian cancer.* Cancer Res, 2012. **72**(9): p. 2197-205.
382. Bixby, D. and M. Talpaz, *Seeking the causes and solutions to imatinib-resistance in chronic myeloid leukemia.* Leukemia, 2011. **25**(1): p. 7-22.
383. Jose-Eneriz, E.S., et al., *Dual epigenetic modifiers for cancer therapy.* Mol Cell Oncol, 2017. **4**(4): p. e1342748.
384. Berube, G., *An overview of molecular hybrids in drug discovery.* Expert Opin Drug Discov, 2016. **11**(3): p. 281-305.
385. Pereira, R., et al., *Indole-derived psammaplin A analogues as epigenetic modulators with multiple inhibitory activities.* J Med Chem, 2012. **55**(22): p. 9467-91.
386. Shao, M., et al., *Structure-based design, synthesis and in vitro antiproliferative effects studies of novel dual BRD4/HDAC inhibitors.* Bioorg Med Chem Lett, 2017. **27**(17): p. 4051-4055.
387. Borretto, E., et al., *Synthesis and Biological Evaluation of the First Example of NO-Donor Histone Deacetylase Inhibitor.* ACS Med Chem Lett, 2013. **4**(10): p. 994-9.
388. Lu, J., et al., *Hijacking the E3 Ubiquitin Ligase Cereblon to Efficiently Target BRD4.* Chem Biol, 2015. **22**(6): p. 755-63.
389. Winter, G.E., et al., *DRUG DEVELOPMENT. Phthalimide conjugation as a strategy for in vivo target protein degradation.* Science, 2015. **348**(6241): p. 1376-81.
390. Gediya, L.K., et al., *Design, synthesis, and evaluation of novel mutual prodrugs (hybrid drugs) of all-trans-retinoic acid and histone deacetylase inhibitors with enhanced anticancer activities in breast and prostate cancer cells in vitro.* J Med Chem, 2008. **51**(13): p. 3895-904.
391. Ganesan, A., *Multitarget Drugs: an Epigenetic Epiphany.* ChemMedChem, 2016. **11**(12): p. 1227-41.
392. Mahboobi, S., et al., *Design of chimeric histone deacetylase- and tyrosine kinase-inhibitors: a series of imatinib hybrides as potent inhibitors of wild-type and mutant BCR-ABL, PDGF-Rbeta, and histone deacetylases.* J Med Chem, 2009. **52**(8): p. 2265-79.
393. Yao, L., et al., *Design and Synthesis of Ligand Efficient Dual Inhibitors of Janus Kinase (JAK) and Histone Deacetylase (HDAC) Based on Ruxolitinib and Vorinostat.* J Med Chem, 2017. **60**(20): p. 8336-8357.
394. Duan, Y.C., et al., *Design and synthesis of tranylcypromine derivatives as novel LSD1/HDACs dual inhibitors for cancer treatment.* Eur J Med Chem, 2017. **140**: p. 392-402.
395. Buchwald, M., O.H. Kramer, and T. Heinzel, *HDACi--targets beyond chromatin.* Cancer Lett, 2009. **280**(2): p. 160-7.
396. Lai, C.J., et al., *CUDC-101, a multitargeted inhibitor of histone deacetylase, epidermal growth factor receptor, and human epidermal growth factor receptor 2, exerts potent anticancer activity.* Cancer Res, 2010. **70**(9): p. 3647-56.
397. Dymock, B.W., et al., *Selective JAK inhibitors.* Future Med Chem, 2014. **6**(12): p. 1439-71.

398. Ko, K.S., et al., *Development of a chimeric c-Src kinase and HDAC inhibitor.* ACS Med Chem Lett, 2013. **4**(8): p. 779-783.
399. Chen, J.B., et al., *Design and synthesis of dual-action inhibitors targeting histone deacetylases and 3-hydroxy-3-methylglutaryl coenzyme A reductase for cancer treatment.* J Med Chem, 2013. **56**(9): p. 3645-55.
400. Woo, L.W., et al., *Hybrid dual aromatase-steroid sulfatase inhibitors with exquisite picomolar inhibitory activity.* ACS Med Chem Lett, 2011. **2**(3): p. 243-7.
401. Chesi, M., et al., *Drug response in a genetically engineered mouse model of multiple myeloma is predictive of clinical efficacy.* Blood, 2012. **120**(2): p. 376-85.
402. Amemiya, S., et al., *Synthesis and evaluation of novel dual BRD4/HDAC inhibitors.* Bioorg Med Chem, 2017. **25**(14): p. 3677-3684.
403. Zhang, Z., et al., *Targeting epigenetic reader and eraser: Rational design, synthesis and in vitro evaluation of dimethylisoxazoles derivatives as BRD4/HDAC dual inhibitors.* Bioorg Med Chem Lett, 2016. **26**(12): p. 2931-2935.
404. Kalin, J.H., et al., *Targeting the CoREST complex with dual histone deacetylase and demethylase inhibitors.* Nat Commun, 2018. **9**(1): p. 53.
405. Knutson, S.K., et al., *Synergistic Anti-Tumor Activity of EZH2 Inhibitors and Glucocorticoid Receptor Agonists in Models of Germinal Center Non-Hodgkin Lymphomas.* PLoS One, 2014. **9**(12): p. e111840.
406. Kirk, J.S., et al., *Top2a identifies and provides epigenetic rationale for novel combination therapeutic strategies for aggressive prostate cancer.* Oncotarget, 2015. **6**(5): p. 3136-46.
407. Johnson, D.P., et al., *HDAC1,2 inhibition impairs EZH2- and BBAP-mediated DNA repair to overcome chemoresistance in EZH2 gain-of-function mutant diffuse large B-cell lymphoma.* Oncotarget, 2015. **6**(7): p. 4863-87.
408. Grinshtein, N., et al., *Small molecule epigenetic screen identifies novel EZH2 and HDAC inhibitors that target glioblastoma brain tumor-initiating cells.* Oncotarget, 2016. **7**(37): p. 59360-59376.
409. Curry, E., et al., *Dual EZH2 and EHMT2 histone methyltransferase inhibition increases biological efficacy in breast cancer cells.* Clin Epigenetics, 2015. **7**: p. 84.
410. Coward, W.R., et al., *A central role for G9a and EZH2 in the epigenetic silencing of cyclooxygenase-2 in idiopathic pulmonary fibrosis.* FASEB J, 2014. **28**(7): p. 3183-96.
411. Huang, W.J., W.W. Chen, and X. Zhang, *Huntington's disease: Molecular basis of pathology and status of current therapeutic approaches.* Exp Ther Med, 2016. **12**(4): p. 1951-1956.
412. Newman, J.C., W. He, and E. Verdin, *Mitochondrial protein acylation and intermediary metabolism: regulation by sirtuins and implications for metabolic disease.* J Biol Chem, 2012. **287**(51): p. 42436-43.
413. Pagans, S., et al., *SIRT1 regulates HIV transcription via Tat deacetylation.* PLoS Biol, 2005. **3**(2): p. e41.
414. Dai, H., et al., *Sirtuin activators and inhibitors: Promises, achievements, and challenges.* Pharmacol Ther, 2018. **188**: p. 140-154.
415. Tervo, A.J., et al., *An in silico approach to discovering novel inhibitors of human sirtuin type 2.* J Med Chem, 2004. **47**(25): p. 6292-8.
416. Smith, M.R., et al., *A potent and selective Sirtuin 1 inhibitor alleviates pathology in multiple animal and cell models of Huntington's disease.* Hum Mol Genet, 2014. **23**(11): p. 2995-3007.
417. Grozinger, C.M., et al., *Identification of a class of small molecule inhibitors of the sirtuin family of NAD-dependent deacetylases by phenotypic screening.* J Biol Chem, 2001. **276**(42): p. 38837-43.
418. Lara, E., et al., *Salermide, a Sirtuin inhibitor with a strong cancer-specific proapoptotic effect.* Oncogene, 2009. **28**(6): p. 781-91.
419. Yang, B., et al., *Aberrant expression of SIRT3 is conversely correlated with the progression and prognosis of human gastric cancer.* Biochem Biophys Res Commun, 2014. **443**(1): p. 156-60.
420. Ivana Scovassi, A. and M. Diederich, *Modulation of poly(ADP-ribosylation) in apoptotic cells.* Biochem Pharmacol, 2004. **68**(6): p. 1041-7.

421. Marshall, G.M., et al., *SIRT1 promotes N-Myc oncogenesis through a positive feedback loop involving the effects of MKP3 and ERK on N-Myc protein stability.* PLoS Genet, 2011. **7**(6): p. e1002135.
422. Hirai, S., et al., *Antitumor effects of a sirtuin inhibitor, tenovin-6, against gastric cancer cells via death receptor 5 up-regulation.* PLoS One, 2014. **9**(7): p. e102831.
423. Yuan, H., et al., *Activation of stress response gene SIRT1 by BCR-ABL promotes leukemogenesis.* Blood, 2012. **119**(8): p. 1904-14.
424. Struhl, K., *Histone acetylation and transcriptional regulatory mechanisms.* Genes Dev, 1998. **12**(5): p. 599-606.
425. Howitz, K.T., et al., *Small molecule activators of sirtuins extend Saccharomyces cerevisiae lifespan.* Nature, 2003. **425**(6954): p. 191-6.
426. Voogd, T.E., et al., *Recent research on the biological activity of suramin.* Pharmacol Rev, 1993. **45**(2): p. 177-203.
427. Mai, A., et al., *Design, synthesis, and biological evaluation of sirtinol analogues as class III histone/protein deacetylase (Sirtuin) inhibitors.* J Med Chem, 2005. **48**(24): p. 7789-95.
428. Kaeberlein, M., M. McVey, and L. Guarente, *The SIR2/3/4 complex and SIR2 alone promote longevity in Saccharomyces cerevisiae by two different mechanisms.* Genes Dev, 1999. **13**(19): p. 2570-80.
429. Rogina, B. and S.L. Helfand, *Sir2 mediates longevity in the fly through a pathway related to calorie restriction.* Proc Natl Acad Sci U S A, 2004. **101**(45): p. 15998-6003.
430. Banks, A.S., et al., *SirT1 gain of function increases energy efficiency and prevents diabetes in mice.* Cell Metab, 2008. **8**(4): p. 333-41.
431. Milne, J.C., et al., *Small molecule activators of SIRT1 as therapeutics for the treatment of type 2 diabetes.* Nature, 2007. **450**(7170): p. 712-6.
432. Smith, B.C. and J.M. Denu, *Sir2 protein deacetylases: evidence for chemical intermediates and functions of a conserved histidine.* Biochemistry, 2006. **45**(1): p. 272-82.
433. Jing, E., et al., *Sirtuin-3 (Sirt3) regulates skeletal muscle metabolism and insulin signaling via altered mitochondrial oxidation and reactive oxygen species production.* Proc Natl Acad Sci U S A, 2011. **108**(35): p. 14608-13.
434. Mai, A., et al., *Study of 1,4-dihydropyridine structural scaffold: discovery of novel sirtuin activators and inhibitors.* J Med Chem, 2009. **52**(17): p. 5496-504.
435. Valente, S., et al., *1,4-Dihydropyridines Active on the SIRT1/AMPK Pathway Ameliorate Skin Repair and Mitochondrial Function and Exhibit Inhibition of Proliferation in Cancer Cells.* J Med Chem, 2016. **59**(4): p. 1471-91.
436. Nayagam, V.M., et al., *SIRT1 modulating compounds from high-throughput screening as anti-inflammatory and insulin-sensitizing agents.* J Biomol Screen, 2006. **11**(8): p. 959-67.
437. Vu, C.B., et al., *Discovery of imidazo[1,2-b]thiazole derivatives as novel SIRT1 activators.* J Med Chem, 2009. **52**(5): p. 1275-83.
438. Bemis, J.E., et al., *Discovery of oxazolo[4,5-b]pyridines and related heterocyclic analogs as novel SIRT1 activators.* Bioorg Med Chem Lett, 2009. **19**(8): p. 2350-3.
439. Jin, L., et al., *Biochemical characterization, localization, and tissue distribution of the longer form of mouse SIRT3.* Protein Sci, 2009. **18**(3): p. 514-25.
440. Huhtiniemi, T., et al., *N(epsilon)-Modified lysine containing inhibitors for SIRT1 and SIRT2.* Bioorg Med Chem, 2010. **18**(15): p. 5616-25.
441. Minor, R.K., et al., *SRT1720 improves survival and healthspan of obese mice.* Sci Rep, 2011. **1**: p. 70.
442. Hubbard, B.P. and D.A. Sinclair, *Small molecule SIRT1 activators for the treatment of aging and age-related diseases.* Trends Pharmacol Sci, 2014. **35**(3): p. 146-54.
443. Mitchell, S.J., et al., *The SIRT1 activator SRT1720 extends lifespan and improves health of mice fed a standard diet.* Cell Rep, 2014. **6**(5): p. 836-43.
444. Pacholec, M., et al., *SRT1720, SRT2183, SRT1460, and resveratrol are not direct activators of SIRT1.* J Biol Chem, 2010. **285**(11): p. 8340-51.

445. Suzuki, K., et al., *SRT1720, a SIRT1 activator, promotes tumor cell migration, and lung metastasis of breast cancer in mice.* Oncol Rep, 2012. **27**(6): p. 1726-32.
446. Hubbard, B.P., et al., *Evidence for a common mechanism of SIRT1 regulation by allosteric activators.* Science, 2013. **339**(6124): p. 1216-9.
447. Sinclair, D.A. and L. Guarente, *Small-molecule allosteric activators of sirtuins.* Annu Rev Pharmacol Toxicol, 2014. **54**: p. 363-80.
448. Mahajan, S.S., et al., *Sirtuin modulators.* Handb Exp Pharmacol, 2011. **206**: p. 241-55.
449. Dai, H., et al., *SIRT1 activation by small molecules: kinetic and biophysical evidence for direct interaction of enzyme and activator.* J Biol Chem, 2010. **285**(43): p. 32695-703.
450. Borra, M.T., et al., *Substrate specificity and kinetic mechanism of the Sir2 family of NAD+-dependent histone/protein deacetylases.* Biochemistry, 2004. **43**(30): p. 9877-87.
451. Park, S.J., et al., *Resveratrol ameliorates aging-related metabolic phenotypes by inhibiting cAMP phosphodiesterases.* Cell, 2012. **148**(3): p. 421-33.
452. Pillai, V.B., et al., *Honokiol blocks and reverses cardiac hypertrophy in mice by activating mitochondrial Sirt3.* Nat Commun, 2015. **6**: p. 6656.
453. Zorn, J.A. and J.A. Wells, *Turning enzymes ON with small molecules.* Nat Chem Biol, 2010. **6**(3): p. 179-188.
454. Li, W., et al., *Sirtuin 2, a mammalian homolog of yeast silent information regulator-2 longevity regulator, is an oligodendroglial protein that decelerates cell differentiation through deacetylating alpha-tubulin.* J Neurosci, 2007. **27**(10): p. 2606-16.
455. Pillai, J.B., et al., *Poly(ADP-ribose) polymerase-1-dependent cardiac myocyte cell death during heart failure is mediated by NAD+ depletion and reduced Sir2alpha deacetylase activity.* J Biol Chem, 2005. **280**(52): p. 43121-30.
456. Yu, W., K.E. Dittenhafer-Reed, and J.M. Denu, *SIRT3 protein deacetylates isocitrate dehydrogenase 2 (IDH2) and regulates mitochondrial redox status.* J Biol Chem, 2012. **287**(17): p. 14078-86.
457. Ren, J.H., et al., *SIRT3 restricts hepatitis B virus transcription and replication through epigenetic regulation of covalently closed circular DNA involving suppressor of variegation 3-9 homolog 1 and SET domain containing 1A histone methyltransferases.* Hepatology, 2018.
458. Gertz, M. and C. Steegborn, *Function and regulation of the mitochondrial sirtuin isoform Sirt5 in Mammalia.* Biochim Biophys Acta, 2010. **1804**(8): p. 1658-65.
459. Ren, J.H., et al., *Protective Role of Sirtuin3 (SIRT3) in Oxidative Stress Mediated by Hepatitis B Virus X Protein Expression.* PLoS One, 2016. **11**(3): p. e0150961.
460. de Lera, A.R. and A. Ganesan, *Epigenetic polypharmacology: from combination therapy to multitargeted drugs.* Clin Epigenetics, 2016. **8**: p. 105.
461. Bracken, A.P., et al., *Genome-wide mapping of Polycomb target genes unravels their roles in cell fate transitions.* Genes Dev, 2006. **20**(9): p. 1123-36.
462. Glozak, M.A. and E. Seto, *Histone deacetylases and cancer.* Oncogene, 2007. **26**(37): p. 5420-32.
463. Miller, T.A., D.J. Witter, and S. Belvedere, *Histone deacetylase inhibitors.* J Med Chem, 2003. **46**(24): p. 5097-116.
464. Huang, H., et al., *Quantitative proteomic analysis of histone modifications.* Chem Rev, 2015. **115**(6): p. 2376-418.
465. Sparmann, A. and M. van Lohuizen, *Polycomb silencers control cell fate, development and cancer.* Nat Rev Cancer, 2006. **6**(11): p. 846-56.
466. Yu, J., et al., *A polycomb repression signature in metastatic prostate cancer predicts cancer outcome.* Cancer Res, 2007. **67**(22): p. 10657-63.
467. Comet, I., et al., *Maintaining cell identity: PRC2-mediated regulation of transcription and cancer.* Nat Rev Cancer, 2016. **16**(12): p. 803-810.
468. Xu, B., et al., *Targeting EZH2 and PRC2 dependence as novel anticancer therapy.* Exp Hematol, 2015. **43**(8): p. 698-712.
469. Shen, L., et al., *Update of research on the role of EZH2 in cancer progression.* Onco Targets Ther, 2013. **6**: p. 321-4.

470. Mai, A., et al., *epigenetic multiple ligands: mixed histone/protein methyltransferase, acetyltransferase, and class III deacetylase (sirtuin) inhibitors.* J Med Chem, 2008. **51**(7): p. 2279-90.
471. Mai, A., et al., *Synthesis and biological validation of novel synthetic histone/protein methyltransferase inhibitors.* ChemMedChem, 2007. **2**(7): p. 987-91.
472. Palacios, D., et al., *TNF/p38alpha/polycomb signaling to Pax7 locus in satellite cells links inflammation to the epigenetic control of muscle regeneration.* Cell Stem Cell, 2010. **7**(4): p. 455-69.
473. Valente, S., et al., *Identification of PR-SET7 and EZH2 selective inhibitors inducing cell death in human leukemia U937 cells.* Biochimie, 2012. **94**(11): p. 2308-13.
474. Ciarapica, R., et al., *Pharmacological inhibition of EZH2 as a promising differentiation therapy in embryonal RMS.* BMC Cancer, 2014. **14**: p. 139.
475. Ciarapica, R., et al., *The Polycomb group (PcG) protein EZH2 supports the survival of PAX3-FOXO1 alveolar rhabdomyosarcoma by repressing FBXO32 (Atrogin1/MAFbx).* Oncogene, 2014. **33**(32): p. 4173-84.
476. Miele, E., et al., *The histone methyltransferase EZH2 as a druggable target in SHH medulloblastoma cancer stem cells.* Oncotarget, 2017. **8**(40): p. 68557-68570.
477. Ragno, R., et al., *Small molecule inhibitors of histone arginine methyltransferases: homology modeling, molecular docking, binding mode analysis, and biological evaluations.* J Med Chem, 2007. **50**(6): p. 1241-53.
478. Castellano, S., et al., *Design, synthesis and biological evaluation of carboxy analogues of arginine methyltransferase inhibitor 1 (AMI-1).* ChemMedChem, 2010. **5**(3): p. 398-414.
479. Cheng, D., et al., *Novel 3,5-bis(bromohydroxybenzylidene)piperidin-4-ones as coactivator-associated arginine methyltransferase 1 inhibitors: enzyme selectivity and cellular activity.* J Med Chem, 2011. **54**(13): p. 4928-32.
480. Castellano, S., et al., *Identification of small-molecule enhancers of arginine methylation catalyzed by coactivator-associated arginine methyltransferase 1.* J Med Chem, 2012. **55**(22): p. 9875-90.
481. Mellini, P., et al., *Pyrazole-based inhibitors of enhancer of zeste homologue 2 induce apoptosis and autophagy in cancer cells.* Philos Trans R Soc Lond B Biol Sci, 2018. **373**(1748).
482. Verma, S.K., et al., *Identification of Potent, Selective, Cell-Active Inhibitors of the Histone Lysine Methyltransferase EZH2.* ACS Med Chem Lett, 2012. **3**(12): p. 1091-6.
483. De, S.K., *Cobalt(II) chloride as a novel and efficient catalyst for the synthesis of 1,2,5-trisubstituted pyrroles under solvent-free conditions.* Heteroatom Chemistry, 2008. **19**(6): p. 592-595.
484. Trisciuoglio, D., et al., *CPTH6, a thiazole derivative, induces histone hypoacetylation and apoptosis in human leukemia cells.* Clin Cancer Res, 2012. **18**(2): p. 475-86.
485. Sundstrom, C. and K. Nilsson, *Establishment and characterization of a human histiocytic lymphoma cell line (U-937).* Int J Cancer, 1976. **17**(5): p. 565-77.
486. Lillico, R., et al., *HDAC inhibitors induce global changes in histone lysine and arginine methylation and alter expression of lysine demethylases.* J Proteomics, 2016. **133**: p. 125-133.
487. Campuzano, V., et al., *Friedreich's ataxia: autosomal recessive disease caused by an intronic GAA triplet repeat expansion.* Science, 1996. **271**(5254): p. 1423-7.
488. Pandolfo, M., *The molecular basis of Friedreich ataxia.* Adv Exp Med Biol, 2002. **516**: p. 99-118.
489. Cossee, M., et al., *Friedreich's ataxia: point mutations and clinical presentation of compound heterozygotes.* Ann Neurol, 1999. **45**(2): p. 200-6.
490. Gellera, C., et al., *Frataxin gene point mutations in Italian Friedreich ataxia patients.* Neurogenetics, 2007. **8**(4): p. 289-99.
491. Deutsch, E.C., et al., *A rapid, noninvasive immunoassay for frataxin: utility in assessment of Friedreich ataxia.* Mol Genet Metab, 2010. **101**(2-3): p. 238-45.
492. Anheim, M., et al., *Exonic deletions of FXN and early-onset Friedreich ataxia.* Arch Neurol, 2012. **69**(7): p. 912-6.

493. Chandok, G.S., et al., *Effects of Friedreich's ataxia GAA repeats on DNA replication in mammalian cells.* Nucleic Acids Res, 2012. **40**(9): p. 3964-74.
494. Ezzatizadeh, V., et al., *The mismatch repair system protects against intergenerational GAA repeat instability in a Friedreich ataxia mouse model.* Neurobiol Dis, 2012. **46**(1): p. 165-71.
495. Campuzano, V., et al., *Frataxin is reduced in Friedreich ataxia patients and is associated with mitochondrial membranes.* Hum Mol Genet, 1997. **6**(11): p. 1771-80.
496. Castaldo, I., et al., *DNA methylation in intron 1 of the frataxin gene is related to GAA repeat length and age of onset in Friedreich ataxia patients.* J Med Genet, 2008. **45**(12): p. 808-12.
497. Bradley, J.L., et al., *Clinical, biochemical and molecular genetic correlations in Friedreich's ataxia.* Hum Mol Genet, 2000. **9**(2): p. 275-82.
498. Koeppen, A.H., et al., *The dentate nucleus in Friedreich's ataxia: the role of iron-responsive proteins.* Acta Neuropathol, 2007. **114**(2): p. 163-73.
499. Wong, A., et al., *The Friedreich's ataxia mutation confers cellular sensitivity to oxidant stress which is rescued by chelators of iron and calcium and inhibitors of apoptosis.* Hum Mol Genet, 1999. **8**(3): p. 425-30.
500. Schulz, J.B., et al., *Diagnosis and treatment of Friedreich ataxia: a European perspective.* Nat Rev Neurol, 2009. **5**(4): p. 222-34.
501. Grabczyk, E., M. Mancuso, and M.C. Sammarco, *A persistent RNA.DNA hybrid formed by transcription of the Friedreich ataxia triplet repeat in live bacteria, and by T7 RNAP in vitro.* Nucleic Acids Res, 2007. **35**(16): p. 5351-9.
502. Wells, R.D., *DNA triplexes and Friedreich ataxia.* FASEB J, 2008. **22**(6): p. 1625-34.
503. Saveliev, A., et al., *DNA triplet repeats mediate heterochromatin-protein-1-sensitive variegated gene silencing.* Nature, 2003. **422**(6934): p. 909-13.
504. Sandi, C., et al., *Epigenetic-based therapies for Friedreich ataxia.* Front Genet, 2014. **5**: p. 165.
505. Sandi, C., S. Al-Mahdawi, and M.A. Pook, *Epigenetics in Friedreich's Ataxia: Challenges and Opportunities for Therapy.* Genet Res Int, 2013. **2013**: p. 852080.
506. Al-Mahdawi, S., et al., *The Friedreich ataxia GAA repeat expansion mutation induces comparable epigenetic changes in human and transgenic mouse brain and heart tissues.* Hum Mol Genet, 2008. **17**(5): p. 735-46.
507. Herman, D., et al., *Histone deacetylase inhibitors reverse gene silencing in Friedreich's ataxia.* Nat Chem Biol, 2006. **2**(10): p. 551-8.
508. Rai, M., et al., *HDAC inhibitors correct frataxin deficiency in a Friedreich ataxia mouse model.* PLoS One, 2008. **3**(4): p. e1958.
509. Greene, E., et al., *Repeat-induced epigenetic changes in intron 1 of the frataxin gene and its consequences in Friedreich ataxia.* Nucleic Acids Res, 2007. **35**(10): p. 3383-90.
510. Evans-Galea, M.V., et al., *FXN methylation predicts expression and clinical outcome in Friedreich ataxia.* Ann Neurol, 2012. **71**(4): p. 487-97.
511. Razin, A., *CpG methylation, chromatin structure and gene silencing-a three-way connection.* EMBO J, 1998. **17**(17): p. 4905-8.
512. De Biase, I., et al., *Epigenetic silencing in Friedreich ataxia is associated with depletion of CTCF (CCCTC-binding factor) and antisense transcription.* PLoS One, 2009. **4**(11): p. e7914.
513. Kim, E., M. Napierala, and S.Y. Dent, *Hyperexpansion of GAA repeats affects post-initiation steps of FXN transcription in Friedreich's ataxia.* Nucleic Acids Res, 2011. **39**(19): p. 8366-77.
514. Kumari, D., R.E. Biacsi, and K. Usdin, *Repeat expansion affects both transcription initiation and elongation in friedreich ataxia cells.* J Biol Chem, 2011. **286**(6): p. 4209-15.
515. Acquaviva, F., et al., *Recombinant human erythropoietin increases frataxin protein expression without increasing mRNA expression.* Cerebellum, 2008. **7**(3): p. 360-5.
516. Sandi, C., et al., *Prolonged treatment with pimelic o-aminobenzamide HDAC inhibitors ameliorates the disease phenotype of a Friedreich ataxia mouse model.* Neurobiol Dis, 2011. **42**(3): p. 496-505.
517. Plummer, R., et al., *Phase I study of MG98, an oligonucleotide antisense inhibitor of human DNA methyltransferase 1, given as a 7-day infusion in patients with advanced solid tumors.* Clin Cancer Res, 2009. **15**(9): p. 3177-83.

518. Sandi, C., et al., *Generation and characterisation of Friedreich ataxia YG8R mouse fibroblast and neural stem cell models.* PLoS One, 2014. **9**(2): p. e89488.
519. Festenstein, R., *Breaking the silence in Friedreich's ataxia.* Nat Chem Biol, 2006. **2**(10): p. 512-3.
520. Sarsero, J.P., et al., *Upregulation of expression from the FRDA genomic locus for the therapy of Friedreich ataxia.* J Gene Med, 2003. **5**(1): p. 72-81.
521. Rai, M., et al., *Two new pimelic diphenylamide HDAC inhibitors induce sustained frataxin upregulation in cells from Friedreich's ataxia patients and in a mouse model.* PLoS One, 2010. **5**(1): p. e8825.
522. Xu, C., et al., *Chemical probes identify a role for histone deacetylase 3 in Friedreich's ataxia gene silencing.* Chem Biol, 2009. **16**(9): p. 980-9.
523. Soragni, E., et al., *Epigenetic therapy for Friedreich ataxia.* Ann Neurol, 2014. **76**(4): p. 489-508.
524. Soragni, E. and J.M. Gottesfeld, *Translating HDAC inhibitors in Friedreich's ataxia.* Expert Opin Orphan Drugs, 2016. **4**(9): p. 961-970.
525. Libri, V., et al., *Epigenetic and neurological effects and safety of high-dose nicotinamide in patients with Friedreich's ataxia: an exploratory, open-label, dose-escalation study.* Lancet, 2014. **384**(9942): p. 504-13.
526. Lynch, D.R. and K.H. Fischbeck, *Nicotinamide in Friedreich's ataxia: useful or not?* Lancet, 2014. **384**(9942): p. 474-5.
527. Chan, P.K., et al., *Heterochromatinization induced by GAA-repeat hyperexpansion in Friedreich's ataxia can be reduced upon HDAC inhibition by vitamin B3.* Hum Mol Genet, 2013. **22**(13): p. 2662-75.
528. Punga, T. and M. Buhler, *Long intronic GAA repeats causing Friedreich ataxia impede transcription elongation.* EMBO Mol Med, 2010. **2**(4): p. 120-9.
529. Janowski, B.A., J. Hu, and D.R. Corey, *Silencing gene expression by targeting chromosomal DNA with antigene peptide nucleic acids and duplex RNAs.* Nat Protoc, 2006. **1**(1): p. 436-43.
530. Janowski, B.A., et al., *Activating gene expression in mammalian cells with promoter-targeted duplex RNAs.* Nat Chem Biol, 2007. **3**(3): p. 166-73.
531. Beck, D.B., et al., *PR-Set7 and H4K20me1: at the crossroads of genome integrity, cell cycle, chromosome condensation, and transcription.* Genes Dev, 2012. **26**(4): p. 325-37.
532. Ma, A., et al., *Discovery of a selective, substrate-competitive inhibitor of the lysine methyltransferase SETD8.* J Med Chem, 2014. **57**(15): p. 6822-33.
533. Blum, G., et al., *Small-molecule inhibitors of SETD8 with cellular activity.* ACS Chem Biol, 2014. **9**(11): p. 2471-8.
534. Bromberg, K.D., et al., *The SUV4-20 inhibitor A-196 verifies a role for epigenetics in genomic integrity.* Nat Chem Biol, 2017. **13**(3): p. 317-324.
535. Silva, A.M., et al., *Expanded GAA repeats impair FXN gene expression and reposition the FXN locus to the nuclear lamina in single cells.* Hum Mol Genet, 2015. **24**(12): p. 3457-71.
536. Lufino, M.M., et al., *A GAA repeat expansion reporter model of Friedreich's ataxia recapitulates the genomic context and allows rapid screening of therapeutic compounds.* Hum Mol Genet, 2013. **22**(25): p. 5173-87.